

12-2007

Stormwater quality characterization, modeling, and management for the greater Milwaukee area, Wisconsin

Puripus Soonthornnonda

Follow this and additional works at: <https://dc.uwm.edu/etd>



Part of the [Engineering Commons](#)

Recommended Citation

Soonthornnonda, Puripus, "Stormwater quality characterization, modeling, and management for the greater Milwaukee area, Wisconsin" (2007). *Theses and Dissertations*. 969.
<https://dc.uwm.edu/etd/969>

This Dissertation is brought to you for free and open access by UWM Digital Commons. It has been accepted for inclusion in Theses and Dissertations by an authorized administrator of UWM Digital Commons. For more information, please contact open-access@uwm.edu.

**STORMWATER QUALITY CHARACTERIZATION, MODELING,
AND MANAGEMENT FOR THE GREATER
MILWAUKEE AREA, WISCONSIN**

By

Puripus Soonthornnonda

A Dissertation Submitted in
Partial Fulfillment of the
Requirements for the Degree of

Doctor of Philosophy

in Engineering

at

The University of Wisconsin – Milwaukee

December 2007

T
9999
-S_n66x
2007

ABSTRACT

**STORMWATER QUALITY CHARACTERIZATION, MODELING,
AND MANAGEMENT FOR THE GREATER
MILWAUKEE AREA, WISCONSIN**

By

Puripus Soonthornnonda

The University of Wisconsin-Milwaukee, 2007
Under the Supervision of Professor Erik R. Christensen

Storm sewer pipes in the Greater Milwaukee area collect polluted stormwater runoff from land surfaces and deliver the polluted water directly to Milwaukee, Menomonee, and Kinnickinnic Rivers and Lake Michigan during rain or snowmelt events. Some amounts of sanitary sewage may on occasion get into the storm sewer system due to inadvertent or improper connections. The combined sewer system delivers polluted stormwater and sanitary sewage to one of the Milwaukee Metropolitan Sewerage District (MMSD)'s two wastewater treatment plants (Jones Island and South Shore). However, during extremely wet conditions, combined sewer overflows (CSOs) may occur. These overflows go directly into the rivers and Lake Michigan. Direct discharges of polluted stormwater and CSOs may cause local waterways to exceed the National Water Quality Criteria (NWQC) for many pollutants, especially nutrients and bacteria.

Meteorological data analysis in the study area was performed. Results indicate that storms of a short duration occur more frequently than storms of a long duration. There was a tendency that the average precipitation intensity is decreasing versus storm duration, except for infrequent rainfall durations. The rainfall intensity averaged over

four rain gauges and rainfall data (2000 – 2005) was 1.35 mm/hr. The average rainfall duration was 8.42 hr. The antecedent dry period was typically from 5 – 25 days. Average rainfall intensity, total depth, and duration in the study area could also be estimated using the Interevent Time Definition (IETD) technique. The corresponding values based on rainfall data from the period 2000 – 2006 were 1.27 mm/hr, 10.2 mm, and 13.7 hr, respectively. The interevent time, defined as a period without rainfall, can be equivalent to an antecedent dry period. The average interevent time of 2.31 days was estimated.

Generally, runoff from winter and spring was found to be more polluted than runoff from other seasons. The highest average concentrations of silver, lead, zinc, total suspended solids, turbidity, total Kjeldahl nitrogen, total phosphorus, *E. coli*, and fecal coliform in stormwater were found in summer.

Geographic Information Systems (GIS) is useful to determine actual drainage areas and runoff coefficients. Runoff coefficients for study drainage areas obtained from an optimization model using GIS land use subareas ranged from 0.162 (SWNB11: new residential and open lands) to 0.697 (SWMI16: highway). In addition to the coefficient for the individual catchment area, runoff coefficients for GIS land use subareas ranged from 0.134 (residential) to 0.700 (freeway) and 0.801 (outdoor and recreational).

The proposed load model was applicable to estimate the stormwater runoff mass (kg) per event for metals, nutrients, and bacteria. Model parameters include the deposition rate (kg/ha/d) as a product of land use factor α (kg/kg_{avg}) and deposition coefficient a (kg_{avg}/ha/d). The effective area (ha) is a product of the drainage area A and runoff coefficient $\hat{\beta}$. Other parameters include antecedent dry period t_d (d), transport coefficient c (cm⁻¹), and rainfall depth (cm) which is a product of rainfall intensity k

(cm/hr) and duration Δt (hr). The load model gave >1.0 land use factors from automobile related drainage areas for most metals, e.g., 3.33 (SWMI04: highway 794 and large residential area), 4.12 (SWMI15: I-94), and 1.60 (SWMI18: Miller Park east parking lot) for copper. Land use factors of *E. coli* were found to be greater than one from residential areas, e.g., 1.96 (SWMI12: residential area) and 31.9 (SWMI04).

A good estimate of the transport coefficient for individual pollutants is necessary because it reflects the removal ability of pollutant mass on surfaces. A washoff mass rate model was developed to estimate the transport coefficient based on the hydrograph. Transport coefficients (cm^{-1}) for metals are in decreasing order lead (6.10 ± 2.55) > silver (4.73 ± 2.44) > zinc (4.69 ± 1.72) > copper (4.59 ± 1.71) > nickel (4.49 ± 1.73) > mercury (3.45 ± 2.98) > cadmium (3.03 ± 1.34), reflecting a decreasing degree of particle association. For BOD₅, suspended solids, bacteria, and phosphorus, the order of transport coefficients are total suspended solids (7.16 ± 2.72) > fecal coliform (6.43 ± 2.79) > *E. coli* (6.12 ± 2.79) > BOD₅ (5.24 ± 4.05) > total phosphorus (2.12 ± 0.907), showing increase in soluble fraction of these pollutants.

Chemical Mass Balance (CMB) and Positive Matrix Factorization (PMF) models were applicable for identification of pollutant sources and computation of pollutant and flow contributions in CSOs. Based on overflow events during 2000 – 2006 for the CMB model and 2004 – 2006 for the PMF model, three possible sources (stormwater, sanitary sewage, and groundwater) in CSOs were found. Between 27 and 56 % of the flow were from sanitary sewage and at least 26 % from stormwater with up to 8 % from groundwater. Metals and total suspended solids from stormwater were found to be predominant pollutants in CSOs. Sanitary sewage contributed ≥ 28 % of the BOD₅,

ammonia, and total phosphorus in CSOs. The contribution of ammonia from sanitary sewage was relative high ($\geq 58\%$). While most fecal coliform bacteria ($52 \pm 19\%$) were from sanitary sewage, the majority of *E. coli* ($84 \pm 21\%$) bacteria were carried by stormwater.

Sewer separation may be implemented to eliminate CSOs with high amounts of BOD₅, ammonia, and total phosphorus in sanitary sewage. However, this method can be inappropriate unless effective BMPs that target removal of metals, total suspended solids, and bacteria from stormwater are implemented in the separated sewer systems. Reduction of CSO pollutants such as cadmium, chromium, copper, nickel, and zinc may be achieved through periodic removal of sewer sediment. In order to reduce CSO pollutants such as total suspended solids and lead, it is important to implement stormwater BMPs prior to combining stormwater and sanitary sewage, for example rain gardens, green parking lots, porous pavement, stormceptor®, vortechs®, and downstream defender®. Mechanisms and benefits of stormceptor, vortechs, and downstream defender systems were described in this study.

This is the first time that a major stormwater quality analysis is performed in the Greater Milwaukee area. It is hoped that the findings from this study can serve as a guide for the design of stormwater drainage areas and appropriate BMPs, which will eventually lead to improvements in the water quality of receiving waters.



Major Professor

12/10/07

Date

ACKNOWLEDGEMENTS

I would like to thank first my advisor, Professor Erik Christensen who has helped me with proofreading my works, developing innovative ideas, and providing invaluable suggestions. I would also like to thank my Ph.D. committee members, Professor Hector Bravo, Professor Jin Li, Professor Jaejin Jang, and Professor Sam Helwany for their time and comments. Thanks also to Professor Qian Liao for substituting for Professor Jin Li who was on maternity leave at the time of my dissertation defense.

I would like to thank the MMSD for supporting my doctoral studies under contact numbers M03023P01 and M03023E01. My dissertation would not have been achievable without data and useful comments from Urbain Boudjou, Mary Singer, Christopher Magruder, Eric Waldmer, and Tim Bate at the Milwaukee Metropolitan Sewerage District (MMSD). I appreciate their assistance.

I would like to thank Betty Warras for cordially helping me with various types of official letters from the dean's office and keeping me informed with many Graduate School forms. I would also like to thank Jean Carlson for helping me with all forms in the beginning of each semester appointment.

I am very thankful for support from my wonderful friends, Yang Liu, Reza Namdar Ghanbari, Peter Shedivy, Indranil Seth, and Marcia Silva. Finally, I would like to thank my wife Suthiya, my daughter Sara, and my parents who have supported me throughout my studies here.

TABLE OF CONTENTS

ABSTRACT.....	iii
ACKNOWLEDGEMENTS.....	vii
LIST OF FIGURES	xi
LIST OF TABLES.....	xxiii
I. INTRODUCTION	1
1.1 Study Areas.....	8
1.2 Sample Collection and Analysis	12
1.3 Measurement of Runoff Flows and Volumes	14
II. METEOROLOGICAL DATA ANALYSIS.....	15
2.1 Interevent Time Definition (IETD).....	22
2.2 Statistics of Rainfall Data by IETD Technique	23
III. CHARACTERIZATION OF STORMWATER QUALITY	28
3.1 Stormwater Quality Pollutants.....	28
3.2 Stormwater Quality Data Analysis	30
3.2.1 Descriptive Statistics	30
3.2.2 Comparison of Stormwater and Combined Sewer Overflows (CSOs) ...	32
3.2.3 Pollutant Trends	33
3.3 Results and Discussion	38
IV. DRAINAGE AREAS AND GEOGRAPHIC INFORMATION SYSTEMS (GIS)	48
4.1 Estimate of the Drainage Area Sizes	48
4.1.1 Measured and Calculated Runoff Coefficients	49

4.1.2	New Drainage Areas Determined By Storm Sewer and Contour lines...	52
4.2	Estimation of Runoff Coefficients Based on Least Squares Method.	54
4.3	Results and Discussion	54
V.	MODELING OF STORMWATER POLLUTANT LOADS	96
5.1	Load Model.....	98
5.2	Results and Discussion	104
5.2.1	Runoff Coefficients	104
5.2.2	Concentrations of Zn and Cu in Stormwater.....	107
5.2.3	Constituent Loads.....	108
5.2.4	Relationship between Mass Loads of Zn, Cu, and Other Metals in Stormwater Runoff.....	118
VI.	MODELING OF STORMWATER POLLUTANT WASHOFF	123
6.1	Pollutant Washoff Rate.....	124
6.2	Results and Discussion	129
6.2.1	Comparison of Modeled and Measured Mass Rates.....	155
6.2.2	Comparison of Modeled and Measured Concentrations	155
6.2.3	Transport Coefficients.....	161
VII.	FRACTION OF STORMWATER IN COMBINED SEWER OVERFLOWS (CSOs).....	165
7.1	CMB Model	167
7.1.1	Pollutant Source Profiles	169
7.2	PMF Model.....	172
7.2.1	Diagnostic Tools.....	173

7.3	Results and Discussion	173
7.3.1	Stormwater, Sanitary sewage, and Groundwater Profiles	173
7.3.2	CMB Model Pollutant Source Contributions	175
7.3.3	PMF Model Pollutant Source Profiles.....	179
7.3.4	PMF Model Pollutant Source Contributions	184
VIII.	STORMWATER BEST MANAGEMENT PRACTICES (BMPs).....	186
8.1	Stormwater BMP Removal Efficiencies of An Individual Storm Load.	190
8.2	Design of Effective Stormwater BMPs.....	191
8.3	Examples of Stormwater BMP Technologies Using Settling for Treatment.	199
8.3.1	Stormceptor®	199
8.3.2	Vortechs®.....	201
8.3.3	Downstream Defender®.....	203
8.3.4	Dry Detention pond	205
IX.	CONCLUSIONS.....	206
X.	RECOMMENDATIONS.....	209
XI.	REFERENCES	211
XII.	APPENDICES	220
XIII.	CURRICULUM VITAE.....	290

LIST OF FIGURES

Figure 1.1.	MMSD's planning area. (Source: MMSD Facilities Information).....	10
Figure 1.2.	Area velocity (AV) sensor and area velocity (AV) module (Source: www.isco.com/).	14
Figure 2.1.	Locations of stormwater study sites and rain gauge stations in the MMSD's planning area. Rain gauge stations, highlighted by , were used to evaluate rainfall statistics.	17
Figure 2.2.	Number of events for each rainfall duration, 4 rain gauge stations (WS1203, 1204, 1206, and 1220), 2000-2005.	19
Figure 2.3.	Average rainfall intensity for each rainfall duration at 4 rain gauge stations (WS1203, 1204, 1206, and 1220), 2000-2005.	21
Figure 2.4.	Autocorrelogram (with 5 % significance upper limit) for determining IETD based on averaged rainfall data (2000-2006) over 22 rain gauge stations in the study area.	23
Figure 2.5.	Number of events for each rainfall duration from average rainfall data (2000-2006) over 22 rain gauge stations.....	25
Figure 2.6.	Average rainfall intensity for each rainfall duration from averaged rainfall data (2000-2006) over 22 rain gauge stations.	26
Figure 2.7.	Average interevent time for each rainfall duration from average rainfall data (2000-2006) over 22 rain gauge stations.	27
Figure 3.1.	Seasonal snowfall at Milwaukee, WI (Wisconsin Climatology Office, 2005).	46
Figure 3.2.	Daily freeway vehicle-miles of travel on freeways for Milwaukee, WI (Texas Transportation Institute, Texas A&M University System, 2005).	47
Figure 4.1.	Measured versus rainfall-based runoff volumes.....	51
Figure 4.2.	Calculated runoff coefficients $\hat{\beta}_{i, calc}$ based on the optimization model vs runoff coefficients $\hat{\beta}_i$ based on new drainage area sizes.....	59
Figure 4.3.	A map of site SWMI01 (Lincoln Memorial Dr & Carferry Dr, Milwaukee) with land uses and new drainage boundary.	60

Figure 4.4.	An aerial photograph of site SWMI01 (Lincoln Memorial Dr & Carferry Dr, Milwaukee) with new drainage boundary.....	61
Figure 4.5.	A map of site SWMI02 (1700 N. Lincoln Memorial Dr @ Lafayette Hill, Milwaukee) with land uses and new drainage boundary.....	62
Figure 4.6.	An aerial photograph of site SWMI02 (1700 N. Lincoln Memorial Dr @ Lafayette Hill, Milwaukee) with new drainage boundary.....	63
Figure 4.7.	A map of site SWFR03 (54th & Ashland, Franklin) with land uses and new drainage boundary.	64
Figure 4.8.	An aerial photograph of site SWFR03 (54th & Ashland, Franklin) with new drainage boundary.	65
Figure 4.9.	A map of site SWMI04 (3500 S. Lake Dr @ Bayview Park, Milwaukee) with land uses and new drainage boundary.	66
Figure 4.10.	An aerial photograph of site SWMI04 (3500 S. Lake Dr @ Bayview Park, Milwaukee) with new drainage boundary.	67
Figure 4.11.	A map of site SWMI05 (1200 E. Singer Circle, Milwaukee) with land uses and new drainage boundary.	68
Figure 4.12.	An aerial photograph of site SWMI05 (1200 E. Singer Circle, Milwaukee) with new drainage boundary.....	69
Figure 4.13.	A map of site SWMI06 (Milwaukee County Zoo, Milwaukee) with land uses and new drainage boundary.	70
Figure 4.14.	An aerial photograph of site SWMI06 (Milwaukee County Zoo, Milwaukee) with new drainage boundary.....	71
Figure 4.15.	A map of site SWMI07 (4345 N. 47th St, Milwaukee) with land uses and new drainage boundary.	72
Figure 4.16.	An aerial photograph of site SWMI07 (4345 N. 47th St, Milwaukee) with new drainage boundary.....	73
Figure 4.17.	A map of site SWMI08 (Hampton & Lincoln Crk Pkwy, Milwaukee) with land uses and new drainage boundary.	74
Figure 4.18.	An aerial photograph of site SWMI08 (Hampton & Lincoln Crk Pkwy, Milwaukee) with new drainage boundary.....	75

Figure 4.19. A map of site SWWB09 (4939 N. Newhall, Whitefish Bay) with land uses and new drainage boundary.	76
Figure 4.20. An aerial photograph of site SWWB09 (4939 N. Newhall, Whitefish Bay) with new drainage boundary.	77
Figure 4.21. A map of site SWGF10 (Boerner Botanical Gardens, Hales Corners, Greenfield) with land uses and new drainage boundary.	78
Figure 4.22. An aerial photograph of site SWGF10 (Boerner Botanical Gardens, Hales Corners, Greenfield) with new drainage boundary.	79
Figure 4.23. A map of site SWNB11 (13380 Eagle Trace & Timber Ridge, New Berlin) with land uses and new drainage boundary.	80
Figure 4.24. An aerial photograph of site SWNB11 (13380 Eagle Trace & Timber Ridge, New Berlin) with new drainage boundary.	81
Figure 4.25. A map of site SWMI12 (3275 S. 72nd St, Milwaukee) with land uses and new drainage boundary.	82
Figure 4.26. An aerial photograph of site SWMI12 (3275 S. 72nd St, Milwaukee) with new drainage boundary.	83
Figure 4.27. A map of site SWWA13 (Ridge Blvd & Harding, Wauwatosa) with land uses and new drainage boundary.	84
Figure 4.28. An aerial photograph of site SWWA13 (Ridge Blvd & Harding, Wauwatosa) with new drainage boundary.	85
Figure 4.29. A map of site SWSF14 (Lake Dr and Tesch Av, St Francis) with land uses and new drainage boundary.	86
Figure 4.30. An aerial photograph of site SWSF14 (Lake Dr and Tesch Av, St Francis) with new drainage boundary.	87
Figure 4.31. A map of site SWMI15 (42nd St & Mt Vernon, I-94 & Menomonee River, Milwaukee) with land uses and new drainage boundary.	88
Figure 4.32. An aerial photograph of site SWMI15 (42nd St & Mt Vernon, I-94 & Menomonee River, Milwaukee) with new drainage boundary.	89
Figure 4.33. A map of site SWMI16 (Marquette interchange, Milwaukee) with land uses and new drainage boundary.	90

Figure 4.34. An aerial photograph of site SWMI16 (Marquette interchange, Milwaukee) with new drainage boundary.....	91
Figure 4.35. A map of site SWWA17 (71st and Chestnut St, Wauwatosa) with land uses and new drainage boundary.	92
Figure 4.36. An aerial photograph site SWWA17 (71st and Chestnut St, Wauwatosa) with land uses and new drainage boundary.	93
Figure 4.37. A map of site SWMI18 (Miller Park east parking lot at sausage house, Milwaukee) with land uses and new drainage boundary.....	94
Figure 4.38. An aerial photograph of site SWMI18 (Miller Park east parking lot at sausage house, Milwaukee) with land uses and new drainage boundary.	95
Figure 5.1. Calculated versus measured loads of zinc (Zn), copper (Cu), cadmium (Cd), and nickel (Ni), considering t_d for two events.	110
Figure 5.2. Calculated versus measured loads of chromium (Cr), lead (Pb), mercury (Hg), and silver (Ag), considering t_d for two events.....	111
Figure 5.3. Calculated versus measured loads of BOD ₅ , total suspended solids (TSS), <i>E. coli</i> (EC), and fecal coliform (FC), considering t_d for two events.....	112
Figure 5.4. Calculated versus measured loads of total soluble phosphorus (TSP) and total phosphorus (TP), considering t_d for two events.....	113
Figure 5.5. Land use factors (\pm std. err. of mean) for (a) Cu, Zn, Cd, (b) Cr, Ni, Pb, (c) Ag, and Hg, considering t_d for two events.	116
Figure 5.6. Land use factors (\pm std. err. of mean) for (a) BOD ₅ , TP, TSP, (b) EC, FC, and TSS, considering t_d for two events.	117
Figure 5.7. Concentrations of Zn, Cu, Cd, Ni, Cr, and Pb vs antecedent dry period, t_d at site 18 (Miller Park stadium parking lot).....	119
Figure 6.1. Hydrographs and hyetographs with sampling times of washoff data for sites SWMI07, SWWB09, SWWA13, and SWMI15 with precipitation gauges WS1202, WS1212, WS1210, and WS1221, respectively. Open symbols indicate data points that are excluded in the calculations.....	130
Figure 6.2. Washoff mass rate plots for Zn at sites SWMI07, SWWB09, and SWWA13. Open symbols indicate that the data were excluded from the calculations.....	131

Figure 6.3. Washoff mass rate plots for <i>E. coli</i> at sites SWMI07, SWWB09, SWWA13, and SWMI15. Open symbols indicate that the data were excluded from the calculations.	132
Figure 6.4. Washoff mass rate plots for TP at sites SWMI07, SWWB09, SWWA13, and SWMI15. Open symbols indicate that the data were excluded from the calculations.	133
Figure 6.5. Washoff mass rate plots for TSS at sites SWMI07, SWWB09, SWWA13, and SWMI15. Open symbols indicate that the data were excluded from the calculations.	134
Figure 6.6. Washoff mass rate plots for fecal coliform at sites SWMI07, SWWB09, SWWA13, and SWMI15. Open symbols indicate that the data were excluded from the calculations.	135
Figure 6.7. Washoff mass rate plots for BOD ₅ at sites SWMI07, SWWB09, and SWWA13. Open symbols indicate that the data were excluded from the calculations.	136
Figure 6.8. Washoff mass rate plots for Hg at sites SWMI07, SWWB09, and SWWA13. Open symbols indicate that the data were excluded from the calculations.	137
Figure 6.9. Washoff mass rate plots for Ag at sites SWMI07, SWWB09, and SWWA13. Open symbols indicate that the data were excluded from the calculations.	138
Figure 6.10. Washoff mass rate plots for Cd at sites SWMI07, SWWB09, and SWWA13. Open symbols indicate that the data were excluded from the calculations.	139
Figure 6.11. Washoff mass rate plots for Cu at sites SWMI07, SWWB09, and SWWA13. Open symbols indicate that the data were excluded from the calculations.	140
Figure 6.12. Washoff mass rate plots for Ni at sites SWMI07, SWWB09, and SWWA13. Open symbols indicate that the data were excluded from the calculations.	141
Figure 6.13. Washoff mass rate plots for Pb at sites SWMI07, SWWB09, and SWWA13. Open symbols indicate that the data were excluded from the calculations.	142

Figure 6.14. Washoff concentration plots for Zn at sites SWMI07, SWWB09, and SWWA13. Open symbols indicate that the data were excluded from the calculations.....	143
Figure 6.15. Washoff concentration plots for <i>E. coli</i> at sites SWMI07, SWWB09, SWWA13, and SWMI15. Open symbols indicate that the data were excluded from the calculations.	144
Figure 6.16. Washoff concentration plots for TP at sites SWMI07, SWWB09, SWWA13, and SWMI15. Open symbols indicate that the data were excluded from the calculations.	145
Figure 6.17. Washoff concentration plots for TSS at sites SWMI07, SWWB09, SWWA13, and SWMI15. Open symbols indicate that the data were excluded from the calculations.	146
Figure 6.18. Washoff concentration plots for fecal coliform at sites SWMI07, SWWB09, SWWA13, and SWMI15. Open symbols indicate that the data were excluded from the calculations.	147
Figure 6.19. Washoff concentration plots for BOD ₅ at sites SWMI07, SWWB09, and SWWA13. Open symbols indicate that the data were excluded from the calculations.....	148
Figure 6.20. Washoff concentration plots for Hg at sites SWMI07, SWWB09, and SWWA13. Open symbols indicate that the data were excluded from the calculations.....	149
Figure 6.21. Washoff concentration plots for Ag at sites SWMI07, SWWB09, and SWWA13. Open symbols indicate that the data were excluded from the calculations.....	150
Figure 6.22. Washoff concentration plots for Cd at sites SWMI07, SWWB09, and SWWA13. Open symbols indicate that the data were excluded from the calculations.....	151
Figure 6.23. Washoff concentration plots for Cu at sites SWMI07, SWWB09, and SWWA13. Open symbols indicate that the data were excluded from the calculations.....	152
Figure 6.24. Washoff concentration plots for Ni at sites SWMI07, SWWB09, and SWWA13. Open symbols indicate that the data were excluded from the calculations.....	153

Figure 6.25. Washoff concentration plots for Pb at sites SWMI07, SWWB09, and SWWA13. Open symbols indicate that the data were excluded from the calculations.....	154
Figure 7.1. Log – linear regressions of PMF estimated normalized source profiles G_{ji} vs. measured source profiles c_{ji} (Table 7.1)	181
Figure 8.1. Downspout disconnection will keep excess water out of the sewer system.	186
Figure 8.2. The rain garden at Calumet Auto Parts, Inc., 8501 West Calumet Road in Milwaukee. (MMSD, 2007c).....	187
Figure 8.3. UWM Great Lakes Water Institute green roof. (MMSD, 2007c).	187
Figure 8.4. Water infiltrates the pervious concrete. (MMSD, 2007c).	188
Figure 8.5. Inlet restrictor locations, Prospect Avenue. The dots indicate the location of the inlets. (MMSD, 2007c).	188
Figure 8.6. Two-acre bioretention system treats stormwater runoff from about 70 acres (28.4 ha) in the Menomonee Valley. (MMSD, 2007c).....	189
Figure 8.7. Bioretention swale and rain garden. (MMSD, 2007c).	189
Figure 8.8. Detention basin with controlled release followed by filter media. Source: Wright Water Engineers, Inc. and GeoSyntec Consultants (2007).....	193
Figure 8.9. Combination of retention pond and media filter. Source: Wright Water Engineers, Inc. and GeoSyntec Consultants (2007).....	193
Figure 8.10. A design chart between the design capture volume or runoff volume and the filter area for a pond based on $h = 0.40$ m and $t_d = 2.17$ days.....	197
Figure 8.11. A design chart between the design capture volume or runoff volume and the filter area for a wet pond based on $h = 0.90$ m and $t_d = 2.19$ days.	198
Figure 8.12. The Stormceptor® under normal operating conditions (frequent rainfall). Source: www.rinkerstormceptor.com	200
Figure 8.13. The Stormceptor® under by-pass operating conditions (infrequent heavy rainfall). Source: www.rinkerstormceptor.com	201

Figure 8.14. The Vortechs system operating under low and high flow conditions. Source: www.contech-cpi.com	202
Figure 8.15. Components of the Downstream Defender® (a) and its system while operating (b). Source: www.hydro-international.biz/	204
Figure 8.16. Example profiles view of a dry detention pond.....	205
Figure A - 1. First flush and later-time concentrations of Ag in stormwater.....	221
Figure A - 2. First flush and later-time concentrations of Alk in stormwater.	222
Figure A - 3. First flush and later-time concentrations of As in stormwater.	223
Figure A - 4. First flush and later-time concentrations of Be in stormwater.	224
Figure A - 5. First flush and later-time concentrations of BOD ₅ in stormwater.....	225
Figure A - 6. First flush and later-time concentrations of Ca in stormwater.	226
Figure A - 7. First flush and later-time concentrations of Cd in stormwater.....	227
Figure A - 8. First flush and later-time concentrations of Cl in stormwater.....	228
Figure A - 9. First flush and later-time concentrations of Cr in stormwater.	229
Figure A - 10. First flush and later-time concentrations of Cu in stormwater.....	230
Figure A - 11. First flush and later-time concentrations of EC in stormwater.	231
Figure A - 12. First flush and later-time concentrations of FC in stormwater.....	232
Figure A - 13. First flush and later-time concentrations of Hard in stormwater.	233
Figure A - 14. First flush and later-time concentrations of Hg in stormwater.....	234
Figure A - 15. First flush and later-time concentrations of Mg in stormwater.....	235
Figure A - 16. First flush and later-time concentrations of NH ₃ in stormwater.	236
Figure A - 17. First flush and later-time concentrations of Ni in stormwater.	237
Figure A - 18. First flush and later-time concentrations of NO ₂ in stormwater.	238
Figure A - 19. First flush and later-time concentrations of NO ₃ in stormwater.	239

Figure A - 20. First flush and later-time concentrations of NO ₅ in stormwater.	240
Figure A - 21. First flush and later-time concentrations of Pb in stormwater.	241
Figure A - 22. First flush and later-time concentrations of Sb in stormwater.	242
Figure A - 23. First flush and later-time concentrations of Se in stormwater.	243
Figure A - 24. First flush and later-time concentrations of TDS in stormwater.	244
Figure A - 25. First flush and later-time concentrations of TKN in stormwater.	245
Figure A - 26. First flush and later-time concentrations of Tl in stormwater.	246
Figure A - 27. First flush and later-time concentrations of TOC in stormwater.	247
Figure A - 28. First flush and later-time concentrations of TP in stormwater.	248
Figure A - 29. First flush and later-time concentrations of TS in stormwater.	249
Figure A - 30. First flush and later-time concentrations of TSP in stormwater.	250
Figure A - 31. First flush and later-time concentrations of TSS in stormwater.	251
Figure A - 32. First flush and later-time concentrations of turbidity in stormwater.	252
Figure A - 33. First flush and later-time concentrations of Zn in stormwater.	253
 Figure B - 1. Box plots of Ag in stormwater per site.	 254
Figure B - 2. Box plots of Alk in stormwater per site.	254
Figure B - 3. Box plots of As in stormwater per site.	255
Figure B - 4. Box plots of Be in stormwater per site.	255
Figure B - 5. Box plots of BOD ₅ in stormwater per site.	256
Figure B - 6. Box plots of Ca in stormwater per site.	256
Figure B - 7. Box plots of Cd in stormwater per site.	257
Figure B - 8. Box plots of Cl in stormwater per site.	257
Figure B - 9. Box plots of Cr in stormwater per site.	258

Figure B - 10. Box plots of Cu in stormwater per site.....	258
Figure B - 11. Box plots of EC in stormwater per site.	259
Figure B - 12. Box plots of FC in stormwater per site.....	259
Figure B - 13. Box plots of Hard in stormwater per site.....	260
Figure B - 14. Box plots of Hg in stormwater per site.....	260
Figure B - 15. Box plots of Mg in stormwater per site.....	261
Figure B - 16. Box plots of NH ₃ in stormwater per site.	261
Figure B - 17. Box plots of Ni in stormwater per site.....	262
Figure B - 18. Box plots of NO ₂ in stormwater per site.	262
Figure B - 19. Box plots of NO ₃ in stormwater per site.	263
Figure B - 20. Box plots of NO ₅ in stormwater per site.	263
Figure B - 21. Box plots of Pb in stormwater per site.	264
Figure B - 22. Box plots of Sb in stormwater per site.	264
Figure B - 23. Box plots of Se in stormwater per site.....	265
Figure B - 24. Box plots of TDS in stormwater per site.	265
Figure B - 25. Box plots of TKN in stormwater per site.	266
Figure B - 26. Box plots of Tl in stormwater per site.....	266
Figure B - 27. Box plots of TOC in stormwater per site.....	267
Figure B - 28. Box plots of TP in stormwater per site.....	267
Figure B - 29. Box plots of TS in stormwater per site.....	268
Figure B - 30. Box plots of TSP in stormwater per site.....	268
Figure B - 31. Box plots of TSS in stormwater per site.....	269
Figure B - 32. Box plots of turbidity in stormwater per site.....	269

Figure B - 33. Box plots of Zn in stormwater per site.	270
Figure C - 1. Box plots of Ag in stormwater per season.....	271
Figure C - 2. Box plots of Alk in stormwater per season.	271
Figure C - 3. Box plots of As in stormwater per season.	272
Figure C - 4. Box plots of Be in stormwater per season.	272
Figure C - 5. Box plots of BOD ₅ in stormwater per season.....	273
Figure C - 6. Box plots of Ca in stormwater per season.	273
Figure C - 7. Box plots of Cd in stormwater per season.....	274
Figure C - 8. Box plots of Cl in stormwater per season.....	274
Figure C - 9. Box plots of Cr in stormwater per season.	275
Figure C - 10. Box plots of Cu in stormwater per season.....	275
Figure C - 11. Box plots of EC in stormwater per season.	276
Figure C - 12. Box plots of FC in stormwater per season.....	276
Figure C - 13. Box plots of Hard in stormwater per season.	277
Figure C - 14. Box plots of Hg in stormwater per season.....	277
Figure C - 15. Box plots of Mg in stormwater per season.....	278
Figure C - 16. Box plots of NH ₃ in stormwater per season.	278
Figure C - 17. Box plots of Ni in stormwater per season.	279
Figure C - 18. Box plots of NO ₂ in stormwater per season.	279
Figure C - 19. Box plots of NO ₃ in stormwater per season.	280
Figure C - 20. Box plots of NO ₅ in stormwater per season.	280
Figure C - 21. Box plots of Pb in stormwater per season.	281
Figure C - 22. Box plots of Sb in stormwater per season.	281

Figure C - 23. Box plots of Se in stormwater per season.	282
Figure C - 24. Box plots of TDS in stormwater per season.	282
Figure C - 25. Box plots of TKN in stormwater per season.	283
Figure C - 26. Box plots of Tl in stormwater per season.	283
Figure C - 27. Box plots of TOC in stormwater per season.	284
Figure C - 28. Box plots of TP in stormwater per season.	284
Figure C - 29. Box plots of TS in stormwater per season.	285
Figure C - 30. Box plots of TSP in stormwater per season.	285
Figure C - 31. Box plots of TSS in stormwater per season.	286
Figure C - 32. Box plots of turbidity in stormwater per season.	286
Figure C - 33. Box plots of Zn in stormwater per season.	287

LIST OF TABLES

Table 1.1. Stormwater study area description.....	11
Table 1.2. List of sample analytical methods.	13
Table 2.1. MMSD's stormwater study sites and rain gauge stations.....	16
Table 2.2. Annual number of events and average rainfall duration, 4 rain gauge stations (WS1203, 1204, 1206, and 1220), 2000-2005.....	20
Table 2.3. Annual average rainfall intensity per event, 4 rain gauge stations (WS1203, 1204, 1206, and 1220), 2000-2005.....	20
Table 2.4. Descriptive statistics of average rainfall data (2000-2006) over 22 rain gauges*.	24
Table 3.1. List of stormwater quality pollutants and their evaluation limits.	29
Table 3.2. Descriptive statistics of various pollutants from CSOs and stormwater.	31
Table 3.3. Combined sewer overflow sampling locations.....	32
Table 3.4. Illustration of seasonal Kendall test.....	37
Table 3.5. Summary of a season indicated the highest average pollutant concentration (2000-2006).....	42
Table 3.6. Seasonal Kendall slope estimations.....	45
Table 4.1. Runoff coefficients for 18 study sites, 2000-2004.....	50
Table 4.2. Summary of new drainage areas, new estimated runoff coefficients, and percent land uses for 18 study sites.....	53
Table 4.3. Runoff coefficients for each type of land use based on the optimization model.....	59
Table 5.1. Effective area and runoff coefficient for each study site.	106
Table 5.2. Multiple correlation coefficients for modeled constituents with and without antecedent dry period, t_d	109

Table 5.3. Comparison of ratios between concentrations of Zn and other metals based on linear expressions in Figure 5.7 with ratios of deposition fluxes (αa) of Zn and other metals at sites 6, 15, 16, and 18.	120
Table 6.1. Summary of α and a values used in eqs 35, 38, and 39.	128
Table 6.2. Summary of c values obtained by plotting eq 35 for metals.	157
Table 6.3. Summary of c values obtained by plotting eq 35 for BOD ₅ , TSS, TP, and bacteria.	158
Table 6.4. Summary of c values obtained by plotting eq 39 for metals.	159
Table 6.5. Summary of c values obtained by plotting eq 39 for BOD ₅ , TSS, TP, and bacteria.	160
Table 7.1. Sanitary sewage, stormwater, and groundwater profiles and CSO measured profile expressed as averages with uncertainties (standard error of the mean) used for CMB modeling (n = number of samples).	171
Table 7.2. Statistical results of the CMB model.	177
Table 7.3. Percent relative contributions of CSO pollutants with uncertainties using CMB model.	178
Table 7.4. Results of coefficient of determination (COD) and Exner function for the Milwaukee's combined sewer overflow data set using PMF with NNLS.	182
Table 7.5. Percent relative contributions of CSO pollutants from Monte Carlo simulation using PMF with NNLS.	183
Table 8.1. A design calculation sheet of a dry pond based on the perfect horizontal plug flow and the overflow velocity.	197
Table 8.2. A design calculation sheet of a wet pond based on the quiescent settling.	198
Table D - 1. Data matrix for PMF modeling.	288

I. INTRODUCTION

Humanity's earliest cities were serviced by sewer systems. The first sewers were built to drain only stormwater runoff and followed the same idea as in Roman times. In the 1840s and 1850s, following the era of industrialization, the cities of London and Paris allowed the discharge of human wastes into stormwater drains because of the increasing urban populations. This was the birth of the combined sewer or the wet-carriage waste disposal system. Existing storm sewers were converted to combined sewers, and new sewers were designed to be combined sewers. This idea was also followed in North America including in Milwaukee, Wisconsin. Subsequently, stormwater runoff flow rates and volumes were significantly increased during wet weather due to increased impervious land cover and the decreased availability of depression storage such as natural ponds and wetlands. In 1994, the Inline Storage System (ISS) in the city of Milwaukee began operating under the Milwaukee Metropolitan Sewerage District (MMSD), which substantially reduced or eliminated combined and sanitary sewer overflows into the rivers and Lake Michigan. A study of water quality of the receiving waters after the ISS indicated significant water quality improvement (Ab Razak and Christensen, 2001). However, these improvements were not sufficient for local waterways to meet the U.S. Environmental Protection Agency (U.S. EPA) Water Quality Criteria for nutrients and bacteria (U.S. Geological Survey, 2004).

The combined sewers are located mostly in the older sections of Milwaukee and Shorewood. They represent about 5% of the MMSD's planning area. The combined sewer system delivers polluted stormwater runoff and sanitary sewage to one of the

MMSD's two wastewater treatment plants, i.e. Jones Island and South Shore. However, during extremely wet condition, combined sewer overflows (CSOs) may occur. These overflows go directly into the rivers and Lake Michigan. Approximate 95% of MMSD's service area contains separate sewers. The separate sewer system consists of two separate sewer pipes: a sanitary sewer and a storm sewer. The sanitary sewer conveys sanitary sewage to one of the MMSD's two wastewater treatment plants for treatment. The storm sewer pipes collect polluted stormwater runoff from land surface and delivers the polluted water directly to a river or lake during rain or melt events. Unfortunately, some amounts of sanitary sewage get into the storm sewer system due to illicit connections. Sanitary sewer overflows can occur after leaky sanitary sewer pipes exceed their capacities during heavy rains due to infiltration and inflow (I/I). This I/I may also cause sewer backup in people's basements.

Stormwater discharges are varied and include visible matter, suspended solids, oxygen-demanding materials, nutrients, pathogenic microorganisms, toxicants such as heavy metals and pesticides, petroleum hydrocarbons, other hazardous contaminants (NSW EPA, 2005). Dry deposition involves the turbulent and gravitational transfer of pollutants from the air to the underlying surface, unaccompanied by atmospheric precipitation (Hicks, 1997). A study of the chemical composition of particulate matter and aerosols over Edmonton, Alberta concluded that industrial emissions and transportation are the major sources of dry deposition from the atmosphere (Klemm and Grey, 1982). A study of U.S. data indicated that the amounts and sources of toxic air pollutants can vary geographically from city to city and from neighborhood to neighborhood and are strongly influenced by types of local sources such as motor

vehicles, wood stoves, combustion of oil and gas, metallurgical industries, chemical production and manufacturing, gasoline marketing, solvent use, and waste oil disposal (Hilborn and Sill, 1990).

Wet deposition is a result of cloud processes that scavenge pollutants from the air at cloud altitudes and deposit them in falling rain, snow, etc. (Hicks, 1997). Studies of pollutant mass loading in precipitation and runoff have concluded that most atmospheric contaminants are washed out during the early stages of rainfall events (Randall et al., 1982). Moreover, the washout of atmospheric pollutants by rainfall droplets is very effective and may contribute to a first-flush effect, indicating that pollutant concentrations in the earlier part of a precipitation event are higher than in the later rainfall (Novotny et al., 1985).

Street refuse accumulation is characterized by locally generated particles of various sizes on street surfaces. The general litter deposits (greater than 3-mm or 1/8-in.) in urban areas include debris, solid wastes, dead animals, animal excreta, etc. The dust and dirt (less than 3-mm or 1/8-in.) include pavement deterioration particles, soil particles, and small organisms. The rate of vegetation input, such as fallen leaves, seeds, and grass clippings increases substantially during the fall season, depending on density of vegetation. A study conducted in Etobicoke, Metropolitan Toronto, showed a significant amount of organic load from autumn leaves in an urban area (James and Boregowda, 1986). The presence of phosphorus in the runoff is commonly attributed to its leaching from vegetation in addition to plant fertilizers. The potential phosphorus content of tree leaves and seeds is found to range from 1.6 to 11 mg/g (Waller and Hart, 1986).

Vehicular traffic constitutes a major source of pollutants in urban area. It contributes to solids (including fine particles) and many chemicals such as heavy metals, polycyclic aromatic hydrocarbons (PAHs), and deicing salts (Thomson et al., 1997). Additionally, pavement conditions also have an effect on pollutant loads. Sartor et al. (1974) reported that streets paved with asphalt could have a higher pollutant loading than streets paved with concrete. A study on the characterization of highway runoff in the Netherlands has indicated that the concentration of pollutants in runoff from impervious asphalt is significantly higher than in runoff from pervious asphalt (Berbee et al., 1999). In snow areas, deicing salts and sand are applied to road surfaces and sidewalks to provide safe driving and walking conditions during winter season. This situation creates increases of chloride content of the runoff.

Pollutant buildup such as deposition, wind erosion, and street cleaning is usually related to land uses of an urban area and to the dry periods between the rainfall events. The quantity of pollutants washed off the impervious area depends on two factors: the amount of pollutant that has accumulated during the dry period preceding a rainfall event and the characteristics of the rainfall, especially rainfall volume and intensity (Huber, 1986). The pollutant buildup on pervious areas is not considered to be significant but the erosion and dissolution mechanisms caused by runoff are considered to contribute significantly to the pollutant washoff (Adams and Papa, 2000). The first-flush concentration is more influenced by antecedent dry period than amount of rainfall (Lee et al., 2004).

Many researchers have proposed stormwater load models based on pollutant buildup and pollutant washoff functions. Sartor et al. (1974) found that the removed

pollutant mass on street surfaces was related to the volume of rainfall during a rainfall event by an exponential model. Alley (1981) developed an exponential washoff model for effective impervious surfaces, and the predicted amount of washoff mass was a direct function of the total volume of storm runoff. Charbeneau and Barrett (1998) predicted the runoff load using event mean concentration for single-land-use catchments. Other runoff models have been widely developed to predict runoff volumes, loads, and concentrations (Brezonik and Stadelmann, 2002; Niehus, 1997). However, none of these models specifically consider the influence of each of several dry periods before a storm event on the estimated load.

Alley and Smith's (1981) model included dry period parameters, but it was studied for only nitrogen, lead, and solids, and for only a single land-use-type drainage area with little pervious area runoff. Only eight periods of runoff were considered. Kim et al. (2005) developed a washoff model for predicting the mass emission rates of highway metals during first-flush runoff. Their model contains four parameters, and none of which appears to have a direct relationship to land use or runoff coefficient. Kim et al. (2005) stated that average daily traffic, antecedent dry period, total rainfall, average rainfall intensity, and runoff coefficient are the main variables that affect total lead mass load. Barrett et al. (1998) reported that a low runoff coefficient resulting from infiltration produces a large reduction in the pollutant load of highway runoff.

One main reason for previous load models' lack of boldness is the absence of an appropriate treatment of antecedent dry conditions, runoff coefficient, and land use in load models for various pollutants. Even though many computer load models are available, e.g., Modeling of Urban Sewers [MOUSE] and Stormwater Management

Model [SWMM], Elliott and Trowsdale (2007), closed-form solution for simulation of multiple sequential dry periods and comprehensive simultaneous parameter estimation for various drainage areas are not included.

The rate of pollutant washoff on effective impervious surfaces was found to be proportional to the remaining pollutant mass (Sartor et al., 1974; Alley, 1981; Alley and Smith, 1981; Grottler, 1987; Akan, 1988; Charbeneau and Barrett, 1998; Osuch-Pajdzinska and Zawilski, 1998). Chen and Adams (2006) proposed a new pollutant load model from which parameters of a washoff rate function can be determined. However, this model was developed based on constant parameters of the buildup function without spatial variation. In most cases, a study catchment does not represent a homogeneous land use (Butcher, 2003).

There are few studies of pollutant washoff rates for residential and open land areas even though these areas are major sources of nutrients and bacteria in stormwater runoff (Bannerman et al., 1993; Soonthornnonda and Christensen, 2007). It is necessary to characterize pollutant removal during different phases of the runoff hydrograph.

As discussed previously, the overflows have been discharged directly into local receiving waters during extremely wet weather conditions. The most common method used to determine the CSO pollutant source during wet weather conditions based on the mass entry-exit totals was explained in Gromaire et al. (2001). This method requires measurements performed at different levels of the same catchment area with given rainfalls, and it can present results with high uncertainties, if it is applied to the large and complicated sewer systems.

Both chemical mass balance (CMB) and positive matrix factorization (PMF) models have been widely used for pollutant source apportionment in air (Cooper and Watson, 1980; Hopke, 1985; Lee et al., 1993; Larsen and Baker, 2003) and aquatic (Bzdusek et al., 2006a; 2006b) environments so that these models should be applicable for studying pollutant sources in drainage systems. Although the CMB modeling was done previously to estimate pollutant source contributions in drainage systems during dry weather flow events (Pitt et al., 1993; Field et al., 1994; Lalor, 1994; Pitt et al., 2004), it had zero degree of freedom, i.e., difference between number of marker compounds and number of sources. Moreover, there is no evidence of any attempts for applying PMF modeling to apportion pollutants in drainage systems.

This study includes characterization, modeling, and management of stormwater runoff quality in the Greater Milwaukee, Wisconsin. Meteorological data analysis in the area will also be performed. The specific objectives of the study are to:

1. Perform statistical analysis of stormwater quality data, i.e., descriptive statistics of 33 pollutants, comparison of stormwater and CSO quality, stormwater pollutant trends, and seasonal variations of stormwater pollutants.
2. Estimate accurate drainage areas based on runoff coefficients using Geographic Information Systems (GIS).
3. Develop a stormwater load model for major 14 pollutants (i.e., zinc, copper, cadmium, nickel, chromium, lead, mercury, Ag, total suspended solids (TSS), *E. coli* (EC), fecal coliform (FC), total soluble phosphorus (TSP), total phosphorus (TP), and 5-day biochemical oxygen demand (BOD₅)) based on multiple

antecedent dry periods and other specific catchment parameters, i.e., land-use factor, deposition coefficient, and effective area used in the pollutant load model.

4. Develop a stormwater pollutant washoff rate model for pollutant mass and concentration during a given runoff event.
5. Estimate pollutant mass and flow fractions of stormwater in the CSOs using Chemical Mass Balance (CMB) with several degrees of freedom and Positive Matrix Factorization (PMF) models.
6. Review appropriate best management practices (BMPs) for stormwater in the area.

This is the first time that a major stormwater quality analysis is performed in the Grater Milwaukee area. The use of GIS to investigate the accuracy of drainage area size was demonstrated. An effort was done to specifically address the influence of each of several dry periods before a storm event on the calculated load in the stormwater load model for mixed land-use drainage areas. The CMB model was applied to apportion pollutant sources of CSOs. Results from the PMF model with least squares non negative rotations were presented and discussed for comparison with the CMB application. After pollutant sources in the CSOs were determined, they would be used to quantify the fraction of pollutant mass and flow fractions of stormwater and sanitary sewage. To the author's knowledge, this is the first application of CMB modeling to apportion pollutant sources in drainage systems during extremely wet weather condition, and also the first application of PMF modeling to apportion pollutant sources in drainage systems.

1.1 Study Areas

The study area can be described as being a part of MMSD's 416 square mile (1077 km²) planning area (Figure 1.1). The MMSD's planning area covers Milwaukee County and parts of Washington, Ozaukee, Waukesha, and Racine Counties. Three major rivers (Milwaukee, Menomonee, and Kinnickinnic Rivers) run through the area and their confluence leads to Milwaukee Harbor and Lake Michigan. On average, the Milwaukee River has the highest flow followed by the Menomonee and the Kinnickinnic Rivers. Lake Michigan provides recreational opportunities and supplies drinking water to approximately 1.3 million people in the Greater Milwaukee area. Only ten percent of the service area drains to the Mississippi River, with the other ninety percent draining to Lake Michigan. The area is heavily urbanized in the center but largely agricultural in the northern and southern parts. Two-thirds of the service area consists of commercial, industrial, and residential areas, including transportation infrastructure and recreational areas (US Geological Survey, 2004). Remaining areas are agricultural, forested, wetlands, and open water.

Stormwater samples were collected between 15 storm sewer locations for the period 2000 - 2006 and 18 storm sewer locations for the period 2000 - 2002 throughout the study area (Table 1.1). These locations represent a variety of land uses (primarily urban in nature) with different sized drainage areas.



Figure 1.1. MMSD's planning area. (Source: MMSD Facilities Information).

Table 1.1. Stormwater study area description.

Site	Community	Location	Land use	Receiving Water
SWMI01	Milwaukee	Lincoln Memorial Dr. AND Carferry Dr.	Institutional, residential, open lands	Lake Michigan
SWMI02	Milwaukee	1700 N. Lincoln Memorial Dr. and Lafayette Hill Rd.	Residential, commercial, recreational, open lands	Lake Michigan
SWFR03	Franklin	54 th and Ashland	Industrial park, open lands	Detention Pond
SWMI04	Milwaukee	3500 S. Lake Dr. and Bay View Park	Institutional, residential, open lands, highway 794, Bay View Park	Lake Michigan
SWMI05	Milwaukee	1200 E. Singer Cir. (inactive in 2003)	Residential, parking lot, open lands	Milwaukee River
SWMI06	Milwaukee	Milwaukee County Zoo	Milwaukee County Zoo, I-94	Underwood Creek
SWMI07	Milwaukee	4345 N. 47 th St.	Residential, recreational	Lincoln Creek
SWMI08	Milwaukee	Hampton and Lincoln Creek Parkway (inactive in 2002)	Residential, commercial	Lincoln Creek
SWWVB09	Whitefish Bay	4939 N. Newhall	Residential, open lands	Lake Michigan
SWGFI10	Greenfield	Boerner Botanical Gardens (formerly 10007 W. Meadow Dr.)	Boerner botanical gardens, parking lot	Detention Pond
SWNB11	New Berlin	13380 Eagle Trace and Timber Ridge	New residential, open lands	Detention Pond
SWMI12	Milwaukee	3275 S. 72 nd St.	Residential, commercial, parking lot	Honey Creek
SWWA13	Wauwatosa	Ridge Blvd. and Harding Blvd.	Residential, open lands	Menomonee River
SWSF14	St. Francis	Lake Dr. and Tesch Ave. (inactive in 2003)	Residential, open lands	Lake Michigan
SWMI15	Milwaukee	42 nd and Mt. Vernon	I-94, flood control area, residential	Menomonee River
SWMI16	Milwaukee	Marquette Interchange	I-94, I-43, highway 794, industrial	Menomonee River
SWWA17	Wauwatosa	71 st AND Chestnut St.	Recreational, open lands, residential, commercial	Menomonee River
SWMI18	Milwaukee	Miller Park East Parking Lot at the Sausage House	Miller Park east parking lot	Menomonee River

1.2 Sample Collection and Analysis

The sampling method used in this study (MMSD, 2003) followed recommendations for stormwater discharge permits by the Wisconsin Department of Natural Resources (WDNR, 2002). The first sample was taken at a specified time triggered by a certain water level in the stormwater sewer. The trigger point level varied from site to site, as a result of adjustments based on baseline flow. A second sample was taken 2 hours later. Sampling was conducted between April and November each year, from 2000 to 2006. The samples are analyzed for 33 constituents by the MMSD (2007a). Table 1.2 shows a list of sample analytical methods. Metals were analyzed based on U.S. Environmental Protection Agency (U.S. EPA) method 6010 (U.S. EPA, 1996), except mercury (U.S. EPA Method 245.1) (U.S. EPA, 1994). Standard Methods (APHA et al., 1998) were used to analyze BOD₅ (5210B), *E. coli* (9223B), fecal coliform (9222D), and TSS (2540D). Unless otherwise specified, total metals concentrations (i.e., both soluble and particulate fractions) are considered.

Table 1.2. List of sample analytical methods.

No.	Pollutant	Analytical Method		Reference
		U.S. EPA	Standard Methods	
1	Silver (Ag)	6010		U.S. EPA (1996)
2	Alkalinity (Alk)	310.2		U.S. EPA (1983a)
3	Arsenic (As)	6010		U.S. EPA (1996)
4	Beryllium (Be)	6010		U.S. EPA (1996)
5	5-day biochemical oxygen demand (BOD ₅)		5210B	APHA et al. (1998)
6	Calcium (Ca)	6010		U.S. EPA (1996)
7	Cadmium (Cd)	6010		U.S. EPA (1996)
8	Chloride (Cl)	325.2		U.S. EPA (1983a)
9	Chromium (Cr)	6010		U.S. EPA (1996)
10	Copper (Cu)	6010		U.S. EPA (1996)
11	<i>E. coli</i> (EC)		9223B	APHA et al. (1998)
12	Fecal coliform (FC)		9222D	APHA et al. (1998)
13	Hardness (Hard)		2340B	APHA et al. (1998)
14	Mercury (Hg)	245.1		U.S. EPA (1994)
15	Magnesium (Mg)	6010		U.S. EPA (1996)
16	Ammonia Nitrogen (NH ₃)	350.1		U.S. EPA (1983a)
17	Nickel (Ni)	6010		U.S. EPA (1996)
18	Nitrite Nitrogen (NO ₂)	353.2		U.S. EPA (1983a)
19	Nitrate Nitrogen (NO ₃)	353.2		U.S. EPA (1983a)
20	Nitrate and Nitrite (NO ₃)	353.2		U.S. EPA (1983a)
21	Lead (Pb)	6010		U.S. EPA (1996)
22	Antimony (Sb)	6010		U.S. EPA (1996)
23	Selenium (Se)	6010		U.S. EPA (1996)
24	Total Dissolved solids (TDS) ^a	-	-	-
25	Total Kjeldahl nitrogen (TKN)	351.2		U.S. EPA (1983a)
26	Thallium (Tl)	6010		U.S. EPA (1996)
27	Total organic carbon (TOC)	415.1		U.S. EPA (1983a)
28	Total Phosphorus (TP)	365.1		U.S. EPA (1983a)
29	Total solids (TS)		2540B	APHA et al. (1998)
30	Total soluble phosphorus (TSP)	365.1		U.S. EPA (1983a)
31	Total suspended solids (TSS)		2540D	APHA et al. (1998)
32	Turbidity (Turb)		2130	APHA et al. (1998)
33	Zinc (Zn)	6010		U.S. EPA (1996)

^a calculated value from TSS and TS.

1.3 Measurement of Runoff Flows and Volumes

An area velocity sensor (Isco model no. 2150, Teledyne Isco, Inc., Lincoln, Nebraska) was used to measure runoff levels and velocities at study sites. The runoff flows, calculated by the area velocity module (Figure 1.2) based on measured runoff levels and velocities, were obtained during the period 2000 to 2006. The event runoff volume was derived by integrating of a runoff hydrograph through storm event duration.

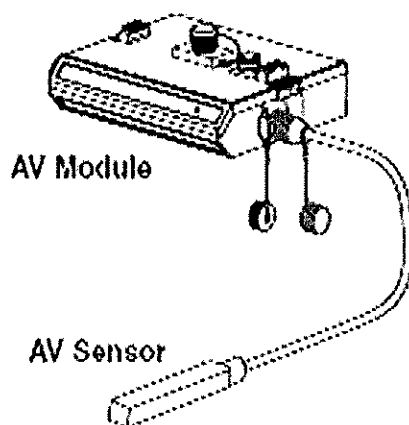


Figure 1.2. Area velocity (AV) sensor and area velocity (AV) module (Source: www.isco.com/).

II. METEOROLOGICAL DATA ANALYSIS

The rainfall data from 2000 to 2005 for 4 rain gauge stations (WS1203 at 245 W. Lincoln Ave., City of Milwaukee Police Station; WS1204 at 300 S. 84th St., City of Milwaukee Fire Station; WS1206 at 3626 W. Fond du Lac Ave., City of Milwaukee Police Station; WS1220 at 5635 S. New Berlin Rd., Hales Corners Village Hall) were analyzed previously by Soonthornnonda et al. (2006). These four rain gauge stations (Table 2.1 and Figure 2.1) are at typical locations throughout the study areas. The annual number of rainfall events, average rainfall duration, and average rainfall intensity were computed based on the visual observation from graphs and tables.

The statistical analysis of averaged rainfall records (2000-2006) over 22 rain gauge stations (Figure 1.1) using an Interevent Time Definition (IETD) as a criterion to isolate single storm events from the continuous record are also demonstrated in this chapter. Rainfall characteristics, e.g., total depth, duration, average intensity, and interevent time, were developed to represent these meteorological data.

Table 2.1. MMSD's stormwater study sites and rain gauge stations.

SITE ID	LOCATION	Rain gauge assignments
SWMI01	LINCOLN MEMORIAL DR. AND CARFERRY DR. (Stormwater discharge to Lake Michigan)	WS1203
SWMI02	1700 N. LINCOLN MEMORIAL DR. @ LAFAYETTE HILL RD. (Stormwater to Lake @ McKinley Marina)	WS1212
SWFR03	54TH AND ASHLAND (Stormwater to Franklin Park to detention pond)	WS1201
SWMI04	3500 S. LAKE DR. @ BAY VIEW PARK (Stormwater to Lake across from St. Francis Seminary)	WS1203
SWMI05	1200 E. SINGER CIR. (Stormwater to Milw. River @ Kern Park) INACTIVE IN 2003	WS1212
SWMI06	MILW CNTY. ZOO (Stormwater to Underwood Creek across from Moose Encl.)	WS1204
SWMI07	4345 N. 47TH ST. (Stormwater to Lincoln Creek)	WS1202
SWMI08	HAMPTON AND LINCOLN CR. PARKWAY (Stormwater to Lincoln Creek under bridge) INACTIVE SINCE 2002	WS1207
SWWB09	4939 N. NEWHALL (Stormwater to Lake @ Big Bay Park)	WS1212
SWGFI0	BOERNER BOTANICAL GARDENS FORMERLY 10007 W. MEADOW DR. (Stormwater to Root River)	WS1220
SWNB11	13380 EAGLE TRACE AND TIMBER RIDGE (Stormwater to wetland residential site)	WS1220
SWMI12	3275 S. 72ND ST. (Stormwater to Honey Creek)	WS1216
SWWA13	RIDGE BLVD. AND HARDING BLVD. (Stormwater to Menomonee River Parkway)	WS1210
SWSF14	LAKE DR. AND TESCH AVE. (Stormwater to Lake Michigan) INACTIVE IN 2003	WS1203
SWMI15	42ND AND MT. VERNON (I-94 x-way Stormwater to Menomonee River)	WS1221
SWMI16	MARQUETTE INTERCHANGE	WS1221
SWWA17	71ST AND CHESTNUT ST. (Stormwater to Menomonee River)	WS1204
SWMI18	MILLER PARK EAST PARKING LOT AT THE SAUSAGE HOUSE (Stormwater to Menomonee River)	WS1221

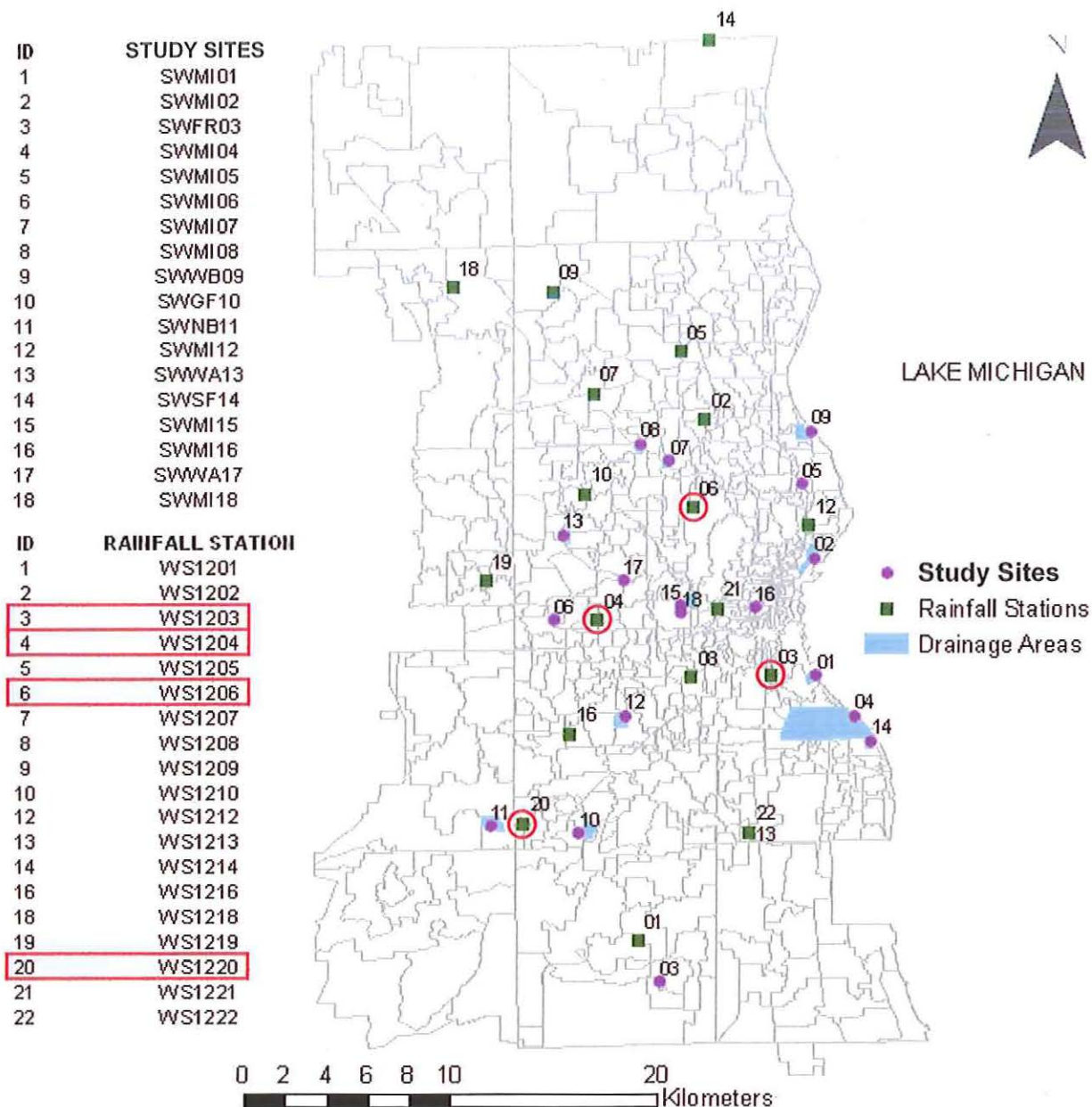


Figure 2.1. Locations of stormwater study sites and rain gauge stations in the MMSD's planning area. Rain gauge stations, highlighted by , were used to evaluate rainfall statistics.

Rainfall data (2000-2005) of 4 rain gauge stations (WS1203, 1204, 1206, and 1220) were selected for comprehensive analysis (Soonthornnonda et. al., 2006). Results indicated that storms of a short duration occur more frequently than storms of a long duration (Figure 2.2). Figure 2.2 shows the near exponential curve of rainfall duration (hr) as x-axis and average number of rainfall events as y-axis. Annual average rainfall durations for all 4 stations (Table 2.2) were computed and ranged from 2.50 (WS1206, 2004) to 19.4 hrs (WS1203, 2004). Annual average rainfall intensities (Table 2.3) ranged from 0.62 to 2.15 mm/hr. Average rainfall intensity (mm/hr) is decreasing versus rainfall duration (hr) (Figure 2.3).

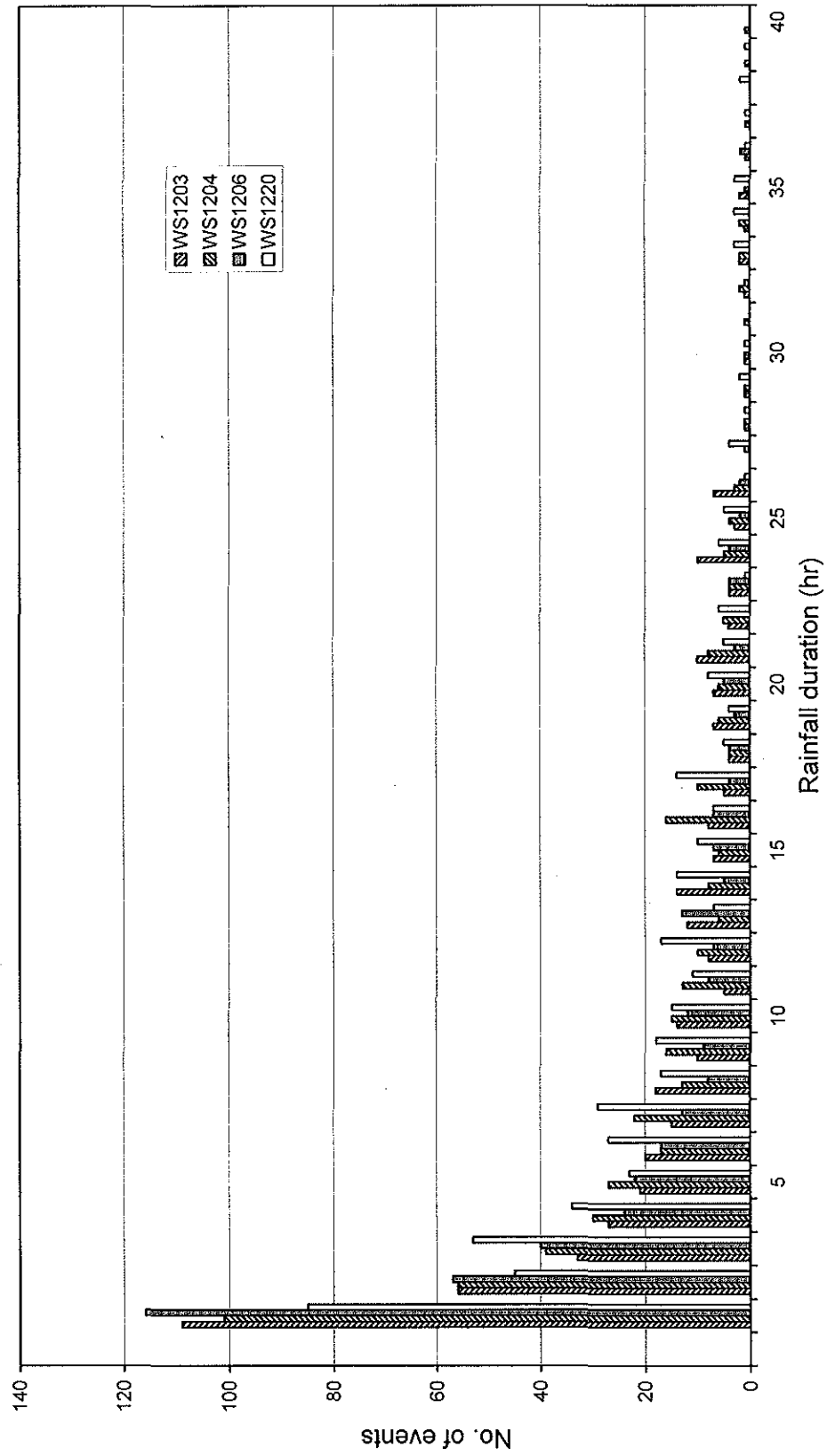


Figure 2.2. Number of events for each rainfall duration, 4 rain gauge stations (WS1203, 1204, 1206, and 1220), 2000-2005.

Table 2.2. Annual number of events and average rainfall duration, 4 rain gauge stations (WS1203, 1204, 1206, and 1220), 2000-2005.

year	WS1203 245 W. Lincoln Ave.		WS1204 300 S. 84 th St.		WS1206 3626 W. Fond du Lac Ave.		WS1220 5635 S. New Berlin Rd.	
	No. of events	Avg rainfall duration (hr)	No. of events	Avg rainfall duration (hr)	No. of events	Avg rainfall duration (hr)	No. of events	Avg rainfall duration (hr)
2000	108	8.46	101	9.01	107	7.0	81	9.77
2001	80	7.62	96	6.69	102	7.3	91	7.53
2002	100	6.19	93	6.23	94	7.0	81	7.37
2003	72	15.3	79	10.0	97	4.2	66	11.7
2004	38	19.4	40	18.8	2	2.5	89	9.72
2005	65	7.77	62	7.45	1	7.0	86	7.53
AVG	77	9.69	79	8.78	67	6.4	82	8.82

Table 2.3. Annual average rainfall intensity per event, 4 rain gauge stations (WS1203, 1204, 1206, and 1220), 2000-2005.

year	Avg rainfall intensity per event (mm/hr)			
	WS1203 245 W. Lincoln Ave.	WS1204 300 S. 84 th St.	WS1206 3626 W. Fond du Lac Ave.	WS1220 5635 S. New Berlin Rd.
2000	1.114	1.364	1.298	1.246
2001	1.722	2.145	1.506	1.804
2002	1.214	1.580	1.241	1.473
2003	0.620	0.829	1.486	0.895
2004	0.936	0.733	0.635	1.501
2005	1.306	1.565	1.016	1.323
AVG	1.176	1.449	1.379	1.398

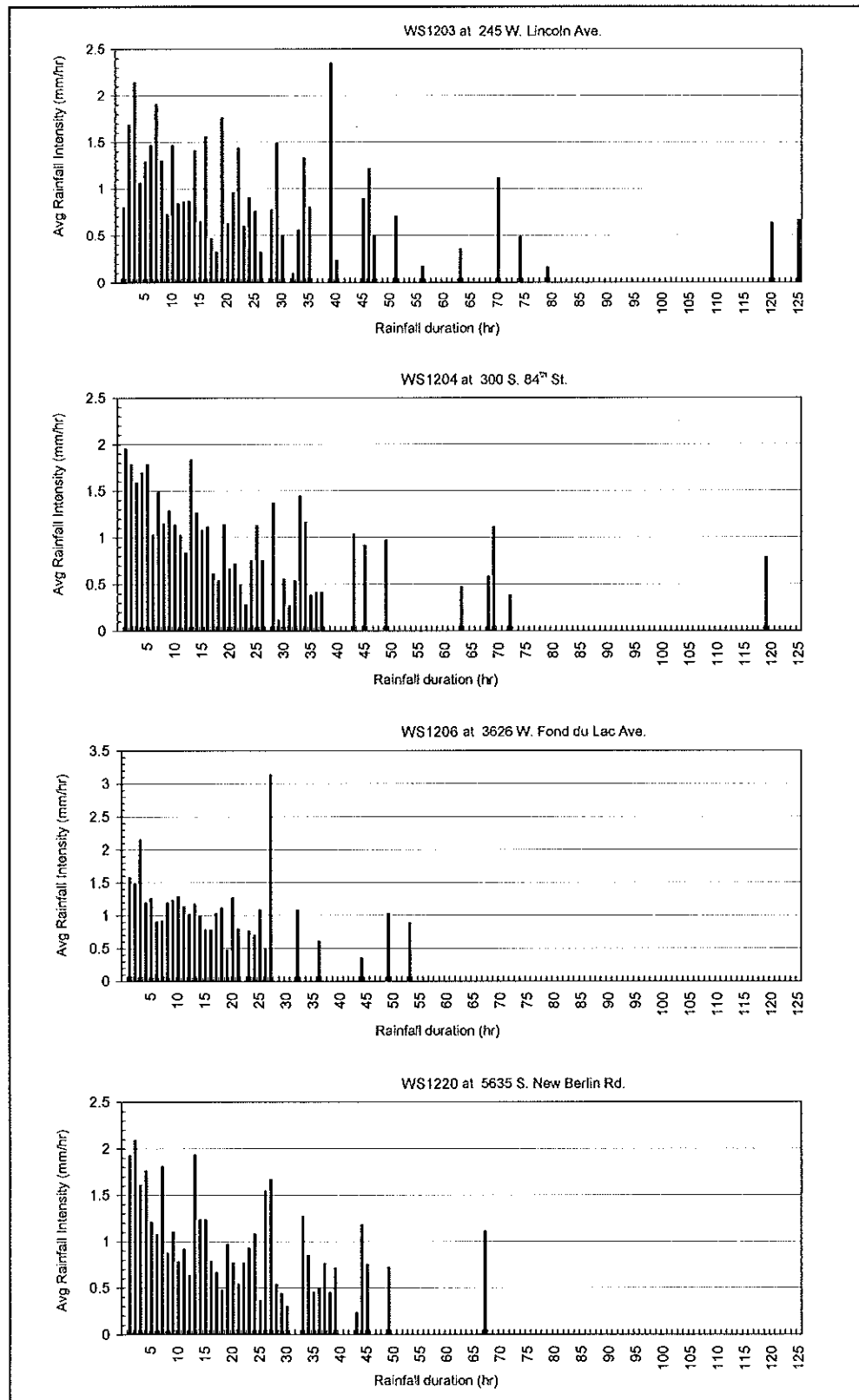


Figure 2.3. Average rainfall intensity for each rainfall duration at 4 rain gauge stations (WS1203, 1204, 1206, and 1220), 2000-2005.

2.1 Interevent Time Definition (IETD)

A rainfall record contains of a series of rainfall pulses through time. A minimum interevent time between consecutive pulses of rainfall (i.e., the interevent time definition, IETD) can be used to isolate an individual storm event from the continuous rainfall record (Adams and Papa, 2000). The IETD can be developed through an autocorrelation analysis due to correlation between observed data with temporal proximity. The autocorrelation coefficient indicates the correlation of data at one point in time with that data at earlier point in time. The autocorrelation coefficient r_k for a lag time k is computed as

$$r_k = \frac{\sum_{i=1}^{N-k} (Y_i - \bar{Y})(Y_{i+k} - \bar{Y})}{\sum_{i=1}^N (Y_i - \bar{Y})^2} \quad (1)$$

where Y_i is the sample of observations at time i , and \bar{Y} is the sample mean of N samples.

The autocorrelogram is a plot of autocorrelation coefficient r_k with respect to the lag time k . Figure 2.4 illustrates the autocorrelogram of averaged rainfall data (2000-2006) over 22 rain gauge stations located throughout the study area. The IETD is defined as the lag time which is sufficient to isolate independent rainfall events statistically within a specified level of significance, meaning that the autocorrelation function sufficiently approaches zero. The autocorrelogram, as shown in Figure 2.4, indicated that the IETD approximately equals 12 hrs for these rainfall data.

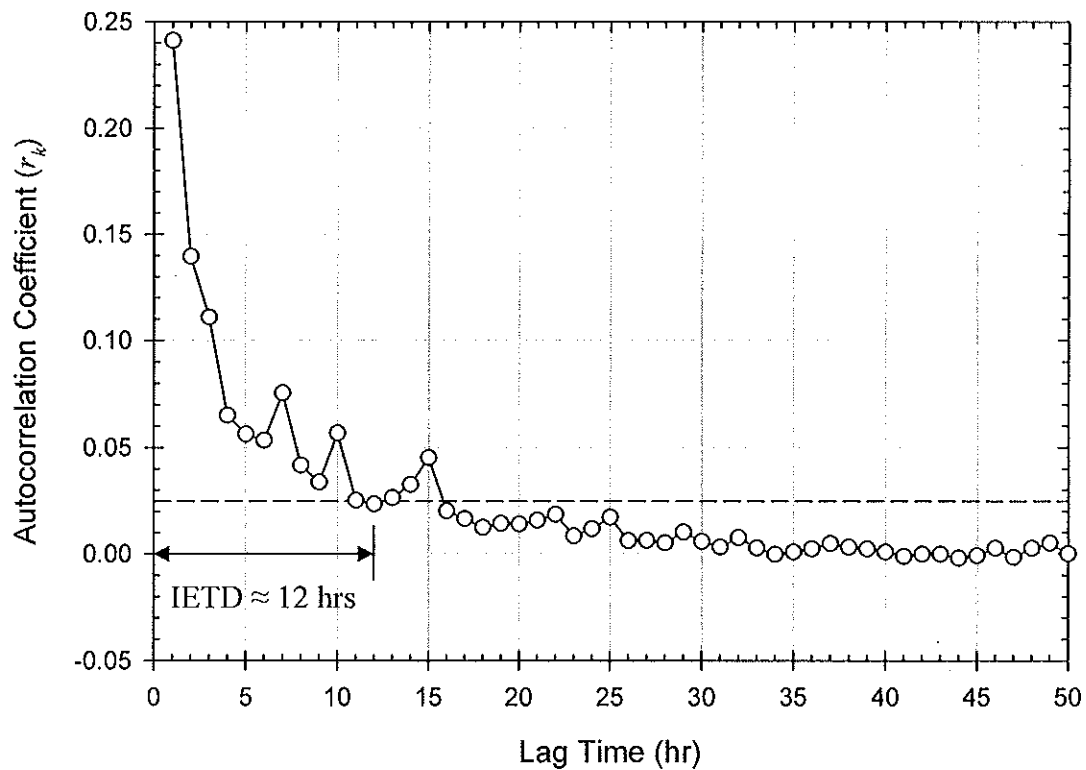


Figure 2.4. Autocorrelogram (with 5 % significance upper limit) for determining IETD based on averaged rainfall data (2000-2006) over 22 rain gauge stations in the study area.

2.2 Statistics of Rainfall Data by IETD Technique

Based on the IETD technique from preceding discussion, descriptive statistics of rainfall characteristics, e.g., duration and intensity, derived from averaged rainfall data (2000-2006) over 22 rain gauge stations in the study area were computed using the EPA's Storm Water Management Model (SWMM), version 5.0 (SWMM5, www.epa.gov/ednnrmrl/models/swmm/index.htm) as shown in Table 2.4. A total 760 rain events were found within a period of seven years. Average rainfall intensity of 1.27 mm/hr, total depth of 10.2 mm., and duration of 13.7 hrs were also obtained. The interevent time, defined as a period without rainfall, can be equivalent to an average dry

period before storm event (i.e., antecedent dry period). The average interevent time of 55.5 hrs were found from these rainfall data.

Results obtained using IETD technique exhibit similar tendency with results from Soonthornnonda et. al. (2006). Figure 2.5 shows the near exponential curve of rainfall duration (hr) as x-axis and number of rainfall events as y-axis, indicating that a short duration occur more frequently than storms of a long duration. Average rainfall intensity (mm/hr) tends to decrease with continuous increasing rainfall duration up to 49 hrs (Figure 2.6). A correlation between average interevent time and rainfall duration was not evident (Figure 2.7).

Table 2.4. Descriptive statistics of average rainfall data (2000-2006) over 22 rain gauges*.

	Rainfall intensity (mm/hr)	Rainfall duration (hr)	Total rainfall depth (mm)	Interevent time (hr)
Minimum Value	0.0508	1.00	0.254	12.0
Maximum Value	133	102	172	377
Mean Value	1.27	13.7	10.2	55.5
Std. Deviation	5.23	15.7	17.3	51.2

* 760 events.

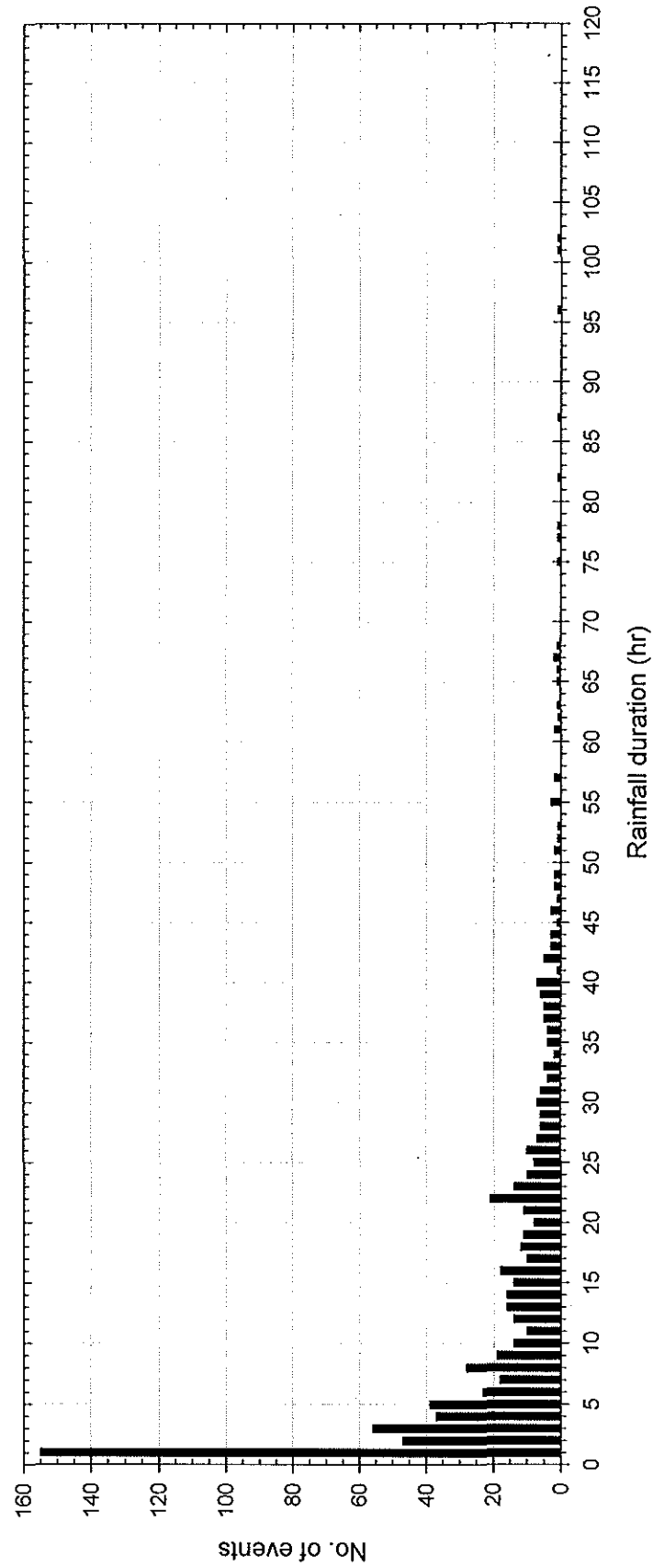


Figure 2.5. Number of events for each rainfall duration from average rainfall data (2000-2006) over 22 rain gauge stations.

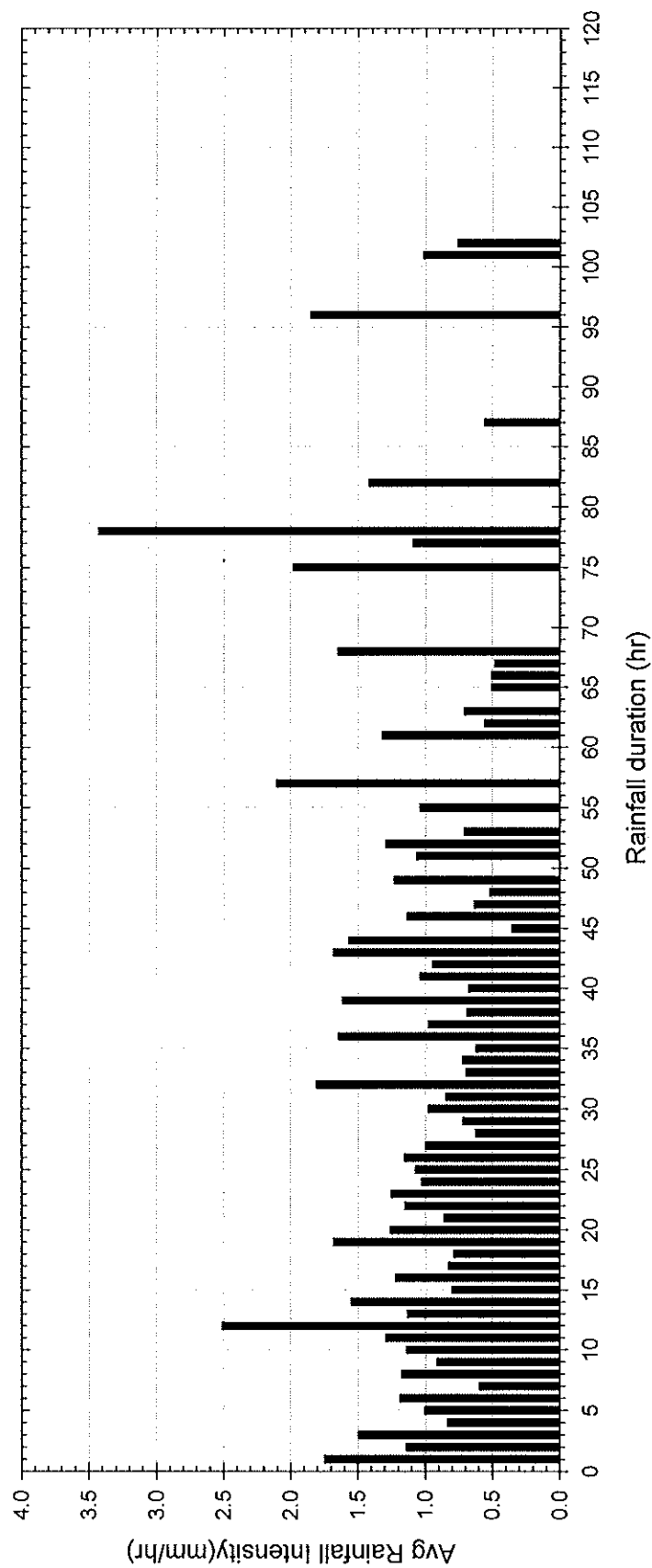


Figure 2.6. Average rainfall intensity for each rainfall duration from averaged rainfall data (2000-2006) over 22 rain gauge stations.

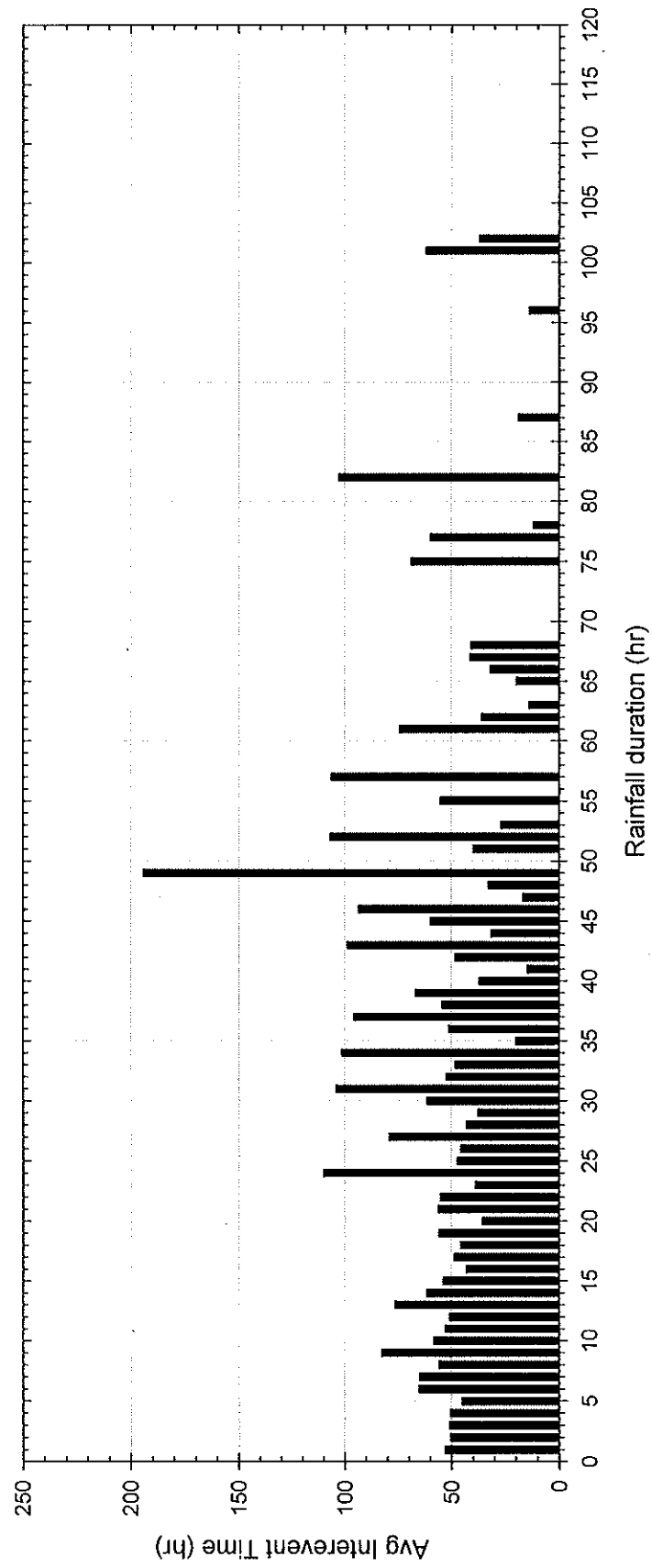


Figure 2.7. Average intervent time for each rainfall duration from average rainfall data (2000-2006) over 22 rain gauge stations.

III. CHARACTERIZATION OF STORMWATER QUALITY

The water quality of receiving waters for a drainage system depends on the quality of combined sewer overflows (CSOs) and stormwater that directly discharge into receiving waters. Different types of runoff pollutants from CSOs and stormwater discharges have different types of impacts on local receiving waters at different seasons. To achieve the better performance of drainage systems, an understanding of characteristics of runoff quality pollutants, pollutant trends, and pollutant seasonal variations is necessary.

3.1 Stormwater Quality Pollutants

There are 33 water quality pollutants (MMSD, 2003; WDNR, NR216, 2002) that are evaluated in this study. Table 3.1 shows the list of pollutants with their limits. It should be noted that these limits are used as guidelines and not required limits.

Table 3.1. List of stormwater quality pollutants and their evaluation limits.

	Pollutant	Limit	Unit of Measure	Limit Reference and Source
1	Silver (Ag)	0.0318	mg/L	NPDES (U.S. EPA, 2000)
2	Alkalinity (Alk)	400	mg/L	National Water Quality Criteria (US EPA, 2004)
3	Arsenic (As)	0.16854	mg/L	NPDES (U.S. EPA, 2000)
4	Beryllium (Be)	0.130	mg/L	NPDES (U.S. EPA, 2000)
5	5-day biochemical oxygen demand (BOD ₅)	30.0	mg/L	WPDES (WDNR, 2003)
6	Calcium (Ca)	- NA -	mg/L	- NA -
7	Cadmium (Cd)	0.0159	mg/L	NPDES (U.S. EPA, 2000)
8	Chloride (Cl)	860	mg/L	NPDES (U.S. EPA, 2000)
9	Chromium (Cr)	0.0160	mg/L	National Water Quality Criteria (US EPA, 2004)
10	Copper (Cu)	0.0636	mg/L	NPDES (U.S. EPA, 2000)
11	<i>E. coli</i> (EC)	126	CFU/100 mL	EPA Gold Book (U.S. EPA, 1986)
12	Fecal coliform (FC)	400	CFU/100 mL	WPDES (WDNR, 2003)
13	Hardness (Hard)	120	mg/L	EPA Gold Book (U.S. EPA, 1986)
14	Mercury (Hg)	2.40	µg/L	NPDES (U.S. EPA, 2000)
15	Magnesium (Mg)	- NA -	mg/L	- NA -
16	Ammonia nitrogen (NH ₃)	19.0	mg/L	NPDES (U.S. EPA, 2000)
17	Nickel (Ni)	1.417	mg/L	NPDES (U.S. EPA, 2000)
18	Nitrite nitrogen (NO ₂)	1.00	mg/L	EPA Gold Book (US EPA, 1986)
19	Nitrate nitrogen (NO ₃)	10.0	mg/L	National Water Quality Criteria (US EPA, 2004)
20	Nitrate and nitrite (NO ₃)	0.680	mg/L	NPDES (U.S. EPA, 2000)
21	Lead (Pb)	0.0816	mg/L	NPDES (U.S. EPA, 2000)
22	Antimony (Sb)	0.636	mg/L	NPDES (U.S. EPA, 2000)
23	Selenium (Se)	0.2385	mg/L	NPDES (U.S. EPA, 2000)
24	Total dissolved solids (TDS)	250	mg/L	EPA Gold Book (U.S. EPA, 1986)
25	Total Kjeldahl nitrogen (TKN)	1.50	mg/L	NPDES (U.S. EPA, 1999)
26	Thallium (Tl)	0.0480	mg/L	EPA Gold Book (U.S. EPA, 1986)
27	Total organic carbon (TOC)	50.0	mg/L	NPDES (U.S. EPA, 1999)
28	Total phosphorus (TP)	1.00	mg/L	WPDES (WDNR, 2003)
29	Total solids (TS)	- NA -	mg/L	- NA -
30	Total soluble phosphorus (TSP)	0.0500	mg/L	EPA Gold Book (U.S. EPA, 1986)
31	Total suspended solids (TSS)	30.0	mg/L	WPDES (WDNR, 2003)
32	Turbidity	5.00	NTU	NPDES (U.S. EPA, 1999)
33	Zinc (Zn)	0.117	mg/L	NPDES (U.S. EPA, 2000)

- NA - : Limits not available

3.2 Stormwater Quality Data Analysis

The purpose of this section is to present the statistical analysis of stormwater quality data (2000-2006). Emphasis will be placed on determining descriptive statistics such as means, medians, and standard errors of the mean and evaluating the quality of stormwater and CSOs. Moreover, trends and seasonal variations of pollutants were also examined.

3.2.1 Descriptive Statistics

The runoff data sets (2000-2006) for 33 pollutants from 18 drainage areas were analyzed. Descriptive statistics consisting of means, median, standard errors of the mean, and geometric means were computed on the pollutants for all drainage areas. A summary of runoff quality pollutants from stormwater is illustrated in Table 3.2.

Various plots of stormwater data (2000-2006) in Appendix A show concentrations of 33 water quality pollutants (first flush and later time concentrations) along with their limits. Box plots of concentrations of 33 water quality pollutants in stormwater (2000-2006) by sampling locations are presented in Appendix B.

Table 3.2. Descriptive statistics of various pollutants from CSOs and stormwater.

No.	Pollutant	Stormwater				CSOs					
		N	Mean	Std Err	Median	Geomean	N	Mean	Std Err	Median	Geomean
1	Ag mg/L	1295	0.000807	0.0000347	0.000275	0.000341	189	0.00219	0.00148	0.00018	0.000367
2	Alk mg/L	651	48.7	5.61	28	27.4					
3	As mg/L	1288	0.00373	0.000194	0.00180	0.00201	190	0.00645	0.00160	0.00115	0.00188
4	Be mg/L	609	0.000982	0.0000943	0.000500	0.000487					
5	BOD ₅ mg/L	1266	22.5	0.846	12.0	12.2	190	24.2	6.35	13.0	13.3
6	Ca mg/L	1296	38.0	1.69	25.0	26.4	136	27.0	1.94	19.0	21.3
7	Cd mg/L	1296	0.000894	0.0000361	0.000500	0.000422	189	0.00240	0.00148	0.000690	0.000611
8	Cl mg/L	854	88.8	9.49	25.0	24.8					
9	Cr mg/L	1296	0.0128	0.00101	0.00630	0.00645	190	0.0153	0.00210	0.00515	0.00822
10	Cu mg/L	1295	0.0442	0.00273	0.0220	0.0241	190	0.0268	0.00230	0.0190	0.0205
11	EC CFU/100 mL	1398	51000	2200	7600	6500	53	136000	16000	100000	95000
12	FC CFU/100 mL	1424	130000	10000	15000	9500	59	730000	410000	160000	180000
13	Hard mg/L	1297	152	7.03	99.0	102	136	105	7.96	71.0	81.4
14	Hg µg/L	1232	0.0454	0.00373	0.0310	0.0290	135	0.0611	0.00729	0.0450	0.0460
15	Mg mg/L	1296	14.0	0.714	8.40	8.49	136	10.1	0.816	6.50	7.54
16	NH ₃ mg/L	1380	0.600	0.0302	0.390	0.270	54	0.831	0.0585	0.810	0.688
17	Ni mg/L	1296	0.00769	0.000352	0.00360	0.00524	190	0.00994	0.00152	0.00700	0.00708
18	NO ₂ mg/L	1319	0.0957	0.00390	0.0580	0.0621					
19	NO ₃ mg/L	1320	1.09	0.0462	0.760	0.626					
20	NO ₅ mg/L	573	1.28	0.100	0.800	0.723					
21	Pb mg/L	1288	0.0305	0.00260	0.0140	0.0115	190	0.0431	0.00386	0.0300	0.0269
22	Sb mg/L	608	0.0173	0.00103	0.0100	0.00837					
23	Se mg/L	1288	0.00684	0.000321	0.00240	0.00272	189	0.00552	0.00149	0.00130	0.00201
24	TDS mg/L	624	333	35.8	160	152					
25	TKN mg/L	1406	3.20	0.0947	2.20	2.26					
26	Tl mg/L	608	0.00496	0.000282	0.00235	0.00287					
27	TOC mg/L	1134	25.2	0.917	15.0	16.6					
28	TP mg/L	1403	0.885	0.0841	0.550	0.569	189	0.815	0.0575	0.58	0.669
29	TS mg/L	1216	493	24.9	300	309					
30	TSP mg/L	660	0.475	0.0223	0.310	0.334					
31	TSS mg/L	1420	194	22.2	64.0	63.4	188	86.8	7.08	60.0	55.8
32	Turbidity NTU	174	144	39.5	34.8	38.4					
33	Zn mg/L	1296	0.185	0.0133	0.0900	0.101	190	0.103	0.00516	0.0870	0.0901

Note: N = number of samples; Std Err = Standard error of the mean.

Note: N = number of samples; Std Err = Standard error of the mean.

3.2.2 Comparison of Stormwater and Combined Sewer Overflows (CSOs)

The CSO samples were collected at 20 locations (Table 3.3) when overflow events occurred during the period 2000 through 2006. Table 3.2 shows a comparison of descriptive statistics of various pollutants between CSOs and stormwater.

Table 3.3. Combined sewer overflow sampling locations.

Site Code	Description	Receiving water
IssCT02	Hawley Road	Menomonee River
IssCT07	N. 16 th St. & W. Canal St.	Menomonee River
IssCT08	S. 3 rd St. & W. Seeboth	Menomonee River
IssCT034	N. 44 th St. & W. Well St.	Menomonee River
IssCT056	N. 25 th & Menomonee River	Menomonee River
IssKK01	S. 6 th St. & W. Cleveland Av.	Kinnickinnic River
IssKK02	S. 1 st & Chase Av.	Kinnickinnic River
IssKK03	S. 4 th St. & W. Becher St.	Kinnickinnic River
IssKK04	S. 1 st St. & W. Lincoln Av.	Kinnickinnic River
IssLMN	LMN E. Bay St. & Ward St.	Lake Michigan
IssLMS	LMS Lincoln memorial Dr. & Russell Av.	Lake Michigan
IssNS04	N. Cambridge & E. Providence	Milwaukee River
IssNS05	E. Burleigh & Milwaukee River	Milwaukee River
IssNS06	Park Place & Milwaukee River	Milwaukee River
IssNS07	Commerce & Booth	Milwaukee River
IssNS08	Commerce & Walnut	Milwaukee River
IssNS09	N. 3rd & Park Freeway East	Milwaukee River
IssNS010	N. Water & St. Paul	Milwaukee River
IssNS011	N. Humboldt & Capitol	Milwaukee River
IssNS012	N. 31st & Capitol	Milwaukee River

There are 19 water quality pollutants to be evaluated in CSO data as follows:

1. Ammonia nitrogen (NH₃)
2. Arsenic (As)
3. 5-day biochemical oxygen demand (BOD₅)
4. Cadmium (Cd),
5. Calcium (Ca)
6. Chromium (Cr)
7. Copper (Cu)

8. *E. coli* (EC)
9. Fecal coliform (FC)
10. Hardness (Hard)
11. Lead (Pb)
12. Magnesium (Mg)
13. Mercury (Hg)
14. Nickel (Ni)
15. Selenium (Se)
16. Silver (Ag)
17. Total phosphorus (TP)
18. Total suspended solids (TSS)
19. Zinc (Zn)

3.2.3 Pollutant Trends

There are variables (e.g. temperature, precipitation, vegetative cover, or lack of cover, use of fertilizers, salting, etc.) or pollutants for which changes between seasons of the year are a major source of variation in many pollutants. A seasonal trend analysis was used to consider these effects, in order to represent the true trends. The seasonal Kendall test was used in this study. For example, spring data of one year should be compared to spring data (not summer or fall data) of another year.

The seasonal Kendall test (Gilbert, 1987) consists of calculating of the Mann-Kendall test statistic, S and its variance, $\text{VAR}(S)$, separately for each season with data collected over years. These seasonal statistics are then combined, and the Z statistic is

computed. The Z value may be referred to the standard normal distribution to test for a statistically significant trend.

Let x_{il} be the datum for the i th season for l th year, x_{ik} be the datum for the i th season for k th season, K the number of seasons, and L the number of years.

For each season the data collected over years (5 years) are used to compute the Mann-Kendall statistic, S . Let S_i be this statistic computed for season i , then

$$S_i = \sum_{k=1}^{n_i-1} \sum_{l=k+1}^{n_i} \text{sgn}(x_{il} - x_{ik}) \quad (2)$$

where $l > k$, n_i is the number of data (over years) for season i , and

$$\begin{aligned} \text{sgn}(x_{il} - x_{ik}) &= 1 & \text{if } x_{il} - x_{ik} > 0 \\ \text{sgn}(x_{il} - x_{ik}) &= 0 & \text{if } x_{il} - x_{ik} = 0 \\ \text{sgn}(x_{il} - x_{ik}) &= -1 & \text{if } x_{il} - x_{ik} < 0 \end{aligned} \quad (3)$$

$\text{VAR}(S_i)$ can be computed as:

$$\begin{aligned} \text{VAR}(S_i) &= \frac{1}{18} \left[n_i(n_i - 1)(2n_i + 5) - \sum_{p=1}^{g_i} t_{ip}(t_{ip} - 1)(2t_{ip} + 5) - \sum_{q=1}^{h_i} u_{iq}(u_{iq} - 1)(2u_{iq} + 5) \right] \\ &+ \frac{\sum_{p=1}^{g_i} t_{ip}(t_{ip} - 1)(t_{ip} - 2) \sum_{q=1}^{h_i} u_{iq}(u_{iq} - 1)(u_{iq} - 2)}{9n_i(n_i - 1)(n_i - 2)} + \frac{\sum_{p=1}^{g_i} t_{ip}(t_{ip} - 1) \sum_{q=1}^{h_i} u_{iq}(u_{iq} - 1)}{2n_i(n_i - 1)} \end{aligned} \quad (4)$$

where g_i is the number of groups of tied data in season i , t_{ip} is the number of tied data in the p th group for season i , h_i is the number of sampling times in season i that contain multiple data, and u_{iq} is the number of multiple data in q th time period in season i .

After getting S_i and $\text{VAR}(S_i)$,

$$S' = \sum_{i=1}^K S_i \quad (5)$$

$$\text{VAR}(S') = \sum_{i=1}^K \text{VAR}(S_i) \quad (6)$$

Next,

$$\begin{aligned} Z &= \frac{(S' - 1)}{[\text{VAR}(S')]^{1/2}} & \text{if } S' > 0 \\ Z &= 0 & \text{if } S' = 0 \\ Z &= \frac{(S' + 1)}{[\text{VAR}(S')]^{1/2}} & \text{if } S' < 0 \end{aligned} \quad (7)$$

To test the null hypothesis, H_o , of no trend versus the alternative hypothesis, H_A , of either an upward or downward trend;

Two tailed test: reject H_o , no trend if absolute value of Z is greater than $Z_{1-\alpha/2}$ (Standard normal distribution table).

One tailed test: reject H_o , no trend in favor of an upward trend if value of Z is greater than $Z_{1-\alpha}$ and reject H_o , no trend in favor of a downward trend if value of Z is negative and absolute value of Z is greater than $Z_{1-\alpha}$.

To compute seasonal kendall slope:

$$Q_i = \frac{x_{il} - x_{ik}}{l - k} \quad (8)$$

where x_{il} is the datum for i th season of l th year, and x_{ik} is the datum for the i th season of k th year, where $l > k$. Rank the $N'_1 + N'_2 + N'_3 + \dots + N'_k = N'$ individual slope estimates and find their median. This median is the seasonal Kendall slope estimator.

To compute the upper limit and lower limit values of the seasonal Kendall slope:

1) choose the desired confidence level, α and find $Z_{1-\alpha}$

2) compute $C_\alpha = Z_{1-\alpha/2} [\text{VAR}(S')]^{1/2}$

- 3) compute $M_1 = (N' - C_\alpha)/2$ and $M_2 = (N' + C_\alpha)/2$
- 4) the lower and upper confidence limits are the M_1 th largest and the (M_2+1) th largest of ranked N'

Table 3.4 shows an example of all computations in seasonal Kendall test. The seasonal Kendall test is described in detail in Gilbert (1987).

Table 3.4. Illustration of seasonal Kendall test

Year	Season 1					Season 2				
	1	2	3	1	2	3	1	2	3	20
Data	8	10	15	15	20	20	15	18	20	
	-	+4	+3.5	2	0	+2.5	3	+3	+2.5	0
		+2	+2.5	2	0	0	0	-	0	0
			+3	1	0	+2	1		+2	0
			$S_1 =$	5	0	$S_2 =$	4	+	0	= 4

Ranking of seasonal slope estimates: 0, 2, 2, 2.5, 2.5, 3, 3, 3.5, 4, 5

Median of seasonal slope estimates: 2.75

$n_1 = 4$ $n_2 = 4$ $g_1 = 0$ $g_2 = 1$, $t_{21} = 2$ $h_1 = 1$, $u_{11} = 2$ $h_2 = 1$, $u_{21} = 2$ $N'_1 = 5$ $N'_2 = 5$, $N' = 10$

$VAR(S_1) = 7.667$

$VAR(S_2) = 6.834$

$[VAR(S_1)]^{1/2} = 2.8$

$[VAR(S_2)]^{1/2} = 2.6$

$S' = S_1 + S_2 = 9$

$VAR(S') = 14.5$

$[VAR(S')]^{1/2} = 3.808$

$Z = 2.1 > Z_{0.95} = 1.645$ (one-tailed: 0.05 level of significance) \rightarrow Reject H_0 (no trend) and accept an upward trend (increasing)

For 90 % confidence interval

$C_\alpha = 1.645$ $[VAR(S')]^{1/2} = 6.264$

$M_1 = 1.868$, lower confidence limit = 1.7

$M_2 + 1 = 9.132$, upper confidence limit = 4.1

Source: Gilbert, 1987 (Example 17.1, p. 228)

3.3 Results and Discussion

Results by plotting first flush and later time concentrations indicate that Cl and bacteria has the least tendency toward first-flush effect. The first flush effect refers to the high concentration that occurs after early storm. Average concentrations of pollutants by location are given in Appendix B. The average concentration of Sb was highest at site SWMI01 (institutional, residential, and open lands). The average concentration of Alk was highest at site SWMI02 (residential, commercial, recreational, and open lands). The average concentration of TDS was highest at site SWMI16 (Marquette interchange). The highest average concentrations of NO_3 , NO_5 , and Tl were found at site SWMI15 (residential and highway). The highest average concentration of turbidity was found at site SWGF10 (botanical gardens and parking lot). The highest average concentrations of TP, TSS, and FC were found at site SWMI12 (residential, commercial, and parking lot). The highest average concentration of TKN was found at site SWWA17 (recreational, open lands, residential, and commercial).

Median values of FC and EC, FC were highest at site SWWA13 (residential, recreational, and open lands), and EC was highest at site SWWA17 (recreational, open lands, residential, and commercial). The highest average concentrations of As, Ca, Cd, Cr, Cu, Hard, Mg, Ni, Pb, and Zn were found at site SWMI15 (residential and highway). The highest average concentrations of Ag, Be, Cl, Hg, Se, TS were found at site SWMI16 (Marquette interchange). The highest average concentrations of BOD_5 , EC, and NO_2 were found at site SWWA17 (recreational, open lands, residential, and commercial). The highest average concentration of NH_3 was found site SWMI15 (residential and highway).

Total phosphorus exceeded the limit (1.00 mg/L) at sites SWWB09 (4939 N. Newhall, Whitefish Bay), SWMI12 (3275 S. 72nd St, Milwaukee), SWWA13 (Ridge Blvd & Harding, Wauwatosa), and SWWA17 (71st and Chestnut St, Wauwatosa). In the soil, TP is rapidly immobilized as calcium or iron phosphates (WATERSHEDSS, 2003). Most of the phosphorus in soils is adsorbed to soil particles or incorporated into organic matter (WATERSHEDSS, 2003). Phosphate is only freely soluble in acid solutions and under reducing conditions (WATERSHEDSS, 2003). Other sources of TP are synthetic detergent and commercial fertilizer (Sawyer et al., 2003). Total soluble phosphorus exceeded the limit (0.05 mg/L) for all 15 measured sites. Two main sources of TSP are synthetic detergent and commercial fertilizer (Sawyer et al., 2003). The increased TP and TSP levels may at least in part be explained by increased detergent and fertilizer usage.

Total Kjeldahl nitrogen exceeded the limit (1.50 mg/L) for all sites. Total Kjeldahl nitrogen is the sum of NH_3 and organic nitrogen. The discharge of NH_3 and its oxidation can rapidly reduce the dissolved-oxygen levels in rivers and estuaries (Sawyer et al., 2003). The amount of NH_3 never exceeded the limit (19.0 mg/L). Nitrite and nitrate exceeded the limit (0.68 mg/L) for all sites. Automobiles in dense urban areas and commercial fertilizer are primary sources of NO_5 (Sawyer et al., 2003).

Calcium and magnesium were high at site SWMI15 (42nd St & Mt Vernon, I-94 & Menominee River, Milwaukee). Chloride was found high at site SWMI16 (Marquette interchange, Milwaukee). The primary source of these pollutants is soil erosion and deicing salts. Both of these sites are transportation corridors which may link deicing salts to the high Ca, Mg, and Cl concentrations at these two sites.

The BOD₅ exceeded the limit (30 mg/L) at sites SWMI08 (Hampton & Lincoln Crk Pkwy, Milwaukee), SWWB09 (4939 N. Newhall, Whitefish Bay), SWMI12 (3275 S. 72nd St, Milwaukee), SWWA13 (Ridge Blvd & Harding, Wauwatosa), and SWWA17 (71st and Chestnut St, Wauwatosa). The BOD₅ is the amount of oxygen required by bacteria while stabilizing decomposable organic matter under aerobic conditions (Sawyer et al., 2003). High BOD₅ reflects high-strength domestic and industrial wastes in terms of the oxygen that will be required under aerobic conditions (Sawyer et al., 2003). Total suspended solids exceeded the limit (30 mg/L) for all sites. Total suspended solids are materials that will be retained by a filter with 2.0-μm nominal average pore size. High TSS deposition is expected to occur through biological and chemical flocculation (Sawyer et al., 2003).

Bacteria levels largely exceeded the limit of 400 CFU/100mL for fecal coliform and the limit of 126 CFU/100mL for *E. coli* at all sites. Sources of fecal coliform are from dogs, cats, rodents in urban areas, from geese, seagulls, and waterfowls in open lands, from farm animals and wild life in rural areas (Burton and Pitt, 2002). Bacteria enter the drainage system by washoff of animal feces (e.g., bird droppings) and organic matter from catchment surfaces, and they may also go into the drainage system through illicit connections (Adams and Papa, 2000).

Chromium exceeded the limit (0.016 mg/L) at sites SWMI15 (42nd St & Mt Vernon, I-94 & Menominee River, Milwaukee) and SWMI16 (Marquette interchange, Milwaukee). Sources of Cr are from metal plating, moving engine parts, and brake lining wear (McCuen, 2004). Copper exceeded the limit (0.0636 mg/L) at sites SWWB09 (4939 N. Newhall, Whitefish Bay), SWMI15 (42nd St & Mt Vernon, I-94 & Menominee River,

Milwaukee), and SWMI16 (Marquette interchange, Milwaukee). The primary sources of Cu are metal plating, bearing and bushing wear, moving engine parts, brake lining wear, and fungicides and insecticides applied by maintenance operations (McCuen, 2004). Lead exceeded the limit (0.0816 mg/L) at site SWMI15 (42nd St & Mt Vernon, I-94 & Menominee River, Milwaukee). Sources of Pb are tire wear, batteries, lubricating oil and grease, and bearing wear (McCuen, 2004). Zinc exceeded the limit (0.117 mg/L) for 12 sites including sites SWMI15 (42nd St & Mt Vernon, I-94 & Menominee River, Milwaukee), SWMI16 (Marquette interchange, Milwaukee), and SWMI18 (Miller park east parking lot at sausage house, Milwaukee). Sources of Zn are tire wear, motor oil, and grease (McCuen, 2004).

Hardness exceeded the limit (120 mg/L: maximum hardness levels accepted by textile industry) for 14 sites. Hardness in water is derived largely from contact with the soil and rock formations. The hard waters also originate in areas where topsoil is thick and limestone formations are present (Sawyer et al., 2003).

Results from Table 3.2 indicate that the average concentrations of various water quality pollutants in CSOs were generally higher than those in stormwater. However, the average concentrations of some water quality pollutants in stormwater were higher than those in CSOs, i.e. Ca, Cu, Hard, Mg, Se, TP, TSS, and Zn.

The different seasonal conditions such as the snowmelt and rainfall periods were found to have a significant impact on the water quality. From Table 3.5, concentrations of Alk, As, Be, Ca, Cd, Cl, Hard, Hg, Mg, Se, TDS, Tl, and TS were highest in winter. The highest concentrations of Ag, Pb, TKN, TP, TSS, turbidity, and Zn were found in summer. Spring had the highest concentrations of Cr, Cu, NH₃, Ni, NO₂, and NO₃.

Concentrations of BOD₅, NO₅, TOC, and TSP were highest in fall. The highest of bacteria levels were found in summer. Explanations for several of these trends are given below. Box plots of 33 pollutant concentrations for spring, summer, fall, and winter are illustrated in Appendix C.

Table 3.5. Summary of a season indicated the highest average pollutant concentration (2000-2006).

No.	Pollutant	Season indicated the highest concentration
1	Ag	Summer
2	Alk	Winter
3	As	Winter
4	Be	Winter
5	BOD ₅	Fall
6	Ca	Winter
7	Cd	Winter
8	Cl	Winter
9	Cr	Spring
10	Cu	Spring
11	EC	Summer
12	FC	Summer
13	Hard	Winter
14	Hg	Winter
15	Mg	Winter
16	NH ₃	Spring
17	Ni	Spring
18	NO ₂	Spring
19	NO ₃	Spring
20	NO ₅	Fall
21	Pb	Summer
22	Sb	Spring
23	Se	Winter
24	TDS	Winter
25	TKN	Summer
26	Tl	Winter
27	TOC	Fall
28	TP	Summer
29	TS	Winter
30	TSP	Fall
31	TSS	Summer
32	Turbidity	Summer
33	Zn	Summer

Results from Table 3.5 and box plots from Appendix C indicated the highest concentrations of TS and many metals except Ag, Pb, and Zn during winter and spring. During snowmelt, the dissolved and particulate pollutants will accompany the snowmelt runoff or become more concentrated in surrounding snowbanks and on the surface. Westerlund et al. (2003) explained that the highest particulate concentration during the snowmelt period was due to lower flow and contribution of pollutants from the melting snowbanks. In addition, the rain-on-snow event, that is more likely to happen in winter and spring, also contributes higher particulate concentrations because rainfall can wash off pollutants accumulated in the snowbanks. The highest bacteria levels (EC and FC) were found in summer from rainfall events, indicating that sources of bacteria are animal feces and bird droppings.

Table 3.6 lists the values of seasonal slopes for 33 pollutants estimated by the seasonal Kendall test. The seasonal slope was computed as the median of all slopes between data pairs of four years (2000-2004) within the same season (spring, summer, and fall). Upward trend is positive seasonal slope (increasing). By contrast, downward trend is negative seasonal slope (decreasing).

In Table 3.6, an upward trend can be found for Ag with seasonal slope of 5.4×10^{-4} mg/L/year, Alk with seasonal slope of 8.75 mg/L/year, As with seasonal slope of 1.5×10^{-3} mg/L/year, Cd with seasonal slope of 1.6×10^{-4} mg/L/year, Cl with seasonal slope of 1 mg/L/year, Cu with seasonal slope of 1×10^{-3} mg/L/year, Hg with seasonal slope of 2.8×10^{-3} µg/L/year, Ni with seasonal slope of 5×10^{-5} mg/L/year, Pb with seasonal slope of 4.4×10^{-3} mg/L/year, Se with seasonal slope of 1.8×10^{-3} mg/L/year, TOC with seasonal

slope of 2 mg/L/year, TP with seasonal slope of 0.08 mg/L/year, and TSP with seasonal slope of 0.05 mg/L/year.

Figure 3.1 shows the seasonal snowfall data in Milwaukee (1899/1990-2004/2005) from Wisconsin state climatology office (2005). Total snowfall of each year is the amount of snowfall accumulated from July of that indicated year to June of next year. Seasonal snowfall data (Figure 3.1) are consistent with the upward trend of Cl since Cl samples were collected from 2002 to 2004 and a primary source of Cl is deicing salt.

A study of urban mobility from Texas Transportation Institute, Texas A&M University System (2005) shows an increase versus year in daily freeway vehicle-miles of travel on freeways in Milwaukee (Figure 3.2), which may explain the upward trends for Cd, Cu, Ni, and Pb because the automobile traffic is a primary source of these pollutants (McCuen, 2004).

Due to exceedances of the guideline limits along with occurrences of upward trends, sites of special concern for Cu and Pb are sites SWMI15 (42nd St & Mt Vernon, I-94 & Menomonee River, Milwaukee) and SWMI16 (Marquette interchange, Milwaukee) (Table 3.6 and Figures E-10 and E-21). Sites of special concern for TP include SWWB09 (4939 N. Newhall, Whitefish Bay), SWMI12 (3275 S. 72nd St, Milwaukee), SWWA13 (Ridge Blvd & Harding, Wauwatosa), and SWWA17 (71st and Chestnut St, Wauwatosa). Because of high TSP values, all 15 sites with TSP measurements (sites 1-4, 6, 7, 9-13, and 15-18) (Table 3.6 and Figure E-30) should be carefully monitored.

Table 3.6. Seasonal Kendall slope estimations.

Stormwater Data 2000 - 2004

Pollutant	% Confidence Interval	Seasonal Trend		Seasonal Kendall Slope Confidence Intervals		
		Two-tailed	One-tailed	Lower Limit	Slope mg/L/year (*µg/L/year)	Upper limit
Ag	95	Upward/Downward	Upward	0.00044	0.00054	0.00071
Alk	95	Upward/Downward	Upward	3	8.75	15
As	95	Upward/Downward	Upward	0.0013	0.0015	0.0018
Be	95	Upward/Downward	Downward	-0.000015	-0.000015	-0.000015
BOD ₅	95	Upward/Downward	Downward	0	-0.6	-1.2
Ca	70	Upward/Downward	Downward	-1.2	-0.67	0
Cd	95	Upward/Downward	Upward	0.00016	0.00016	0.00026
Cl	75	Upward/Downward	Upward	0	1	2.34
Cr	85	Upward/Downward	Downward	-0.0001	-0.00005	0
Cu	85	Upward/Downward	Upward	0	0.001	0.0017
EC	95	No trend	No trend	-300	0	75
FC	95	Upward/Downward	Downward	-1145	-370	-1.67
Hard	65	Upward/Downward	Downward	-4.33	-2	0
Hg	95	Upward/Downward	Upward	0.0028*	0.0028*	0.0028*
Mg	45	Upward/Downward	Downward	-0.25	-0.1	0
NH ₃	95	No trend	No trend	-0.02	0	0.023
Ni	95	Upward/Downward	Upward	0	0.00005	0.000067
NO ₂	95	Upward/Downward	Downward	-0.0083	-0.0057	-0.0033
NO ₃	90	Upward/Downward	Downward	-0.06	-0.03	0
NO ₅	95	na	na	na	na	na
Pb	95	Upward/Downward	Upward	0.0025	0.0044	0.0063
Sb	95	Upward/Downward	Downward	-0.078	-0.053	-0.012
Se	95	Upward/Downward	Upward	0.00073	0.0018	0.0031
TDS	70	Upward/Downward	Downward	-39.5	-20	0
TKN	95	Upward/Downward	Downward	-0.3	-0.22	-0.13
TI	95	Upward/Downward	Downward	-0.0011	-0.0011	-0.0011
TOC	90	Upward/Downward	Upward	0	2	3.5
TP	95	Upward/Downward	Upward	0.05	0.08	0.11
TS	55	Upward/Downward	Downward	-10.67	-6.67	0
TSP	95	Upward/Downward	Upward	0.02	0.05	0.05
TSS	95	Upward/Downward	Downward	-8.75	-4.4	-0.5
Turbidity	95	na	na	na	na	na
Zn	95	No trend	No trend	-0.0043	0	0.005

Note: na = not sufficient data to compute seasonal slope

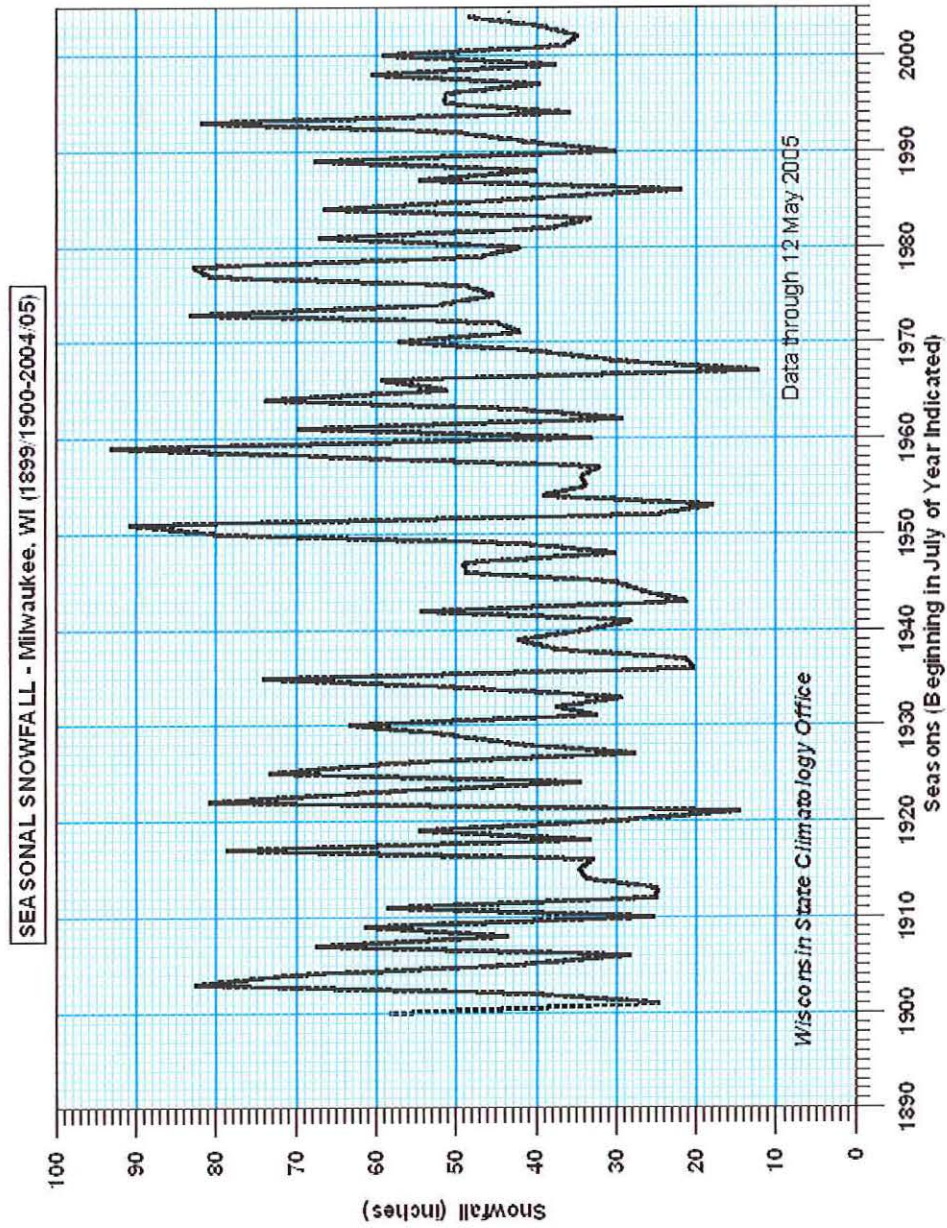


Figure 3.1. Seasonal snowfall at Milwaukee, WI (Wisconsin Climatology Office, 2005).

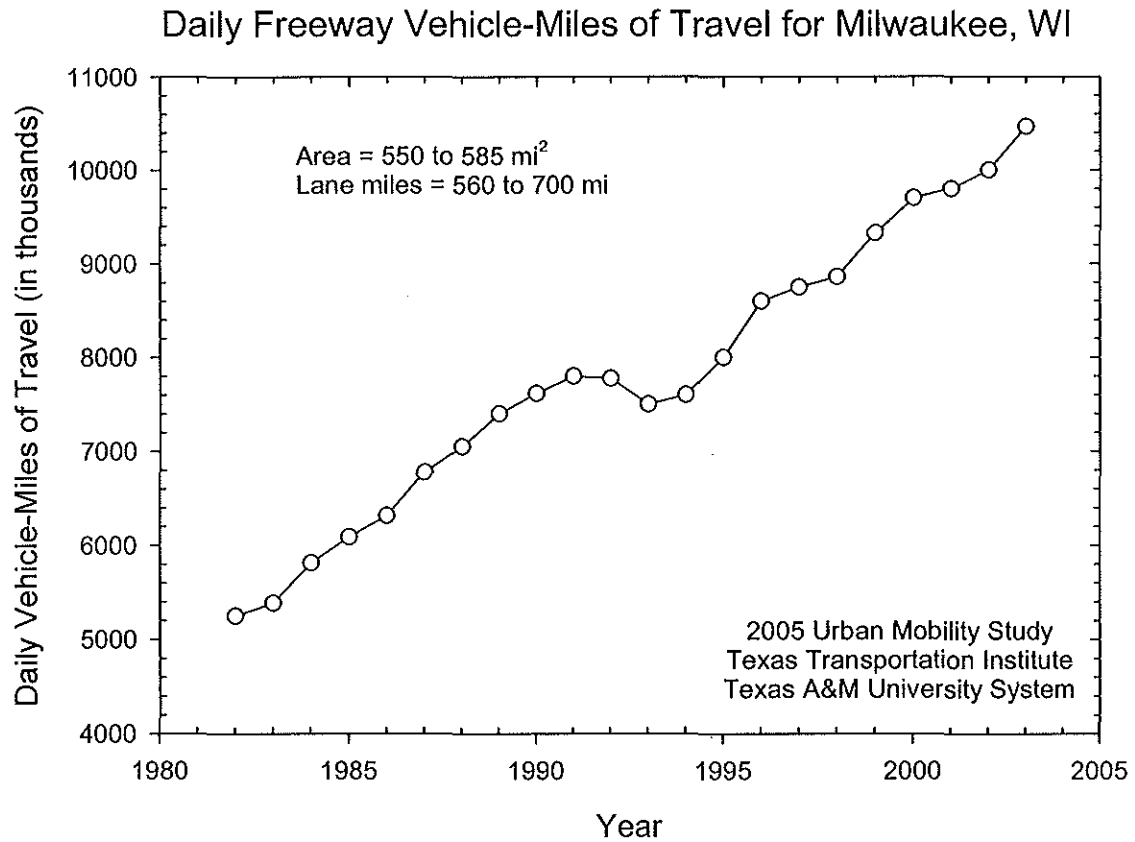


Figure 3.2. Daily freeway vehicle-miles of travel on freeways for Milwaukee, WI (Texas Transportation Institute, Texas A&M University System, 2005).

IV. DRAINAGE AREAS AND GEOGRAPHIC INFORMATION SYSTEMS (GIS)

Maps of 18 stormwater study sites using ArcGIS are illustrated in this chapter. The feature of a landscape (e.g., pattern of terrain and slope) represented by contour lines in a topographic map for each storm catchment may not reflect the complete drainage pattern. Then, GIS maps of drainage area's infrastructures (buildings, streets, and storm sewers) and natural condition (imperviousness) are generally preferred. Contour lines, types of land use, available storm sewers, and suggested drainage boundaries are included in the maps shown.

The actual drainage area of the GIS maps may be estimated based on runoff coefficients for the areas, along with contour data and storm sewer lines. GIS may show how stormwater runoff is actually drained. For example, a runoff coefficient > 1 usually indicates that the drainage area is underestimated. Collectively, these maps will enhance the understanding of the drainage pattern of the study area, and will provide information required to make decisions related to the stormwater best management practices (BMPs).

4.1 Estimate of the Drainage Area Sizes

Application of ArcGIS for the estimation of the accurate drainage area size is recommended. The runoff coefficient is a key to accomplish this estimation. Moreover, overlaying the storm sewer lines on the land use map in ArcGIS is also helpful method in order to examine the drainage boundary for each study site. In the case of unavailable storm sewer pipes, the investigation of surface topography using contour lines may be helpful.

4.1.1 Measured and Calculated Runoff Coefficients

Runoff coefficients were computed as total runoff volume divided by total rainfall volume. Coefficients ranged from 0.00096 to 16.1. Mean coefficients for 18 monitoring sites ranged from 0.0052 to 3.88. Median coefficients for 18 monitoring sites (Table 4.1) ranged from 0.0036 to 3.71. The mean coefficient over all sites was 0.87 ± 0.33 , and the median was 0.13.

Coefficients were greater than 1.0 at sites SWMI06, SWMI07, SWMI08, and SWMI18. The reason for these >1.0 coefficients is that drainage areas are underestimated. Very low values of coefficients due to overestimation of drainage areas are also evident, e.g., for sites SWMI02 and SWMI15. Runoff volume from rainfall was estimated based on the median coefficient of each site. A plot of the measured runoff volume versus the calculated runoff volume (Figure 4.1) had $R^2 = 0.897$ ($n = 372$), which indicates that runoff coefficients are nearly constant for a given area and all events, except low rainfall events where depression volumes sometime can give low measured runoff volume, and therefore low runoff coefficients (e.g., site SWWB09).

Table 4.1. Runoff coefficients for 18 study sites, 2000-2004.

Site ID	Location	Comments	Runoff coefficient*
SWM101	Lincoln Memorial Dr & Carferry Dr, Milwaukee	Institutional, residential, open lands	0.0306 (0.0658,0.00563)
SWM102	1700 N. Lincoln Memorial Dr @ Lafayette Hill, Milwaukee	Residential, commercial, recreational, open lands	0.00355 (0.0165,0.000965)
SWFR03	54th & Ashland, Franklin	Industrial park, open lands	0.183 (0.386,0.0219)
SWM104	3500 S. Lake Dr @ Bayview Park, Milwaukee	Institutional, residential, open lands, highway 794, Bay View Park	0.0771 (0.138,0.0491)
SWM105	1200 E. Singer Circle, Milwaukee	Residential, parking lot, open lands	0.270 (3.01,0.0641)
SWM106	Milwaukee County Zoo, Milwaukee	Milwaukee County Zoo, I-94	2.18 (16.1,0.721)
SWM107	4345 N. 47th St, Milwaukee	Residential, recreational	3.71 (8.29,0.335)
SWM108	Hampton & Lincoln Crk Pkwy, Milwaukee	Residential, commercial	3.41 (8.99,0.962)
SWWB09	4939 N. Newhall, Whitefish Bay	Residential, open lands	0.0980 (0.201,0.00224)
SWG10	Boerner Botanical Gardens, Hales Corners (10007 W. Meadow Dr), Greenfield	Boerner botanical gardens, parking lot	0.00865 (0.0220,0.00164)
SWNB11	13380 Eagle Trace & Timber Ridge, New Berlin	New residential, open lands	0.0151 (0.0494,0.00604)
SWM112	3275 S. 72nd St, Milwaukee	Residential, commercial, parking lot	0.0813 (0.167,0.031)
SWWA13	Ridge Blvd & Harding, Wauwatosa	Residential, open lands	0.265 (0.505,0.0159)
SWSF14	Lake Dr and Tesch Av, St Francis	Residential, open lands	0.0341 (0.0581,0.00346)
SWM115	42nd St & Mt Vernon (I-94 & Menomonee River), Milwaukee	I-94, flood control area, residential	0.0335 (0.0948,0.0175)
SWM116	Marquette Interchange, Milwaukee	I-94, I-43, highway 794, industrial	0.237 (0.350,0.171)
SWWA17	71st and Chestnut St, Wauwatosa	Recreational, open lands, residential, commercial	0.725 (0.973,0.428)
SWM118	Miller Park east parking lot at sausage house, Milwaukee	Miller Park east parking lot	3.01 (5.99,0.208)

*median with maximum and minimum

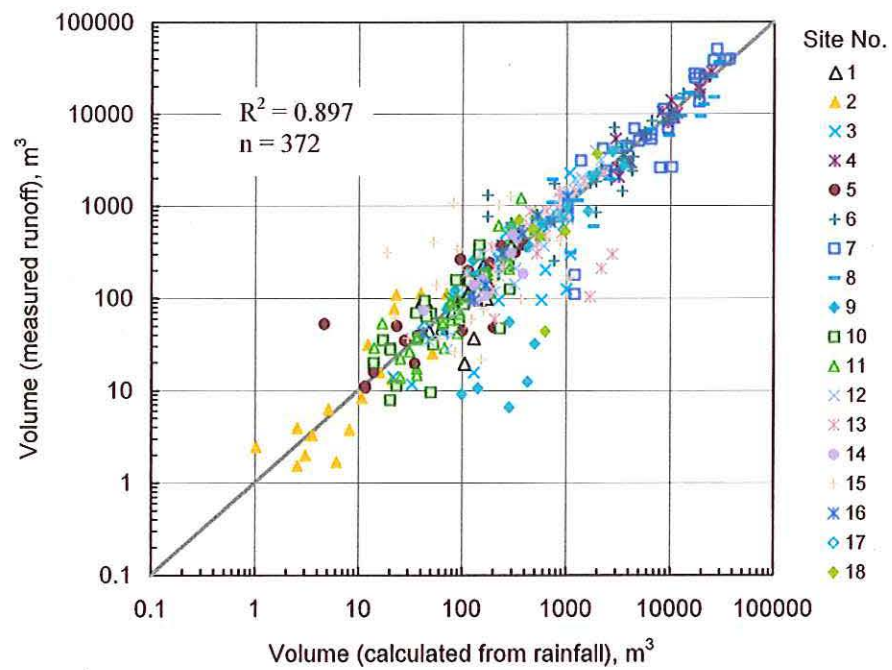


Figure 4.1. Measured versus rainfall-based runoff volumes.

4.1.2 New Drainage Areas Determined By Storm Sewer and Contour lines

Table 4.2 shows a summary of new drainage areas and percent land uses for 18 study sites. Residential area is dominant at site SWNB11 (13380 Eagle Trace & Timber Ridge, New Berlin). Transportation is prevailing at sites SWMI01 (Lincoln Memorial Dr & Carferry Dr, Milwaukee) and SWMI16 (Marquette interchange, Milwaukee). Outdoor recreational area and open lands are predominantly found at site SWMI06 (Milwaukee County Zoo, Milwaukee).

All GIS maps and aerial photographs with the suggested drainage boundary are illustrated in Figures 4.3 - 4.38. New drainage areas were determined in two stages. First, original runoff coefficients $\hat{\beta}$ were used as a guide to determine if an area adjustment appeared to be necessary. Adjustments were then done according to the GIS map considering storm sewer lines and topography. The second stage is a further adjustment of the drainage area and resulting runoff coefficient $\hat{\beta}$ such that it becomes consistent with a calculated runoff coefficient $\hat{\beta}_{calc}$ based on optimized runoff coefficients β_i for each subarea i of given GIS land use type, e.g., residential, etc. This optimization is illustrated below with reference to Table 4.2.

Table 4.2. Summary of new drainage areas, new estimated runoff coefficients, and percent land uses for 18 study sites.

Site No.	Original Area (ha)	New Area (ha)	Original runoff coefficient	New runoff coefficient	Percent land use									
					Residential	Business and Commercial	Industrial	Freeway related land	Roads	Parking	Communication and Utilities	Governmental services and Institutional	Outdoor Recreational	Open Lands
SWMI01	23.8	2.19	0.0306	0.333	0	0	0	0	81.0	2.80	0	1.00	0	5.70
SWMI02	57.2	0.509	0.00355	0.399	0	0	0	0	40.0	0	19.0	0	21.0	19.0
SWFR03	11.7	9.53	0.183	0.225	0	4.01	18.5	0	17.1	24.7	0	0	0	35.7
SWMI 04	608	250	0.0771	0.187	54.0	9.20	0	0	6.40	3.30	1.60	16.0	1	7.90
SWMI 05	3.42	3.67	0.270	0.252	66.0	0	0	0	23.0	9.10	0	0	0	2.20
SWMI06	10.6	38.8	2.18	0.597	0	0	0	0	0	28.9	0	0	54.7	15.5
SWMI 07	18.4	256	3.71	0.266	44.0	5.20	0	0	22.0	12.0	0	9.20	8.30	1.80
SWMI 08	21.2	320	3.41	0.225	59.0	3	0	0	27.0	2.10	0	3.90	3.20	0
SWWB09	57.3	45.1	0.0980	0.125	73.5	0.77	0	0	25.7	0	0	0	0	0
SWGFI0	71.3	1.27	0.00865	0.486	0	0	0	0	18.2	81.8	0	0	0	0
SWNB 11	73.8	5.28	0.0151	0.211	81.0	0	0	0	19.0	0	0	0	0	0
SWMI 12	38.8	17.8	0.0813	0.177	70.0	0	0	0	28.0	0	0	0	260	0
SWWA13	20.5	44.1	0.265	0.123	70.0	0	0	0	30.0	0	0	0	0	0
SWSF14	21.5	3.91	0.0341	0.187	75.0	0	0	0	25.0	0	0	0	0	0
SWMI 15	44.2	2.99	0.0335	0.495	32.0	0	0	29.0	17.0	0	1.50	0	17.0	260
SWMI 16	6.39	2.23	0.237	0.679	0	0	0	100	0	0	0	0	0	0
SWWA17	13.3	40.8	0.725	0.237	42.9	5.77	0.11	3.07	19.4	9.22	2.79	0.24	12.8	3.07
SWMI 18	1.92	10.3	3.01	0.561	0	0	25.0	6.00	5.80	43.0	16.0	0	4.00	0

Note: 1 ha = 0.00386 mi²

4.2 Estimation of Runoff Coefficients Based on Least Squares Method.

Data from Table 4.2 can be used directly to formulate the following optimization model:

$$\text{Minimize} \quad S = \sum_{i=1}^{18} (\hat{\beta}_i - \hat{\beta}_{i, calc})^2 \quad (9)$$

$$\text{where} \quad \hat{\beta}_{i, calc} = \sum_{j=1}^{10} f_{ij} \cdot \beta_j \quad i = 1, 2, 3, \dots, 18 \quad (10)$$

subject to

$$\sum_{j=1}^{10} f_{ij} = 1 \quad i = 1, 2, 3, \dots, 18 \quad \text{and} \quad 0 \leq \beta_j \leq 1 \quad (11)$$

By guessing initial values of β_j for j^{th} land use, the $\hat{\beta}_{i, calc}$ was estimated using the fractional area distribution f_{ij} for j^{th} land use of site i . The Solver command in Microsoft Excel was used to find optimized solutions β_j (minimum S value) for this nonlinear objective function.

4.3 Results and Discussion

In order to develop the actual drainage area, the original drainage area was mapped using ArcGIS, and maps included contour data, storm sewer lines, and types of land use. Unreasonable values of the calculated runoff coefficient from runoff volume and rainfall volume based on original drainage area size would lead to incorrect drainage areas. Many storm sewer lines were provided in several formats such as hard copies, AutoCAD files, and ArcGIS shapfiles by local cities, e.g., city of Milwaukee for site SWMI, city of Whitefish Bay for site SWWB, etc.

For site SWMI01 (Figure 4.3), the original runoff coefficient was found to be 0.0306, indicating the overestimation of drainage area size. Unfortunately, available storm sewer lines were incomplete for this site. The estimate of drainage area boundary had to be done based on available adjacent storm sewer lines, and the runoff coefficient then became 0.333. The original runoff coefficient was very low for site SWMI02. After reducing the drainage area size, the new coefficient of 0.399 was obtained. In this case, the new drainage area boundary was determined based on contour lines in Figure 4.5 and the impervious area from aerial photograph in Figure 4.6 due to unavailability of storm sewer lines. This was done by an assumption that most storm sewers are commonly constructed to drain runoff from pavement. Then, the proposed drainage area should cover only the area of Alterra coffee shop.

For site SWFR03, the complete storm sewer lines were obtained in a hard copy. It was obvious that the original area boundary was incorrect (Figure 4.7). The new runoff coefficient was estimated to be 0.225, which is similar to the old coefficient. Site SWMI04 contains the most complicated storm sewer system compared to others. Fortunately, the AutoCAD file and hard copy of complete storm sewer lines were obtained. The new drainage area boundary was drawn to cover these sewer lines (Figure 4.9), and the new runoff coefficient was 0.187. Site SWMI05 covers a small area and contains simple storm sewer lines (Figure 4.11). The new runoff coefficient was estimated to be 0.252, which is close to the old coefficient. The storm sewer lines for site SWMI06 were obtained from Milwaukee County in the shapefile format. The original runoff coefficient was 2.18, showing the underestimation of the drainage area. Considering storm sewer lines in Figure 4.13, the drainage area had to extend to cover a

major part of the east parking lot area. For site SWMI07, the original runoff coefficient was very high (3.71), indicating the underestimation of the drainage area. The new drainage area covers more areas along the storm sewer lines into the southwest of the original area (Figure 4.15). Site SWMI08 had the original runoff coefficient of 3.41, pointing to the underestimation of the drainage area. The complete storm sewer lines were obtained, and the new drainage area boundary was drawn based on these sewer lines. The drainage area had to extend to cover all sewer lines in the west (Figure 4.17). The runoff coefficient was then reduced to 0.225.

For site SWWB09, the drainage area boundary was extended to the south of the original area to cover the storm sewer lines (Figure 4.19). The contour lines in Figure 4.21 and the site inspection were mainly used to determine the new drainage area boundary for site SWGF10. The original runoff coefficient for this site was very low (0.00865), indicating the overestimation of the drainage area. The runoff coefficient based on the new drainage area became 0.486. Site SWNB11 had a very low value of original runoff coefficient (0.0151), specifying the overestimation of the drainage area. The complete storm sewer lines for this site were obtained (Figure 4.23). The new drainage area gave a runoff coefficient of 0.211. Also, the aerial photograph of this site indicated small impervious area. Site SWMI12 had a low value of runoff coefficient (0.0813) so that the original drainage area was overestimated. The new drainage area was determined based on complete storm sewer lines, giving a runoff coefficient of 0.177 (Figure 4.25).

The new drainage area for site SWWA13 had to be estimated based on the site inspection accordance with contour lines in Figure 4.27 due to incorrect storm sewer

lines. The runoff coefficient of 0.123 obtained using new drainage area boundary was lower than the original runoff coefficient (0.265). The original drainage area for site SWSF14 was overestimated due to a small original runoff coefficient (0.0341). The complete storm sewer lines from the hard copy were used to determine the new drainage area boundary for this site. The new drainage area (Figure 4.29) gave a runoff coefficient of 0.187. The original runoff coefficient was 0.0335 for site SWMI15, indicating the overestimation of the drainage area. As seen in Figure 4.31, site SWMI15 contains simple storm sewer lines so that the new drainage area was easy to estimate. Then, the new runoff coefficient based on the new area was 0.495.

Site SWMI16 was located at the old Marquette interchange. The hard copy of complete storm sewer lines was obtained from the Wisconsin Department of Transportation (WisDOT). The new drainage area (Figure 4.33) gave a runoff coefficient of 0.679. The new drainage area for site SWWA17 was determined based on the site inspection and contour lines. The drainage area was extended into the north of the old drainage area boundary (Figure 4.35). The new upper boundary is located on top of a small hill, showing a downhill drain path. It gave a runoff coefficient of 0.237. The incomplete storm sewer lines were received for site SWMI18, and the original drainage area was underestimated based on a very high value of runoff coefficient (3.01). Considering contour lines (Figure 4.37) and the impervious area from aerial photograph (Figure 4.38), the new drainage area was determined, and the runoff coefficient of 0.561 was obtained.

New runoff coefficients computed based on new drainage area sizes are reasonable (Table 4.2 and Figure 4.2). Results from the optimization model indicated the

similarity between calculated runoff coefficients $\hat{\beta}_{i,calc}$ for all 18 sites and runoff coefficients estimated from new drainage sizes (Figure 4.2). Values of decision variables β_j obtained from the optimization modeling (Table 4.3) are reasonable, except for business and commercial areas, and open lands.

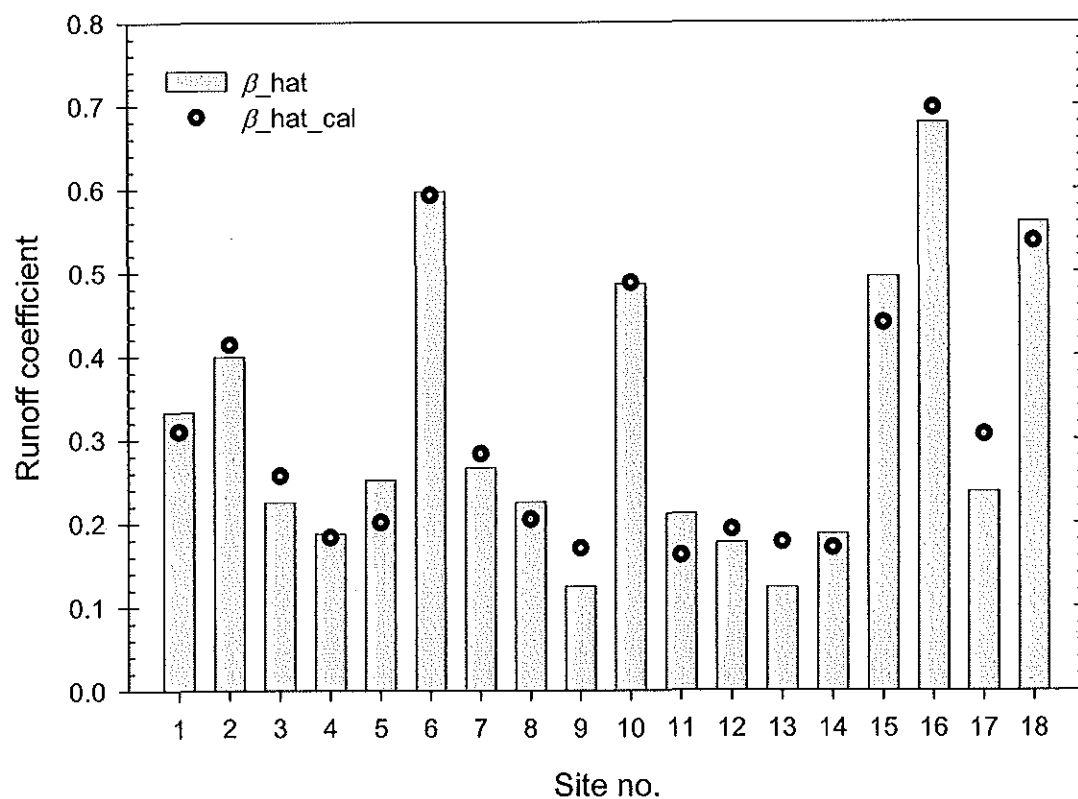


Figure 4.2: Calculated runoff coefficients $\hat{\beta}_{i, \text{calc}}$ based on the optimization model vs runoff coefficients $\hat{\beta}_i$ based on new drainage area sizes.

Table 4.3. Runoff coefficients for each type of land use based on the optimization model.

Types of land use	Runoff coefficient, β_j
Residential	0.134
Business and Commercial	0
Industrial	0.417
Freeway related land	0.697
Roads	0.278
Parking	0.534
Communication and Utilities	0.707
Governmental services and Institutional	0.349
Outdoor Recreational	0.801
Open Lands	0

SWMI01

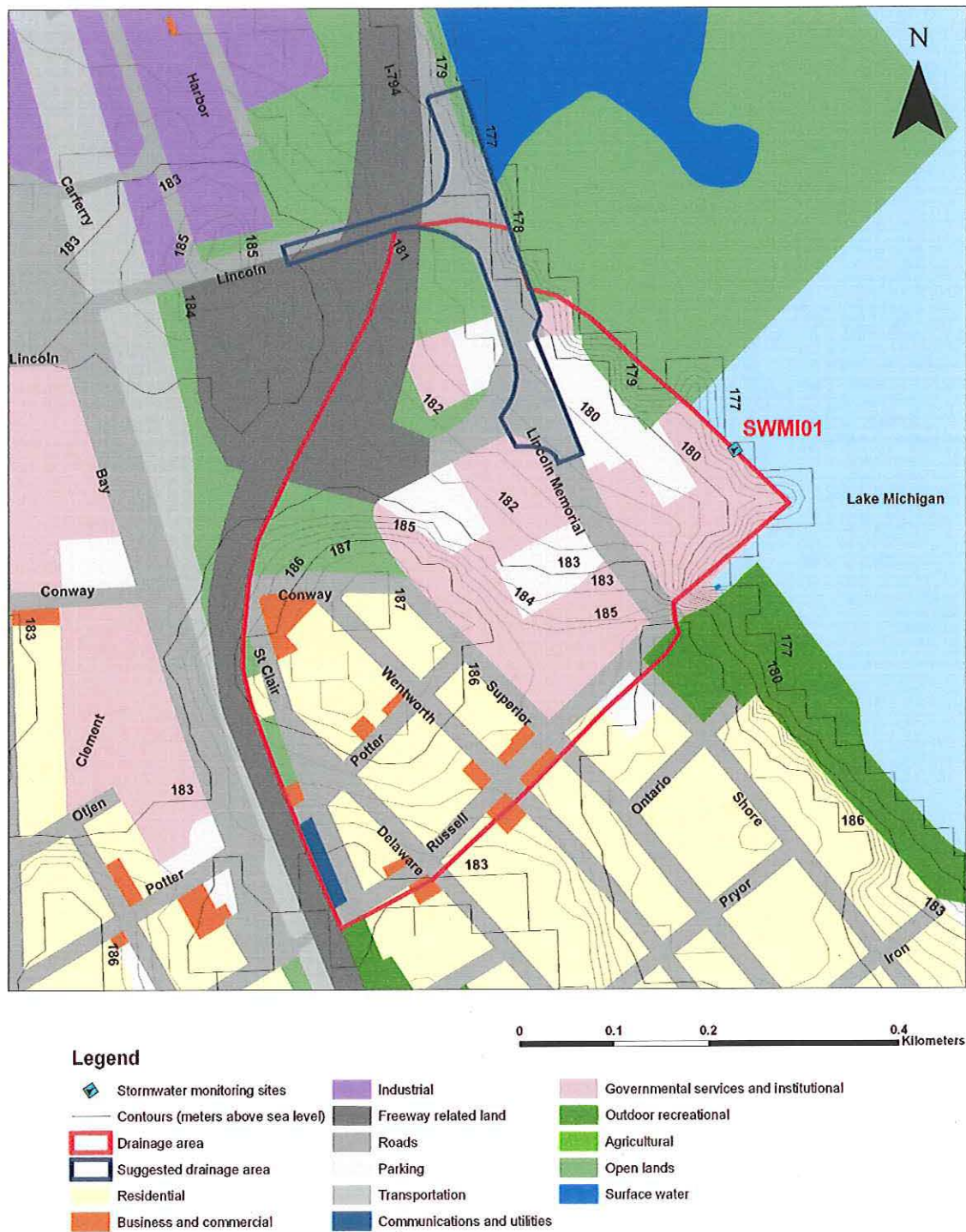


Figure 4.3. A map of site SWMI01 (Lincoln Memorial Dr & Carferry Dr, Milwaukee) with land uses and new drainage boundary.

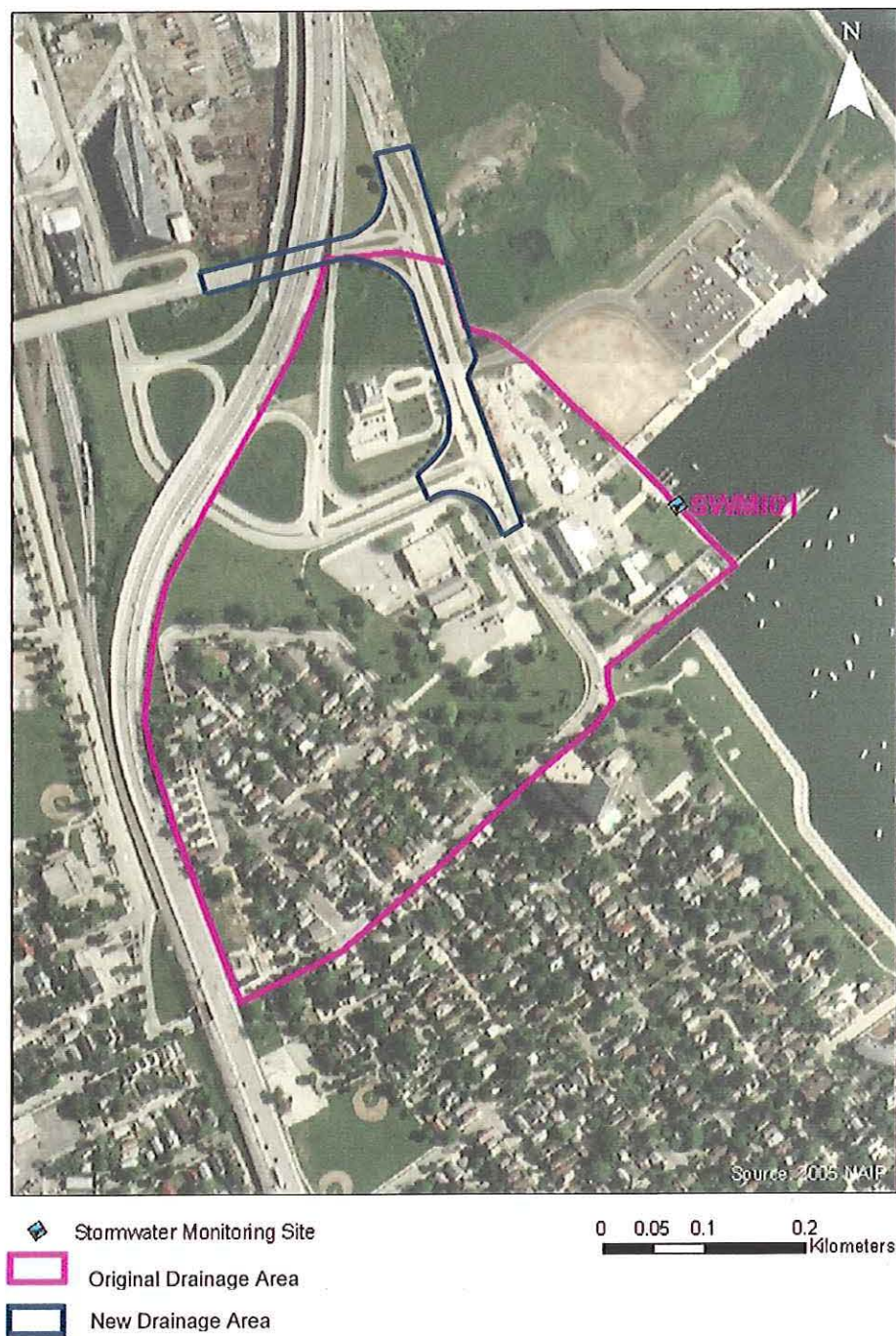


Figure 4.4. An aerial photograph of site SWMI01 (Lincoln Memorial Dr & Carferry Dr, Milwaukee) with new drainage boundary.

SWMI02

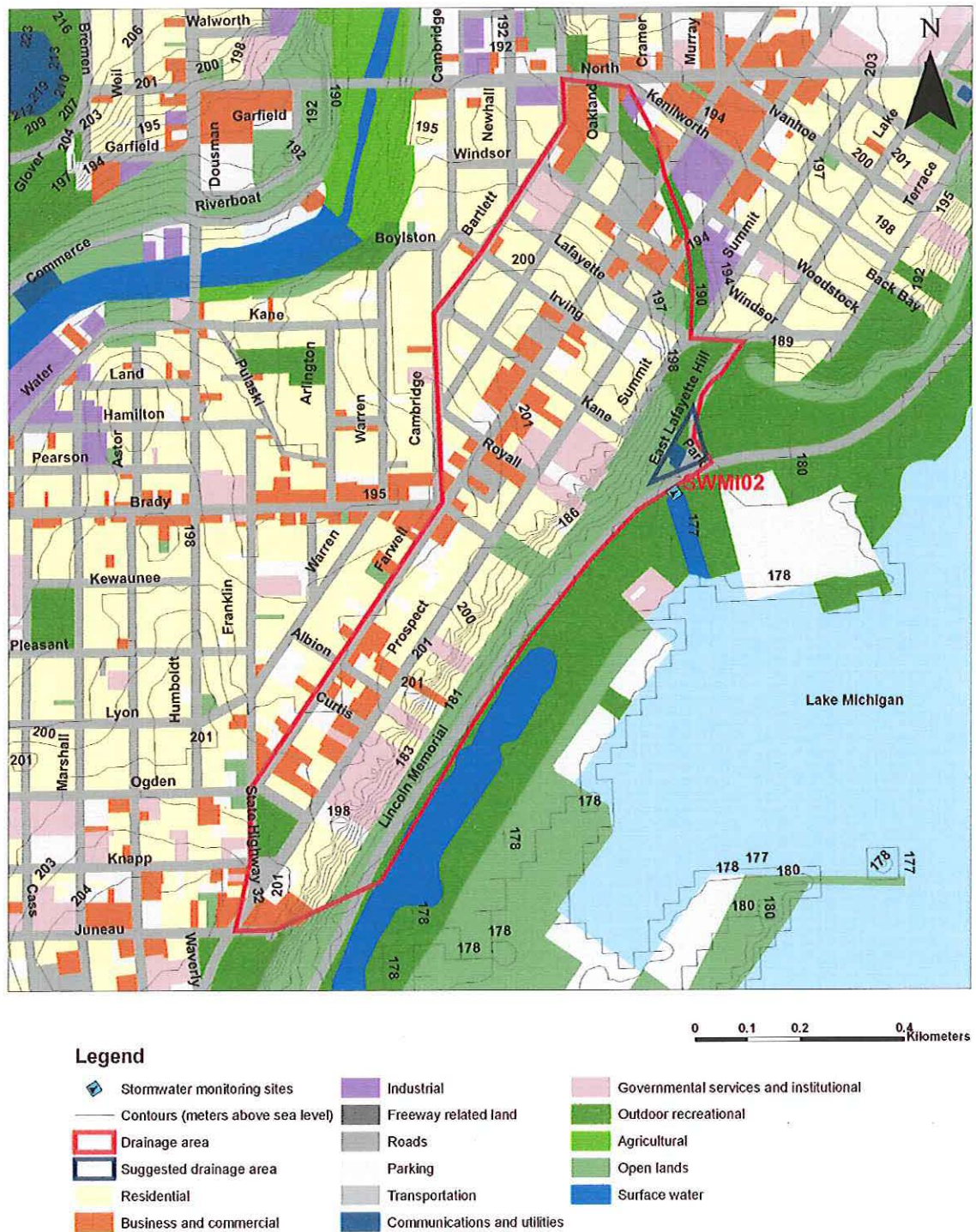


Figure 4.5. A map of site SWMI02 (1700 N. Lincoln Memorial Dr @ Lafayette Hill, Milwaukee) with land uses and new drainage boundary.

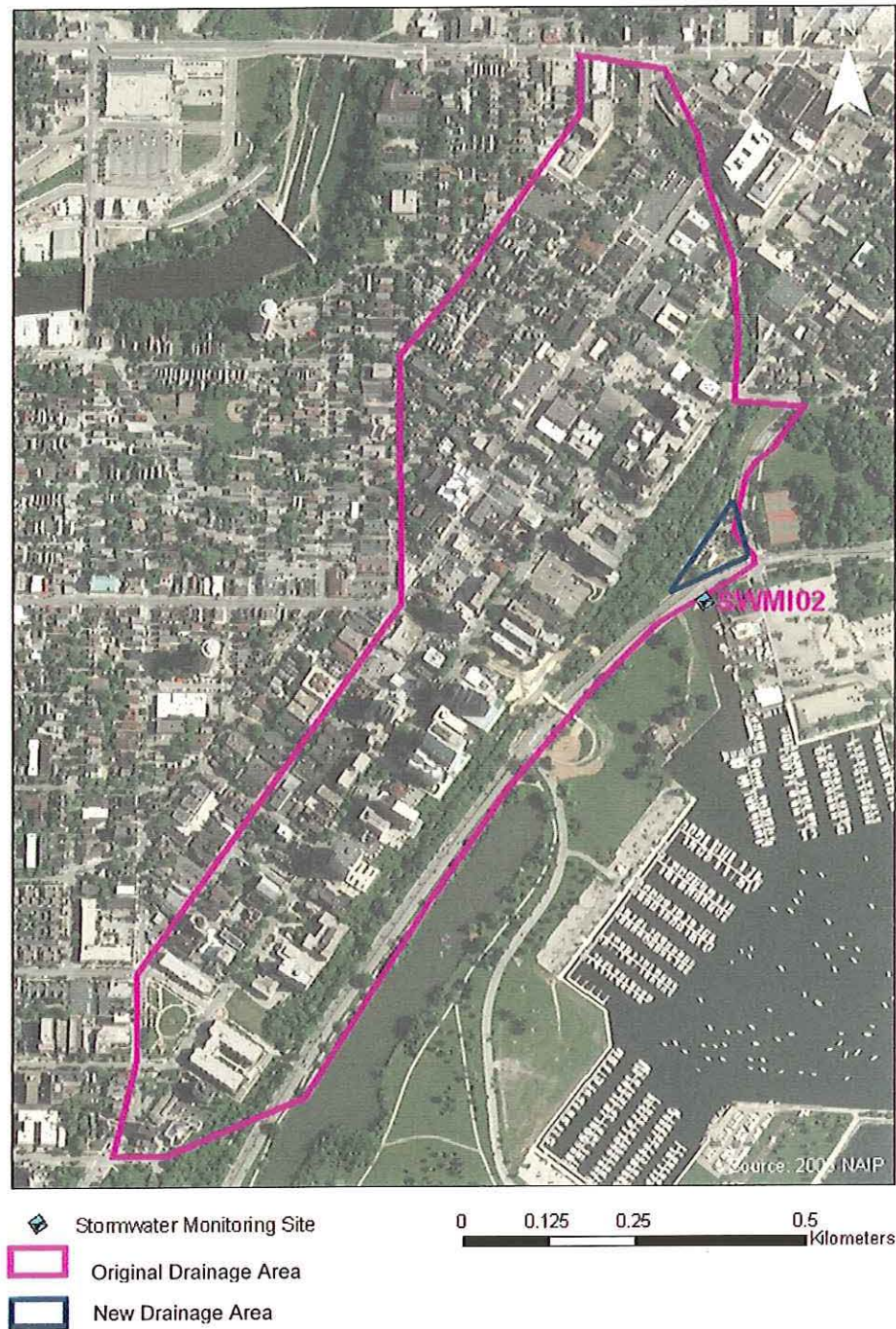


Figure 4.6. An aerial photograph of site SWMI02 (1700 N. Lincoln Memorial Dr @ Lafayette Hill, Milwaukee) with new drainage boundary.

SWFR03

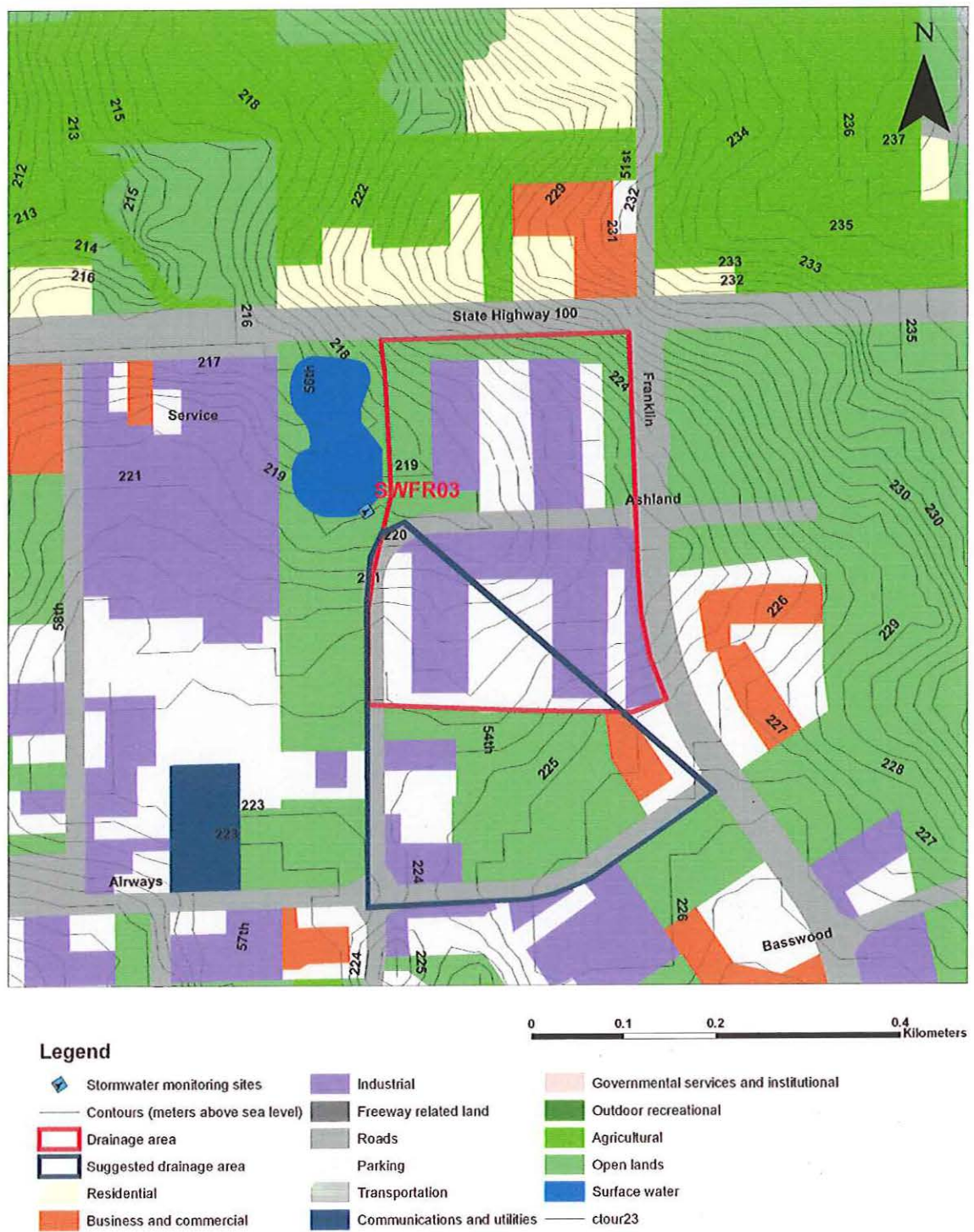


Figure 4.7. A map of site SWFR03 (54th & Ashland, Franklin) with land uses and new drainage boundary.

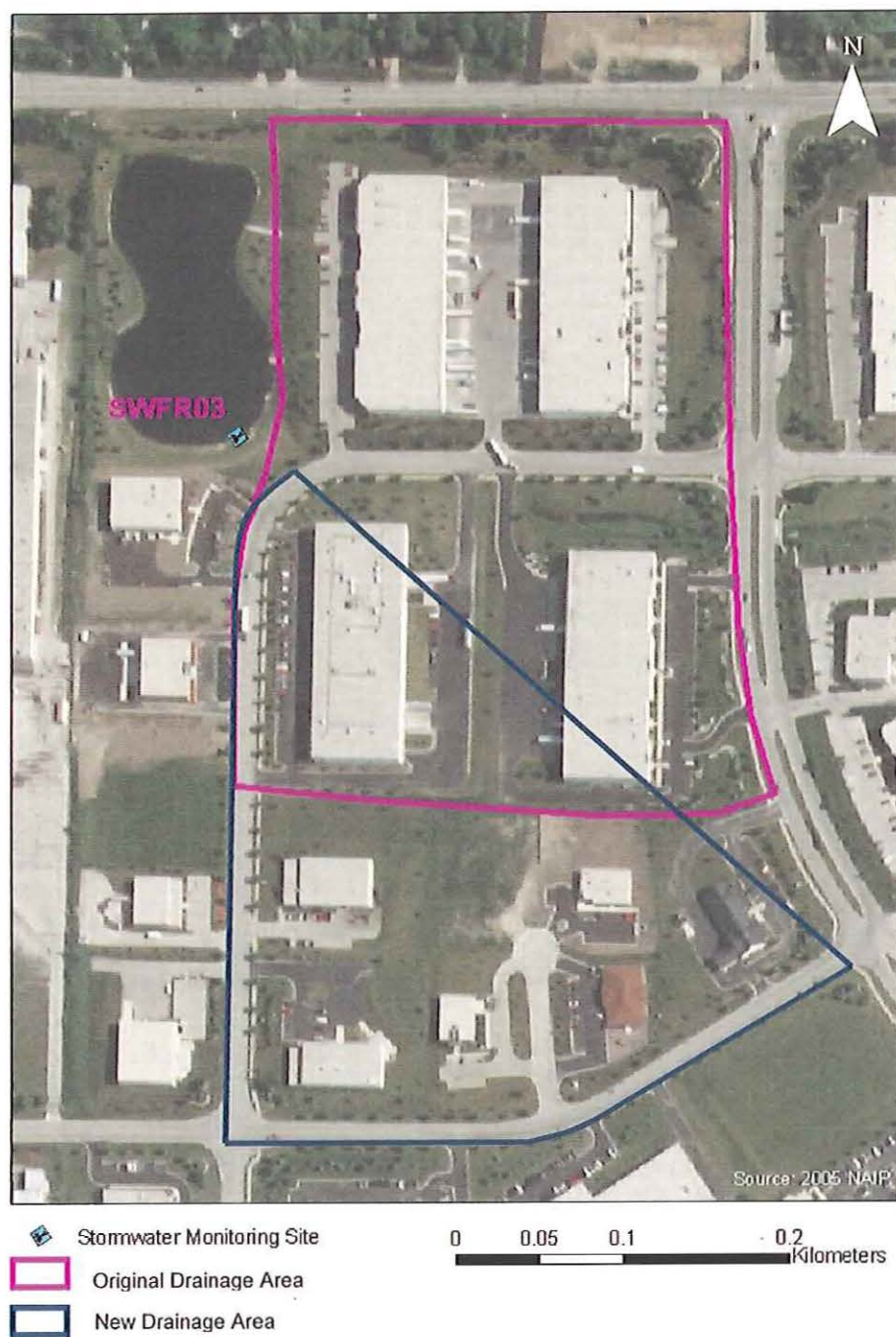


Figure 4.8. An aerial photograph of site SWFR03 (54th & Ashland, Franklin) with new drainage boundary.

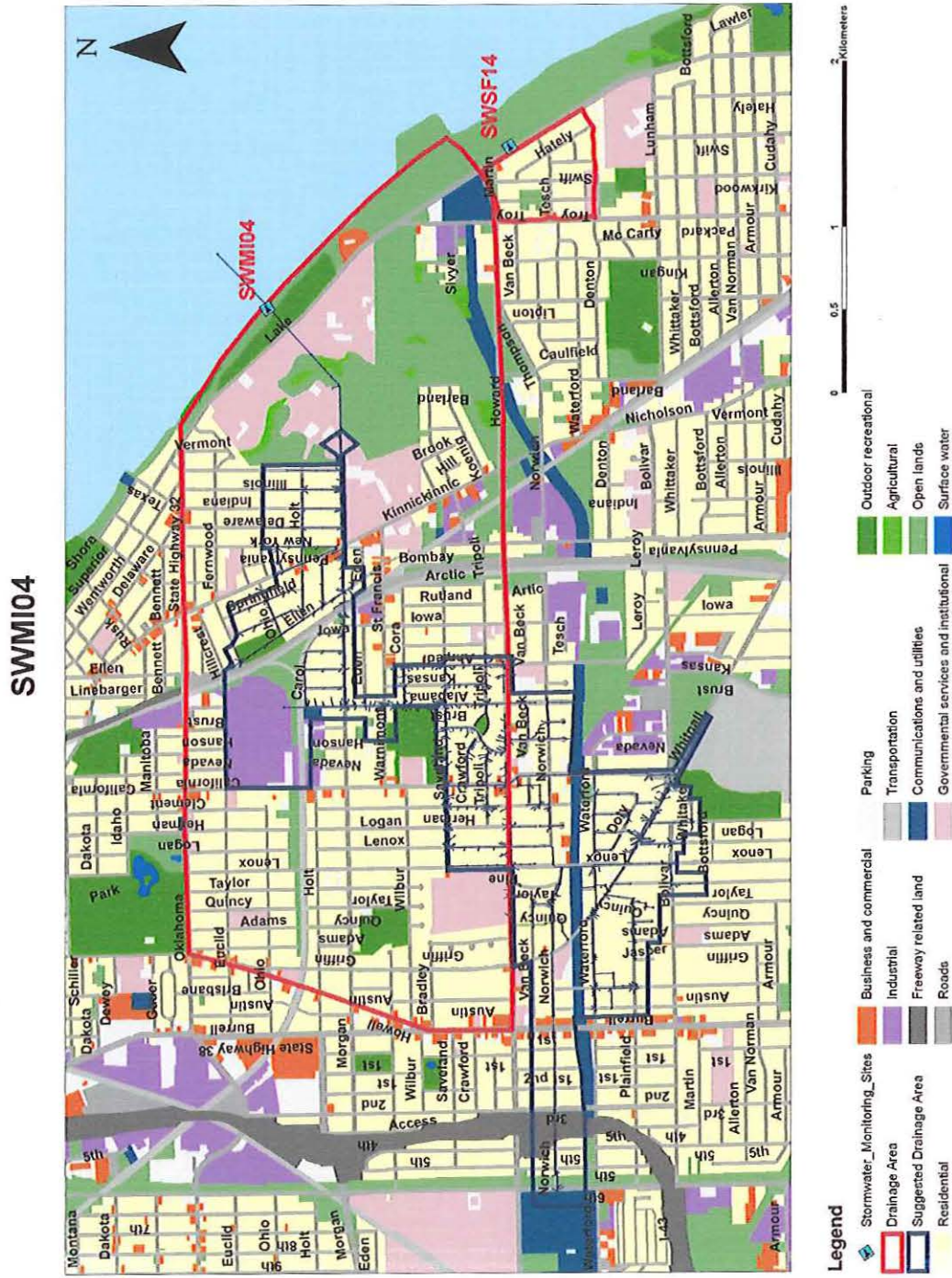


Figure 4.9. A map of site SWMI04 (3500 S. Lake Dr @ Bayview Park, Milwaukee) with land uses and new drainage boundary.

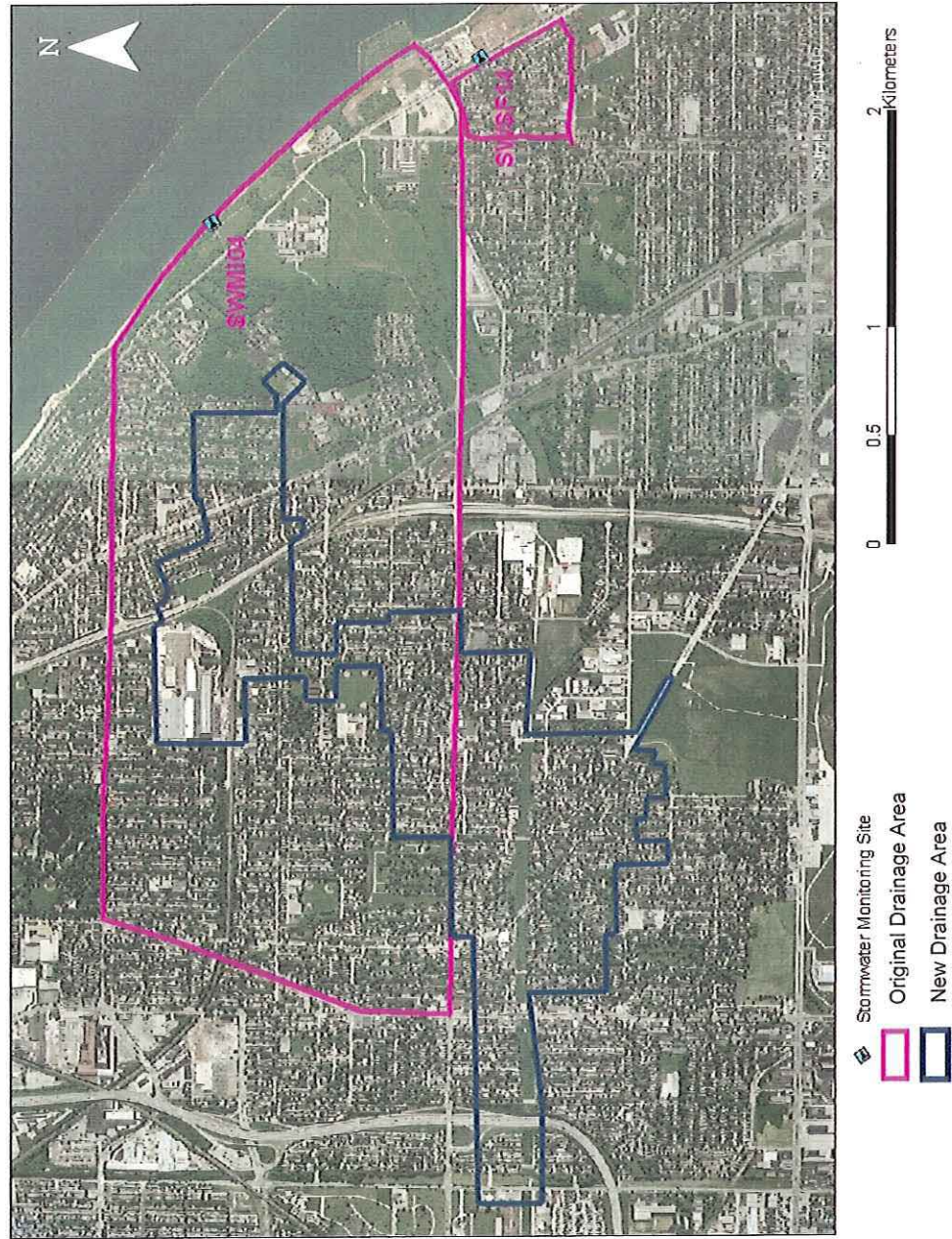


Figure 4.10. An aerial photograph of site SWMI04 (3500 S. Lake Dr @ Bayview Park, Milwaukee) with new drainage boundary.

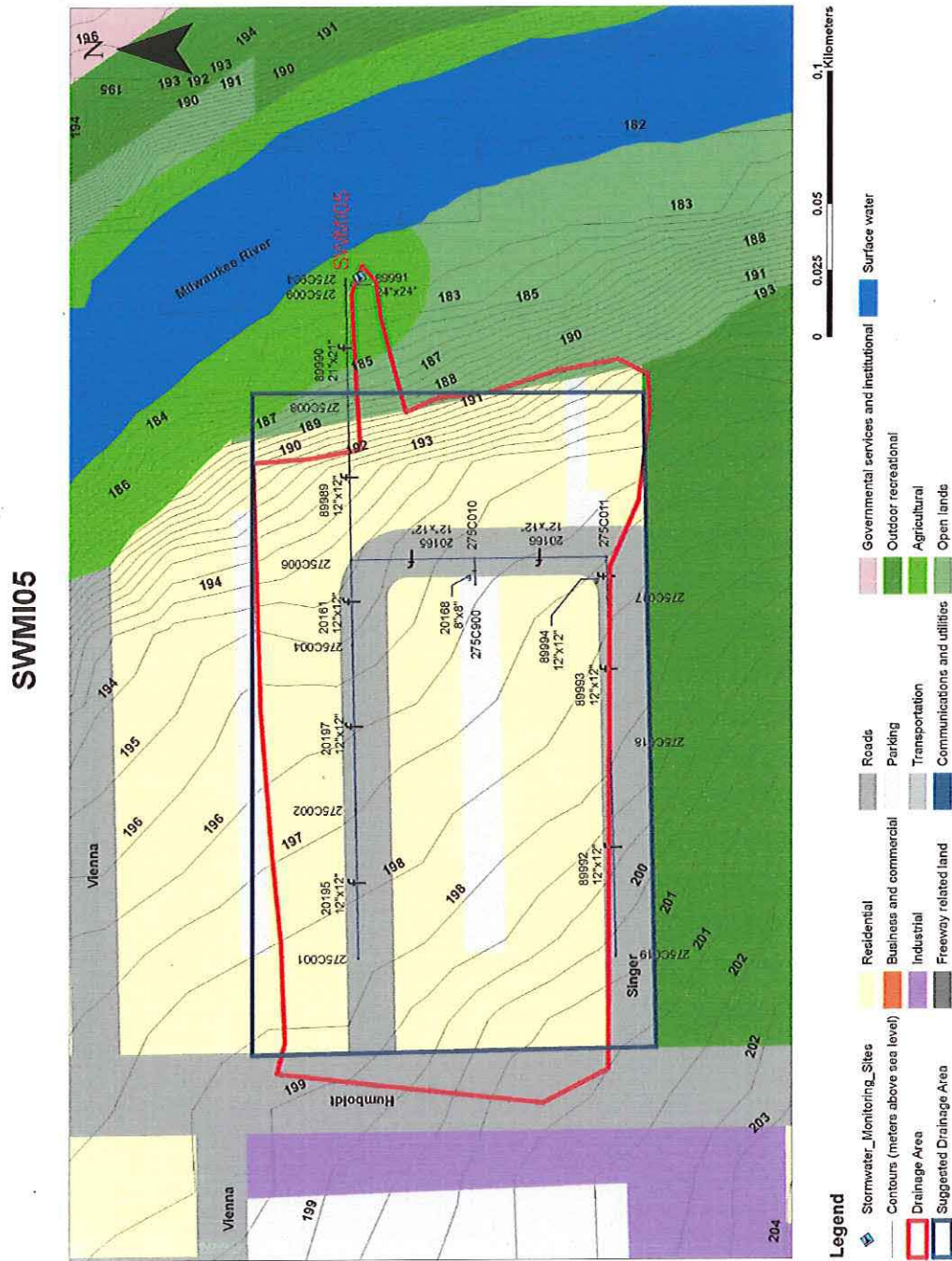


Figure 4.11. A map of site SWMI05 (1200 E. Singer Circle, Milwaukee) with land uses and new drainage boundary.

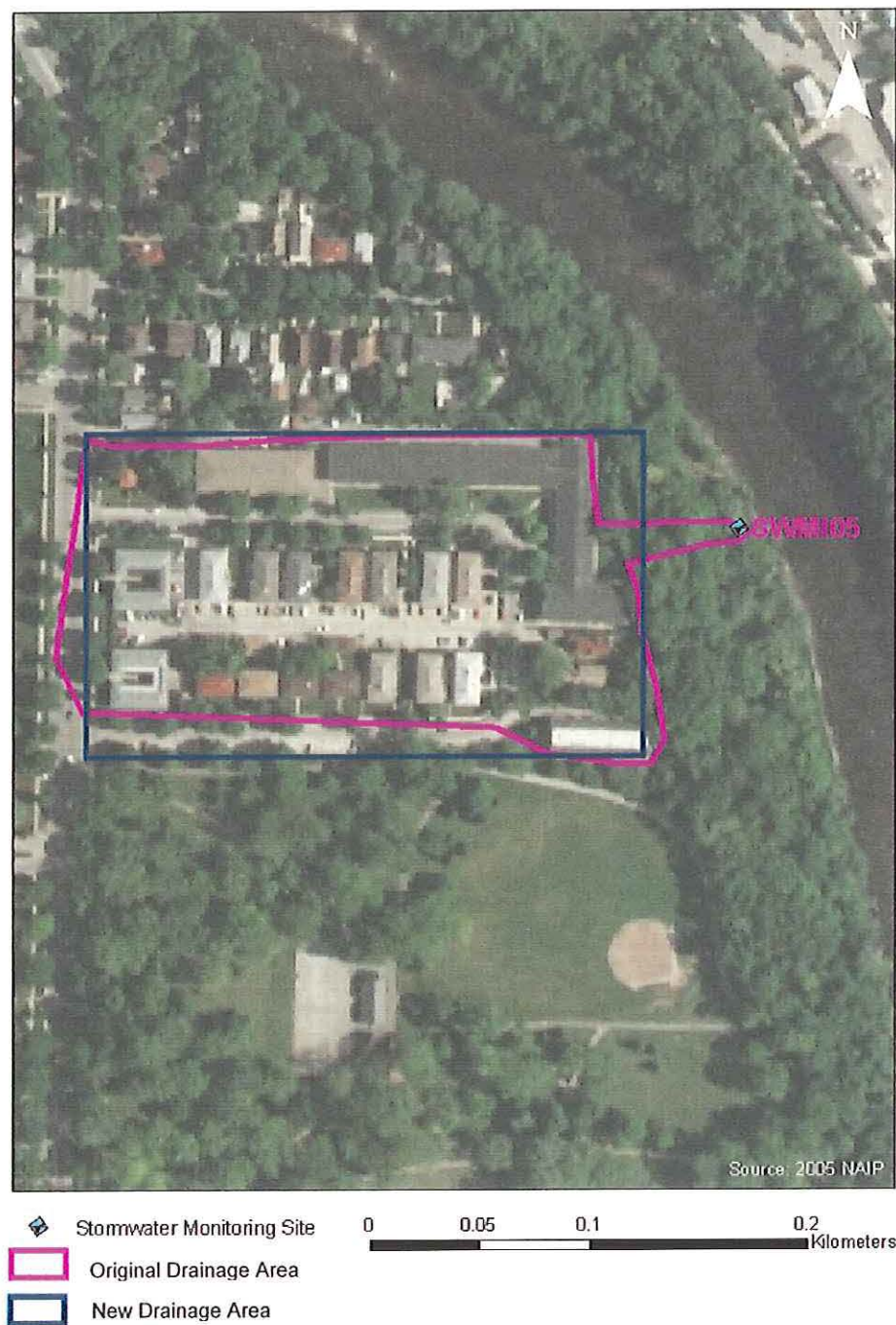


Figure 4.12. An aerial photograph of site SWMI05 (1200 E. Singer Circle, Milwaukee) with new drainage boundary.

SWMI06



Legend

- | | | |
|-----------------------------------|------------------------------|---|
| Stormwater monitoring sites | Industrial | Governmental services and institutional |
| Contours (meters above sea level) | Freeway related land | Outdoor recreational |
| Drainage area | Roads | Agricultural |
| Suggested drainage area | Parking | Open lands |
| Residential | Transportation | Surface water |
| Business and commercial | Communications and utilities | |

Figure 4.13. A map of site SWMI06 (Milwaukee County Zoo, Milwaukee) with land uses and new drainage boundary.

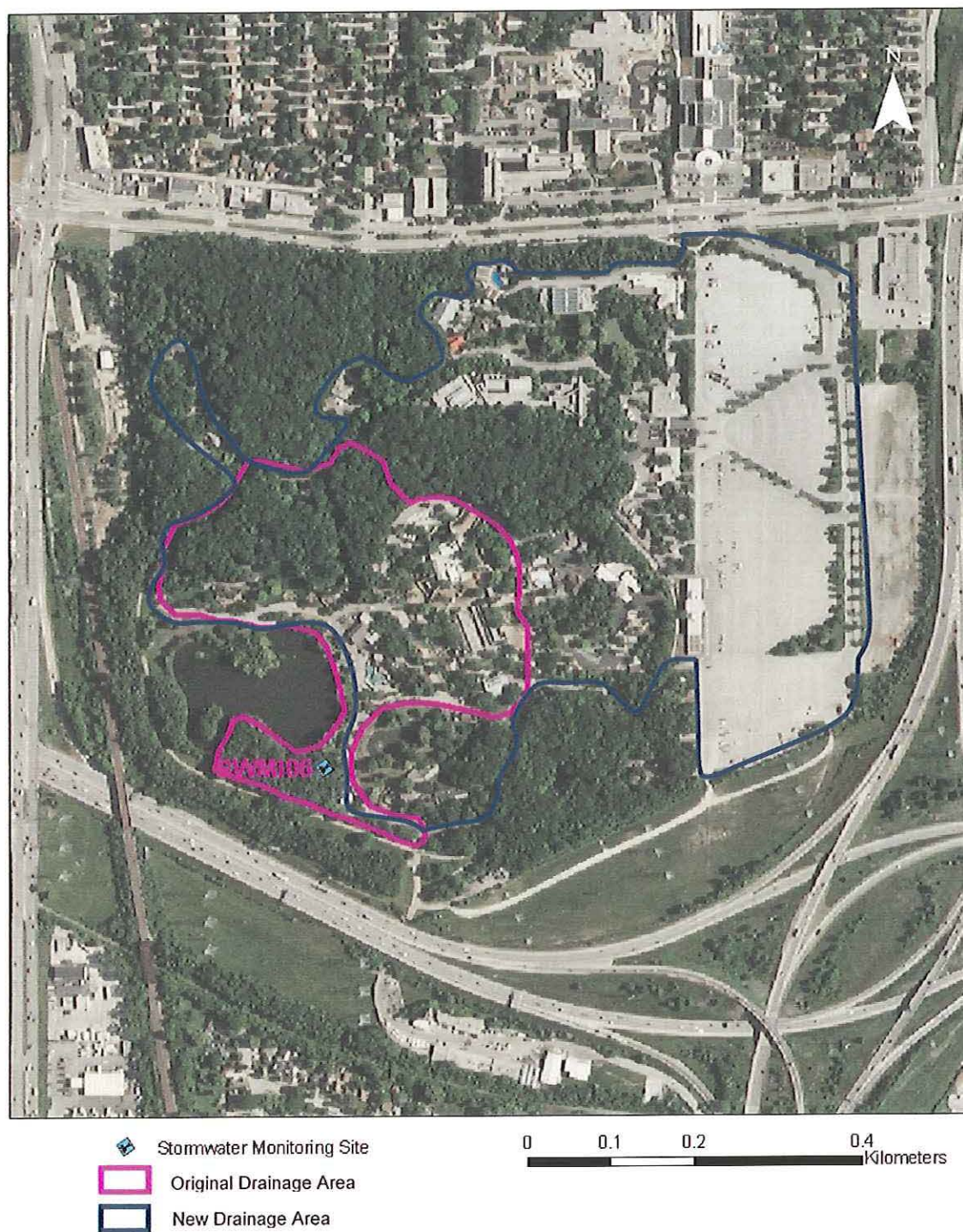


Figure 4.14. An aerial photograph of site SWMI06 (Milwaukee County Zoo, Milwaukee) with new drainage boundary.

SWMI07

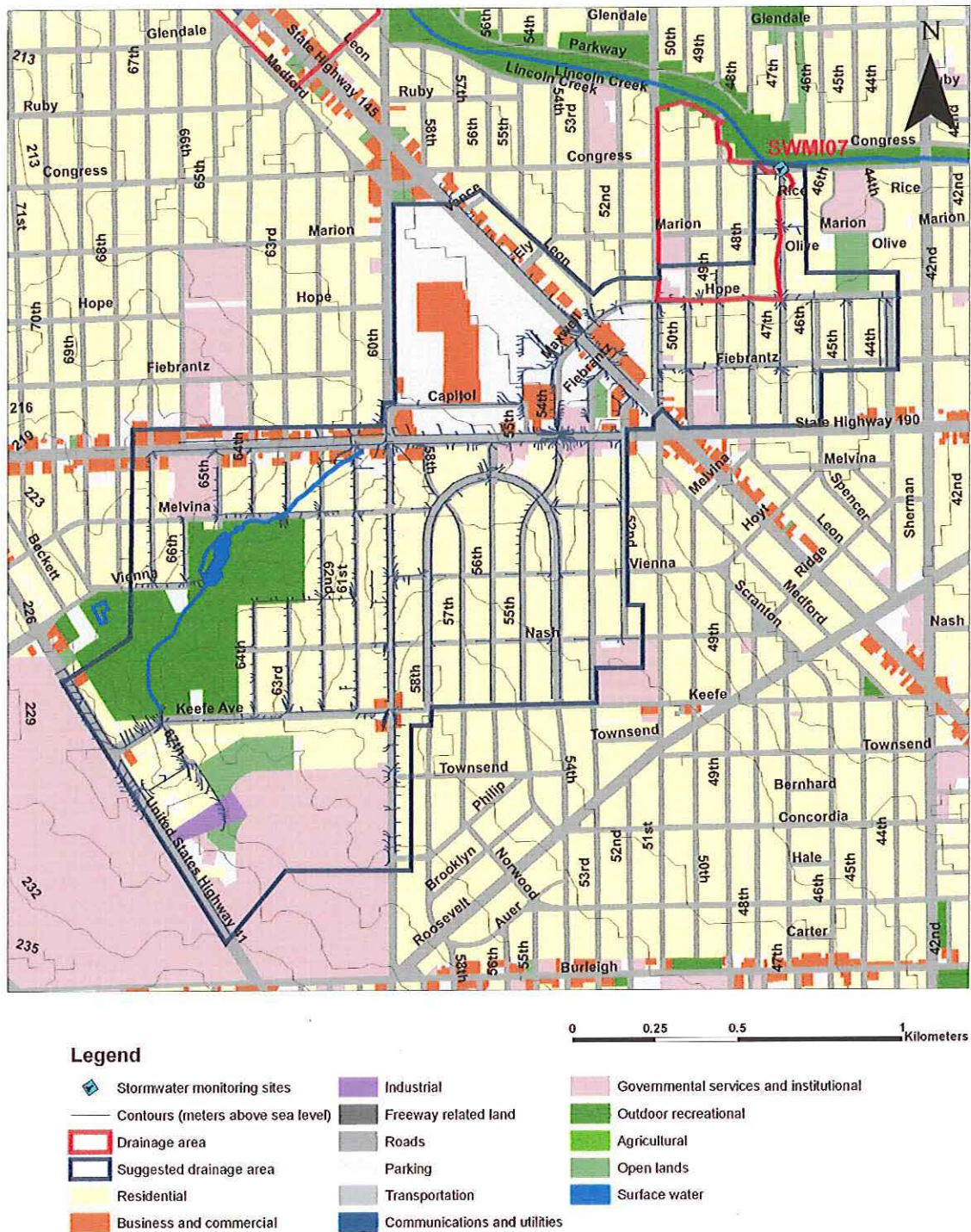


Figure 4.15. A map of site SWMI07 (4345 N. 47th St, Milwaukee) with land uses and new drainage boundary.

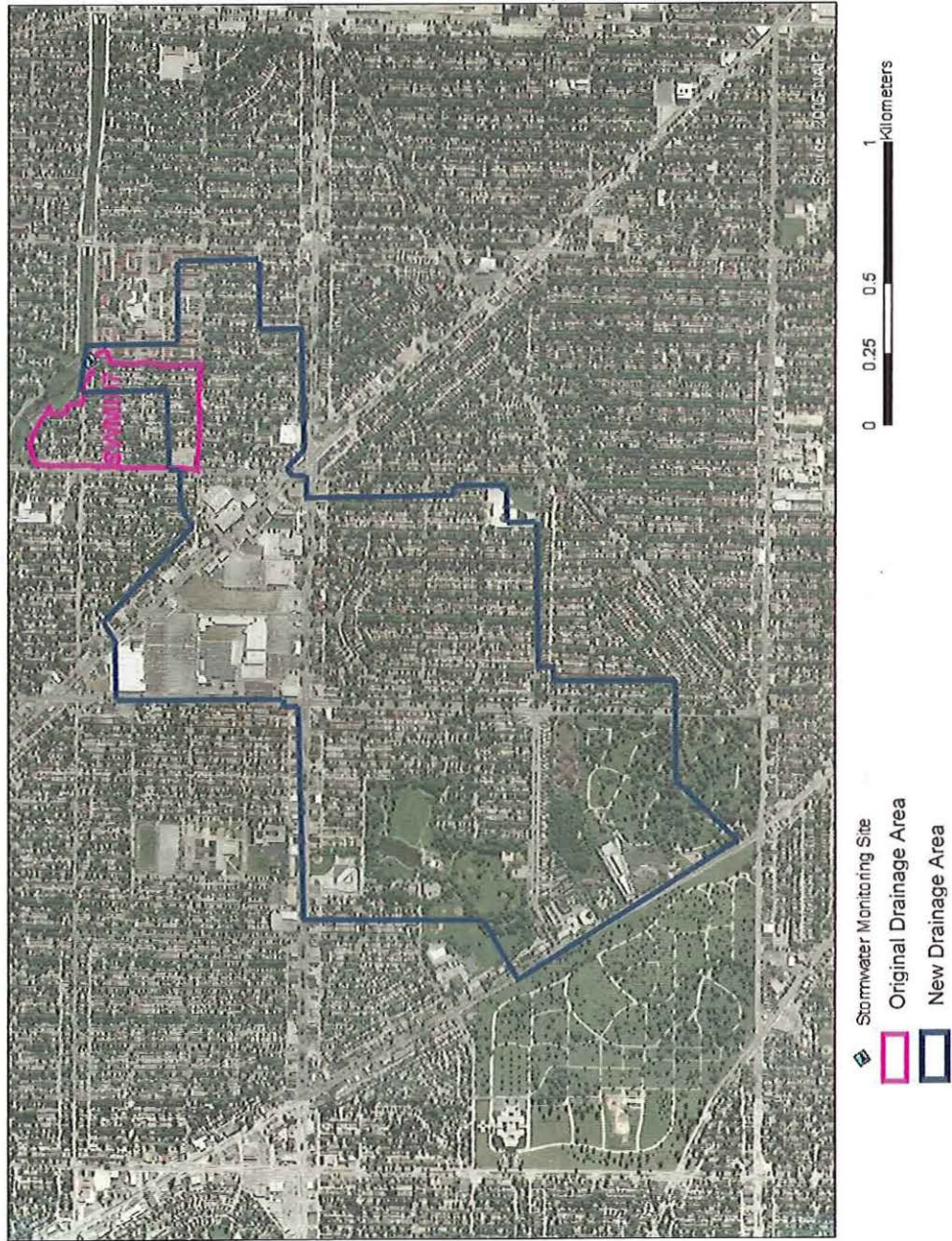


Figure 4.16. An aerial photograph of site SWMI07 (4345 N. 47th St, Milwaukee) with new drainage boundary.

SWMI08

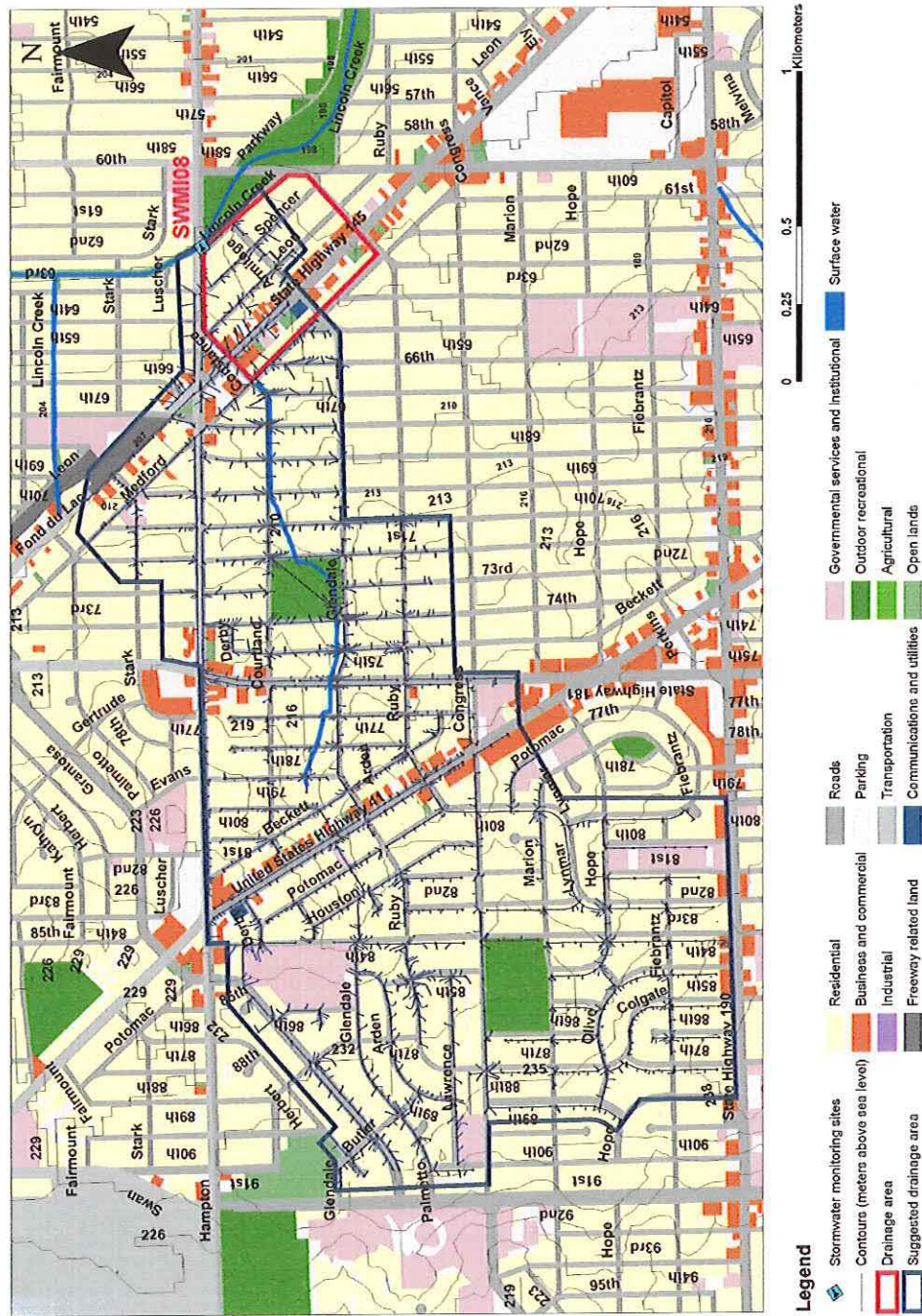


Figure 4.17. A map of site SWMI08 (Hampton & Lincoln Crk Pkwy, Milwaukee) with land uses and new drainage boundary.

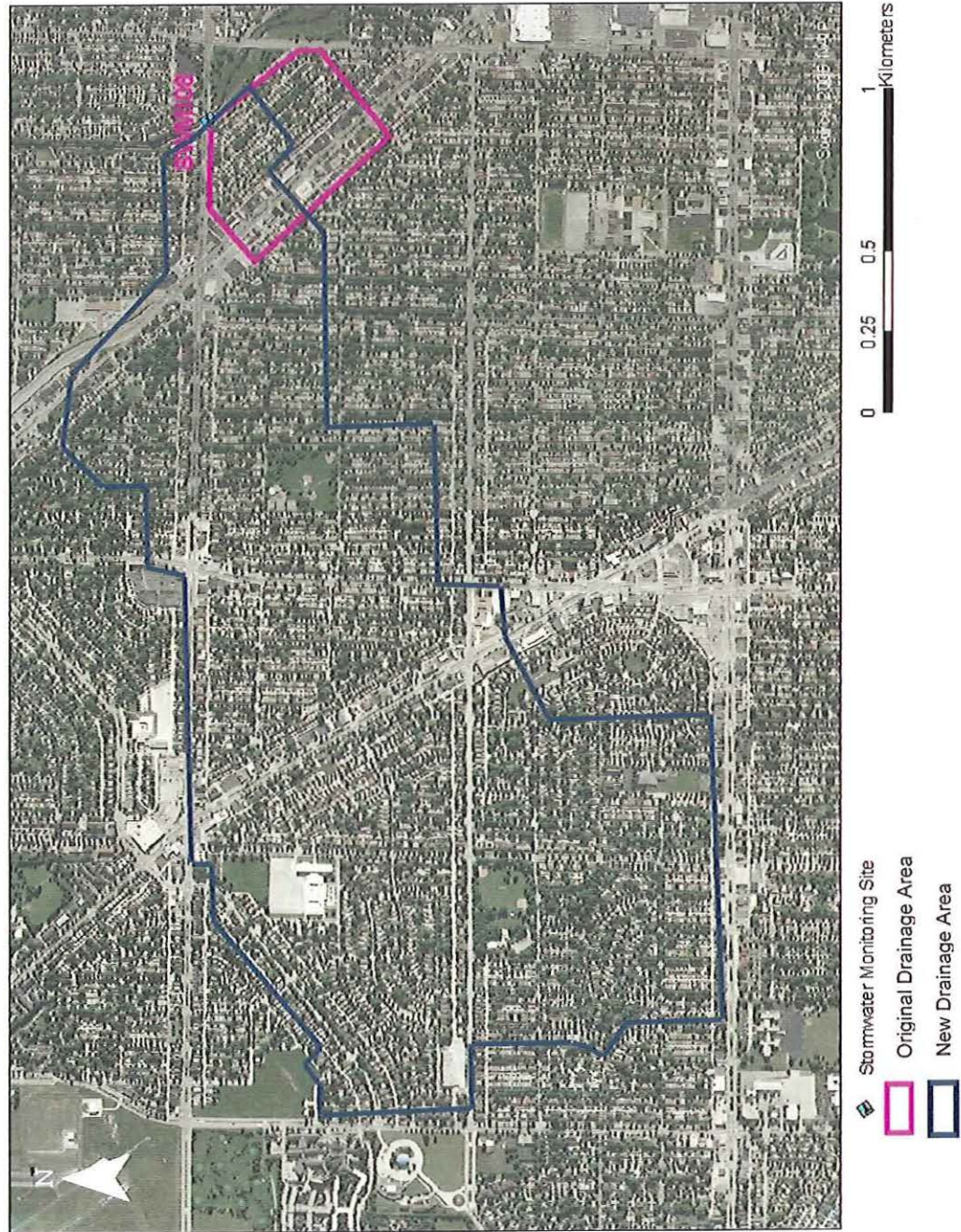


Figure 4.18. An aerial photograph of site SWMI08 (Hampton & Lincoln Crk Pkwy, Milwaukee) with new drainage boundary.

SWWB09

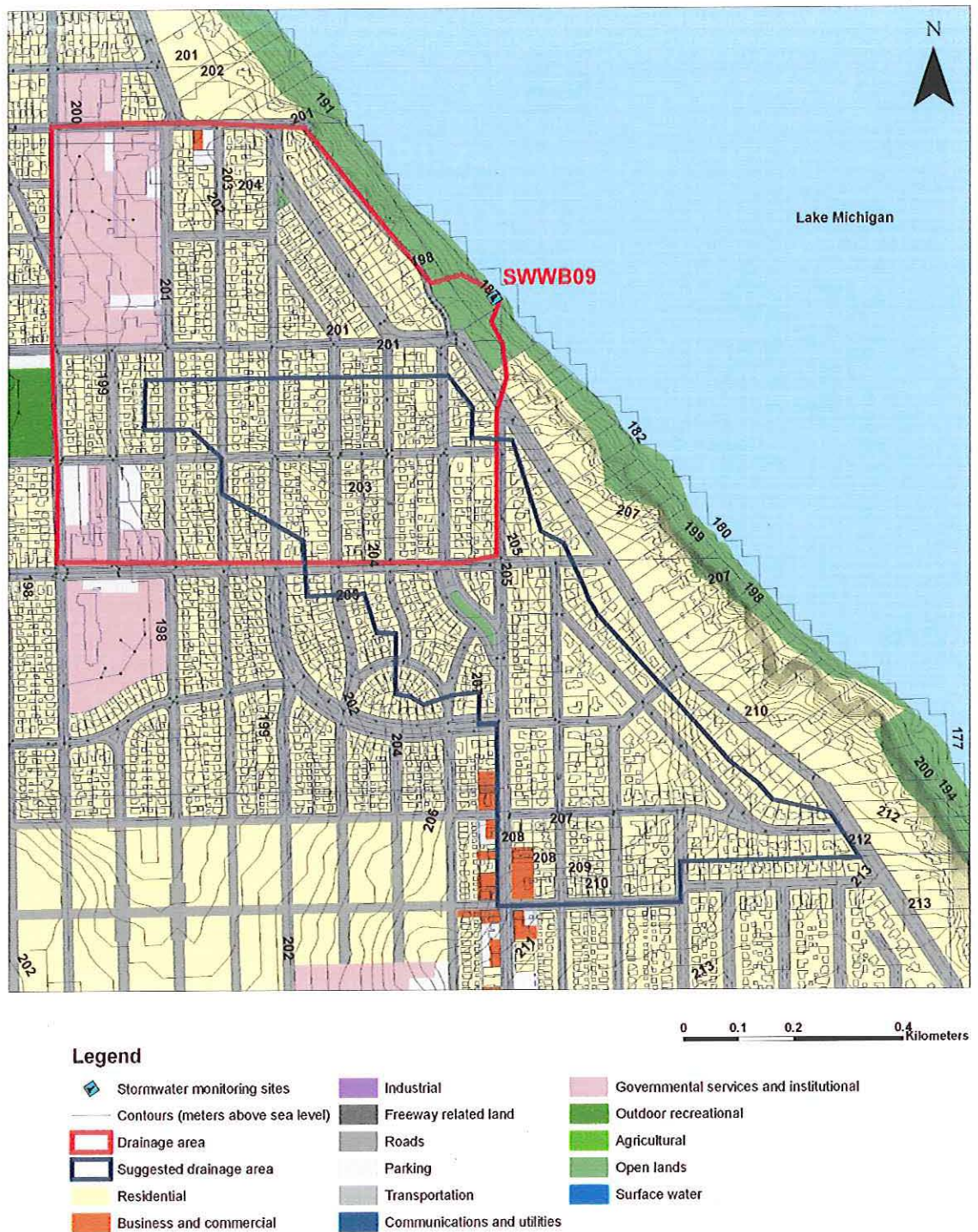


Figure 4.19. A map of site SWWB09 (4939 N. Newhall, Whitefish Bay) with land uses and new drainage boundary.

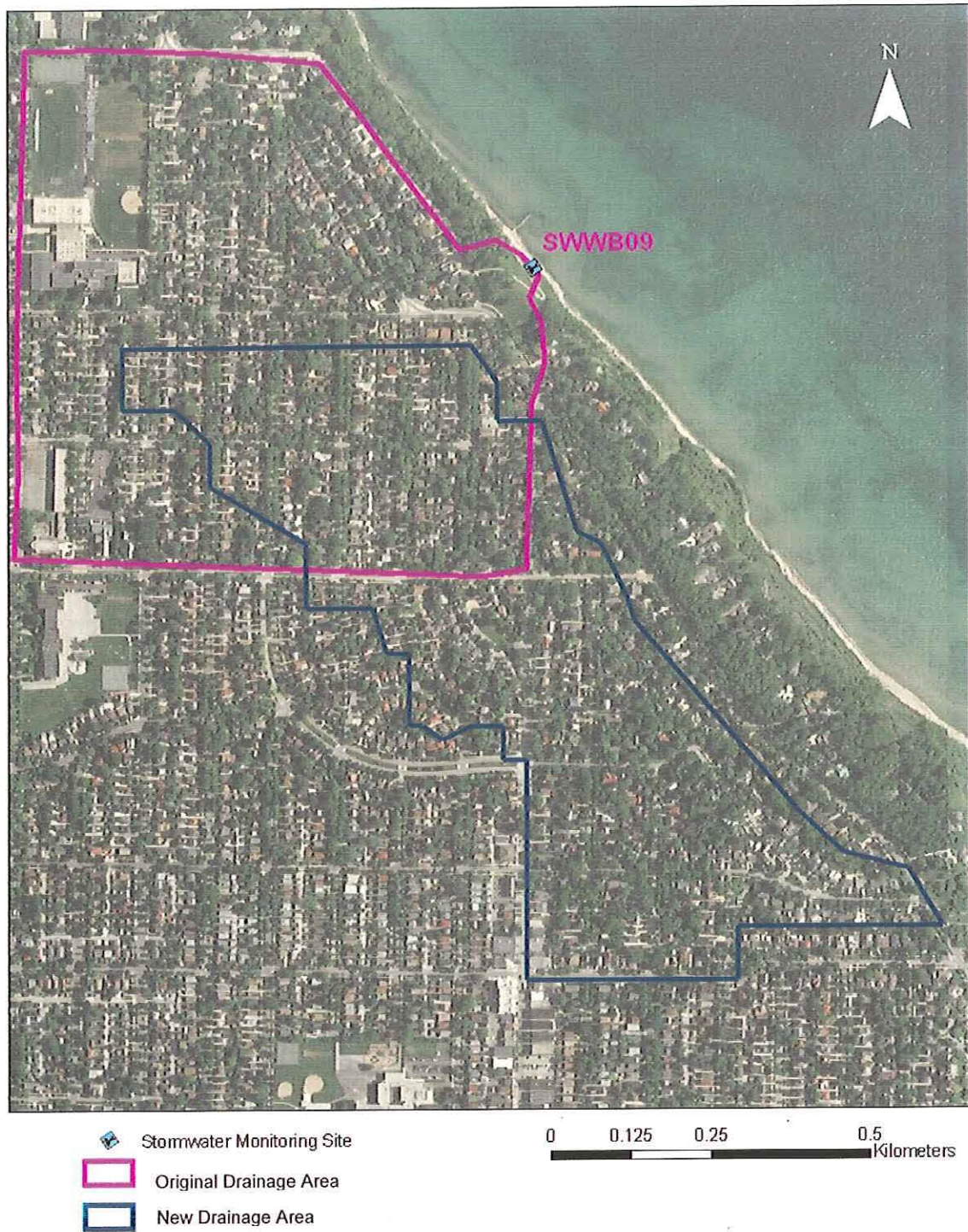


Figure 4.20. An aerial photograph of site SWWB09 (4939 N. Newhall, Whitefish Bay) with new drainage boundary.

SWGF10

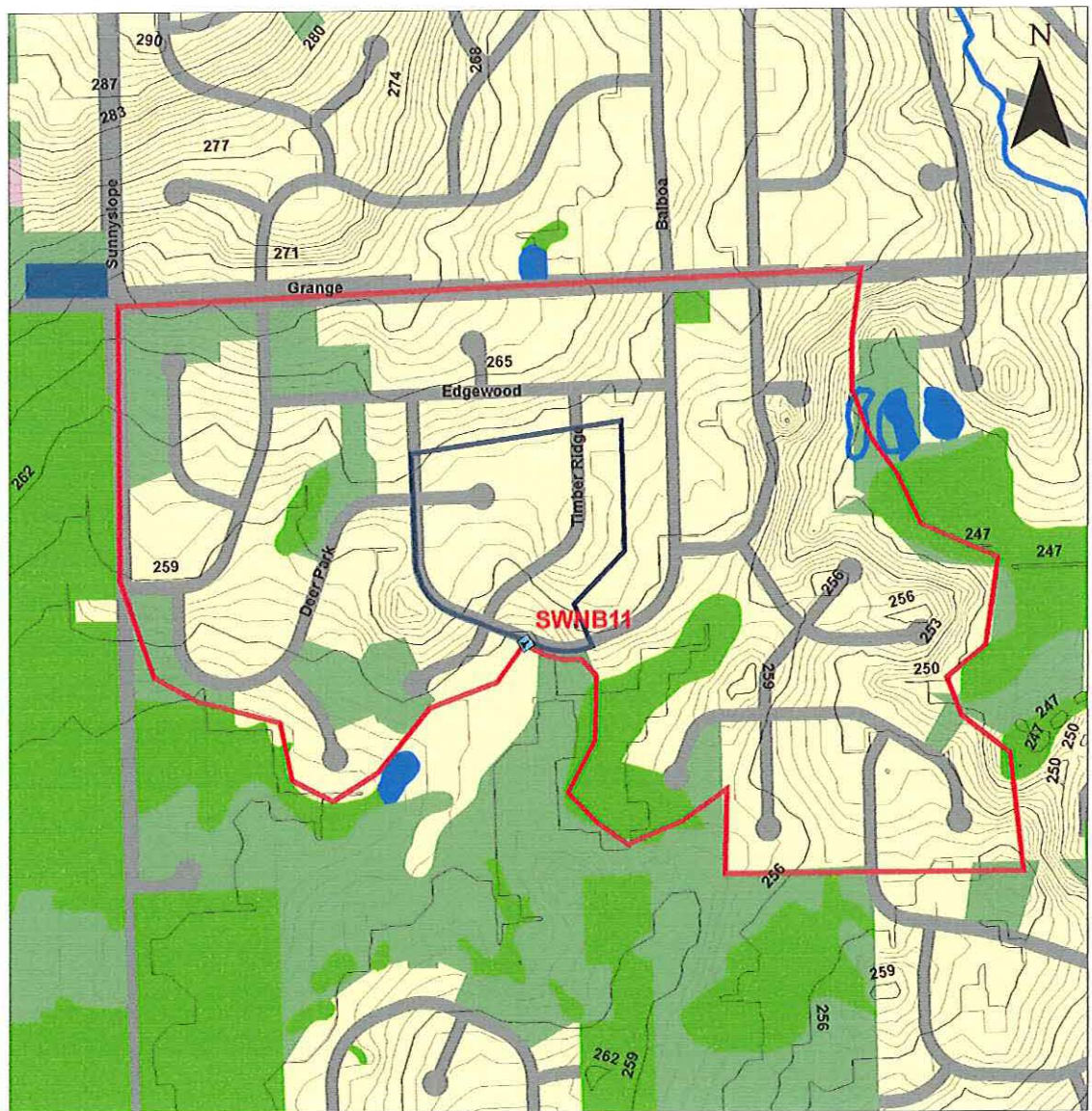


Figure 4.21. A map of site SWGF10 (Boerner Botanical Gardens, Hales Corners, Greenfield) with land uses and new drainage boundary.



Figure 4.22. An aerial photograph of site SWGF10 (Boerner Botanical Gardens, Hales Corners, Greenfield) with new drainage boundary.

SWNB11



Legend

- | | | |
|-----------------------------------|------------------------------|---|
| Stormwater_Monitoring_Sites | Industrial | Governmental services and institutional |
| Contours (meters above sea level) | Freeway related land | Outdoor recreational |
| Drainage area | Roads | Agricultural |
| Suggested drainage area | Parking | Open lands |
| Residential | Transportation | Surface water |
| Business and commercial | Communications and utilities | |

0 0.1 0.2 0.4 Kilometers

Figure 4.23. A map of site SWNB11 (13380 Eagle Trace & Timber Ridge, New Berlin) with land uses and new drainage boundary.

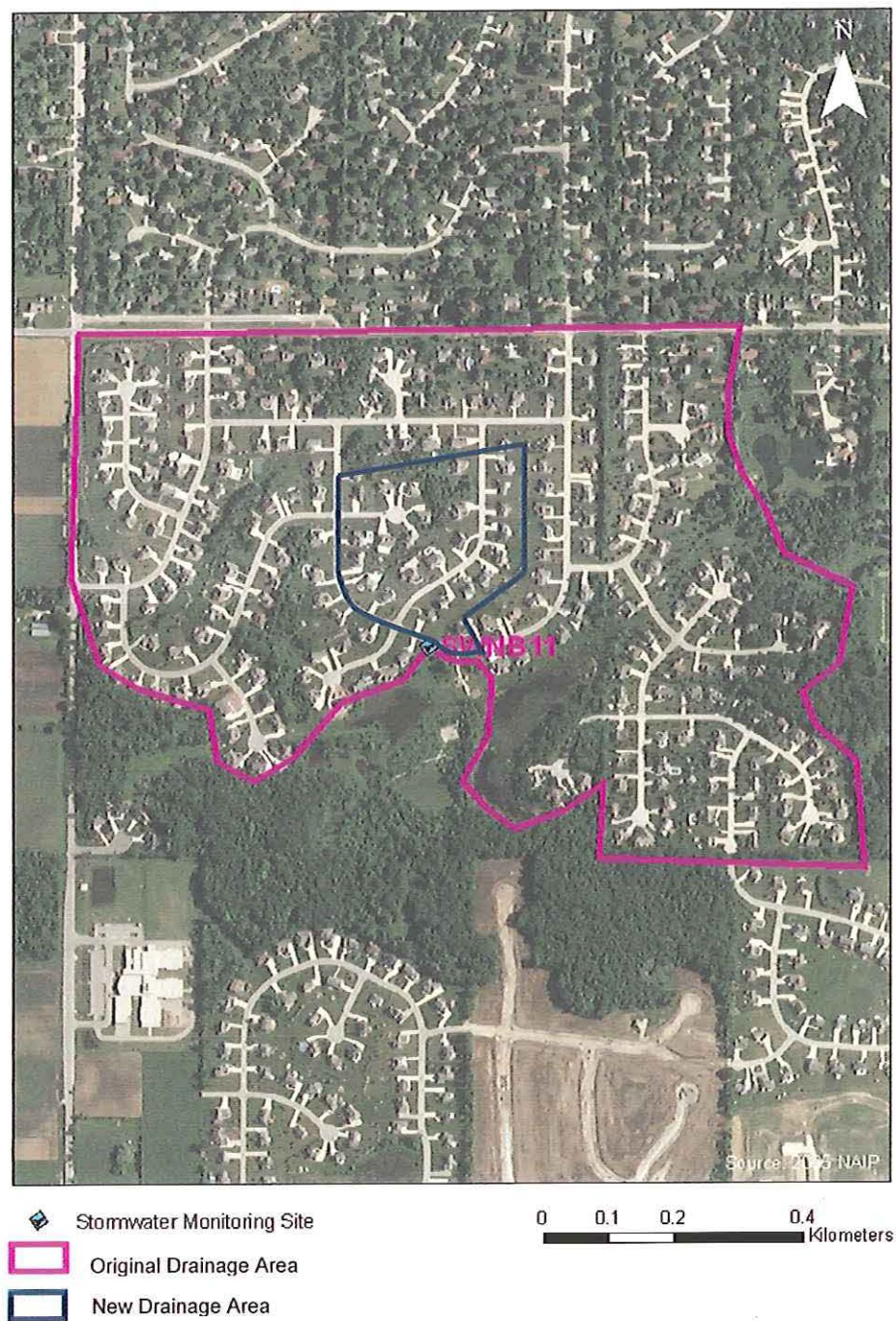
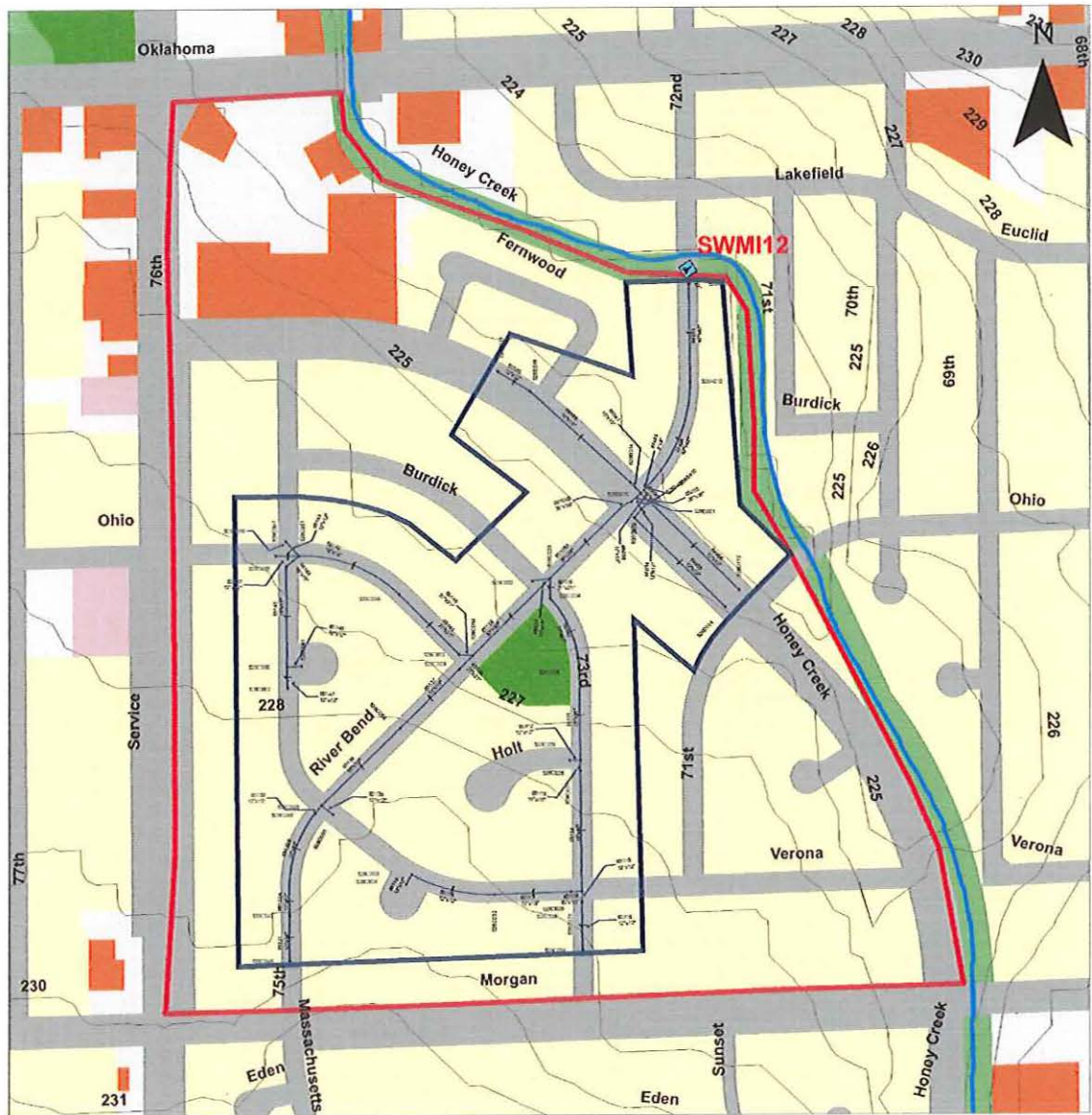


Figure 4.24. An aerial photograph of site SWNB11 (13380 Eagle Trace & Timber Ridge, New Berlin) with new drainage boundary.

SWMI12



Legend

- | | | |
|-----------------------------------|------------------------------|---|
| Stormwater monitoring sites | Industrial | Governmental services and institutional |
| Contours (meters above sea level) | Freeway related land | Outdoor recreational |
| Drainage area | Roads | Agricultural |
| Suggested drainage area | Parking | Open lands |
| Residential | Transportation | Surface water |
| Business and commercial | Communications and utilities | |

Figure 4.25. A map of site SWMI12 (3275 S. 72nd St, Milwaukee) with land uses and new drainage boundary.



Figure 4.26. An aerial photograph of site SWMI12 (3275 S. 72nd St, Milwaukee) with new drainage boundary.

SWWA13



Legend

- | | | |
|-----------------------------------|------------------------------|---|
| Stormwater monitoring site | Industrial | Governmental services and Institutional |
| Contours (meters above sea level) | Freeway related land | Outdoor Recreational |
| Drainage area | Roads | Agricultural |
| Suggested drainage area | Parking | Open lands |
| Residential | Transportation | Surface water |
| Business and commercial | Communications and Utilities | |

0 0.1 0.2 0.4 Kilometers

Figure 4.27. A map of site SWWA13 (Ridge Blvd & Harding, Wauwatosa) with land uses and new drainage boundary.

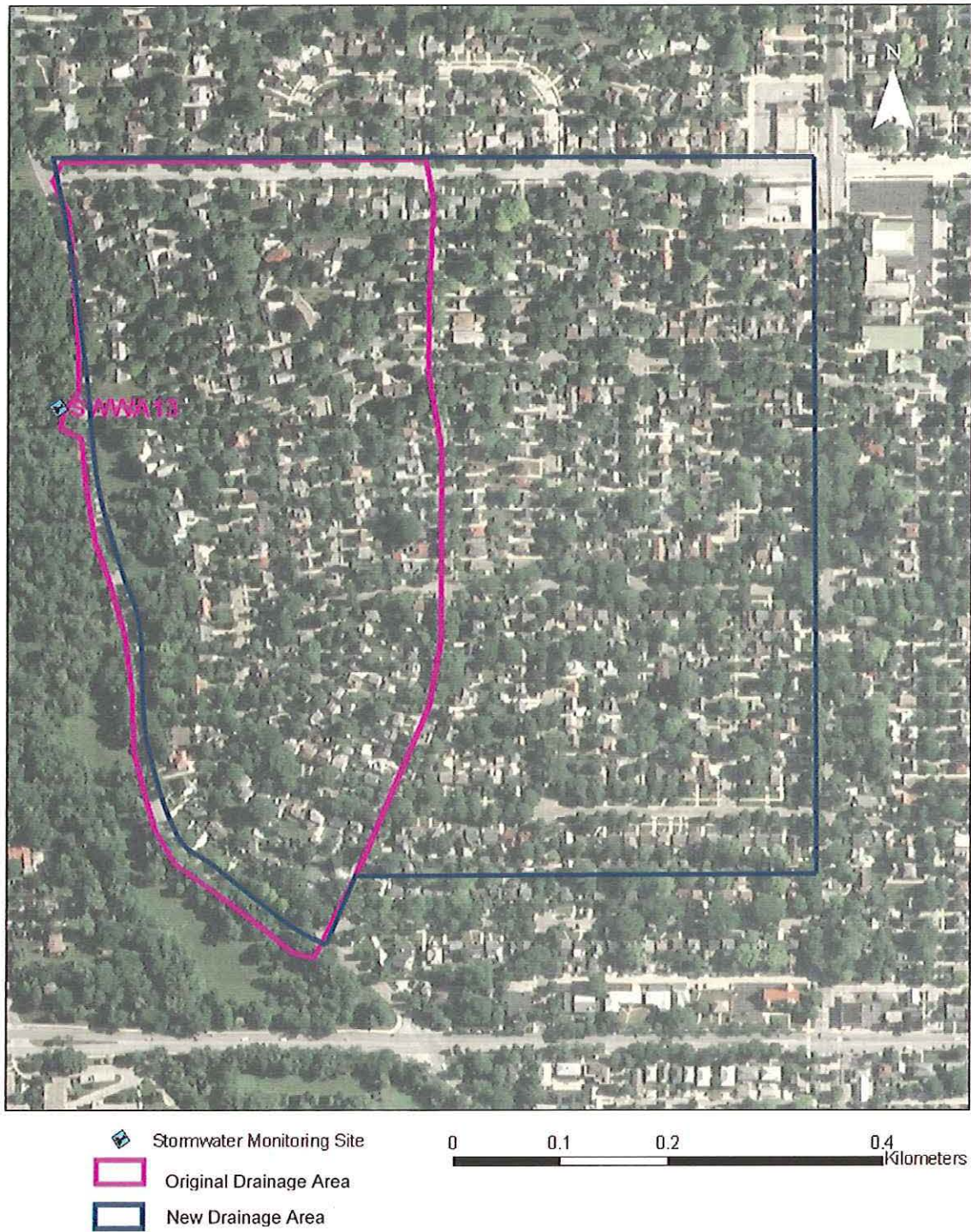


Figure 4.28. An aerial photograph of site SWWA13 (Ridge Blvd & Harding, Wauwatosa) with new drainage boundary.

SWSF14

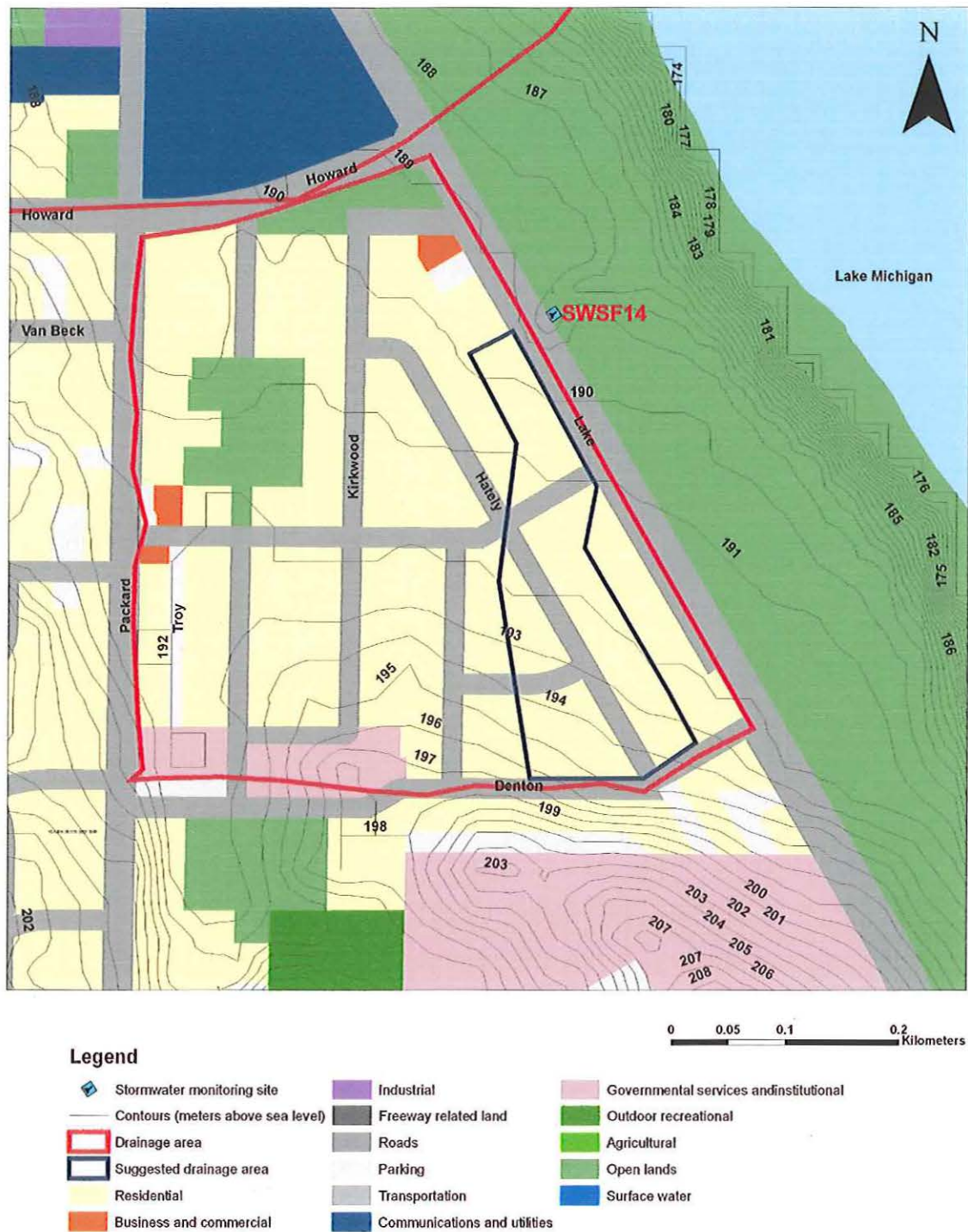


Figure 4.29. A map of site SWSF14 (Lake Dr and Tesch Av, St Francis) with land uses and new drainage boundary.



Figure 4.30. An aerial photograph of site SWSF14 (Lake Dr and Tesch Av, St Francis) with new drainage boundary.

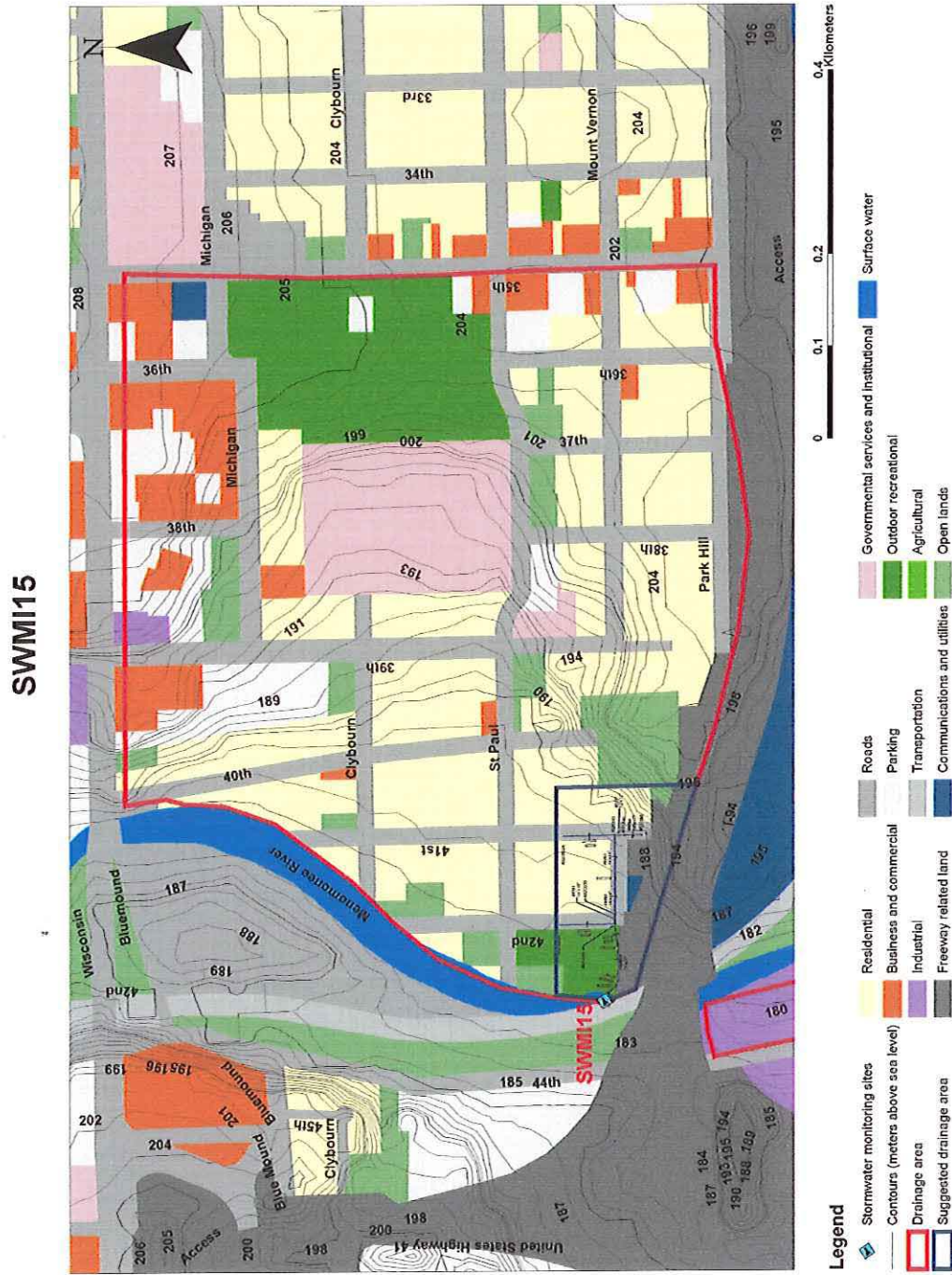


Figure 4.31. A map of site SWMI15 (42nd St & Mt Vernon, I-94 & Menomonee River, Milwaukee) with land uses and new drainage boundary.

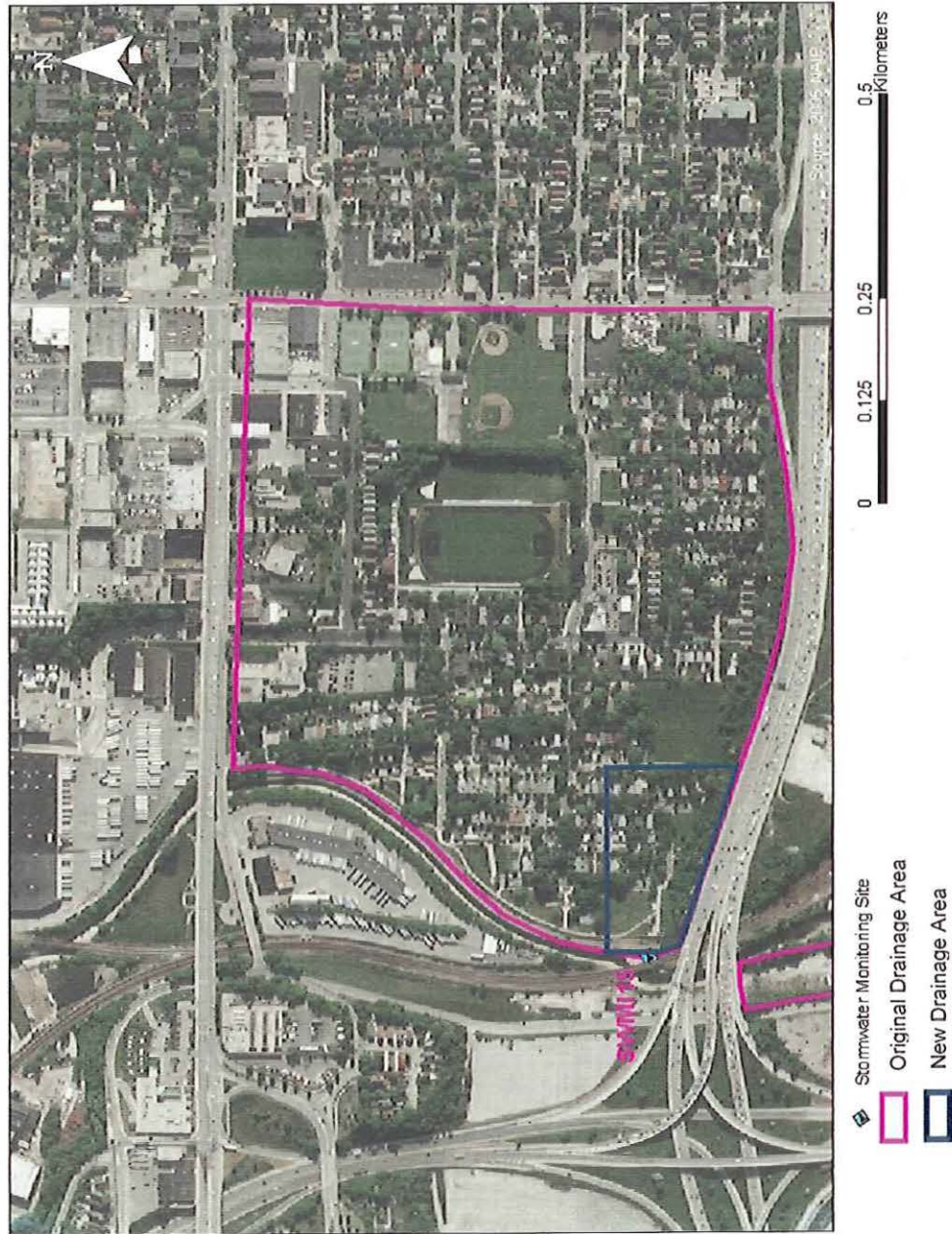


Figure 4.32. An aerial photograph of site SWMI15 (42nd St & Mt Vernon, I-94 & Menomonee River, Milwaukee) with new drainage boundary.

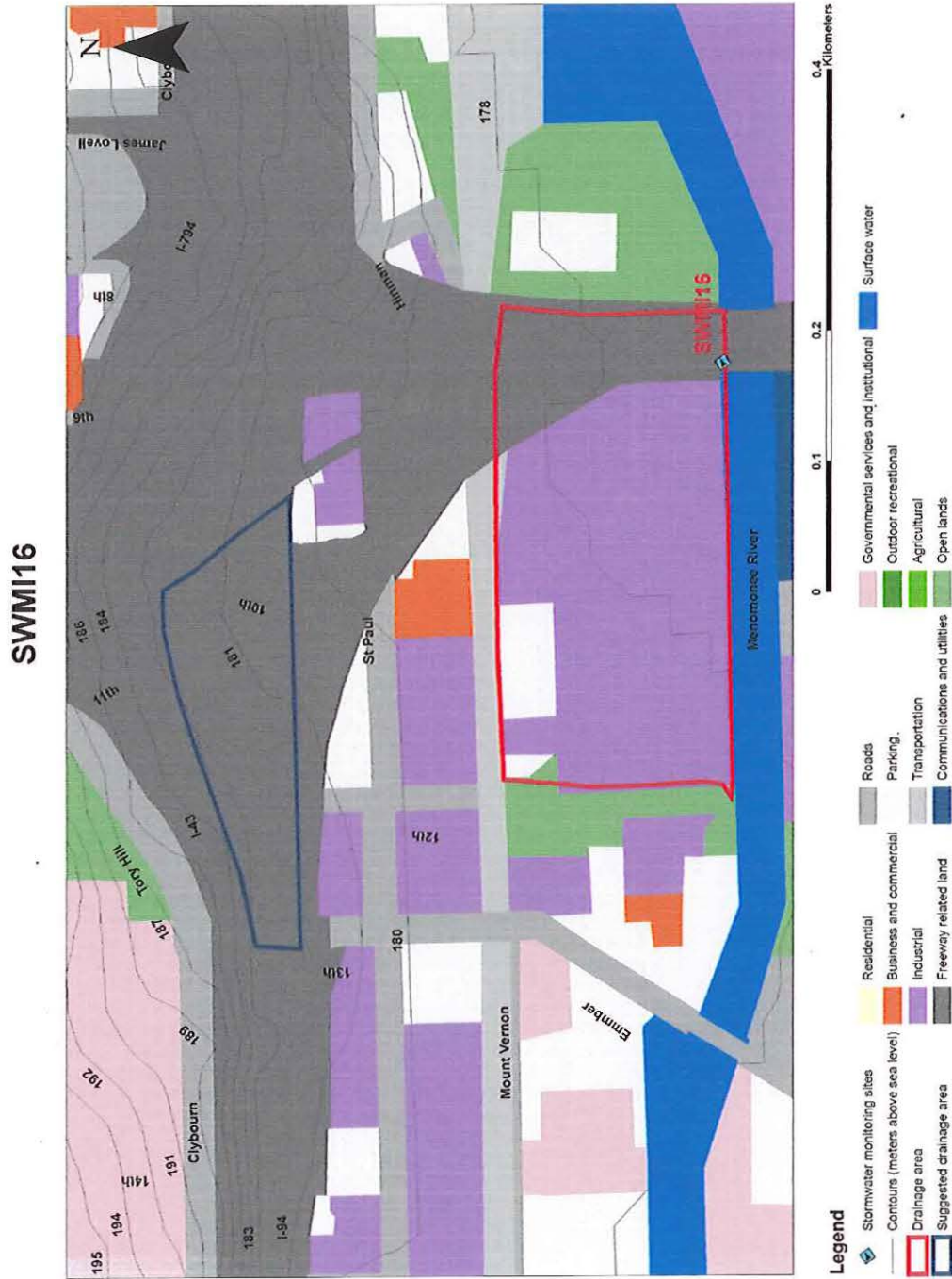


Figure 4.33. A map of site SWMI16 (Marquette interchange, Milwaukee) with land uses and new drainage boundary.

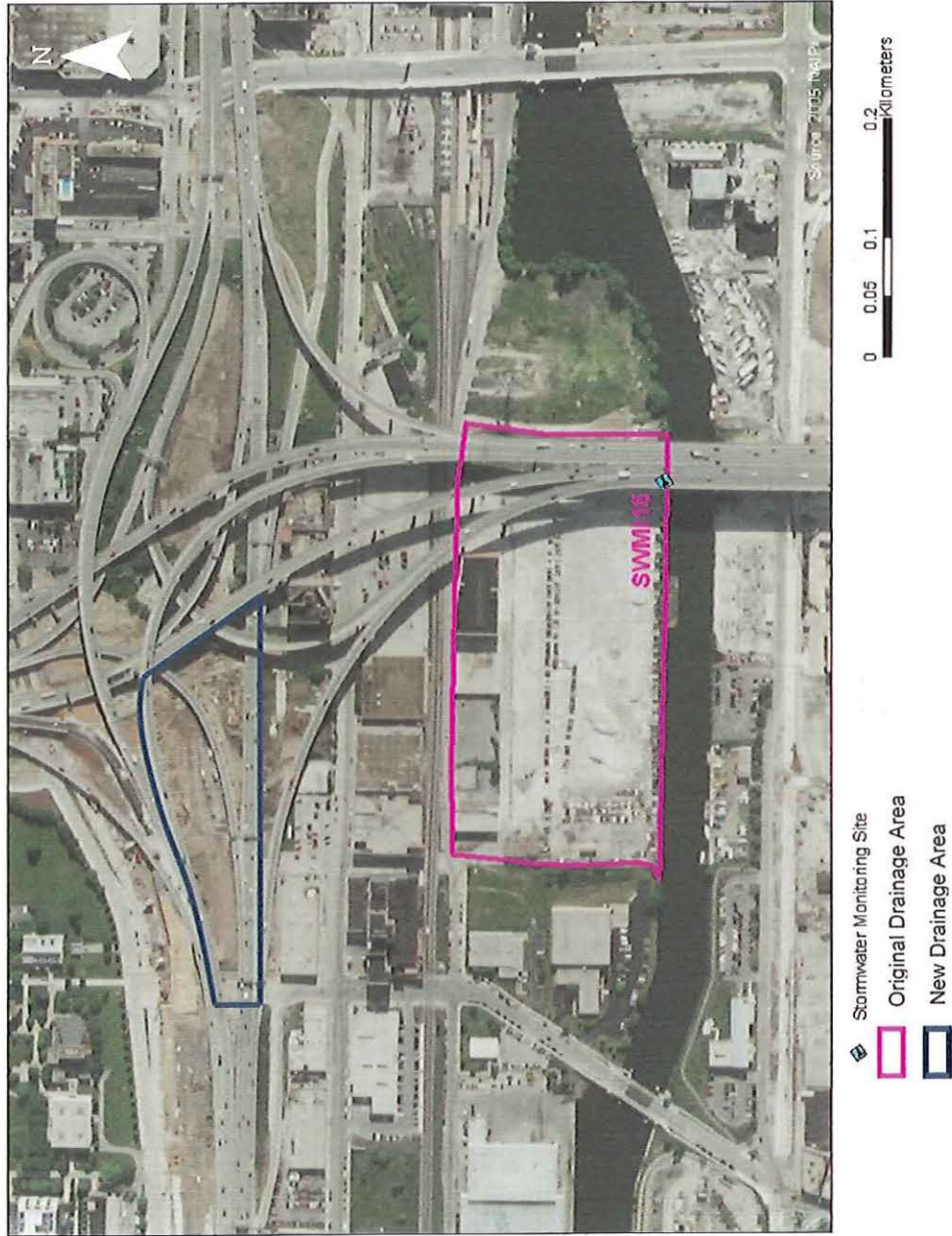
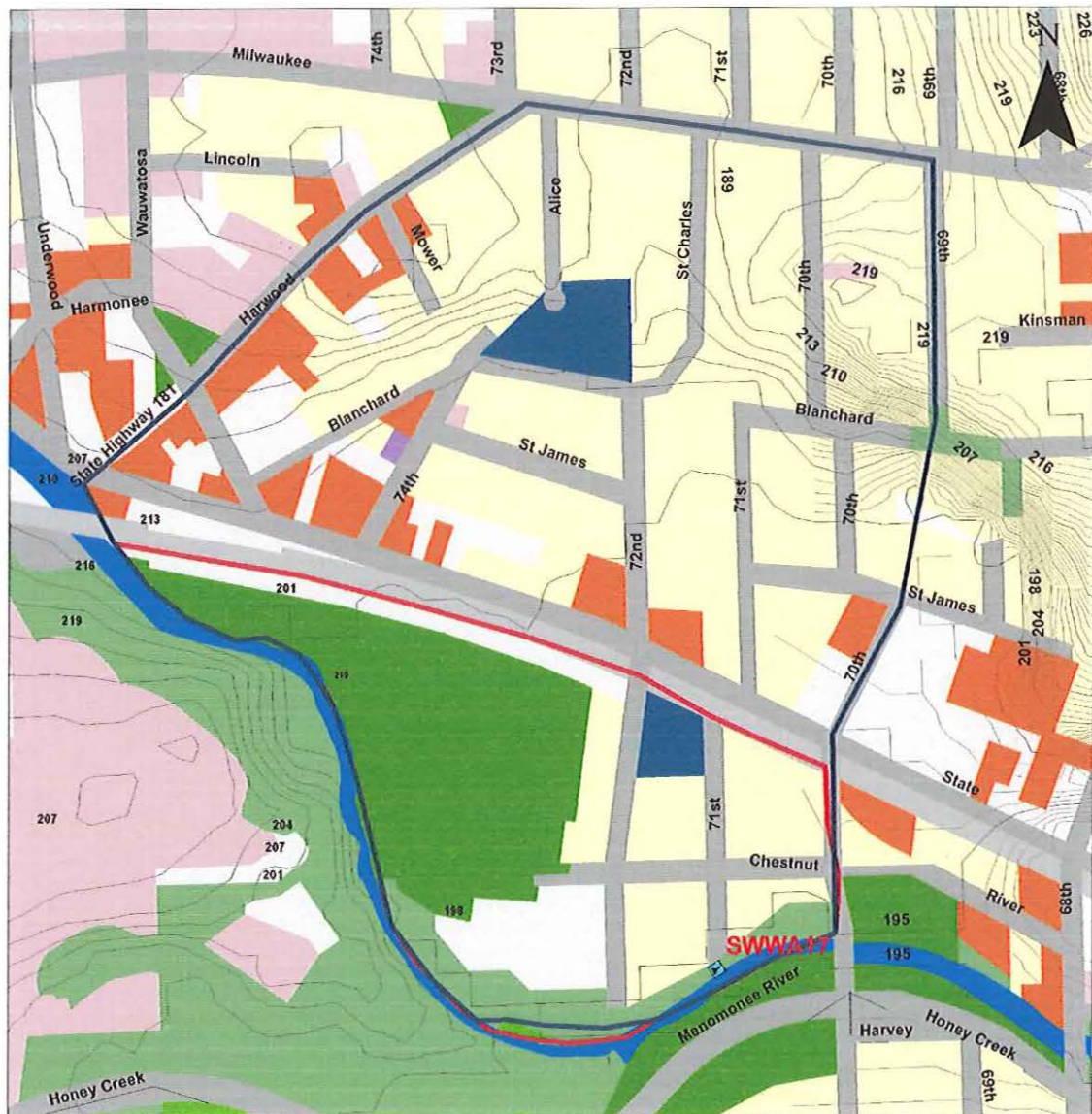


Figure 4.34. An aerial photograph of site SWMI16 (Marquette interchange, Milwaukee) with new drainage boundary.

SWWA17



Legend

- | | | |
|-----------------------------------|------------------------------|---|
| Stormwater monitoring sites | Industrial | Governmental services and institutional |
| Contours (meters above sea level) | Freeway related land | Outdoor recreational |
| Drainage area | Roads | Agricultural |
| Suggested drainage area | Parking | Open lands |
| Residential | Transportation | Surface water |
| Business and commercial | Communications and utilities | |

0 0.1 0.2 0.4 Kilometers

Figure 4.35. A map of site SWWA17 (71st and Chestnut St, Wauwatosa) with land uses and new drainage boundary.

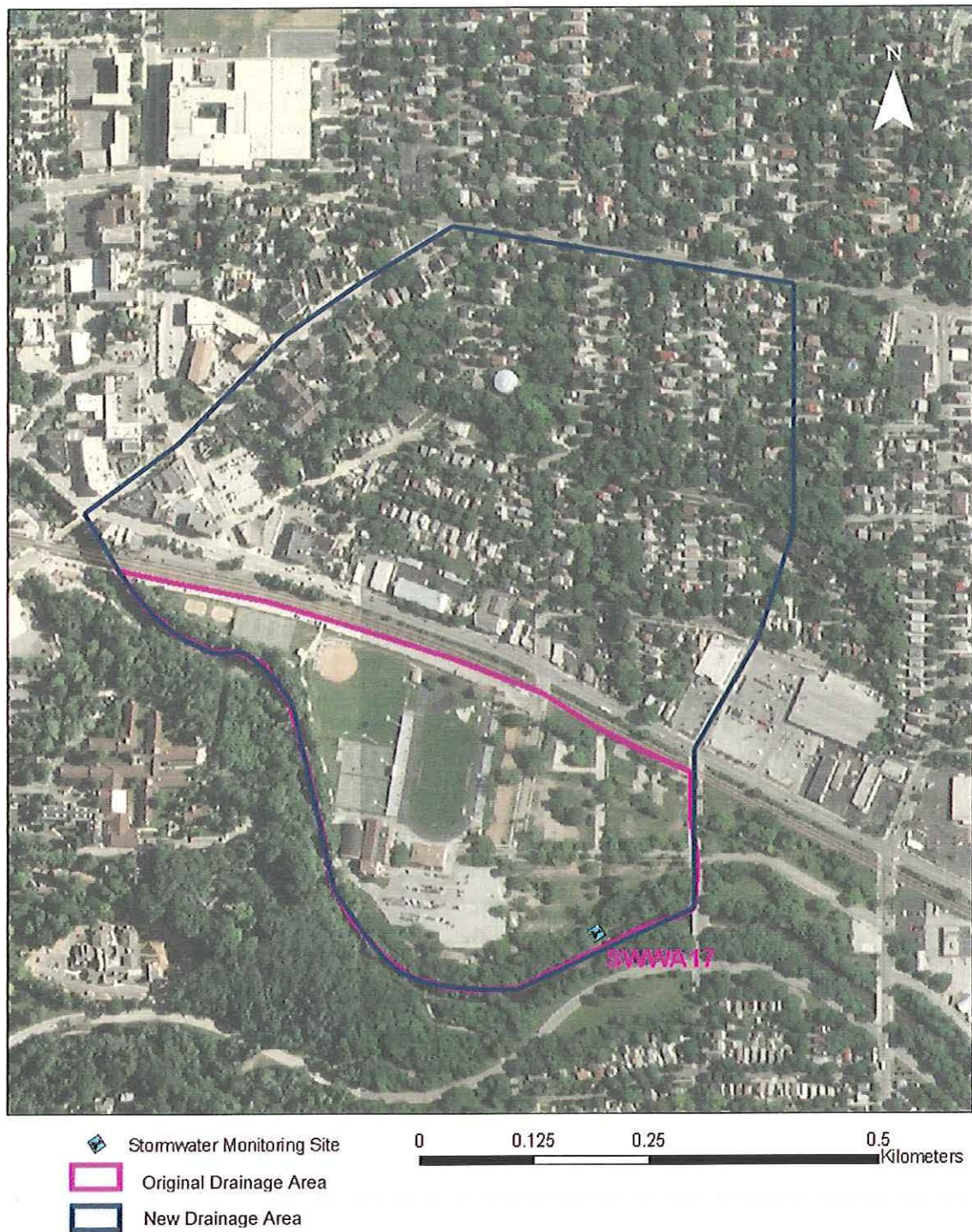


Figure 4.36. An aerial photograph site SWWA17 (71st and Chestnut St, Wauwatosa) with land uses and new drainage boundary.

SWMI18

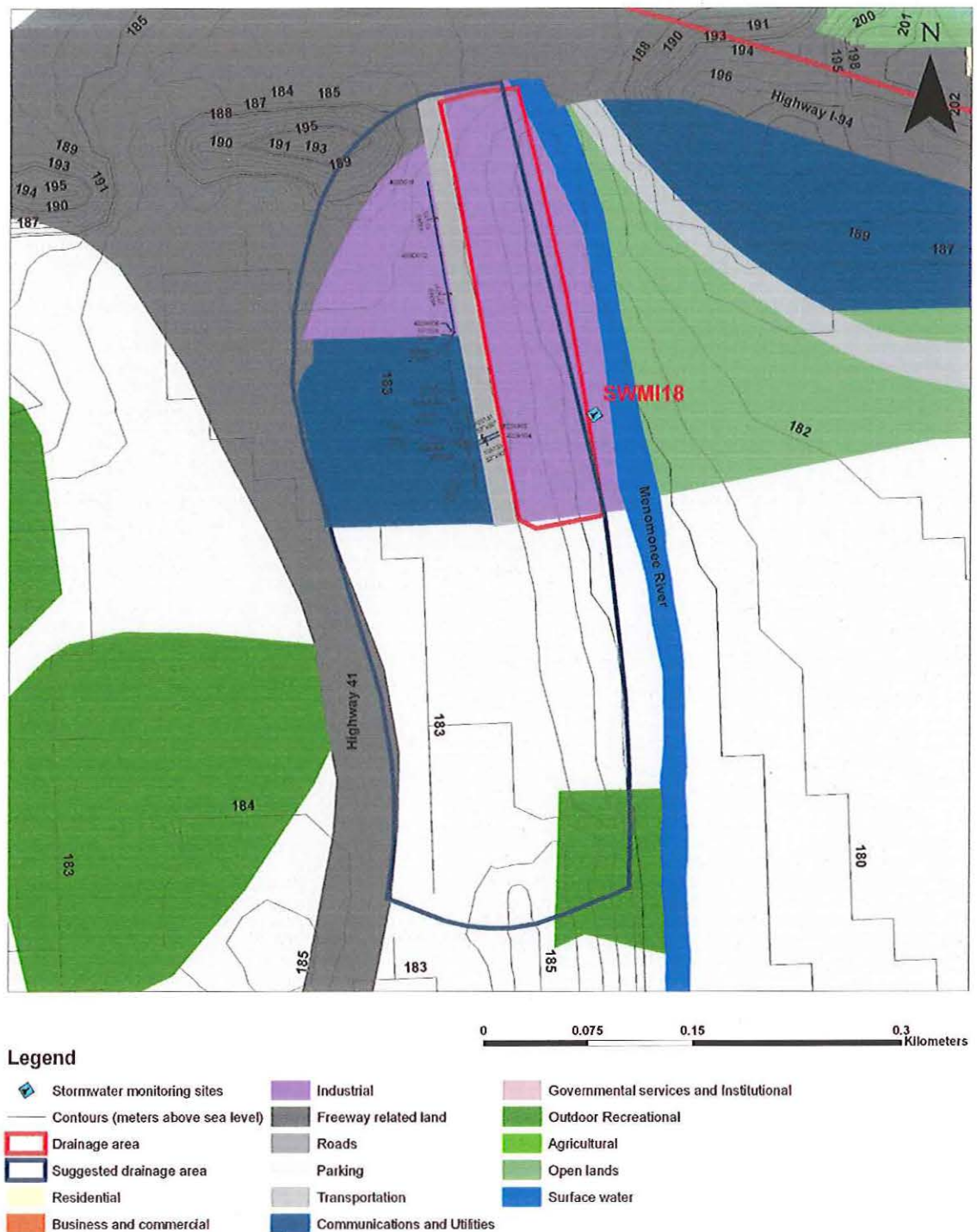
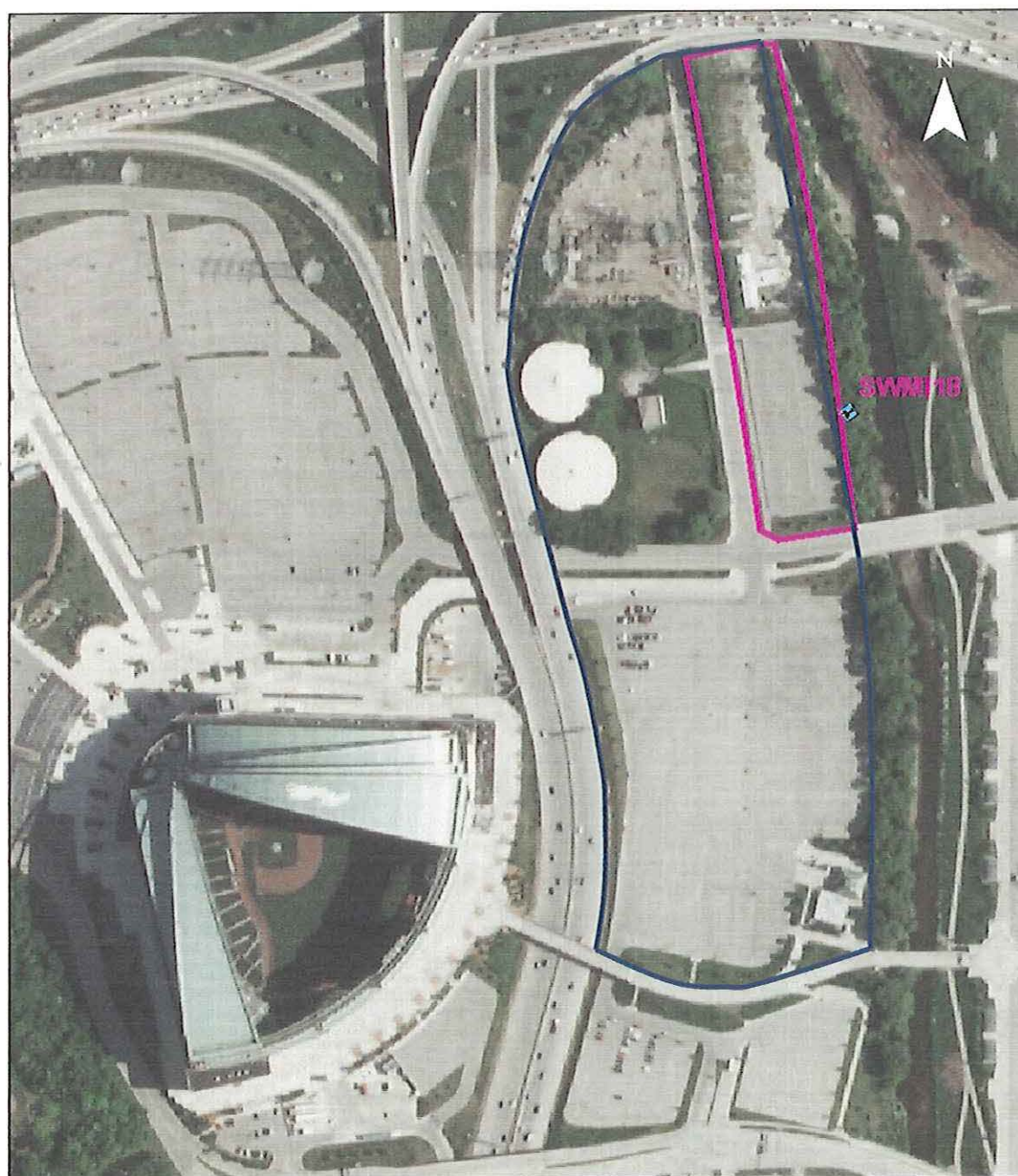





Figure 4.37. A map of site SWMI18 (Miller Park east parking lot at sausage house, Milwaukee) with land uses and new drainage boundary.



-  Stormwater Monitoring Site
-  Original Drainage Area
-  New Drainage Area

0 0.05 0.1 0.2
Kilometers

Figure 4.38. An aerial photograph of site SWMI18 (Miller Park east parking lot at sausage house, Milwaukee) with land uses and new drainage boundary.

V. MODELING OF STORMWATER POLLUTANT LOADS

Common sources of urban runoff include dry and wet atmospheric deposition, accumulation of street refuse (litter, dirt, organic residues, and vehicular traffic emissions), vegetation, urban area erosion, and road deicing chemicals (Adams and Papa, 2000). The quality of stormwater runoff in each drainage area depends on land use. Runoff from traffic-related drainage areas can display high levels of heavy metals and chloride. By comparison, residential runoff typically has high levels of nutrients and bacteria (Soonthornnonda and Christensen, 2005). Further characterization of runoff quantity and quality is desirable to obtain predictive models and evaluate the need for treatment before discharge into receiving waters.

Sartor et al. (1974) simulated washoff of stormwater pollutants from street surfaces by an exponential model. They found that the removed pollutant mass was related to the volume of rainfall during a rainfall event. Alley (1981) developed an exponential washoff model for effective impervious surfaces, in which the predicted amount of constituent washoff was a direct function of the total volume of storm runoff. Charbeneau and Barrett (1998) proposed a model that predicts pollutant load using event mean concentration for single-land-use catchments. Other runoff quality analysis models have been widely developed to predict runoff volumes, mass loads, and concentrations (Brezonik and Stadelmann, 2002; Niehus, 1997); however, to our knowledge, there is no model that specifically considers the influence of each of several dry periods before a storm event on the calculated load. Although Alley and Smith's (1981) model included antecedent condition parameters, it was tested only for nitrogen, lead, and solids, and

only for a single land-use-type drainage area with little pervious area runoff. Only eight periods of runoff were considered. Kim et al. (2005) created a washoff model for predicting the mass emission rates of highway metals during first-flush runoff. Their model has four parameters—none of which appears to have a direct relationship to land use or runoff coefficient. Kim et al. (2005) reported that average daily traffic, antecedent dry period, total rainfall, average rainfall intensity, and runoff coefficient are the main variables that affect total lead mass load. Barrett et al. (1998) reported that a low runoff coefficient resulting from infiltration produces a large reduction in the pollutant load of highway runoff. An appropriate treatment of antecedent conditions, runoff coefficient, and land use in load models has not been satisfactorily demonstrated, to date. Even though many computer load models for continuous simulation are available, i.e., Modeling of Urban Sewers [MOUSE] and Stormwater Management Model [SWMM], Elliott and Trowsdale (2007), important conditions, such as closed-form solution for simulation of multiple sequential dry periods or comprehensive simultaneous parameter estimation for several drainage areas, are not included.

The main objective of this chapter is to develop a load model for urban runoff constituents with emphasis on Zn, Cu, Cd, Ni, Cr, Pb, Hg, Ag, BOD₅, TSS, EC, FC, TSP, and TP. The model contains a buildup component, including consideration of runoff coefficient, drainage area, land use, and one to three antecedent dry period(s) before a given storm event and a washoff component reflecting intensity and duration of the storm. A comprehensive parameter estimation scheme is included. Other objectives are to determine runoff coefficients for sampling areas, evaluate constituent concentrations relative to their guideline values or limits, and estimate the contribution of traffic-related

sources to Zn, Cu, Cd, Ni, Cr, and Pb in urban runoff. More than 400 storm events will be considered in 18 watersheds of Milwaukee, Wisconsin, during the period 2000 through 2004. This chapter will also elaborate the work done previously by Soonthornnonda and Christensen (2007a).

5.1 Load Model

Washoff models proposed by Alley (1981) and Sartor et al. (1974) have been used by a number of researchers. In these models, the rate of pollutant removed from an effective impervious surface is assumed to be proportional to the amount remaining on this surface. The amount of pollutant washoff predicted is a function of the volume of storm runoff or rainfall and initial amount of pollutant. The initial amount of pollutant is a function of the maximum amount of pollutant on the effective impervious area and time since the last period of street sweeping or storm runoff (Alley and Smith, 1981). Alley and Smith (1981) stated that it was an important assumption in their model that effective impervious surfaces were the predominant source of stormwater loads and that the watershed had uniform land use. With regard to antecedent dry conditions, they recognized that the surface load (L_e) after the previous period of storm runoff or street sweeping should be considered, and they gave an expression for the equivalent accumulation time (t_e) in terms of L_e and buildup parameters. However, L_e was not expressed in terms of parameters for previous storm(s) and associated antecedent dry period(s).

Many complex load models that use continuous simulation (i.e., SWMM, Hydrologic Simulation Program-Fortran [HSPF], and Source Loading and Management

Model [SLAMM]) do not give better information for the accumulation rate of constituents on the drainage area. The accumulation rate is often obtained by trial and error during data calibration, with little, if any, actual direct measurements (Pitt et al., 2004).

To overcome the above limitations, the modified model, described below, includes multiple subwatersheds, each with a specific runoff coefficient and land-use factor. Antecedent dry conditions are considered, in terms of an equivalent accumulation time reflecting the antecedent dry period and up to two appropriately reduced previous antecedent dry periods.

The model, which relates the load per event (P) of a given pollutant to the runoff coefficient, average rainfall, antecedent dry period, and land-use factor for a site, is as follows:

$$P = \alpha a \hat{\beta} A f(t_d) [1 - e^{-ck\Delta t}] \quad (12)$$

where

P = event load (kg/event),

α = land-use factor (kg/kg_{average}),

$\hat{\beta}$ = median runoff coefficient,

a = deposition coefficient (kg_{average}/ha/d),

A = drainage area (ha),

c = transport coefficient (cm⁻¹),

k = average rainfall intensity (cm/d),

Δt = storm duration (days), and

$f(t_d)$ = function of antecedent dry period, t_d .

The storm duration (Δt) is determined as the period of time between the starting point of each storm hydrograph and the point where 10% of discharge peak value has occurred at the recession limb of the hydrograph.

The effective area is $\hat{\beta} A$. The pollutant mass accumulated at the beginning of the storm event (j) is $\alpha a \hat{\beta} A f(t_d)$. If a load (L_e) is remaining on the drainage area after the previous storm, L_e should be added to this expression. In this model, the expression in the square bracket in eq 12, optimum approximately 78%, represents the fraction of the initial pollutant mass washed off after the runoff event.

If the accumulation of pollutant mass between storm events $j-1$ and j does not depend on t_d , $f(t_d)$ may be written as a constant, as follows:

$$f(t_d) = 1 \quad (13)$$

However, if the accumulation of pollutant mass between storm events $j-1$ and j is dependent on t_d , $f(t_d)$ may be written as follows:

$$f(t_d) = t_{d,j} \quad (14)$$

Where it is assumed that the surface is clean after the previous storm $j-1$.

Advancing one step further, the pollutant mass retained after storm event $j-1$ may be included in the model, and $f(t_d)$ is the following:

$$f(t_d) = t_{d,j-1} e^{-ck_{j-1}\Delta t_{j-1}} + t_{d,j} \quad (15)$$

Where it is assumed that the surface is clean after storm $j-2$.

The pollutant masses retained after storm events $j-1$ and $j-2$ may also be included in the model, and $f(t_d)$ becomes the following:

$$f(t_d) = t_{d,j-2} e^{-c(k_{j-2}\Delta t_{j-2} + k_{j-1}\Delta t_{j-1})} + t_{d,j-1} e^{-ck_{j-1}\Delta t_{j-1}} + t_{d,j} \quad (16)$$

The assumption is here that the surface is clean after storm $j-3$. The model expressed by eqs 14 to 16 is a linear buildup model. In eq 16 and its extensions to further dry periods (i.e., $t_{d,j-3}$), the effective antecedent dry period is written as a sum of the preceding dry period followed by downweighted or reduced previous dry periods. For a sufficient number of terms, the actual previous dry periods become downweighted, such that their contribution is small and the assumption of initial clean surfaces (i.e., after storm $j-3$) is inconsequential.

In case of significant removal of pollutants by wind or pollutant decay during buildup, the general expression for buildup may be written as follows:

$$P = \frac{\alpha \hat{\beta} A}{K} (1 - e^{-K t_d}) + L e^{-K t_d} \quad (17)$$

where K is a removal coefficient (days^{-1}).

This equation is a version of the buildup model considered by Charbeneau and Barrett (1998), modified to include the runoff coefficient $\hat{\beta}$. The expression for $f(t_d)$, corresponding to eqs 14 to 16, and including pollutant removal according to eq 6 during buildup, are in the same order.

$$f(t_d) = \frac{1 - e^{-K t_{d,j}}}{K} \quad (18)$$

$$f(t_d) = \frac{1 - e^{-K t_{d,j-1}}}{K} e^{-(c k_{j-1} \Delta t_{j-1} + K t_{d,j})} + \frac{1 - e^{-K t_{d,j}}}{K} \quad (19)$$

$$\begin{aligned} f(t_d) = & \frac{1 - e^{-K t_{d,j-2}}}{K} e^{-\{c k_{j-2} \Delta t_{j-2} + c k_{j-1} \Delta t_{j-1} + K(t_{d,j-1} + t_{d,j})\}} + \frac{1 - e^{-K t_{d,j-1}}}{K} e^{-(c k_{j-1} \Delta t_{j-1} + K t_{d,j})} \\ & + \frac{1 - e^{-K t_{d,j}}}{K} \end{aligned} \quad (20)$$

Note that these equations become eqs 14 to 16 when $Kt_d \ll 1$, which we assume here to be the case, as a result of frequent rainfall events in the Midwest of the United States. The antecedent dry period (t_d) was defined as the dry period before any runoff event, in which both the previous peak discharge and the current peak discharge are ≥ 5 % of the overall average peak flow during rainfall events from 2000 to 2004. By using this definition, values of t_d will be more realistic by disregarding minor runoff events.

Land-use factors α (i.e., mass load at specific site divided by mass load for all regions) were estimated as a measure of that site's relative contribution to the pollutant load. The pollutant deposition flux on a surface is αa . The values of a and c were determined by a least-squares fit of calculated to measured loads for all areas, with $\alpha = 1$. Next, α values for individual drainage areas were estimated based on average factors needed to give a better fitting model. The factor α for a drainage area can be determined from the following:

$$\text{Min } \left\{ S = \sum_{i=1}^n (Y_i - A - Bx_i)^2 \right\} \quad (21)$$

Where Y_i = calculated load, and

x_i = measured load for the drainage area in a log-log load plot.

Here, the value of $B = 1$ and the number of data points = n .

A necessary condition for an optimum solution is the following:

$$\frac{\partial S}{\partial A} = \sum_{i=1}^n 2(Y_i - A - Bx_i) = 0 \quad (22)$$

Rearranging eq 22, we obtain the following:

$$A = \frac{\sum_{i=1}^n Y_i - Bx_i}{n} \quad (23)$$

The standard deviation of A is computed as follows:

$$\sigma A = \sqrt{\frac{\sum_{i=1}^n [Y_i - (A + Bx_i)]^2}{n-1}} \quad (24)$$

and the uncertainty of the mean δA is given by the following:

$$\delta A = \frac{\sigma A}{\sqrt{n}} \quad (25)$$

Thus,

$$\log \alpha = -A \pm \delta A \quad (26)$$

and

$$\alpha = 10^{-A} (10^{-A-\delta A}, 10^{-A+\delta A}) \quad (27)$$

Multiplication of the overall calculated load with α will then ensure that the new calculated points are centered around the line $Y = x$ in the log-log loading plot.

Measured loads P_m were determined as follows:

$$P_m = \frac{1}{2} (c_1 Q_1 + c_2 Q_2) \Delta t \quad (28)$$

where c_1 and c_2 = first and 2-hour-later concentrations of pollutant (kg/m^3), respectively, and

Q_1 and Q_2 = corresponding flows (m^3/d).

Values of P_m based on eq 28 were compared with those based on a limited data set ($n = 12$ storms, representing the full range of storm variability), with approximately six measurements during each storm event. Results indicated that loads calculated from eq 28 were overestimated by a factor of 1.54 ± 0.15 (average \pm standard error of mean, $n =$

12). Thus, the use of eq 28 to estimate measured loads may be acceptable, especially because load uncertainties typically are one cycle (a factor of 10) in log–log load plots.

Pollutant concentrations in stormwater runoff are difficult to model because of many uncertain factors, such as source strength, dispersion, runoff percolation, and so forth. However, order-of-magnitude estimates can be made for some metals where the major source is known. For example, automobile tires are a major source of Zn (Christensen and Guinn, 1979), and aqueous concentrations can be calculated as the emission rate times the number of vehicle kilometers traveled in the watershed during the antecedent dry period divided by the runoff volume.

By contrast, ratios between deposition fluxes $\alpha\alpha$ can, in some cases, be modeled reasonably well, based on known emission rates (i.e., rates of Zn from tire wear and Cu from brake linings [Brewer, 1997; Legret and Pagotto, 1999]).

5.2 Results and Discussion

5.2.1 Runoff Coefficients

As discussed in Chapter 4, runoff coefficients were computed as total runoff volume divided by total rainfall volume. Coefficients ranged from 0.00096 to 16.1. The mean coefficients for the 18 monitoring sites ranged from 0.0052 to 3.88. The median coefficients ranged from 0.0036 to 3.71 (Table 5.1). The mean coefficient over all sites was 0.87 ± 0.33 , and the median was 0.13. Coefficients were greater than 1.0 at sites 6, 7, 8, and 18. Typically, runoff coefficients vary for different storm events, being larger for larger storms and shorter dry periods between storms (less influence of depression

storage and limited infiltration), but would not exceed a value of one, nor would they be very small for urban areas.

Three possible explanations of obtaining runoff coefficients larger than one for these sites are illegal discharges of sanitary wastewater, groundwater infiltration, and underestimated drainage areas. Substantial contribution from sanitary wastewater should influence the water quality (higher concentrations of nutrients, BOD₅, and EC). The substantial contribution from groundwater would also influence water quality; for example, concentrations of heavy metals (i.e., Zn, Cu, Pb, and Cr) would be lower because of a dilution effect. The results in Chapter 3 do not support these hypotheses.

It is more likely that these four drainage areas (sites 6, 7, 8, and 18) have been underestimated. We have recently confirmed this for sites 6 and 7, from the fact that the drainage piping networks extend significantly beyond the originally indicated drainage areas for these sites. The extension is in rough proportion to the amount by which the runoff coefficient exceeds unity. The low values of measured runoff coefficient may be the result of infiltration in unsaturated soil at low rainfall (sites 1, 9, 10, and 14) and overestimated drainage areas (i.e., site 15). The value much smaller than 1 (0.033) of the runoff coefficient for site 15 is confirmed by the fact that the slopes and outfalls for drainage pipes of site 15 indicate that the effective drainage area is much smaller than the one that was indicated originally. Despite these modifications, the product $\hat{\beta}A$ remains valid, even for $\hat{\beta} > 1$, because $\hat{\beta}$ is multiplied by the same factor by which A is divided.

Table 5.1. Effective area and runoff coefficient for each study site.

Site No.	Location	Land use	Receiving Water	Drainage area (ha)		Runoff coefficient ^a , $\hat{\beta}$
				Total, A	Effective, $\hat{\beta}$ A	
1	Milwaukee	Institutional, residential, open lands	Lake Michigan	23.8	0.73	0.0306 (0.0658,0.00563)
2	Milwaukee	Residential, commercial, recreational, open lands	Lake Michigan	57.2	0.20	0.00355 (0.0165,0.000965)
3	Franklin	Industrial park, open lands	Detention Pond	11.7	2.15	0.183 (0.386,0.0219)
4	Milwaukee	Institutional, residential, open lands, highway 794, Bay View Park	Lake Michigan	608	46.9	0.0771 (0.138,0.0491)
5	Milwaukee	Residential, parking lot, open lands	Milwaukee River	3.42	0.92	0.270 (3.01,0.0641)
6	Milwaukee	Milwaukee County Zoo, I-94	Underwood Creek	10.6	23.2	2.18 (16.1,0.721)
7	Milwaukee	Residential, recreational	Lincoln Creek	18.4	68.2	3.71 (8.29,0.335)
8	Milwaukee	Residential, commercial	Lincoln Creek	21.2	72.3	3.41 (8.99,0.962)
9	Whitefish Bay	Residential, open lands	Lake Michigan	57.4	5.62	0.0980 (0.201,0.00224)
10	Greenfield	Boerner botanical gardens, parking lot	Detention Pond	71.4	0.62	0.00865 (0.0220,0.00164)
11	New Berlin	New residential, open lands	Detention Pond	73.9	1.12	0.0151 (0.0494,0.00604)
12	Milwaukee	Residential, commercial, parking lot	Honey Creek	38.8	3.16	0.0813 (0.167,0.0310)
13	Wauwatosa	Residential, open lands	Menomonee River	20.5	5.43	0.265 (0.505,0.0159)
14	St. Francis	Residential, open lands	Lake Michigan	21.5	0.73	0.0341 (0.0581,0.00346)
15	Milwaukee	I-94, flood control area, residential	Menomonee River	44.3	1.48	0.0335 (0.0948,0.0175)
16	Milwaukee	I-94, I-43, highway 794, industrial	Menomonee River	6.40	1.51	0.237 (0.350,0.171)
17	Wauwatosa	Recreational, open lands, residential, commercial	Menomonee River	13.4	9.69	0.725 (0.973,0.428)
18	Milwaukee	Miller Park east parking lot	Menomonee River	1.92	5.78	3.01 (5.99,0.208)

^a median with maximum and minimum

5.2.2 Concentrations of Zn and Cu in Stormwater

Regarding the estimation of metal concentrations in runoff volume, consider Zn and Cu from site 15 during the 6-hour rainfall event from August 12, 2002, 6:00 p.m., to August 13, 2002, 12:00 a.m. (midnight). Assuming that a 1.5-km stretch of the 6-lane I-94 freeway is the source and that the freeway system in Milwaukee includes 1100 lane km (700 lane miles), the fraction of total Zn and Cu deposition is 8.04×10^{-3} .

The primary source of Cu in urban runoff is automobile brake linings (McCuen, 2004). The average brake wear rate is 8.8 mg/vehicle km (Warner et al., 2002). The average brake lining is assumed to have a Cu concentration of 79 000 mg/kg (7.9%) (Brewer, 1997; Legret and Pagotto, 1999). Thus, the average deposition rate of Cu is $8.8 \times 0.079 = 0.70$ mg/vehicle km. Christensen and Guinn (1979) reported that the average deposition rate of Zn is 3.0 mg/vehicle km.

Consequently, with an antecedent dry period of 8.6 days, 1.685×10^7 vehicle freeway km traveled per day (1.047×10^7 vehicle freeway miles traveled per day), a runoff volume of 1274 m³, Zn concentration of 2.73 mg/L, and Cu concentration of 0.63 mg/L are obtained, compared with measured event mean concentrations of 2.23 and 0.51 mg/L, respectively. Hydraulic and pollutant data are from the MMSD (2003) and highway data from the Texas Transportation Institute (2005). Because of several uncertainties, for example, in contributing freeway length and amounts of Zn and Cu deposition in the watershed, the agreement between measured and calculated values should only be taken as an indication within an order of magnitude, that Zn and Cu from highways appear to be a significant source of Zn and Cu in runoff.

5.2.3 Constituent Loads

Event mass loads of Zn, Cu, Cd, Ni, Cr, Pb, Hg, Ag, BOD₅, TSS, EC, FC, TSP, and TP were estimated according to eqs 12 to 16 and also using eqs 18 to 20. Results using eqs 12 to 16 are shown in Table 5.2, which presents the deposition coefficient a and R^2 from the model fit. The model performed better for all constituents, except TSP, when t_d was included in the buildup term. This indicates that the release of soluble phosphorus may be more dependent on storm duration and intensity than accumulation during dry periods. The R^2 values for all constituents, except TSS and Ag, based on an assumption of a clean surface after the last storm in eq 14, are less than the R^2 values obtained from eq 15, suggesting that the load retained after the previous storm is significant and that constituents such as metals, phosphorus, and bacteria, associated with smaller particles, are more likely to be trapped on the drainage area at the end of the previous storm than bulk TSS. Figures 5.1, 5.2, 5.3, and 5.4 show a comparison of measured and predicted loads of Zn, Cu, Cd, Ni, Cr, Pb, Hg, Ag, BOD₅, TSS, EC, FC, TSP, and TP. The load model based on the retained mass after two previous storms (eq 16) gave less accurate results, as shown in Table 5.2.

Table 5.2. Multiple correlation coefficients for modeled constituents with and without antecedent dry period, t_d .

Constituent	No. of events monitored	Deposition coefficient, a (kg/ha/d)			R^2			
		one event included eq 14	two events included eq 15	three events included eq 16	without t_d eq 13	with t_d for one event eq 14	with t_d for two events eq 15	with t_d for three events eq 16
Zn	410	9.83×10^{-3}	7.43×10^{-3}	6.59×10^{-3}	0.480	0.537	0.557	0.555
Cu	410	1.92×10^{-3}	1.45×10^{-3}	1.28×10^{-3}	0.498	0.531	0.552	0.551
Cd	411	4.29×10^{-5}	3.20×10^{-5}	2.84×10^{-5}	0.273	0.413	0.417	0.403
Ni	411	6.29×10^{-4}	4.62×10^{-4}	4.08×10^{-4}	0.468	0.497	0.519	0.517
Cr	411	7.36×10^{-4}	5.45×10^{-4}	4.82×10^{-4}	0.363	0.431	0.448	0.443
Pb	411	1.43×10^{-3}	1.09×10^{-3}	9.71×10^{-4}	0.347	0.426	0.439	0.435
Hg	423	1.72×10^{-6}	1.26×10^{-6}	1.12×10^{-6}	0.460	0.462	0.476	0.475
Ag	411	2.96×10^{-5}	2.25×10^{-5}	1.98×10^{-5}	-0.115	0.178	0.150	0.129
BOD ₅	443	1.30	0.992	0.879	0.491	0.557	0.571	0.568
TSS	437	19.7	14.8	13.1	0.226	0.383	0.367	0.361
EC ^(a)	441	3.73×10^9	2.66×10^9	2.44×10^9	0.469	0.525	0.545	0.536
FC ^(a)	445	6.27×10^9	4.49×10^9	4.11×10^9	0.243	0.349	0.355	0.346
TSP	83	4.15×10^{-3}	4.16×10^{-3}	4.13×10^{-3}	0.510	0.404	0.446	0.445
TP	437	7.85×10^{-2}	5.62×10^{-2}	4.95×10^{-2}	0.477	0.520	0.542	0.536

^(a) CFU/ha/d

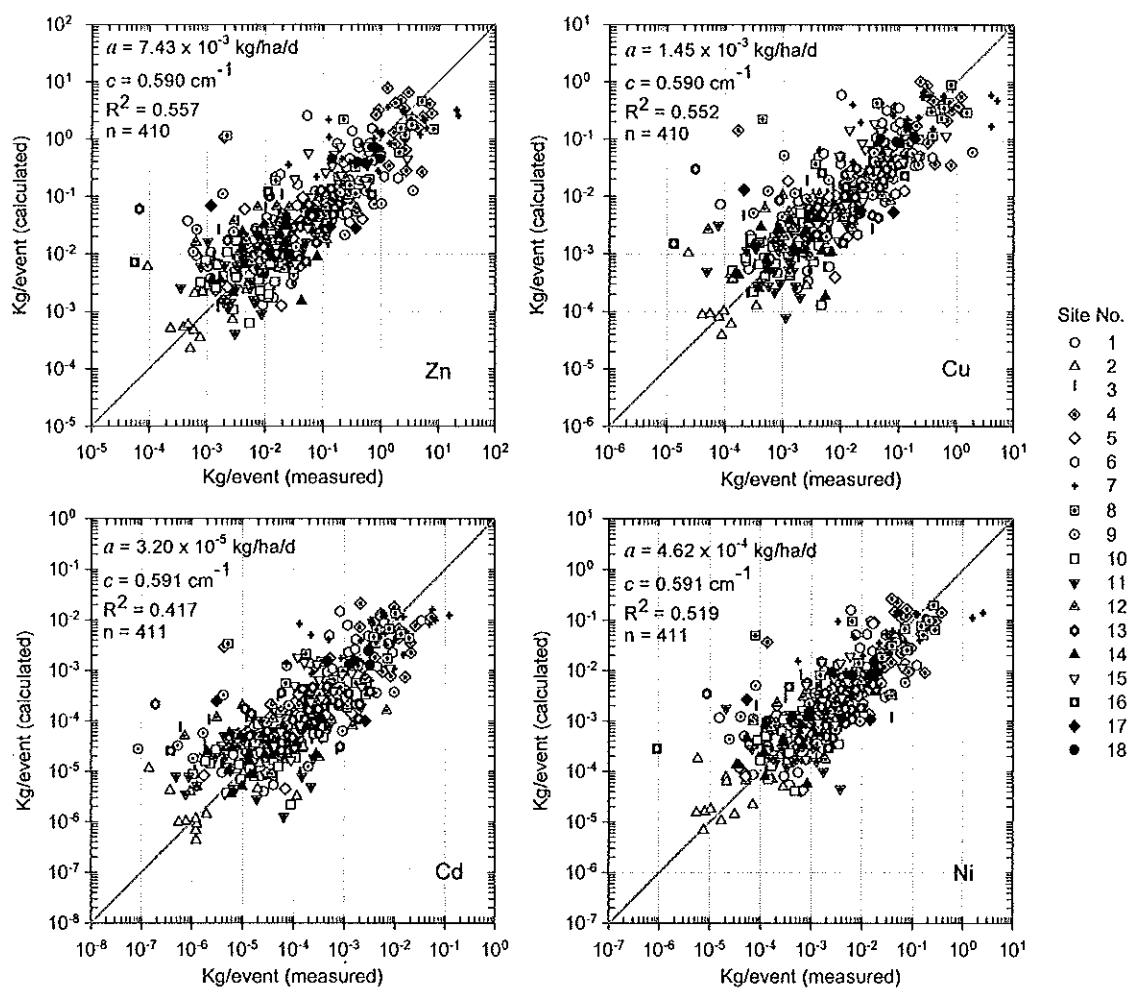


Figure 5.1. Calculated versus measured loads of zinc (Zn), copper (Cu), cadmium (Cd), and nickel (Ni), considering t_d for two events.

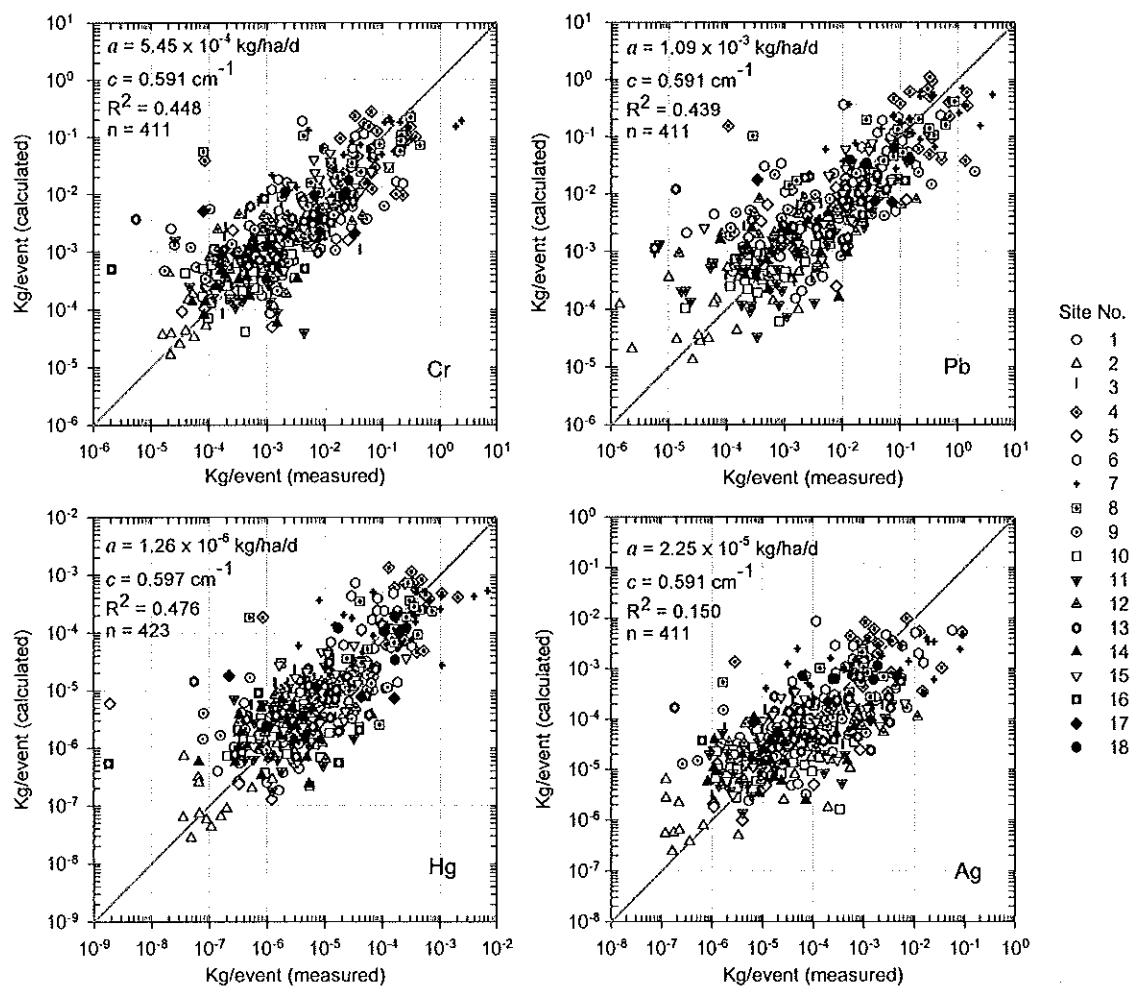


Figure 5.2. Calculated versus measured loads of chromium (Cr), lead (Pb), mercury (Hg), and silver (Ag), considering td for two events.

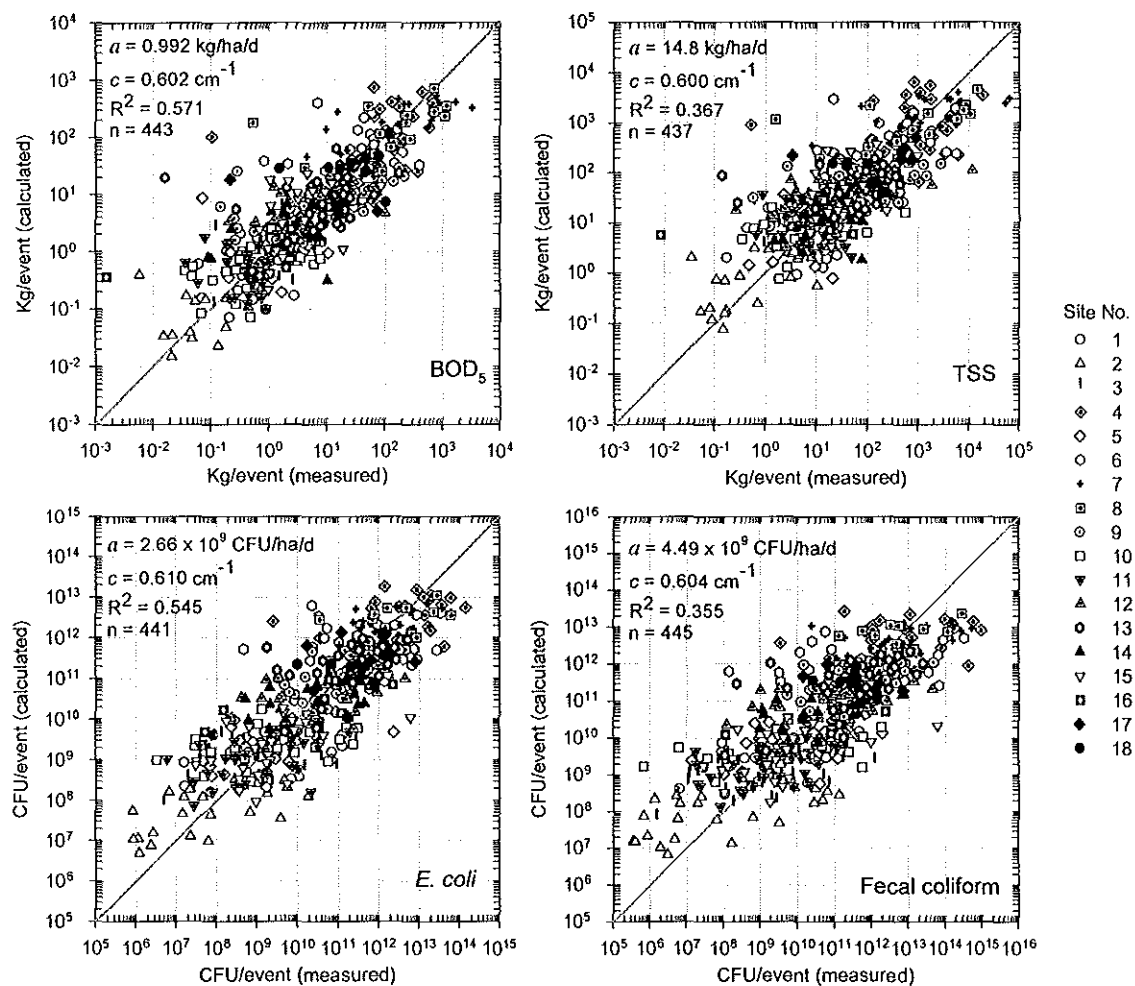


Figure 5.3. Calculated versus measured loads of BOD_5 , total suspended solids (TSS), *E. coli* (EC), and fecal coliform (FC), considering td for two events.

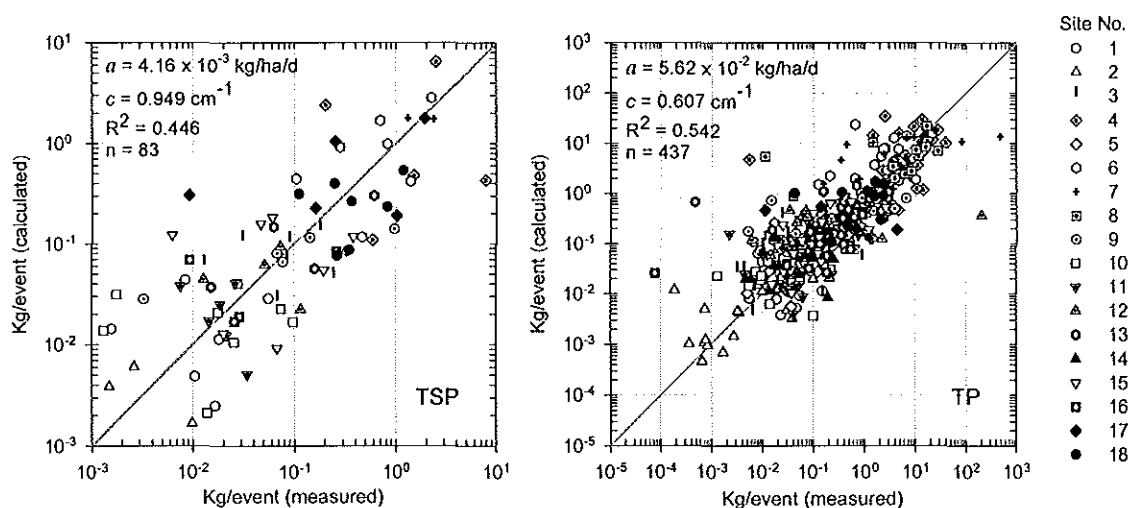


Figure 5.4. Calculated versus measured loads of total soluble phosphorus (TSP) and total phosphorus (TP), considering t_d for two events.

An average of 78% removal of pollutant mass (i.e., the square bracket in eq 12) was selected as an optimum, giving c values for all constituents of approximately 0.6 cm^{-1} . Alley (1981) reported that a runoff volume of 12.7 mm would wash off 90% of a pollutant from effective impervious surfaces, regardless of duration and whether or not the runoff was uniform. The corresponding c is 1.81 cm^{-1} . Charbeneau and Barrett (1998) found that approximately 85% of TSS was actually removed. Alley (1981) reported that average c values for eight storms based on total runoff ranged from 0.63 cm^{-1} (nitrogen) to 1.30 cm^{-1} (suspended solids). Grottke (1987) found c values based on effective rainfall ranging from 0.21 cm^{-1} (Cd) to 3.20 cm^{-1} (Ni).

There was some improvement in the model fit, as shown by an increasing R^2 , when losses of Cu, Ni, and Hg during buildup according to eqs 18 to 20 were included. The optimal K values were 0.036 day^{-1} for Cu and Ni and 0.2 day^{-1} for Hg. Thus, characteristic times for losses $1/K$ (days) were 28 days for Cu and Ni and 5 days for Hg.

The reason for the shorter time for Hg is probably that this element exists in many volatile compounds and therefore is more likely to undergo relatively rapid losses.

Land use factors α (mass load at specific site divided by mass load for all regions) were estimated as a measure of that site's relative contribution to the pollutant load. These factors, based on eqs 12 and 15, are shown in Figures 5.5 and 5.6. Factors (α) for many metals were greater than 1.0 at sites 4, 5, 15, and 18. Also, α factors for BOD₅ and TP were greater than 1 at site 4. The values of α factors for EC and FC were greater than 1 at 10 sites (4, 6, 7, 8, 9, 12, 13, 14, 17, and 18). The land-use factor can be used as a parameter to understand the relative contribution of pollutant load in each stormwater catchment. A catchment with significant highway(s) and parking lot(s) will give a high α value for metals, as seen in Table 5.1 and Figure 5.5. Catchments with residential, open lands, or recreational areas display high α values for BOD₅, TP, EC, and FC (Table 5.1 and Figure 5.6).

Deposition fluxes $\alpha\alpha$ of Cu, Cd, and Pb based on eqs 12 and 15, at site 15, were 5.96×10^{-3} , 5.84×10^{-5} , and 2.47×10^{-3} kg/ha/d, respectively. Deposition fluxes of Cu, Cd, and Pb at site 18 were 2.31×10^{-3} , 3.46×10^{-5} , and 8.93×10^{-4} kg/ha/d, respectively. By comparison, Harrison and Johnston (1985) reported that deposition fluxes of Cu, Cd, and Pb on the verges of a major highway in northwest England range between 1.43×10^{-4} and 2.07×10^{-3} , 1.43×10^{-5} and 2.43×10^{-4} , and 3.29×10^{-4} and 0.016 kg/ha/d, respectively. Thus, fluxes of Cd and Pb at sites 15 and 18 were within the ranges reported above. The deposition fluxes of Cu at sites 15 and 18 were just above the above-mentioned range. The load model gave deposition fluxes of Zn of 0.0236 (site 15) and 0.0102 (site 18) kg/ha/d. Sabin et al. (2005) determined atmospheric deposition rates in Los Angeles,

California, of 10 and 43 $\mu\text{g}/\text{m}^2/\text{d}$ (1.0×10^{-4} and 4.3×10^{-4} $\text{kg}/\text{ha}/\text{d}$) within a 5-ha area of limited local metal sources for Cu and Zn, respectively, further indicating that local inputs generally are significantly higher than atmospheric inputs.

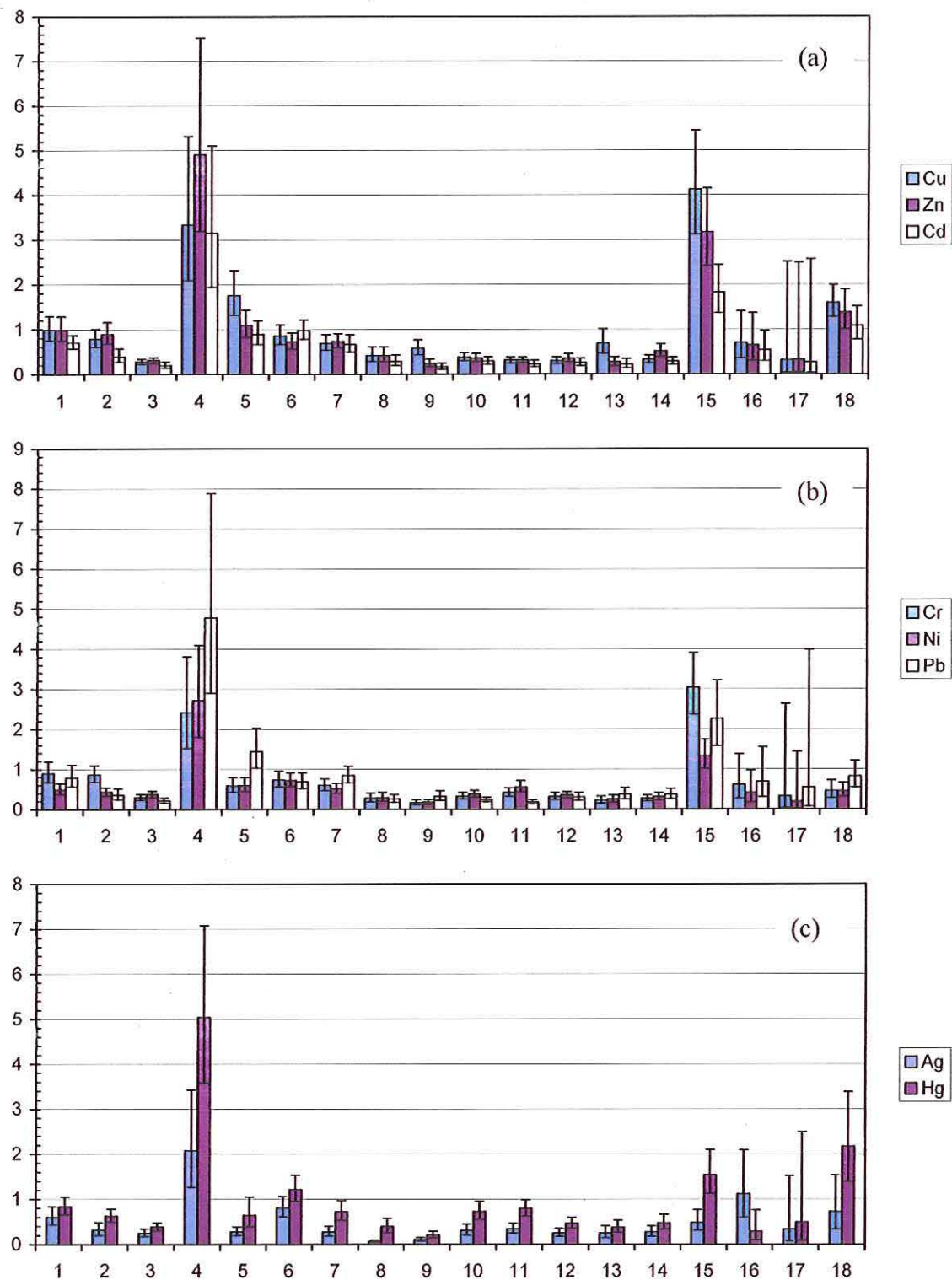


Figure 5.5. Land use factors (\pm std. err. of mean) for (a) Cu, Zn, Cd, (b) Cr, Ni, Pb, (c) Ag, and Hg, considering t_d for two events.

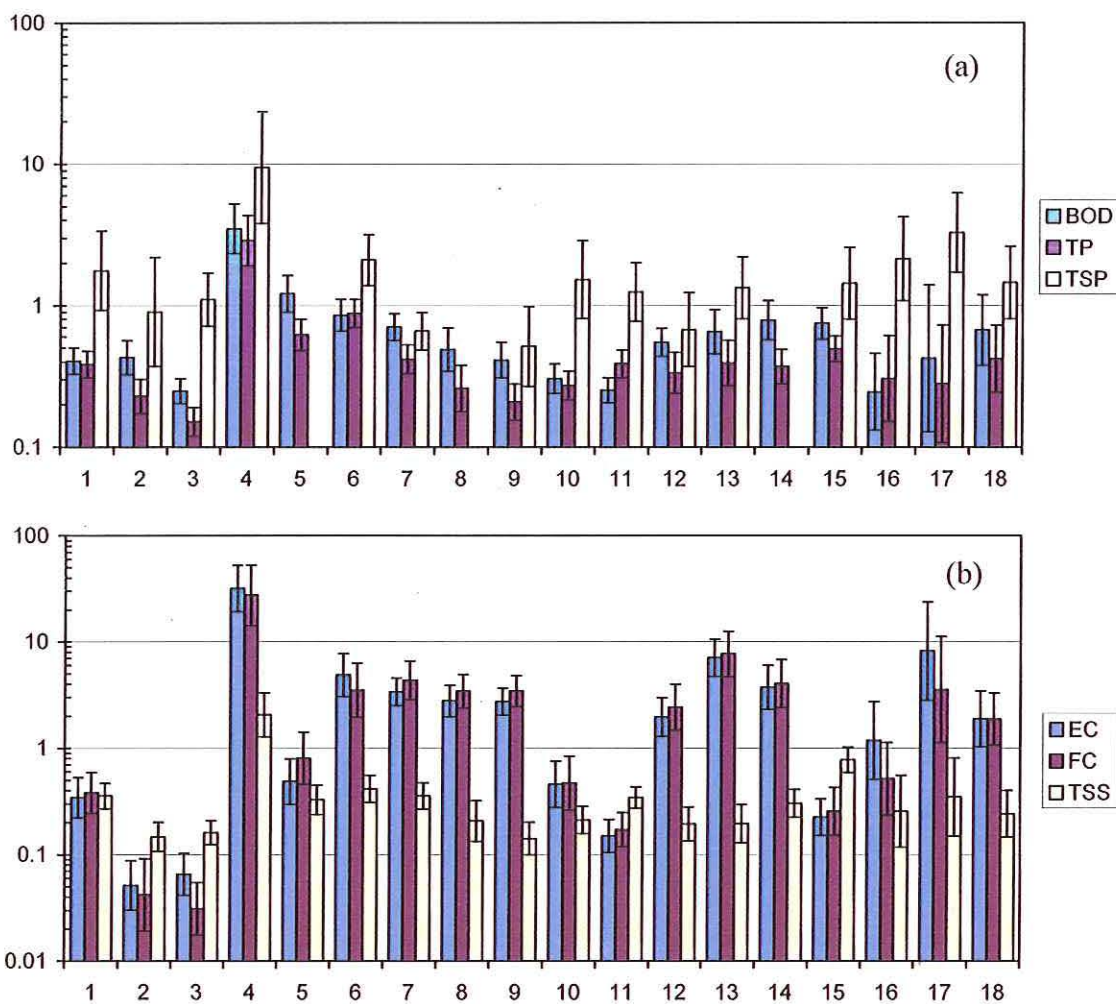


Figure 5.6. Land use factors (\pm std. err. of mean) for (a) BOD₅, TP, TSP, (b) EC, FC, and TSS, considering t_d for two events.

5.2.4 Relationship between Mass Loads of Zn, Cu, and Other Metals in Stormwater Runoff

Ratios between Zn and Cu deposition fluxes $\alpha\alpha$ are 4.0 (site 15), 4.7 (site 16), and 4.4 (site 18). These three sites have significant automobile traffic. The ratio between the average Zn and Cu vehicle deposition rates is 3.0 mg Zn/vehicle km/0.70 mg Cu/vehicle km = 4.3. Also, the ratio between Zn and Cu concentrations at site 18, at $t_d = 25$ days in Figure 5.7, is 1.43 mg/L / 0.3 mg/L = 4.77. This is in agreement with the ratio between the range of ratios of Zn and Cu deposition fluxes $\alpha\alpha$ (4.0 to 4.7) and average Zn and Cu vehicle deposition rates (4.3), which, with the linear correlation of metal concentrations versus antecedent dry period, as illustrated in Figure 5.7, indicate that the measured Zn and Cu in fact is derived from automobile traffic.

Table 5.3 summarizes the comparison of ratios between concentrations of Zn and other metals with ratios of deposition fluxes (eqs 12 and 15) of Zn and other metals (Cu, Cd, Ni, Cr, and Pb) at sites 6, 15, 16, and 18. Ratios of deposition fluxes at sites 18 and associated concentration ratios from Figure 5.7 are assumed to be indicators of traffic-related sources. Table 5.3 shows that all metals at these sites can be viewed as having automobiles as a main source, except Cr at site 6, 15, and 16; Cd and Ni at site 6; and Pb at site 6. Possible nonautomotive sources of selected metals include metal plating (Cr and Ni), asphalt paving (Ni), and insecticide application (Cd) (Colman et al., 2001).

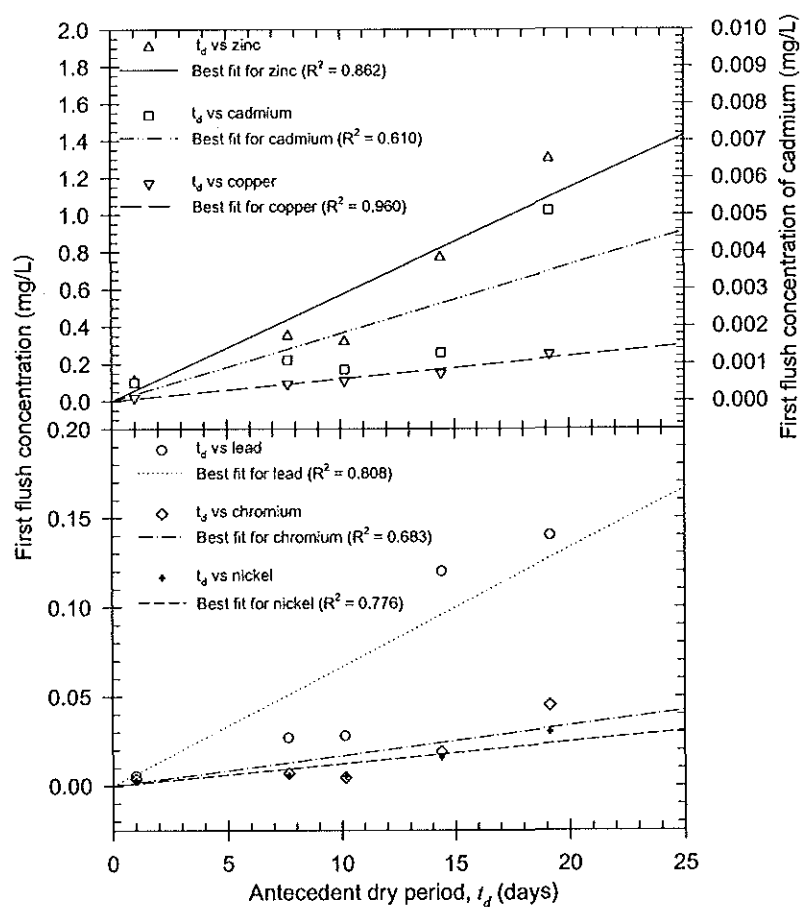


Figure 5.7. Concentrations of Zn, Cu, Cd, Ni, Cr, and Pb vs antecedent dry period, t_d at site 18 (Miller Park stadium parking lot).

Table 5.3. Comparison of ratios between concentrations of Zn and other metals based on linear expressions in Figure 5.7 with ratios of deposition fluxes ($\alpha\alpha$) of Zn and other metals at sites 6, 15, 16, and 18.

Metals	Summary of Figure 5.7		Ratio ^a of deposition flux ($\alpha\alpha$) of Zn / Me ^b			
	R ²	Ratio of Zn / Me* concentrations (site 18)	Site 6	Site 15	Site 16	Site 18
Zn	0.862	1.00	1.00	1.00	1.00	1.00
Cu	0.960	4.77	4.35 (3.01,6.07)	3.95 (2.61,5.71)	4.74 (1.30,11.8)	4.43 (2.94,6.40)
Cd	0.610	311	172 (122,236)	404 (264,588)	281 (86.7,668)	295 (179,456)
Ni	0.776	47.7	16.1 (11.3,22.3)	38.4 (25.7,55.0)	25.2 (5.52,69.4)	48.3 (28.6,76.3)
Cr	0.683	34.0	13.4 (9.18,18.9)	14.2 (9.62,20.2)	14.3 (3.38,38.2)	41.2 (22.3,70.0)
Pb	0.808	9.23	7.11 (4.80,10.1)	9.54 (5.91,14.5)	6.33 (1.50,16.8)	11.4 (6.59,18.4)

^a Ratio with upper and lower limits based on standard error of the mean.

^b Denominator metals are Zn, Cu, Cd, Ni, Cr, and Pb.

The main new points developed here are the following:

- (1) A new dry-period-based load model for pollutants in urban runoff, in which the influence of each dry period before a storm event on the calculated load can be evaluated; and
- (2) Demonstration of the fact that including not only the immediately preceding dry period, but also a weighted contribution from one additional preceding dry period improves the model fit for the following constituents:
Zn, Cu, Cd, Ni, Cr, Pb, Hg, BOD₅, bacteria, TSP, and TP.

The additional term reflects the load retained on the drainage area after the previous storm. Only the model fits for TSS and Ag are not improved by the consideration of an additional dry period.

Previous models as developed by, for example, Alley and Smith (1981) and Kim et al. (2006) are limited to parameters such as nitrogen, lead, TSS, and chemical oxygen demand and do not express the calculated load in terms of a closed-form expression with previous dry periods as parameters. Also, only Alley and Smith (1981) compare models with different antecedent dry conditions (nitrogen, lead, and TSS).

Although the developed model can consider maximum pollutant buildup on the drainage area resulting from removal by wind or decay, we find that a linear model appears to be sufficient for the data considered here, based on linear metal concentrations versus the dry period in Figure 5.7, except perhaps for Hg, and, to a lesser extent, Cu and Ni. Data for the bacteria concentrations versus the dry period (not shown) also support a linear model, up to $t_d = 25$ days. It may be expected that exponential buildup terms, as in eqs 18 to 20, would apply to drier climates with long antecedent dry periods, as is found

in the southwestern United States. In addition to introducing new theoretical and practical aspects mentioned above, this work can also serve as basis for comparisons with load estimates for other drainage areas.

VI. MODELING OF STORMWATER POLLUTANT WASHOFF

Many stormwater mass models are based on the assumption that the rate of pollutant washoff on effective impervious surfaces is proportional to the remaining pollutant mass (Sartor et al., 1974; Alley, 1981; Alley and Smith, 1981; Grottke, 1987; Akan, 1988; Charbeneau and Barrett, 1998; Osuch-Pajdzinska and Zawilski, 1998). Most previous studies have focused on determining the pollutant mass from buildup and washoff models mainly on impervious highway catchments.

Chen and Adams (2006) proposed a new pollutant mass model from which parameters of a washoff rate function can be determined. However, this model was developed based on constant parameters of the buildup function without spatial variation. In most cases, a study catchment does not represent a homogeneous land use (Butcher, 2003). There are few studies of pollutant washoff rates for residential and open land areas even though these areas are major sources of nutrients and bacteria in stormwater runoff (Bannerman et al., 1993; Soonthornmonda and Christensen, 2007a). There is also a need to characterize pollutant removal during different phases of the runoff hydrograph. In addition, little information is available on bacteria removal during storm events. Bacteria (e.g., EC and FC) are microbial indicators of recreational water quality. Wade et al. (2003) reported that it is more consistent to use EC as a predictor for gastrointestinal illness.

In this chapter, a washoff rate equation for stormwater pollutant mass was derived based on a linear buildup formulation. The transport coefficient c in the washoff rate reflects the ability to remove the pollutant mass from the catchment surface (Segarra-

Garcia and Loganathan, 1994). Thus, it is important to have a good estimate of the proper value of c for individual pollutants. Values of c for seven metals (i.e., Zn, Cu, Cd, Ni, Pb, Hg, and Ag), TSS, BOD₅, TP, EC, and FC were estimated using the proposed washoff rate equation. Pollutant removal is described relative to characteristic phases of the stormwater hydrographs for drainage areas of mixed land uses.

Four study areas, i.e., sites SWMI07, SWWB09, SWWA13, and SWMI15), from 18 study sites were investigated. Sites SWMI07, SWWB09, and SWWA13 are a combination of residential, recreational, and open land areas, located in Milwaukee, Whitefish Bay, and Wauwatosa. Site SWMI15 is a combination of major highway (I-94) and residential areas. Stormwater runoff from site SWMI07 drains to Lincoln Creek. The runoff from site SWWB09 drains to Lake Michigan, and Menomonee River receives stormwater runoff from sites SWWA13 and SWMI15.

Three rain events, i.e., September 22, 2005, November 5, 2005, and November 14, 2005, were selected to study (Figure 6.1). The antecedent dry periods for these events were 2.63, 12.7, and 2.0 days, respectively. The first sample for each event was taken at a specified time triggered by a certain water level in the storm sewer. The trigger point varied from site to site due to adjustments based on baseline flow. Up to seven additional samples were taken at subsequent half-hour intervals, with the last sample typically corresponding to the end of significant runoff. Parts of the work shown in this chapter can be also found in Soonthornnonda et al. (2007b).

6.1 Pollutant Washoff Rate

This washoff model is based on the following first order equation describing the pollutant mass remaining on a surface at time t after onset of a storm,

$$\frac{dM}{dt} = -ckM \quad (29)$$

where, M = pollutant mass (kg); c = transport coefficient (cm^{-1}); k = average event rainfall intensity (cm/hr). By integration we obtain $M = M_o e^{-ckt}$ where M_o is the initial mass on the area at $t = 0$. Thus, the rate of mass removal \dot{M} is

$$\dot{M} = -\frac{dM}{dt} = ckM_o e^{-ckt} \quad (30)$$

Eqs 29 and 30, or similar equations, were formulated by Sartor et al. (1974), Alley (1981), and Alley and Smith (1981). Assuming that the area was completely cleaned by the previous storm, in Chapter 5, the initial mass M_o was described as a linear buildup function,

$$M_o = \alpha a \hat{\beta} A t_d \quad (31)$$

where, α = land use factor ($\text{kg}/\text{kg}_{\text{average}}$); a = deposition coefficient ($\text{kg}_{\text{average}}/\text{ha}/\text{d}$); $\hat{\beta}$ = runoff coefficient; A = catchment area (ha); t_d = antecedent dry time (d). The effective area A_e is $\hat{\beta} A$. The runoff coefficient $\hat{\beta}$ in eq 31 indicates that only the fraction $\hat{\beta}$ of the accumulated mass is available to be removed by the stormwater.

According to eqs 30 and 31, the mass washoff rate can be described as follows:

$$\frac{dM}{dt} = ck(\alpha a \hat{\beta} A t_d) e^{-ckt} \quad (32)$$

Rearranging eq 32,

$$\frac{\frac{dM}{dt}}{\alpha a \hat{\beta} A t_d k} = c e^{-ckt} \quad (33)$$

Taking natural logs of both sides, we obtain

$$\ln \left(\frac{\frac{dM}{dt}}{\alpha a \hat{\beta} A t_d k} \right) = \ln c - ckt \quad (34)$$

By letting $\frac{dM}{dt} = Q(t) C(t)$ where $Q(t)$ and $C(t)$ are the flow (m^3/sec) and the pollutant concentration (kg/m^3), respectively, eq 34 becomes

$$\ln \left(\frac{Q(t) C(t)}{\alpha a \hat{\beta} A t_d k} \right) = \ln c - ckt \quad (35)$$

Thus, log of the normalized mass rate $Q(t)C(t)/\alpha a A_e t_d k$ (cm^{-1}) vs. the cumulative rainfall kt (cm) should be a straight line with intercept $\ln c$ and slope c . For these plots, examples of which will be described later, we used flow, concentration, and rainfall data from MMSD (2003) and deposition rates from Table 6.1. If the plots are linear, or nearly so, that would support the validity of eq 32.

An approximate expression for the pollutant concentration $C(t)$ can be developed as follows. During the time dt the pollutant mass and runoff volume are

$$dM = ck (\alpha a \hat{\beta} A t_d) e^{-ckt} dt \quad (36)$$

$$dV = A \hat{\beta} k dt \quad (37)$$

Thus, the concentration $C(t) = dM/dV$ is

$$C(t) = \frac{dM}{dV} = c \alpha a t_d e^{-ckt} \quad (38)$$

Equation 36 follows from eq 32, and eq 37 expresses the volume of runoff as the runoff fraction $\hat{\beta}$ of the total rainfall volume. Note that the derivation of eq 38 is related to the formulation of Charbeneau and Barrett (1998), but modified to include specific consideration of the runoff coefficient $\hat{\beta}$, deposition rate (αa), and antecedent dry period t_d .

It is interesting to note that if the runoff coefficient can be written as a ratio of steady-state rates of runoff and rainfall, $\hat{\beta} = Q(t)/Ak$, rather than as a ratio between corresponding volumes, eq 35 becomes

$$\ln\left(\frac{C(t)}{\alpha a t_d}\right) = \ln c - ckt \quad (39)$$

The right-hand side of this equation is identical to the right-hand side of eq 34. The general features of results obtained from this equation will be discussed and considered a few examples of the application of eq 38 for pollutant concentrations.

Table 6.1. Summary of α and a values used in eqs 35, 38, and 39.

Pollutant	Land use factor α , kg/kg _{average} ^a				Deposition coefficient a , kg _{average} /ha/d ^b
	SWMI07	SWWB09	SWWA13	SWMI15	
Zn	0.730	0.238	0.268	3.17	7.43×10^{-3}
Cu	0.687	0.576	0.684	4.12	1.45×10^{-3}
Cd	0.657	0.163	0.223	1.82	3.20×10^{-5}
Ni	0.514	0.177	0.249	1.33	4.62×10^{-4}
Pb	0.842	0.316	0.366	2.26	1.09×10^{-3}
Hg	0.723	0.213	0.378	1.54	1.26×10^{-6}
Ag	0.277	0.108	0.248	0.485	2.25×10^{-5}
BOD ₅	0.705	0.413	0.655	0.748	0.992
TSS	0.356	0.142	0.196	0.780	14.8
EC	3.39	2.74	7.09	0.225	2.66×10^9
FC	4.37	3.45	7.73	0.255	4.49×10^9
TP	0.418	0.208	0.393	0.494	5.62×10^{-2}

^aCFU/CFU_{average} for *E. coli* and fecal coliform.^bCFU_{average}/ha/d for *E. coli* and fecal coliform.

6.2 Results and Discussion

The washoff rate and concentration models (eqs 35 – 38) were applied to data from three rainfall events and twelve pollutants. The washoff models represented by eqs 35 and 39 are derived from eq 29 where the flow Q is assumed to be constant and they were therefore applied to the near constant portion of the hydrographs at peak flows. An improvement of fits was in fact achieved by omitting points in the early and late portions of the hydrographs.

Most regressions for 12 pollutants, i.e., Zn, Cu, Cd, Ni, Pb, Hg, Ag, TSS, BOD₅, TP, EC, and FC (Figures 6.2 – 6.25) provide substantial support for log-linear fits. The initial portion of hydrograph limb reflects that rain impact on a dry surface results in more splash related energy, compared to later periods when there is a thin film of flowing water moving across the surface that can wash off larger materials (Pitt et al., 2004). The late portion of declining hydrograph limb can indicate increased loading of large particles that may not be source limited, or may show the effect of armor shielding. When the corresponding points are omitted from the regressions, the resulting linear fits improve (Figures 6.2 and 6.25). Calculated values of the transport coefficient c for pertinent pollutants, sites, and events based on eq 35 are listed in Tables 6.2 and 6.3.

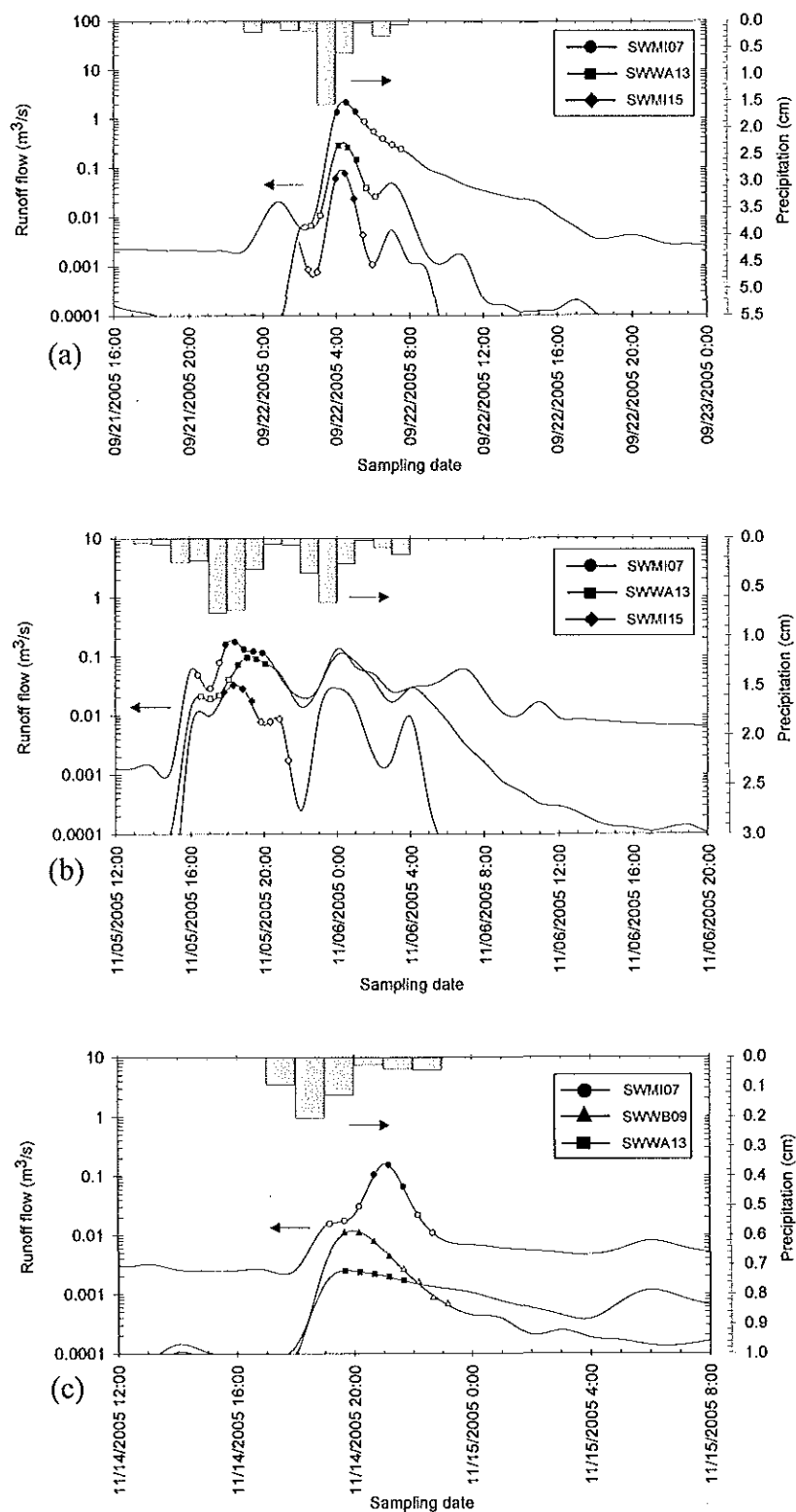


Figure 6.1. Hydrographs and hyetographs with sampling times of washoff data for sites SWMI07, SWWB09, SWWA13, and SWMI15 with precipitation gauges WS1202, WS1212, WS1210, and WS1221, respectively. Open symbols indicate data points that are excluded in the calculations.

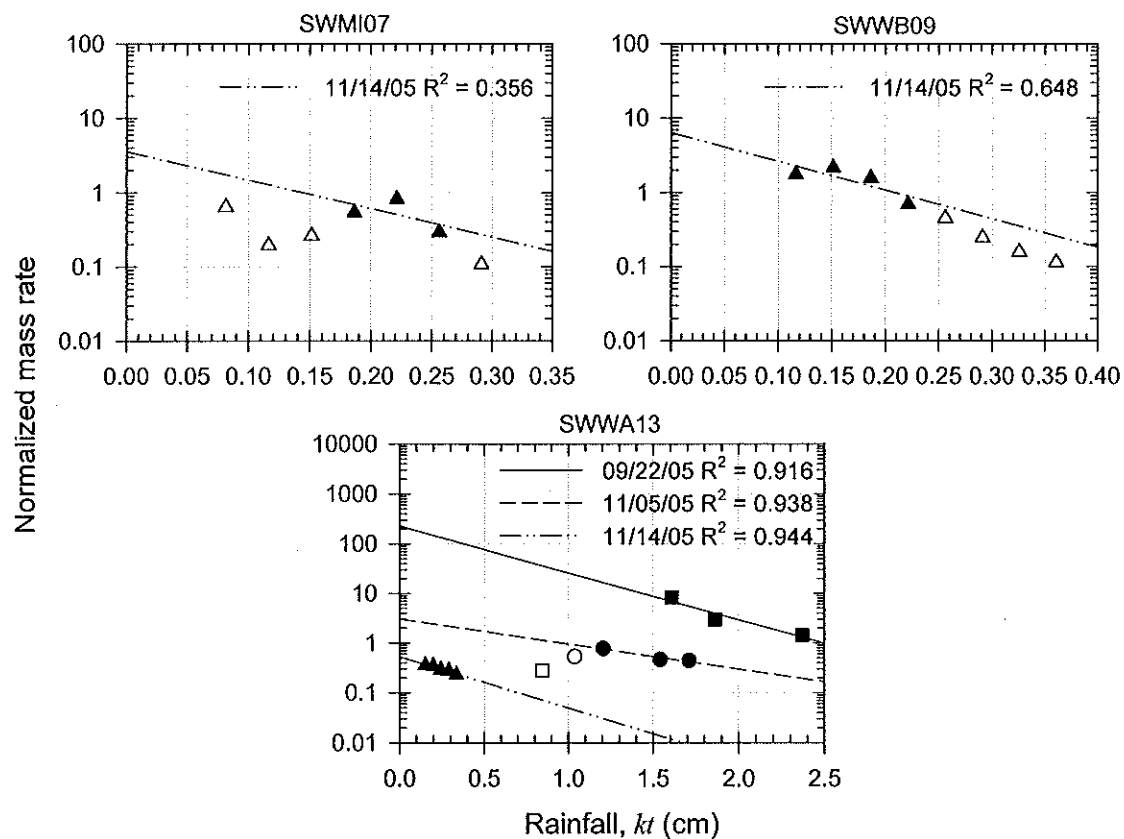


Figure 6.2. Washoff mass rate plots for Zn at sites SWMI07, SWWB09, and SWWA13. Open symbols indicate that the data were excluded from the calculations.

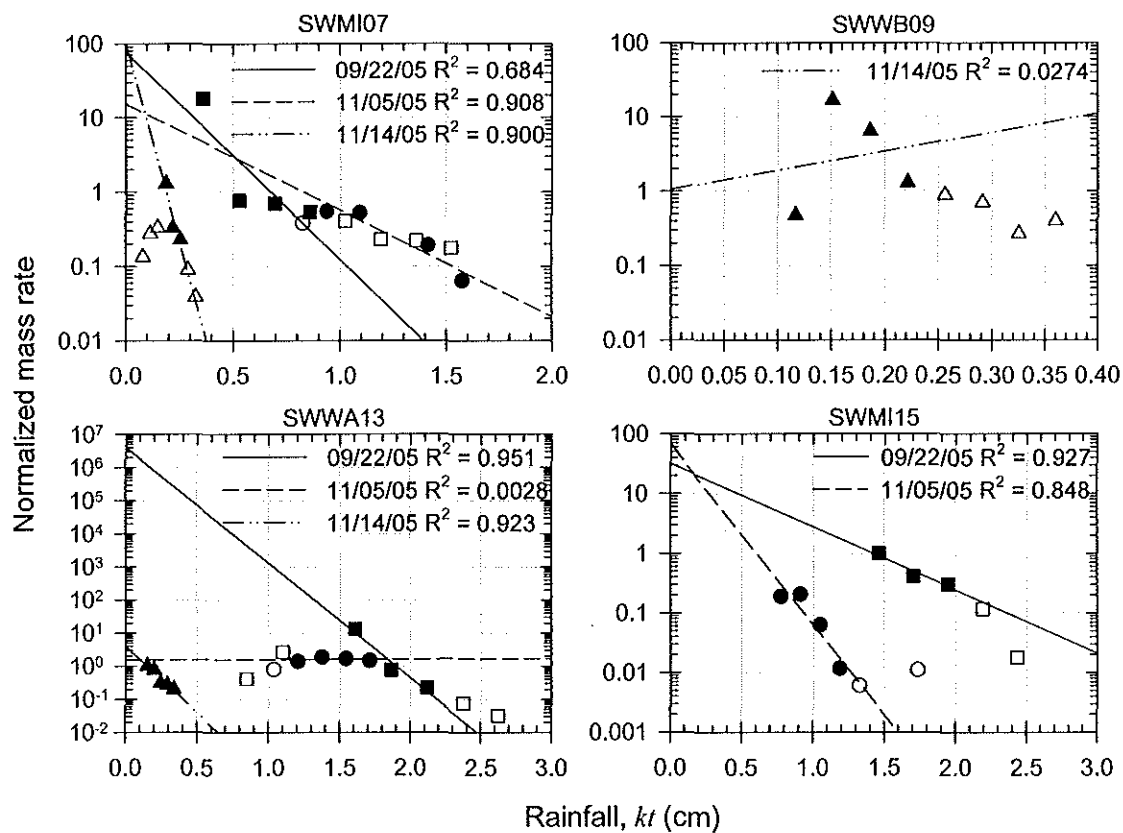


Figure 6.3. Washoff mass rate plots for *E. coli* at sites SWMI07, SWWB09, SWWA13, and SWMI15. Open symbols indicate that the data were excluded from the calculations.

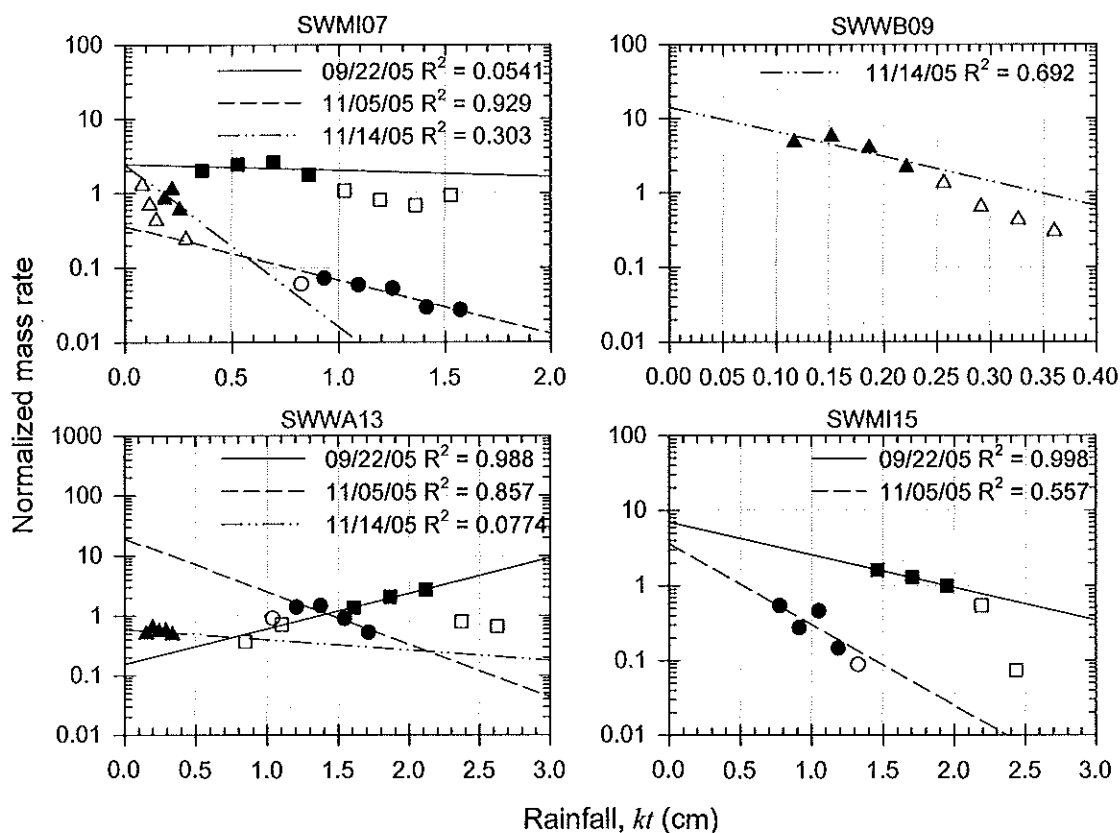


Figure 6.4. Washoff mass rate plots for TP at sites SWMI07, SWWB09, SWWA13, and SWMI15. Open symbols indicate that the data were excluded from the calculations.

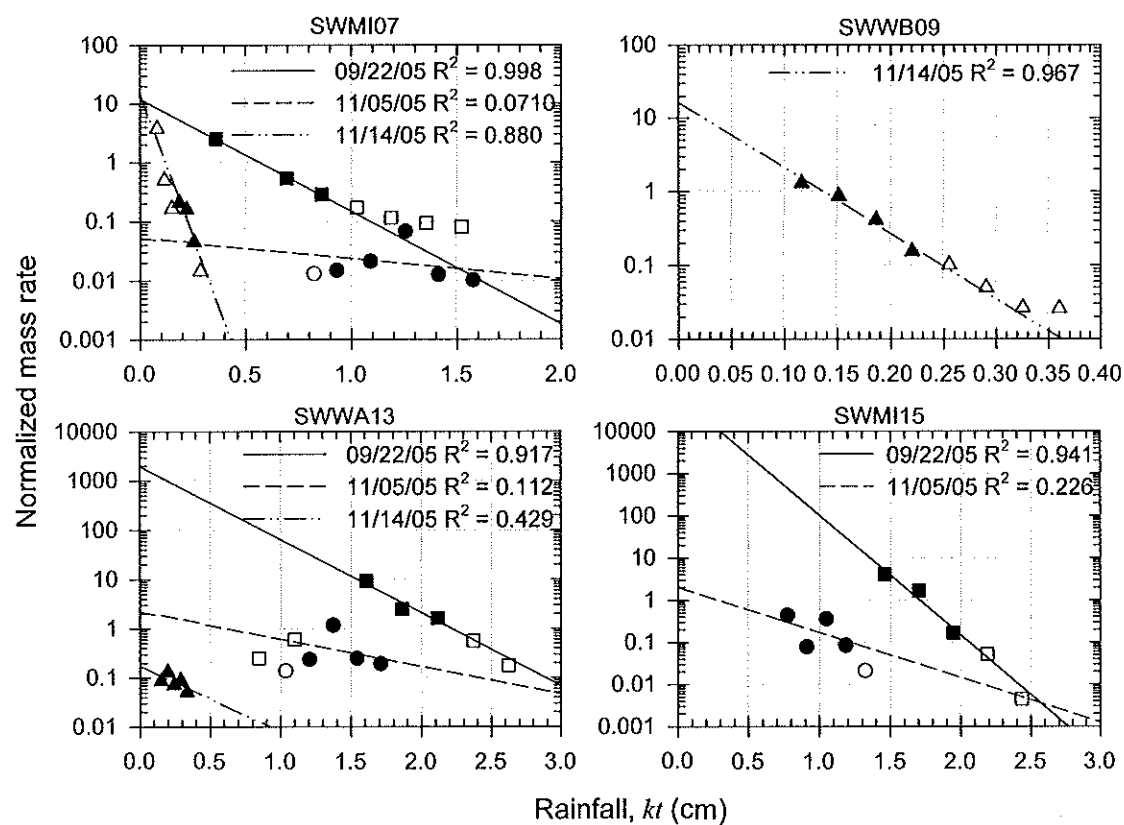


Figure 6.5. Washoff mass rate plots for TSS at sites SWMI07, SWWB09, SWWA13, and SWMI15. Open symbols indicate that the data were excluded from the calculations.

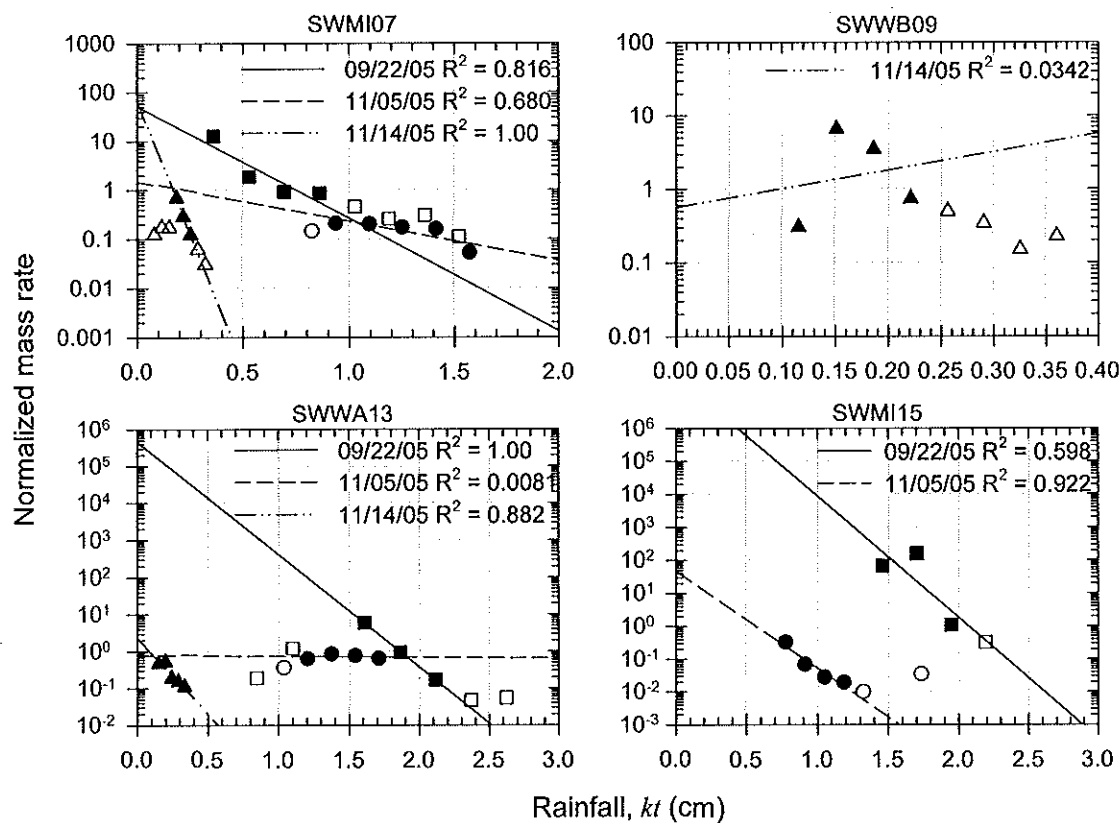


Figure 6.6. Washoff mass rate plots for fecal coliform at sites SWMI07, SWWB09, SWWA13, and SWMI15. Open symbols indicate that the data were excluded from the calculations.

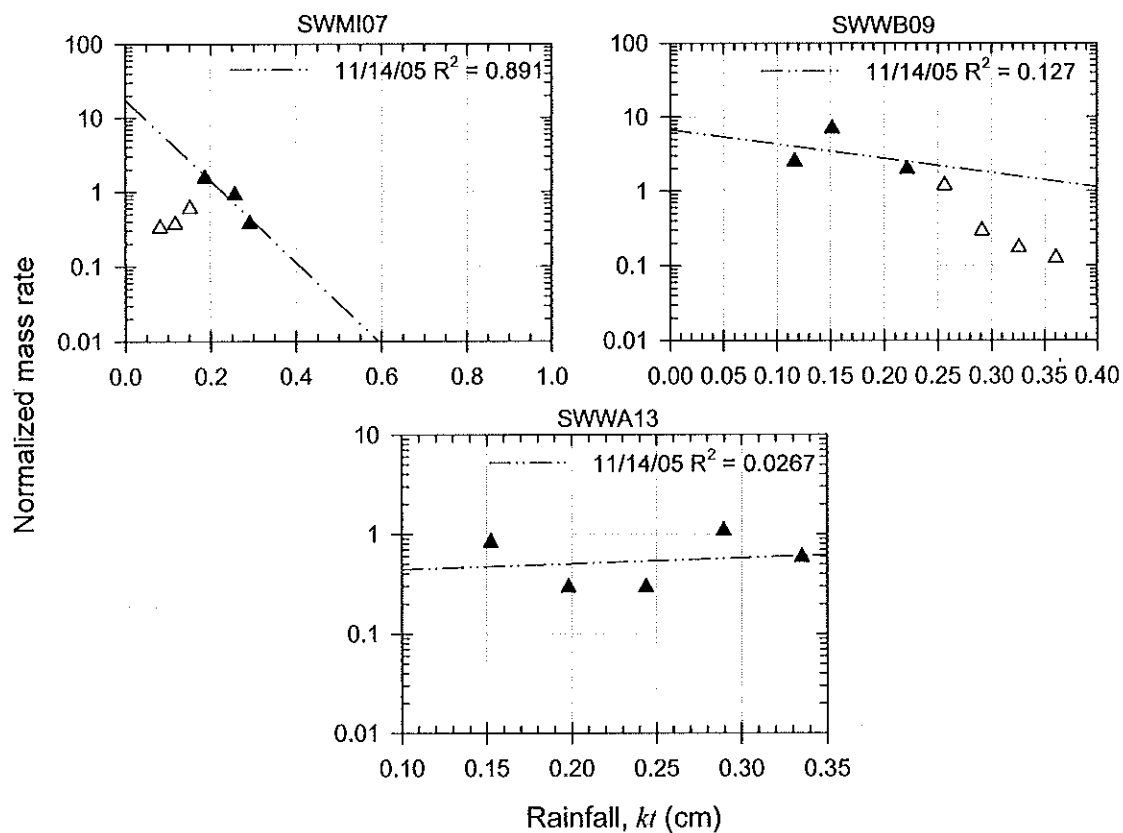


Figure 6.7. Washoff mass rate plots for BOD₅ at sites SWMI07, SWWB09, and SWWA13. Open symbols indicate that the data were excluded from the calculations.

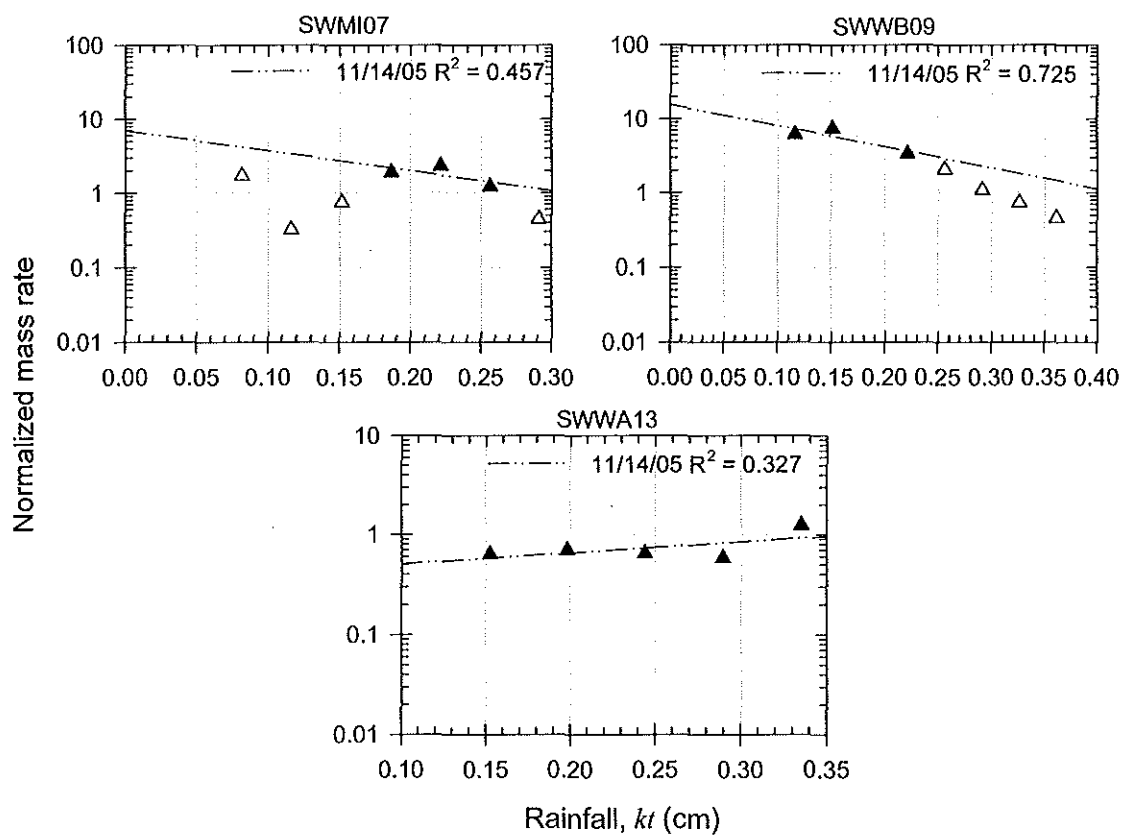


Figure 6.8. Washoff mass rate plots for Hg at sites SWMI07, SWWB09, and SWWA13. Open symbols indicate that the data were excluded from the calculations.

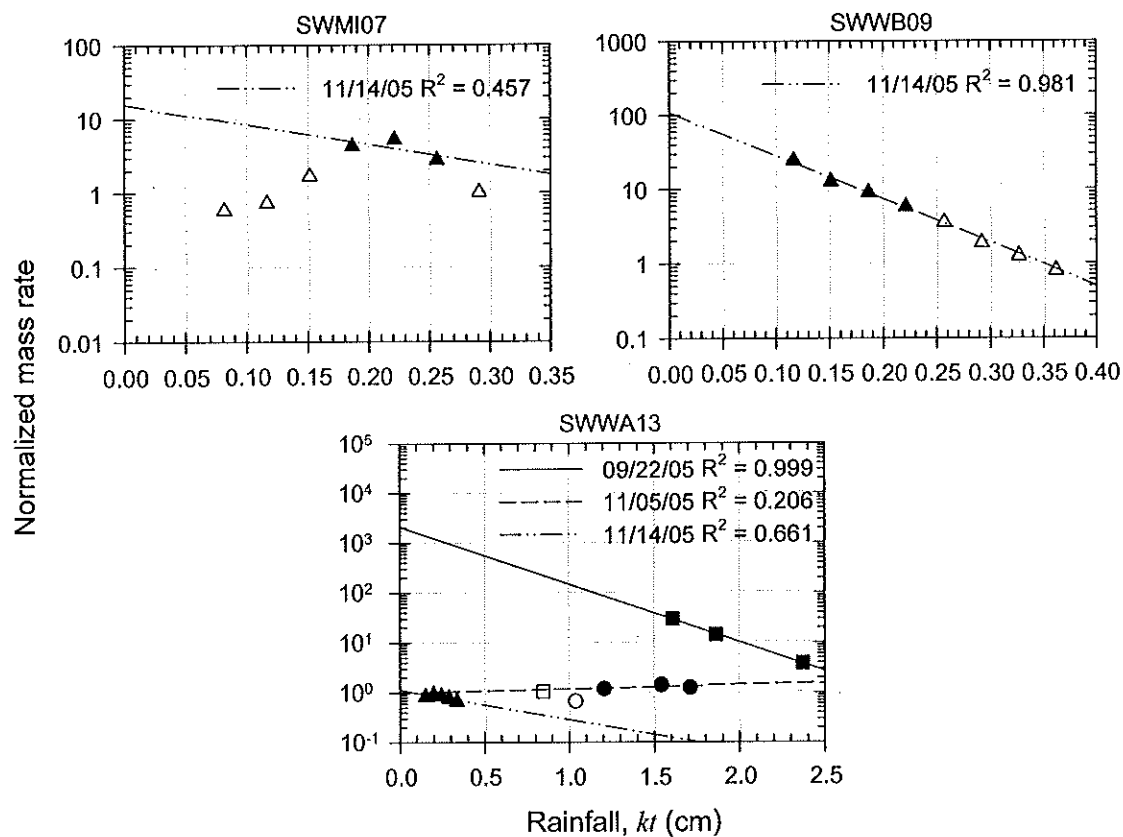


Figure 6.9. Washoff mass rate plots for Ag at sites SWMI07, SWWB09, and SWWA13. Open symbols indicate that the data were excluded from the calculations.

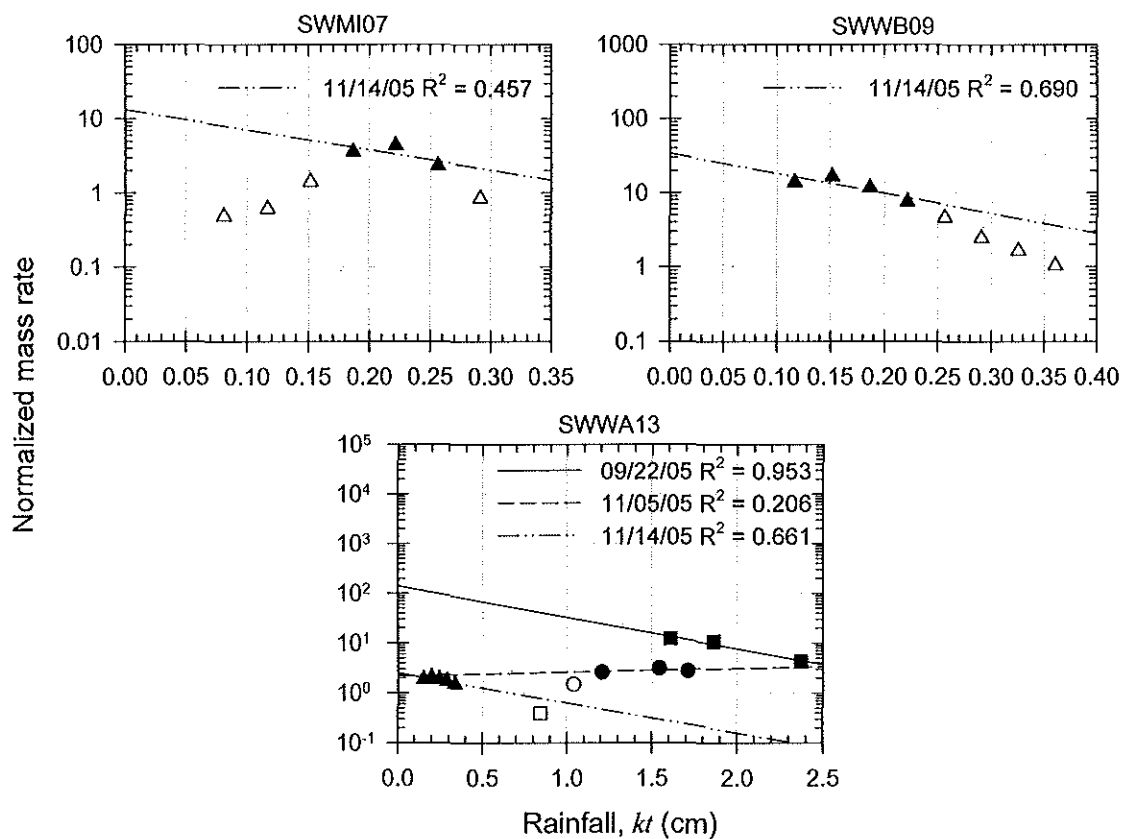


Figure 6.10. Washoff mass rate plots for Cd at sites SWMI07, SWWB09, and SWWA13. Open symbols indicate that the data were excluded from the calculations.

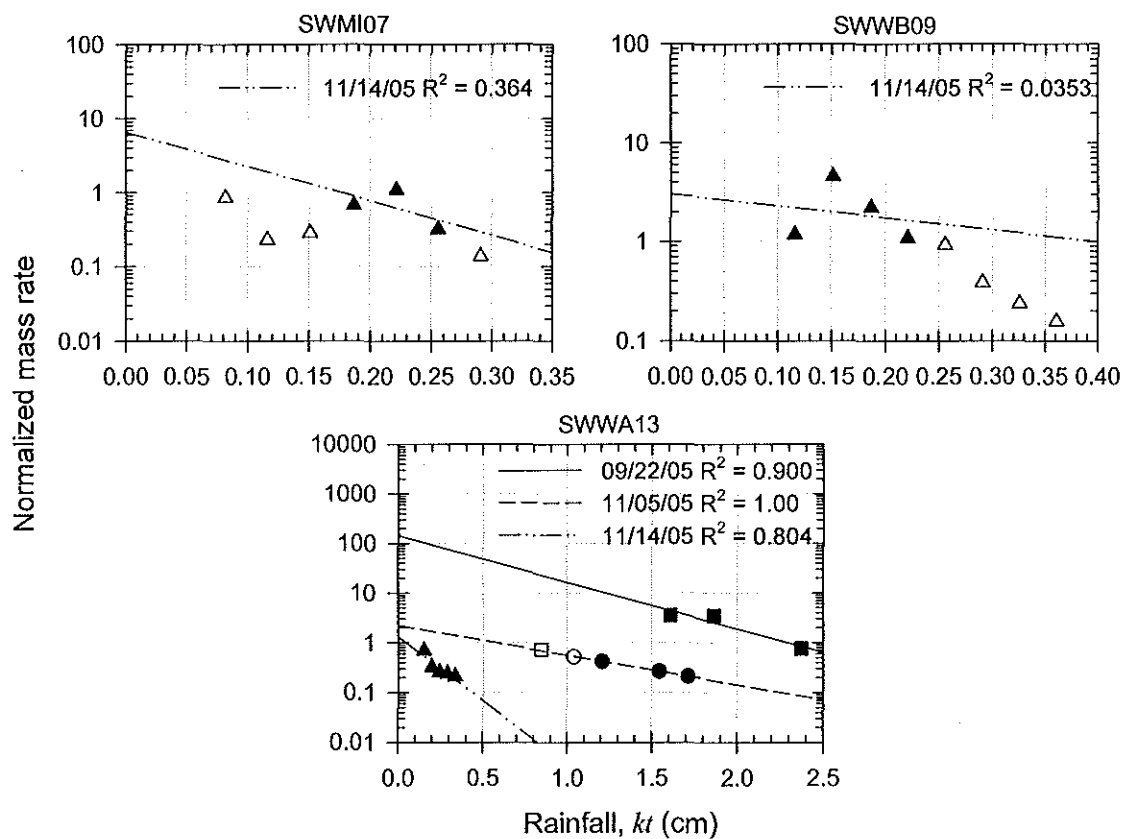


Figure 6.11. Washoff mass rate plots for Cu at sites SWMI07, SWWB09, and SWWA13. Open symbols indicate that the data were excluded from the calculations.

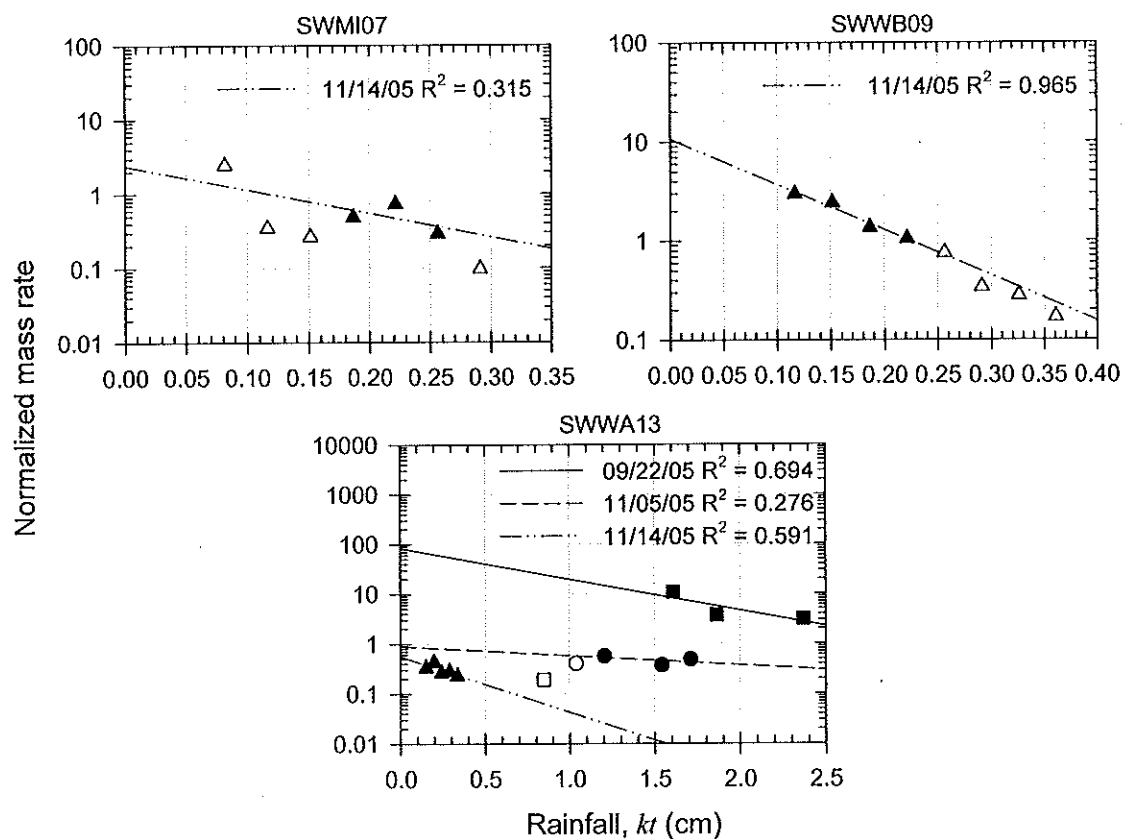


Figure 6.12. Washoff mass rate plots for Ni at sites SWMI07, SWWB09, and SWWA13. Open symbols indicate that the data were excluded from the calculations.

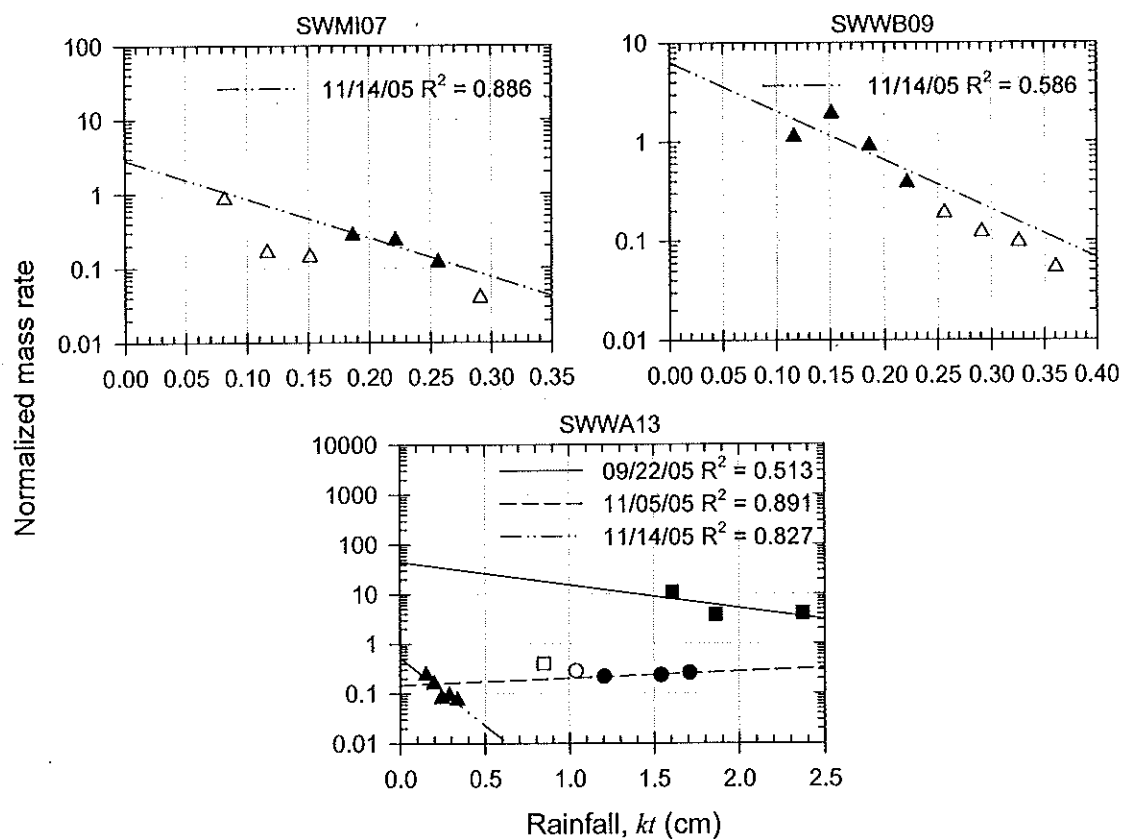


Figure 6.13. Washoff mass rate plots for Pb at sites SWMI07, SWWB09, and SWWA13. Open symbols indicate that the data were excluded from the calculations.

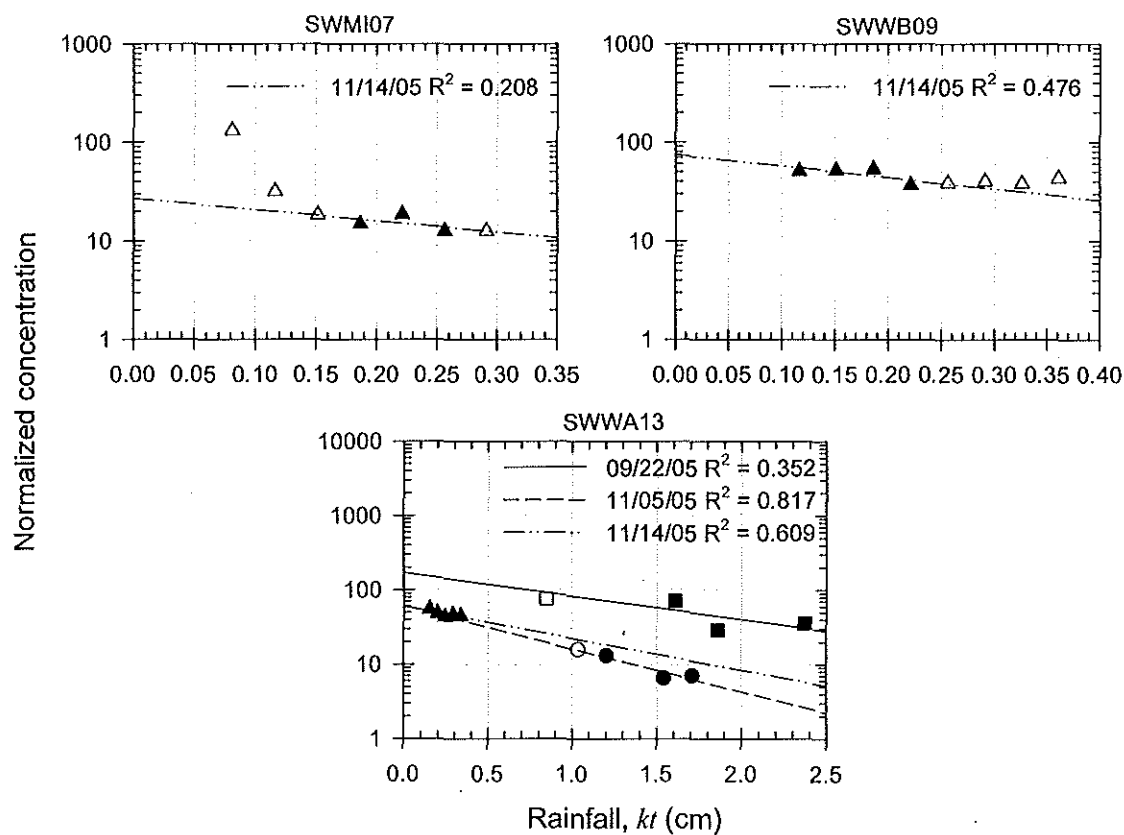


Figure 6.14. Washoff concentration plots for Zn at sites SWMI07, SWWB09, and SWWA13. Open symbols indicate that the data were excluded from the calculations.

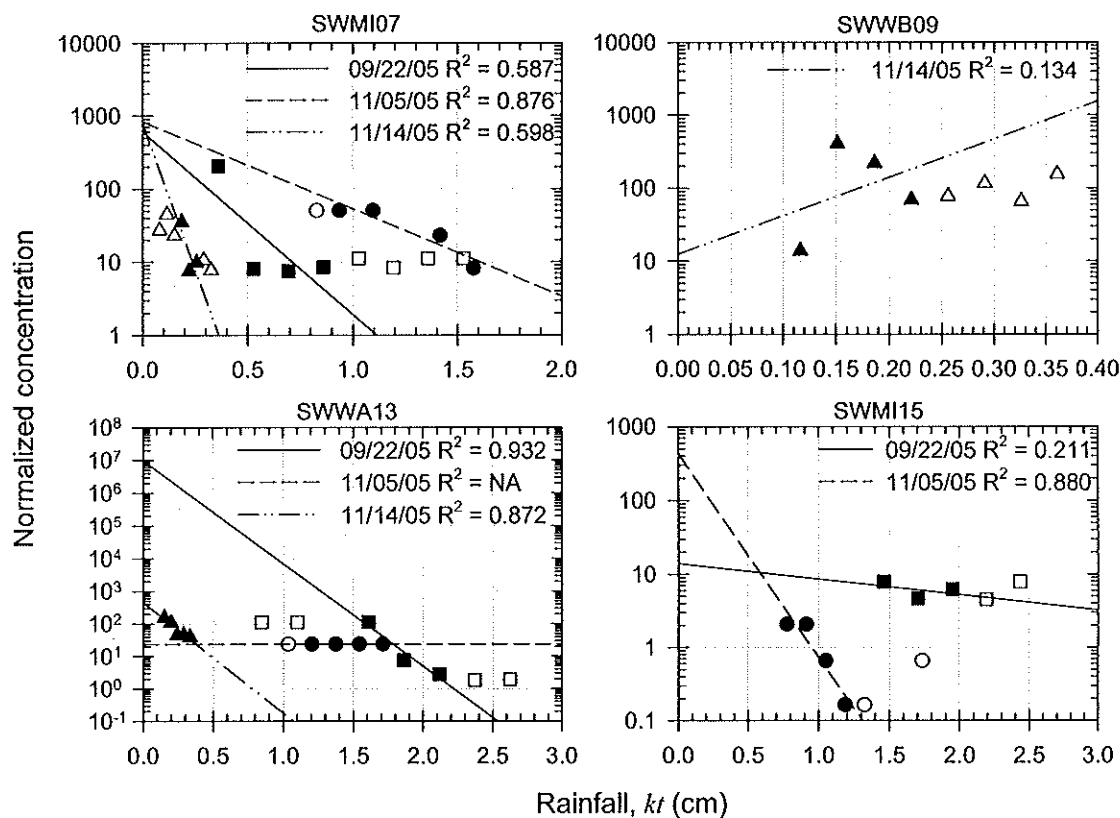


Figure 6.15. Washoff concentration plots for *E. coli* at sites SWMI07, SWWB09, SWWA13, and SWMI15. Open symbols indicate that the data were excluded from the calculations.

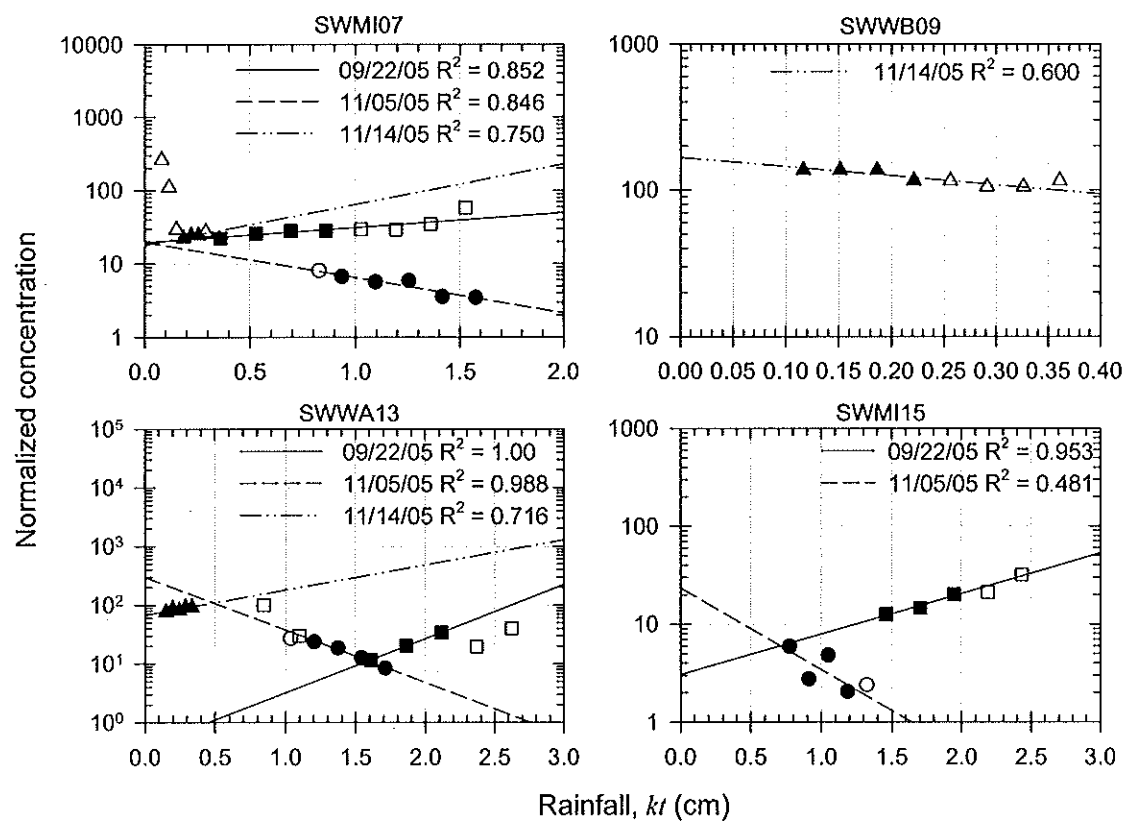


Figure 6.16. Washoff concentration plots for TP at sites SWMI07, SWWB09, SWWA13, and SWMI15. Open symbols indicate that the data were excluded from the calculations.

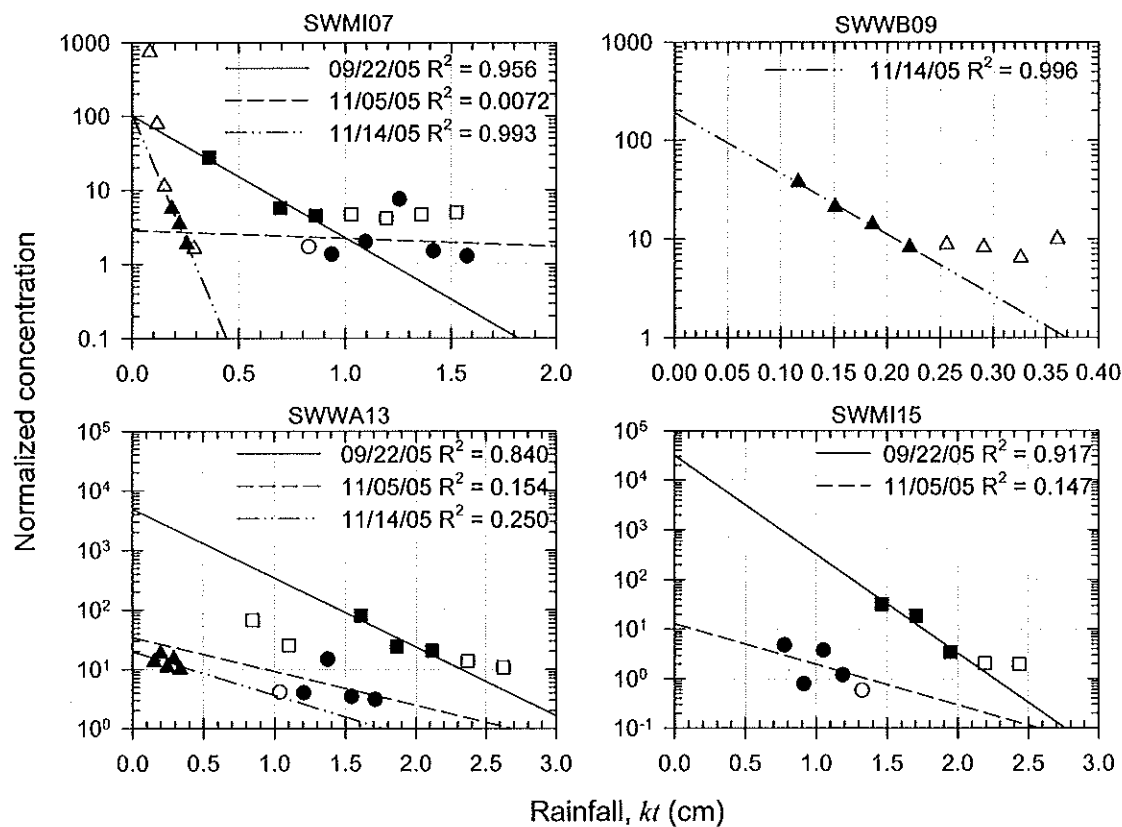


Figure 6.17. Washoff concentration plots for TSS at sites SWMI07, SWWB09, SWWA13, and SWMI15. Open symbols indicate that the data were excluded from the calculations.

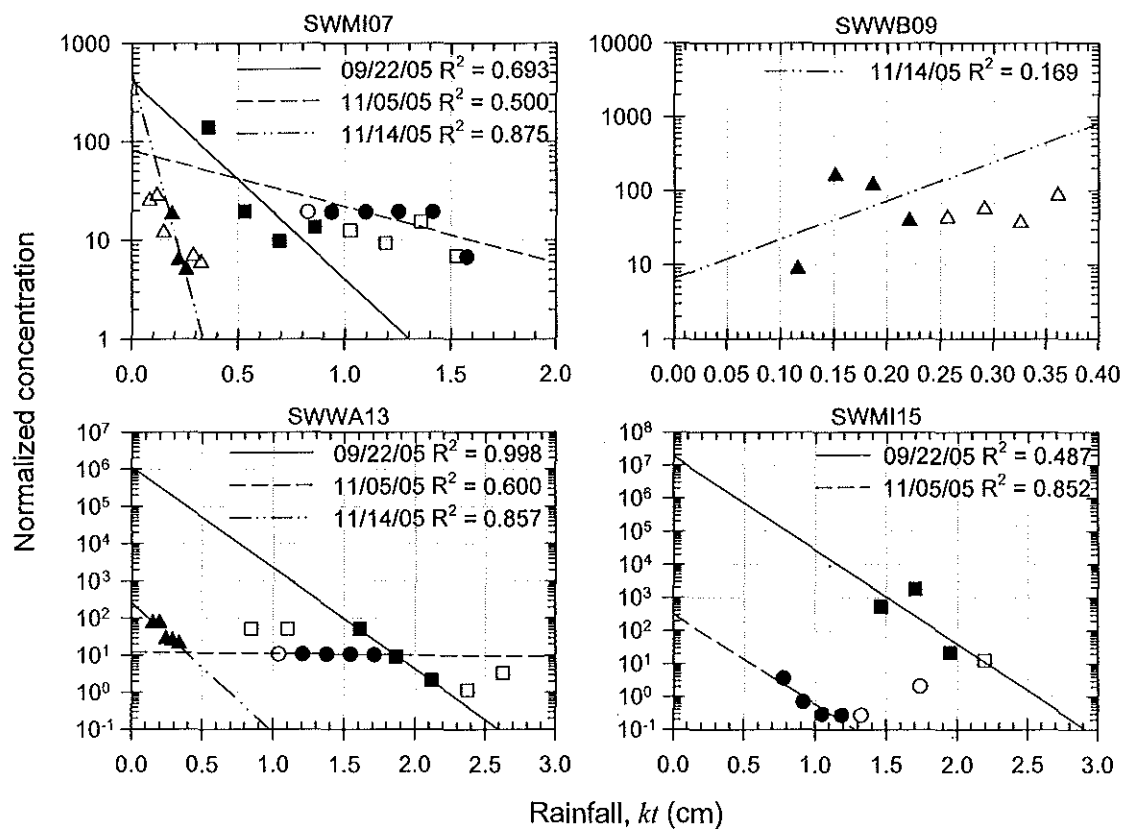


Figure 6.18. Washoff concentration plots for fecal coliform at sites SWMI07, SWWB09, SWWA13, and SWMI15. Open symbols indicate that the data were excluded from the calculations.

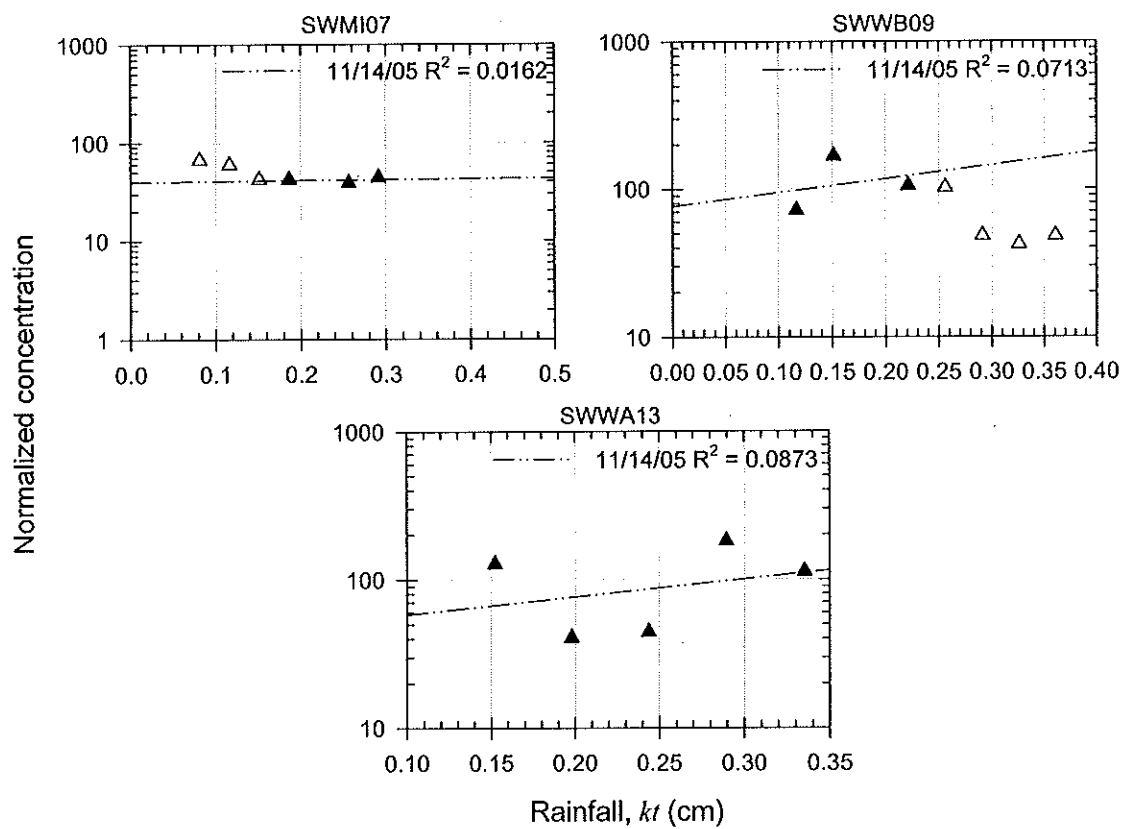


Figure 6.19. Washoff concentration plots for BOD_5 at sites SWMI07, SWWB09, and SWWA13. Open symbols indicate that the data were excluded from the calculations.

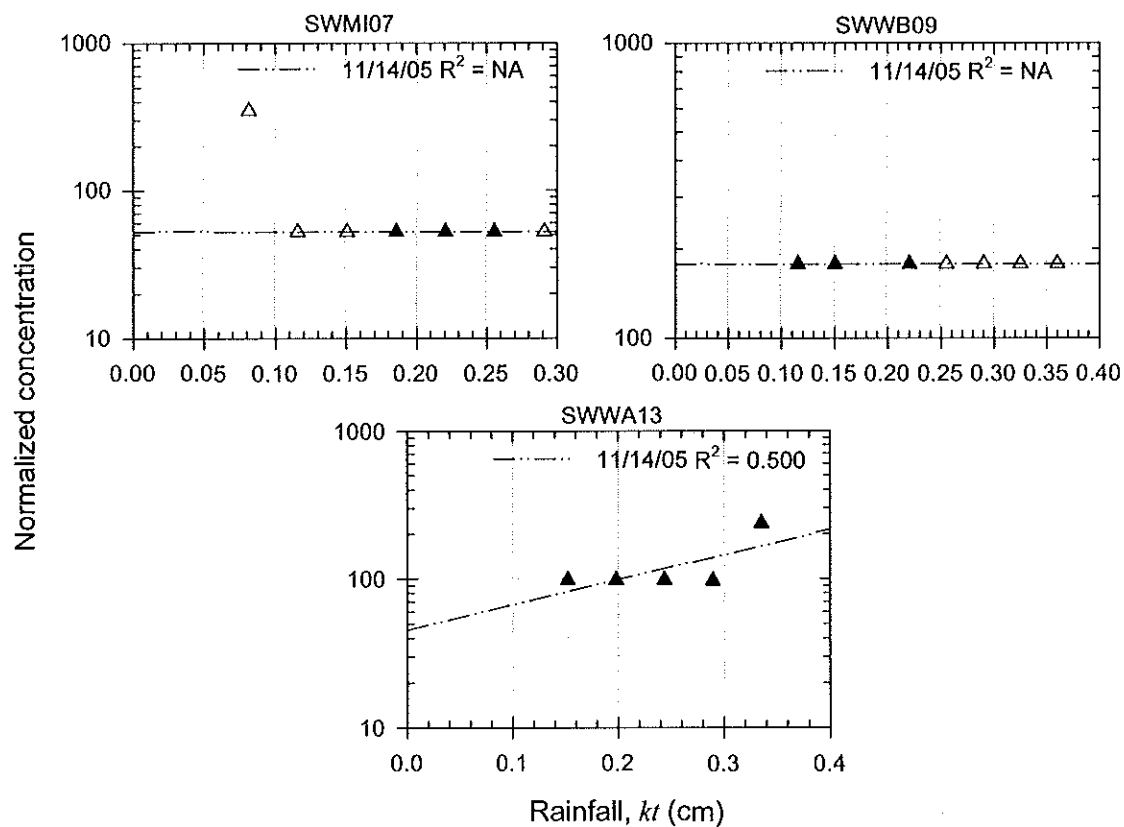


Figure 6.20. Washoff concentration plots for Hg at sites SWMI07, SWWB09, and SWWA13. Open symbols indicate that the data were excluded from the calculations.

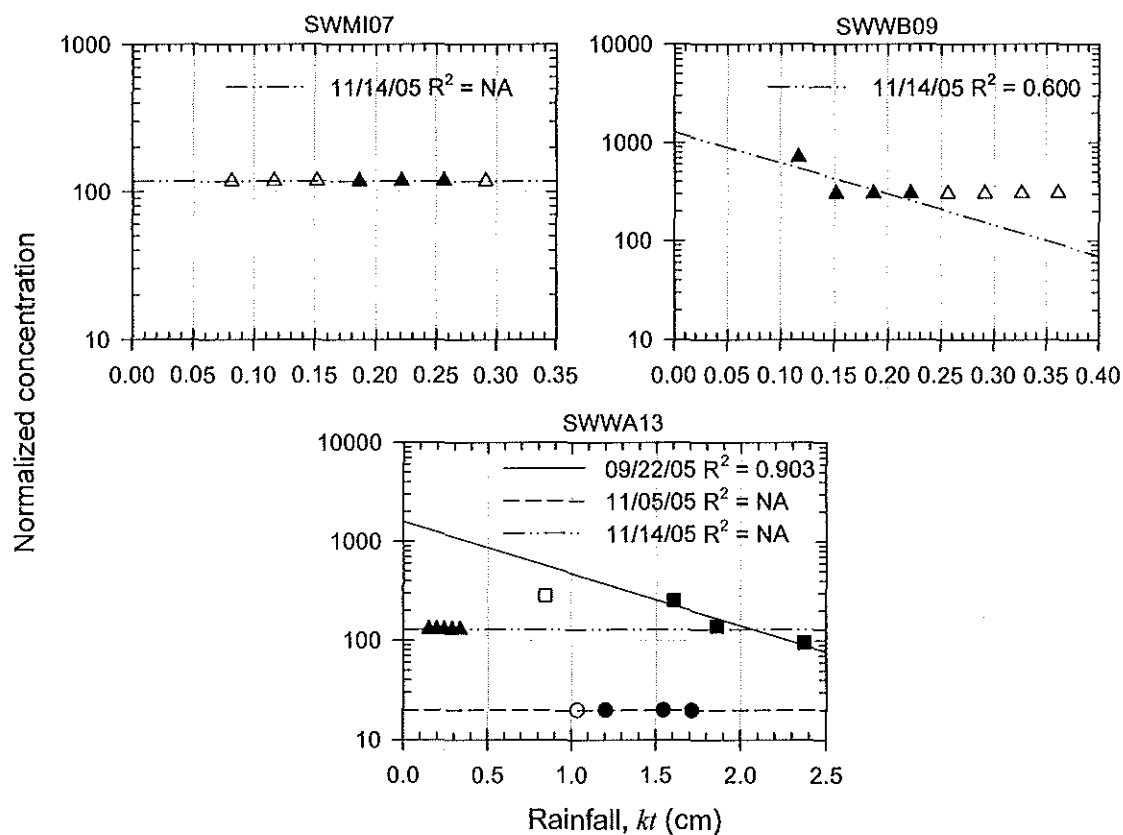


Figure 6.21. Washoff concentration plots for Ag at sites SWMI07, SWWB09, and SWWA13. Open symbols indicate that the data were excluded from the calculations.

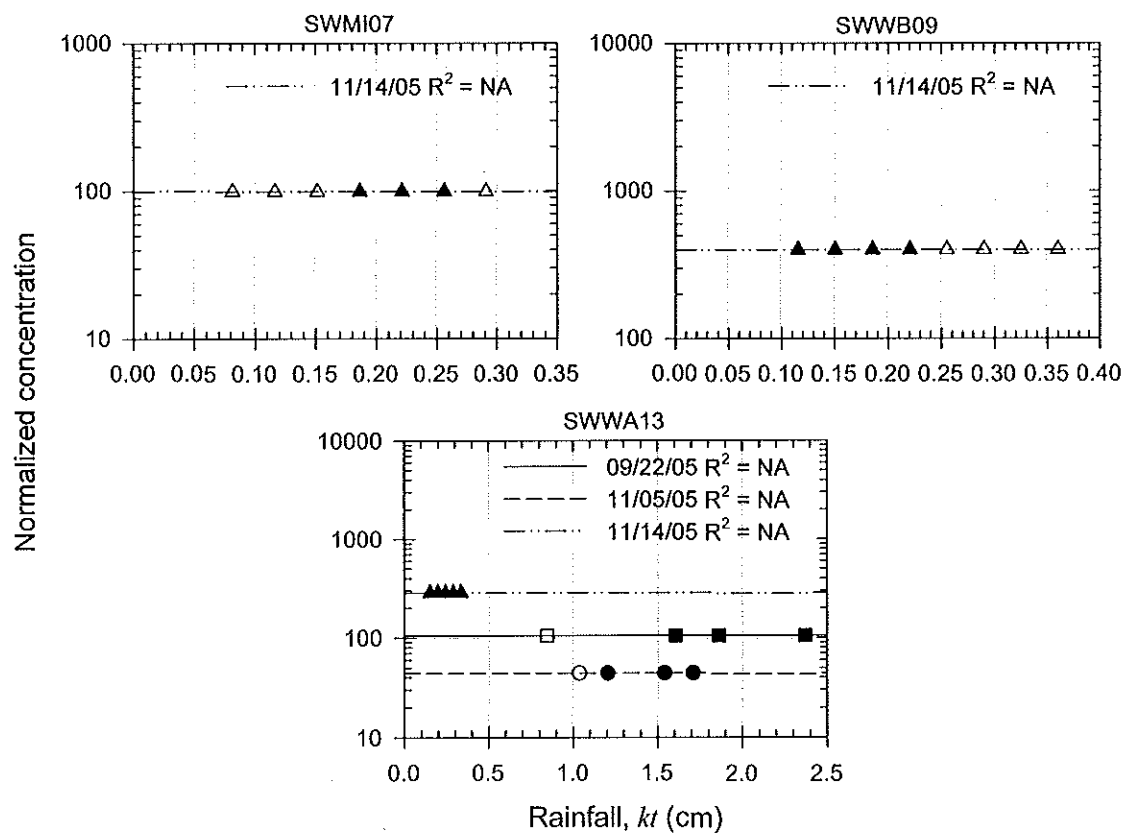


Figure 6.22. Washoff concentration plots for Cd at sites SWMI07, SWWB09, and SWWA13. Open symbols indicate that the data were excluded from the calculations.

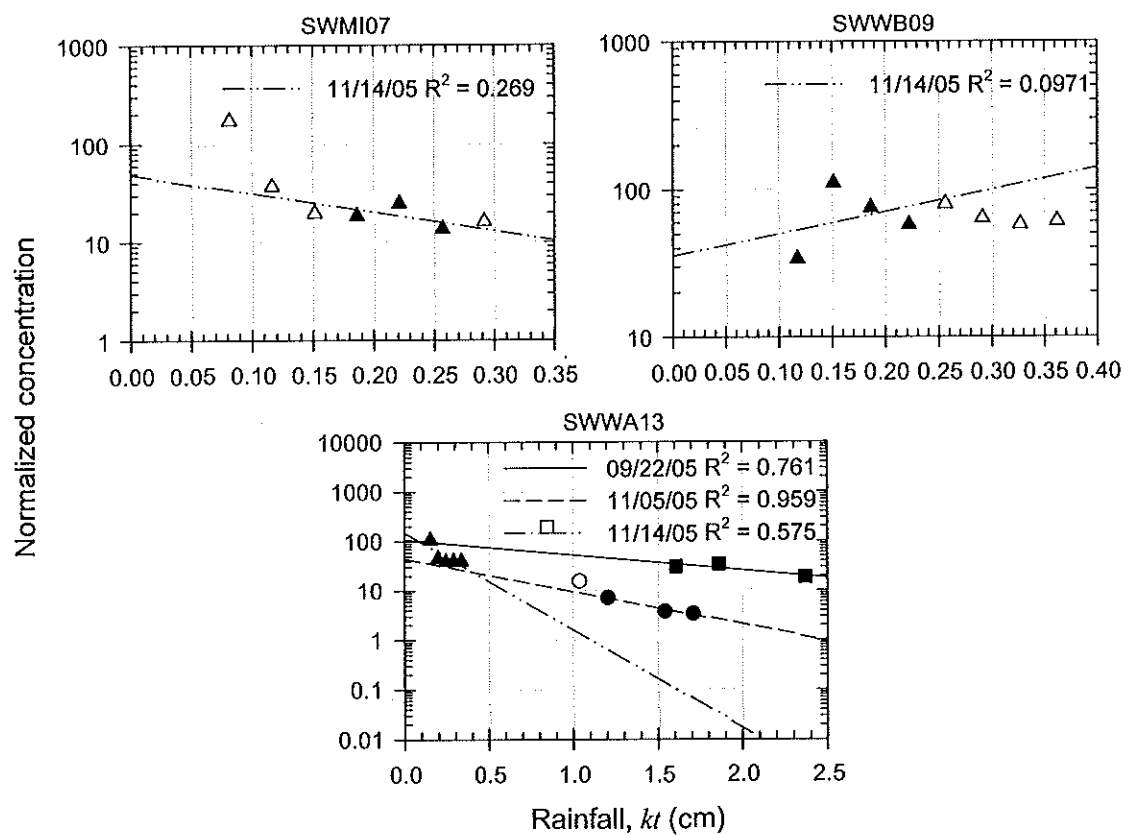


Figure 6.23. Washoff concentration plots for Cu at sites SWMI07, SWWB09, and SWWA13. Open symbols indicate that the data were excluded from the calculations.

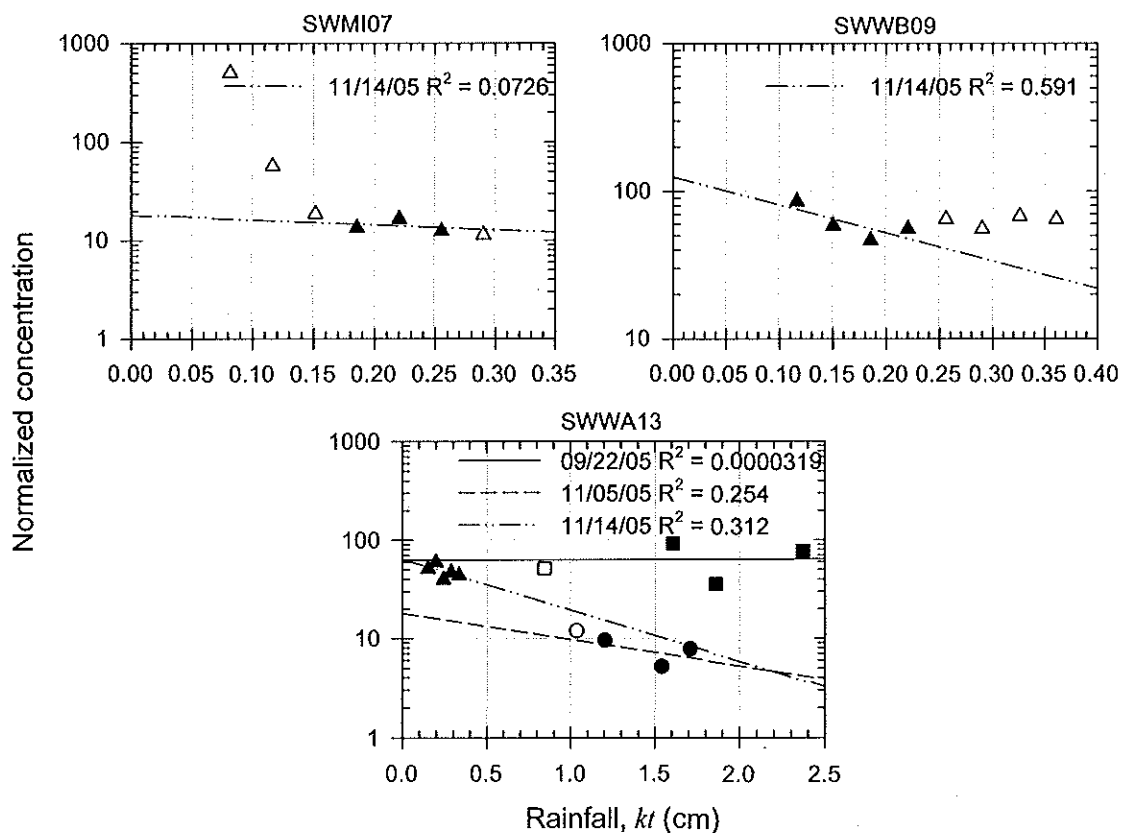


Figure 6.24. Washoff concentration plots for Ni at sites SWMI07, SWWB09, and SWWA13. Open symbols indicate that the data were excluded from the calculations.

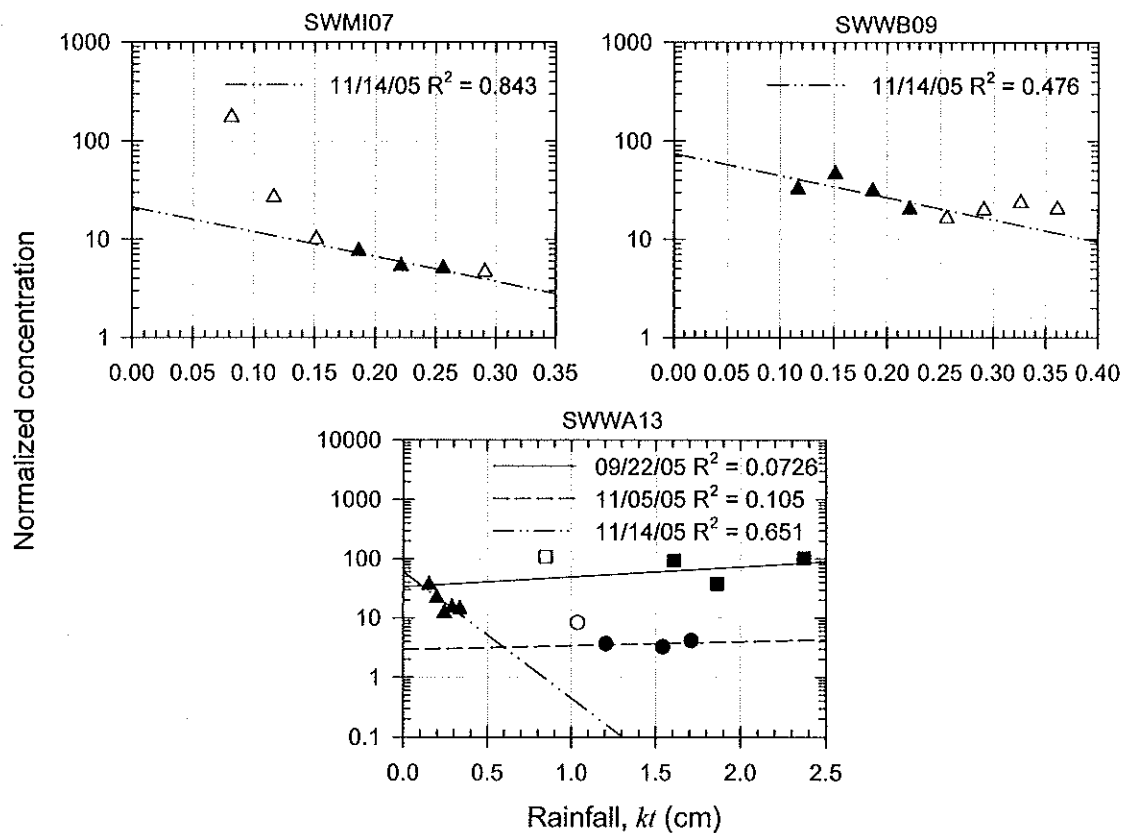


Figure 6.25. Washoff concentration plots for Pb at sites SWMI07, SWWB09, and SWWA13. Open symbols indicate that the data were excluded from the calculations.

6.2.1 Comparison of Modeled and Measured Mass Rates

Figures 6.2 – 6.13 show plots of eq. 35 for all 13 pollutants, i.e., Zn, Cu, Cd, Ni, Pb, Hg, Ag, TSS, BOD₅, TP, EC, and FC. The negative slopes of the linear regressions represent the transport coefficients c in cm^{-1} . Sixty seven percent of all monitored data from seven metals, three storm events, and three sites indicate R^2 values of >0.50 with the number of points between 3 and 5 (Table 6.2).

Plots of eq 35 for EC are illustrated in Figure 6.3. The linear correlations are also here reasonably good with most $R^2 \geq 0.60$. For FC the quality of the linear regressions are also favorable (Table 6.3). The 11/05/2005 event displays smaller c values for most pollutants from sites SWWA13 and SWMI07. This may reflect that the hydrograph has reached the near constant flow washoff segment which can be seen from Figure 6.1b. Note that a load model indicates comparable low c values around 0.60 cm^{-1} (Soonthornnonda and Christensen, 2007a). Total suspended solids for events 09/22/2005 and 11/14/2005 show good linearity (Table 6.3). The BOD₅ gave good fits for one event in site SWMI07. The linearity of the TP plots is comparable to that of other constituents of Table 6.3.

6.2.2 Comparison of Modeled and Measured Concentrations

Using eq 38 for Zn with $c = 4.69 \text{ cm}^{-1}$ gives calculated Zn concentrations ranging from 0.0942 to 0.0299 mg/L for $kt = 0.116$ to 0.361 cm considering site SWWB09 for the 11/14/2005 event. This should be compared with measured Zn concentrations ranging from 0.073 to 0.063 mg/L. Similarly, calculated EC concentrations for site SWMI07

during the 11/14/2005 event are between 65,700 and 14,700 CFU/100 mL, to be compared with measured values of 20,000 and 5,700 CFU/100 mL with corresponding kt values of 0.0815 and 0.326 cm. Other comparisons are less favorable although calculated and measured concentrations mostly are within an order of magnitude of each other.

Plots of log normalized concentrations vs. rainfall kt (not shown) using eq 39 (Figures 6.14 -6.25) are comparable to those for normalized mass rate (Figures 6.2 – 6.13), except that the linearity, measured by R^2 , and the transport coefficients c both generally are lower (Tables 6.4 and 6.5). Some concentrations plots show nearly constant values (Hg and Cd) vs. kt for selected sites and events.

Table 6.2. Summary of c values obtained by plotting eq 35 for metals.

Constituent	Event	Transport coefficient, slope, c (cm^{-1})										Average \pm standard error of the mean
		SWMI07			SWWB09				SWWA13			
		c	R^2	n^a	c	R^2	n	c	R^2	n		
Zn	09/22/05							2.17	0.916	3		
	11/05/05							1.16	0.938	3		
	11/14/05	8.87	0.356	3	8.90	0.648	4	2.37	0.944	5	4.69 \pm 1.72	
Cu	09/22/05							2.16	0.900	3		
	11/05/05							1.37	1.00	3		
	11/14/05	10.7	0.364	3	2.79	0.0353	4	5.92	0.804	5	4.59 \pm 1.71	
Cd	09/22/05							1.45	0.953	3		
	11/05/05							-0.168	0.206	3		
	11/14/05	6.26	0.457	3	6.22	0.690	4	1.38	0.661	5	3.03 \pm 1.34	
Ni	09/22/05							1.45	0.694	3		
	11/05/05							0.442	0.276	3		
	11/14/05	7.40	0.315	3	10.6	0.965	4	2.57	0.591	5	4.49 \pm 1.73	
Pb	09/22/05							1.07	0.513	3		
	11/05/05							-0.320	0.891	3		
	11/14/05	12.1	0.886	3	11.4	0.586	4	6.28	0.828	5	6.10 \pm 2.55	
Hg	09/22/05											
	11/05/05											
	11/14/05	6.26	0.457	3	6.60	0.725	3	-2.51	0.363	5	3.45 \pm 2.98	
Ag	09/22/05							2.66	1.00	3		
	11/05/05							-0.168	0.206	3		
	11/14/05	6.26	0.457	3	13.5	0.981	4	1.38	0.661	5	4.73 \pm 2.44	

^a n = number of data points

^a n = number of data points4.69 \pm 1.724.59 \pm 1.713.03 \pm 1.344.49 \pm 1.736.10 \pm 2.553.45 \pm 2.984.73 \pm 2.44

Table 6.3. Summary of c values obtained by plotting eq 35 for BOD₅, TSS, TP, and bacteria.

Constituent	Event	Transport coefficient, slope, c (cm ⁻¹)										Average ± standard error of the mean	
		SWMI07		SWWB09		SWWA13		SWMI15		n			
		c	R ²	n ^a	c	R ²	n	c	R ²		c		R ²
BOD ₅	09/22/05												
	11/05/05												
TSS	11/14/05	12.6	0.891	3	4.47	0.127	3	-1.35	0.0267	5			5.24 ± 4.05
	09/22/05	4.41	0.998	3				3.42	0.917	3	6.54	0.941	3
	11/05/05	0.789	0.0710	5				1.29	0.112	4	2.46	0.226	4
	11/14/05	22.0	0.880	3	20.4	0.967	4	3.08	0.429	5			7.16 ± 2.72
E. coli	09/22/05	6.43	0.684	4				8.02	0.951	3	2.44	0.927	3
	11/05/05	3.29	0.908	4				-0.0321	0.00280	4	6.95	0.848	4
Fecal coliform	11/14/05	24.6	0.900	3	-5.85	0.0274	4	9.22	0.923	5			6.12 ± 2.79
	09/22/05	5.29	0.816	4				7.02	1.00	3	8.48	0.598	3
	11/05/05	1.85	0.680	5				0.0593	0.00810	4	6.83	0.922	4
	11/14/05	24.7	1.00	3	-5.79	0.0342	4	9.44	0.882	5			6.43 ± 2.79
TP	09/22/05	0.194	0.0541	4				-1.36	0.988	3	1.00	0.998	3
	11/05/05	1.65	0.929	5				2.03	0.857	4	2.49	0.557	4
	11/14/05	4.99	0.303	3	7.66	0.692	4	0.400	0.0774	5			2.12 ± 0.907

^a n = number of data points

^a n = number of data points

Table 6.4. Summary of c values obtained by plotting eq 39 for metals.

Constituent	Event	Transport coefficient, slope, c (cm^{-1})										Average \pm standard error of the mean
		SWMI07			SWWB09			SWWA13				
		c	R^2	n^a	c	R^2	n	c	R^2	n		
Zn	09/22/05							0.721	0.352	3		
	11/05/05							1.33	0.817	3		
	11/14/05	2.61	0.208	3	2.67	0.476	4	0.988	0.609	5	1.67 \pm 0.411	
Cu	09/22/05							0.709	0.761	3		
	11/05/05							1.54	0.959	3		
	11/14/05	4.44	0.269	3	-3.43	0.0971	4	4.54	0.575	5	1.56 \pm 1.46	
Cd	09/22/05											
	11/05/05											
	11/14/05											
Ni	09/22/05											
	11/05/05							0.610	0.254	3		
	11/14/05	1.15	0.0726	3	4.37	0.591	4	1.19	0.312	5	1.83 \pm 0.857	
Pb	09/22/05							-0.382	0.0726	3		
	11/05/05							-0.151	0.150	3		
	11/14/05	5.81	0.843	3	5.17	0.476	4	4.90	0.651	5	3.07 \pm 1.37	
Hg	09/22/05											
	11/05/05											
	11/14/05							-3.90	0.500	5		
Ag	09/22/05							1.21	0.903	3		
	11/05/05											
	11/14/05				7.28	0.600	4				4.24 \pm 3.03	

^a n = number of data points

Table 6.5. Summary of c values obtained by plotting eq 39 for BOD₅, TSS, TP, and bacteria.

Constituent	Event	Transport coefficient, slope, c (cm ⁻¹)												Average ± standard error of the mean	
		SWM107			SWWB09			SWWA13			SWM115				
		c	R ²	n ^a	c	R ²	n	c	R ²	n	c	R ²	n		
BOD ₅	09/22/05														
	11/05/05														
TSS	11/14/05	-0.156	0.0162	3	-2.13	0.0713	3	-2.73	0.0873	5					
	09/22/05	3.80	0.956	3				2.67	0.840	3	4.58	0.917	3		
	11/05/05	0.247	0.0072	5				1.32	0.154	4	1.89	0.147	4		
	11/14/05	15.7	0.993	3	14.2	0.996	4	1.70	0.250	5					
<i>E. coli</i>	09/22/05	5.76	0.587	4				7.26	0.932	3	0.488	0.211	3		
	11/05/05	2.75	0.876	4							6.39	0.880	4		
	11/14/05	18.4	0.598	3	-12.1	0.134	4	7.84	0.872	5					
	09/22/05	4.63	0.693	4				6.26	0.998	3	6.52	0.487	3		
Fecal coliform	11/05/05	1.31	0.500	5				0.0914	0.600	4	6.26	0.852	4		
	11/14/05	18.4	0.875	3	-12.0	0.169	4	8.06	0.857	5					
TP	09/22/05	-0.473	0.852	4				-2.12	1.00	3	-0.953	0.953	3		
	11/05/05	1.11	0.846	5				2.06	0.988	4	1.92	0.481	4		
	11/14/05	-1.27	0.750	3	1.44	0.600	4	-0.982	0.716	5					
0.0816 ± 0.519															

^a n = number of data points

^a n = number of data points

6.2.3 Transport Coefficients

The transport coefficients c for seven metals, BOD₅, TSS, TP, and bacteria based on eq 35 are shown in Tables 6.2 and 6.3. Considering metals, the highest c value (6.10 cm⁻¹) is for Pb and the lowest (3.03 cm⁻¹) for Cu. These results indicate that the ability of metals to be removed from the surface is ranked in the order Pb>Ag>Zn>Cu>Ni>Hg>Cd which may reflect a decreasing degree of particle association with Pb having the highest, and Hg and Cd the least particle affinity. A related but not directly comparable result was obtained by Ellis et al. (1987) who investigated average removal rates to a catchment outfall from highway surface runoff in the northwestern London for Cd, Cu, Pb, and Zn. The order of removal rates (μg/m²/cm runoff) was Pb (370) > Zn (348) > Cu (92.2) > Cd (4.80). These values indicate total removal rates whereas obtained coefficients are relative rates, $-dM/(Mk dt)$, see eq 29.

Four negative slopes for Cd, Hg, Pb, and Ag may indicate that while the particulate fraction is removed to some extent, contaminants in the soluble phase or additional solids are being replenished, and will only drop for larger kt values. Colman et al. (2001) suggested that a possible nonautomotive source of Cd is insecticide application. Cameron and Green (2005) stated that common sources of Hg are latex paint and household detergents and that of Ag are batteries, fungicides, and medical supplies. Sansalone et al. (2005) indicated that Pb can come from anti-caking agents used on deicing salt.

The transport of Zn, Cu, Ni, and Pb, especially from traffic emission (Sansalone et al., 2005), depends on deposition fluxes, and transport coefficients. Thus for a given

deposition flux, washoff is enhanced by a large transport coefficient which is found in area such as Whitefish Bay (SWWB09) with accessible and easily washable roads.

Evidence for higher average particulate concentration of Cd ($\mu\text{g/g}$) in stormwater solids than that on road surface was confirmed by Revitt et al. (1990) even though Cd showed less ability to be washed than other pollutants. Also, Ellis et al. (1987) reported that Cd has the highest ratio of soluble to insoluble metal out of Cu, Pb, and Zn in road runoff. The high c values of TSS $7.16 \pm 2.72 \text{ cm}^{-1}$ (Table 6.3) confirms that solids are preferentially removed from drainage areas.

The ability of TP to be washed from the surface is comparatively small, probably because much of the TP is in the dissolved phase. Waschbusch et al. (1999) reported that lawns are the largest contributors of TP and streets are the largest source of TSS. The negative slopes in Table 6.3, which are noticeable for BOD₅, TP, and EC, indicate pollutant replenishment.

In terms of cumulative rainfall kt capable of causing a 10-fold reduction in removal rates, we see that kt values for Zn at site SWMI07 and SWWB09 are relatively small ($\sim 0.25 \text{ cm}$) whereas more rainfall is required for such a reduction at site SWWA13 (Figure 6.2). Metals are mainly on the streets at the two former sites, and therefore removal is enhanced even by small amounts of precipitation. By comparison, EC shows a more varied picture (Figure 3) indicating that EC can be associated with roads, residential areas such as lawns, and commercial areas.

Transport coefficients for EC and FC are virtually identical, and only a little less than the c values of TSS. It is generally believed EC and FC come to stormwater runoff from pervious and impervious surfaces, failing septic systems, and direct deposition of

animal feces (Petersen, 2005). Transport and removal of microbial contamination is mediated in part by soil and sedimentation of attached organisms. Muirhead et al. (2006) investigated the transport mechanisms of microorganisms during the rainfall events, and concluded that the majority of bacteria attach to the fine particles ($< 2 \mu\text{m}$), and appeared to move rapidly across the study area. In contrast, bacterial transport could be significantly reduced if the cells were pre-attached to large soil particles ($> 45 \mu\text{m}$), which mainly came from lawns, and are generally less mobile in the environment, settle faster, and may have different rate of mortality than their free phase counterparts (Fries et al., 2006). The majority of the EC and FC that were detected in the stormwater runoff may have come from free phase bacteria or bacteria attached to fine particles, and are associated with animal feces on roads. Pitt et al. (2004) found that most washoff particles were less than $63 \mu\text{m}$ in size.

The order of removal efficiency for all pollutants (Tables 6.2 and 6.3) are $\text{TSS} > \text{FC} > \text{EC} > \text{Pb} > \text{BOD}_5 > \text{Ag} > \text{Zn} > \text{Cu} > \text{Ni} > \text{Hg} > \text{Cd} > \text{TP}$. This order is nearly the same as obtained from concentration vs. kt plots (eq 39): $\text{TSS} > \text{EC} > \text{FC} > \text{Ag} > \text{Pb} > \text{Ni} > \text{Zn} > \text{Cu} > \text{TP}$. On the basis of a load model (Soonthornnonda and Christensen, 2007a) the ease of removal ranking is $\text{TSS} > \text{Cd} > \text{FC} > \text{BOD}_5 > \text{Hg} > \text{Pb} > \text{Zn} > \text{EC} > \text{Cr} > \text{Cu} > \text{TP} > \text{Ni}$ which is similar to the above two rankings except for Cd and EC. The load model sequence follows the ratio R_2^2/R_1^2 where R_1^2 and R_2^2 are multiple correlation coefficients for modeled constituents with consideration of one and two dry periods, respectively, prior to the storm being analyzed. A large value of this ratio indicates that the drainage area is not clean after the previous storm so that it is important to consider the pollutant mass

accumulated in the dry period before the previous storm. In this case the pollutant is relatively difficult to remove.

The values of c listed in Table 6.2 and 6.3 are generally a factor 4 - 8 higher than most values determined for single land use areas (Alley, 1981; Grottker, 1987; Charbeneau and Barrett, 1998) or from a load model applied to the same mixed land use drainage areas ($\sim 0.60 \text{ cm}^{-1}$) (Soonthornnonda and Christensen, 2007a). Values of c comparable to this value were obtained with this washoff model from the event of 11/05/2005 where there is a nearly constant flow over 2 - 3 hours. Thus, the results of the washoff model considered here lend support to the value of the transport coefficient used in the load model, but indicate also that these coefficients tend to be higher when they are based on narrow peaks of the hydrograph.

VII. FRACTION OF STORMWATER IN COMBINED SEWER OVERFLOWS (CSOs)

Combined sewer overflows (CSOs) can have significant impacts on the water quality of local waterways. For example, Ab Razak and Christensen (2001) reported that since a 19.5 mile (31.4 km) inline storage system (ISS) in Milwaukee began operating in 1994, concentrations of BOD₅, TP, Zn, and TSS have decreased in the Milwaukee's combined sewer service area (CSSA). Elimination of overflows by increasing ISS pumping and storage capacity showed improvements of water quality in the area (MMSD, 2007b). However, these improvements are not sufficient for local waterways to meet the US Environmental Protection Agency (US EPA) Water Quality Criteria for nutrients and bacteria (US Geological Survey, 2004).

It is often assumed that sanitary sewage is the dominant factor in CSOs that deteriorates the water quality of local waterways. However, the average annual stormwater volume simulated using data from the period 1997 through 2002 was within ten percent of total sanitary sewage volume generated in the Milwaukee's CSSA (Brown and Caldwell, 2004). This raises a question whether sanitary sewage or stormwater in CSOs has the larger pollutant contribution and if there are any additional pollutant sources.

Quantification of CSO pollutant source contributions is useful for evaluating the impacts of CSOs on the water quality of local receiving waters. The pollutant contribution of stormwater in CSOs can be used to guide local communities in the selection of appropriate stormwater best management practices (BMPs).

Both chemical mass balance (CMB) and positive matrix factorization (PMF) models have been widely used for the pollutant source apportionment in air (Cooper and Watson, 1980; Hopke, 1985; Lee et al., 1993; Larsen and Baker, 2003) and aquatic (Bzdusek et al., 2006a; 2006b) environments. While CMB modeling has been done previously to estimate pollutant source contributions in drainage systems during dry weather flow events (Pitt et al., 1993; Field et al., 1994; Lalor, 1994; Pitt et al., 2004), to our knowledge, only recently has a CMB model been used for pollutant source apportionment during rain events (Soonthornmonda et al., 2007a). Also, we are not aware of any attempts to apply PMF modeling to apportion pollutants in drainage systems.

The main objective of this chapter is to investigate the CSO pollutant source contributions using CMB and PMF models. Three possible sources, i.e., stormwater, sanitary sewage, and groundwater, and eleven pollutants (BOD_5 , TSS, NH_3 , TP, Cd, Cr, Cu, Pb, Ni, Hg, and Zn) from the sampling period 2000 through 2006 were used for CMB modeling. Selected sets of CSO data (2000-2006) for the same pollutants (except for Hg) were applied to the PMF model to generate three normalized source profiles. Relative pollutant source contributions in CSOs were estimated based on both CMB and PMF models. Additionally, source flow contributions were computed for both CMB and PMF models. The raw influent data were obtained from the MMSD's two wastewater treatment plants (i.e., Jones Island and South Shore). Influent data for events of <0.10 inch (0.25 cm) rainfall were selected to represent the sanitary sewage data. Groundwater data (2000-2006) were derived from Wisconsin Department of Natural Resources' Groundwater Retrieval Network (WDNR GRN) (Wisconsin Department of Natural Resources, 2007). Pollutant concentrations of 53 samples of CSOs used for PMF

modeling are shown in Appendix D. Parts of the work shown in this chapter can be also found in Soonthornnonda and Christensen (2007b).

7.1 CMB Model

The CMB model is a receptor modeling technique that uses a mass balance approach to determine pollutant contributions from different sources based on observations at sampling sites. The basic idea of the CMB model is that a given measured profile can be reproduced by linear combinations of several sources. The measured CSO concentration F_j (mg/L) of pollutant j ($1 \leq j \leq m$) is expressed as

$$F_j = \sum_{i=1}^n \Phi_{ji} \alpha_i + e_j \quad (40)$$

where Φ_{ji} is the concentration (mg/L) of j^{th} pollutant in the i^{th} source, α_i is the source contribution factor of the i^{th} source, e_j is the error associated with the concentration of the j^{th} pollutant, n is the number of sources, and m is the number of pollutants used in the model.

The aim of the modeling is to determine the contribution factors α_i for each of the i source using the effective variance least-squares method. The effective variance least-squares method is described in detail by Henry et al. (1984), Watson et al. (1984), and Christensen et al. (1997). In order to evaluate the goodness of fit, χ^2 , the multiple linear correlation coefficient R^2 , and the relative error for $\chi^2 = \text{df}$ (number of degrees of freedom, $m - n$) were used.

The χ^2 is calculated as

$$\chi^2 = \sum_{j=1}^m \frac{(F_j - F'_j)^2}{(r.e._k F_j)^2 + \sum_{i=1}^n \{\alpha_i (r.e._i \Phi_{ji})\}^2} \quad (41)$$

where

$$F'_j = \sum_{i=1}^n \Phi_{ji} \alpha_i \quad (42)$$

is the calculated concentration of the j^{th} pollutant in the CSO sample, $r.e._k$ is the relative error of pollutant measurement, and $r.e._i$ is the relative error of CSO source profile i . It is assumed that these relative errors of all pollutants are characterized by a single value as

$$\sigma F_j = r.e._k F_j \quad (43)$$

$$\sigma \Phi_{ji} = r.e._i \Phi_{ji} \quad (44)$$

where σ indicates standard error.

The multiple linear correlation coefficient R^2 is defined as described in Su and Christensen (1997). The relative contribution f_{ji} of pollutant j in a CSO sample from source i is calculated as

$$f_{ji} = \frac{\Phi_{ji} \alpha_i}{\Phi_{j1} \alpha_1 + \Phi_{j2} \alpha_2 + \dots + \Phi_{jn} \alpha_n} \quad (45)$$

The uncertainty δf_{ji} is given here as

$$\delta f_{ji} = f_{ji} \sqrt{\left(\frac{\delta \alpha_i}{\alpha_i}\right)^2 + \left(\frac{\left((\Phi_{j1} \delta \alpha_1)^2 + (\Phi_{j2} \delta \alpha_2)^2 + \dots + (\Phi_{jn} \delta \alpha_n)^2\right)^{1/2}}{\Phi_{j1} \alpha_1 + \Phi_{j2} \alpha_2 + \dots + \Phi_{jn} \alpha_n}\right)^2} \quad (46)$$

and the flow contribution P_i from source i is computed as

$$P_i = \frac{k_i \alpha_i}{\sum_{i=1}^n k_i \alpha_i} \quad (47)$$

where

$$\Phi_{ji} = k_i c_i \quad (48)$$

Here, c_i is the concentration of pollutant j in stream i , e.g., stormwater, sanitary sewage, or groundwater, and k_i is the factor between source profiles and actual concentrations of pollutant j . This factor is assumed to be one for stormwater and groundwater, and it was found to be about 6.44 for sanitary sewage. The reason for the >1 value for the latter is that the sanitary sewage profile (Table 7.1) is based on measurements at the inflow to treatment plants, i.e., Jones Island and South Shore, where turbulence to a higher degree keeps the solids in suspension producing high pollutant concentrations.

7.1.1 Pollutant Source Profiles

Three possible types of CSO pollutant source profiles, i.e., stormwater, sanitary sewage, and groundwater, were applied to the CMB model. The pollutant profiles of three sources with uncertainties (standard error of the mean) are shown in Table 7.1. The pollutant profiles for stormwater and sanitary sewage were generated as described in Soonthornnonda et al. (2007a). The pollutant profiles for groundwater were averages derived from WDNR GRN data. The derived data were detects only sampling data from public water supplies, private water supplies, and landfill wells located throughout the State of Wisconsin. The number of groundwater samples ranged from 33 to 1,721. Wisconsin's groundwater is contained in four major aquifers: the sand and gravel aquifer, the Silurian dolomite aquifer, the sandstone aquifer, and the crystalline bedrock aquifer.

Groundwater connects to and feeds wetlands, streams, and lakes (Wisconsin Academy of Sciences, Arts and Letters, 2003).

Table 7.1. Sanitary sewage, stormwater, and groundwater profiles and CSO measured profile expressed as averages with uncertainties (standard error of the mean) used for CMB modeling (n = number of samples).

Pollutant	Sanitary Sewage ^a	Stormwater ^d	Groundwater ^a	Combined Sewer Overflows
BOD ₅	281 ± 2.39 (n = 3101)	22.5 ± 0.846 (n = 1266)	19 ± 2.7 (n = 192)	24.2 ± 6.35 (n = 190)
TSS	284 ± 4.64 (n = 3102)	194 ± 22.2 (n = 1420)	133 ± 47.6 (n = 145)	86.8 ± 7.08 (n = 188)
NH ₃	13.8 ± 0.0874 (n = 3101)	0.600 ± 0.0302 (n = 1380)	0.356 ± 0.0423 (n = 306)	0.831 ± 0.0585 (n = 54)
TP	5.45 ± 0.0306 (n = 3104)	0.885 ± 0.0841 (n = 1403)	0.207 ± 0.0166 (n = 358)	0.815 ± 0.0575 (n = 189)
Cd	0.00158 ± 0.0000624 (n = 460)	0.000894 ± 0.0000361 (n = 1296)	0.000413 ± 0.0000622 (n = 195)	0.00240 ± 0.00148 (n = 189)
Cr	0.0436 ± 0.00271 (n = 460)	0.0128 ± 0.00101 (n = 1296)	0.00547 ± 0.000606 (n = 1127)	0.0153 ± 0.00210 (n = 190)
Cu	0.0726 ± 0.00203 (n = 458)	0.0442 ± 0.00273 (n = 1295)	0.0241 ± 0.0022 (n = 668)	0.0268 ± 0.00230 (n = 190)
Pb	0.0107 ± 0.000850 (n = 234)	0.0305 ± 0.00260 (n = 1288)	0.00607 ± 0.000579 (n = 1067)	0.0431 ± 0.00386 (n = 190)
Ni	0.0111 ± 0.000415 (n = 458)	0.00769 ± 0.000352 (n = 1296)	0.00639 ± 0.000702 (n = 1721)	0.00994 ± 0.00152 (n = 190)
Hg (µg/L)	0.158 ± 0.0138 (n = 298)	0.0454 ± 0.00000373 (n = 1232)	0.298 ± 0.0397 (n = 266)	0.0611 ± 0.00729 (n = 135)
Zn	0.164 ± 0.00339 (n = 786)	0.185 ± 0.0133 (n = 1296)	0.110 ± 0.0124 (n = 797)	0.103 ± 0.00516 (n = 190)
EC (CFU/100mL)	141,000 ± 49,000 (n = 10)	50,900 ± 2,210 (n = 1398)	30.1 ± 24.9 (n = 33)	136,000 ± 15,900 (n = 53)
FC (CFU/100mL)	2,140,000 ± 1,990,000 (n = 12)	134,000 ± 10,100 (n = 1424)	NA ^b	730,000 ± 406,000 (n = 59)

Note: all concentrations are in mg/L unless otherwise noted.

^a average relative errors (r.e.'s) of sanitary sewage, stormwater, and groundwater profiles = 0.128, 0.0616, and 0.194, respectively.

^b NA = data not available.

7.2 PMF Model

The PMF model used for this study is based on equations described by Paatero (1997). The governing equation of the PMF model is

$$X = G F \quad (49)$$

where X ($m \times n$) is the data matrix consisting of the CSO measurements of m pollutants in n samples, G ($m \times p$) is the factor loading matrix (source profiles), F ($p \times n$) is the factor score matrix (source contributions), and p is the number of pollutant sources.

The model minimizes a weighted sum of squares of differences between calculated and measured elements of the data matrix by normal equations, and uses rotations based on the nonnegative least squares (NNLS) procedure (Lawson and Hanson, 1974) to eliminate negative elements of G and F . The data matrix X is initially average scaled by dividing the pollutant concentrations in each CSO sample by their respective average concentration for all samples and then backscaled (multiply by averages) after rotations. Description of our PMF model can be found in detail in Bzdusek et al. (2006a). The PMF solutions incorporate weighting of individual data points so that both high and low pollutant concentrations will be modeled accurately (Bzdusek et al., 2006b).

The relative contribution h_{ji} of pollutant j in a CSO sample k from source i is then,

$$h_{ji} = \frac{G_{ji}F_{ik}}{G_{j1}F_{1k} + G_{j2}F_{2k} + \dots + G_{jp}F_{pk}} \quad (50)$$

Note that this equation is analogous to eq 45 for the CMB model with k referring to a particular sample and the number of sources p corresponding to n of eq 45.

The flow fraction H_i from source i can be calculated from

$$H_i = \frac{k_i F_{ik}}{\sum_{i=1}^p k_i F_{ik}} \quad (51)$$

and

$$G_{ji} = k_i c_i, \quad (52)$$

where k_i is the factor between estimated normalized source profiles and actual concentrations of pollutant j .

Ten different data sets for the data matrix X were created using a Monte Carlo simulation method. The original data matrix was assumed to be average values, and random variations were generated based on a relative error of 0.20. Ten CSO pollutant source profiles and relative source contributions were estimated using the PMF model. The average of estimated source profiles were then compared with the source profiles listed in Table 7.1.

7.2.1 Diagnostic Tools

The coefficient of determination (COD) and Exner function were used to evaluate the goodness of fit between the estimated data set and measured data set. The COD for each pollutant and Exner function approach 1.0 and zero for a perfect fit. The weighted sum of squares of differences between estimated and measured data, Q , should approximately equal the number of degrees of freedom, $df = n \times m - p \times (n + m)$ for a good fit.

7.3 Results and Discussion

7.3.1 Stormwater, Sanitary sewage, and Groundwater Profiles

Considering the pollutant source profiles (stormwater, sanitary sewage, and groundwater) and CSO data (Table 7.1), sanitary sewage is found to have higher concentrations of most pollutants than stormwater (except Pb and Zn), groundwater (except Hg), and CSOs (except Cd and Pb). Most pollutants exhibit higher concentrations in stormwater than in groundwater (except Hg). Stormwater is found to have higher TSS, TP, Cu, and Zn concentrations than CSOs. Groundwater has higher Zn concentration than CSOs. Bacteria levels from sanitary sewage, stormwater, groundwater, and CSOs were also included in Table 7.1, and the highest bacteria levels are found in sanitary sewage.

The highest concentrations of Pb and Cd found in CSOs may be explained by the erosion of sewer deposits or remobilization of in-sewer settled particles (Gromaire et al., 2001). Analyses of sewer deposit samples and sediment transport in the study area would have to be carried out in order to verify this hypothesis. The highest concentration of Hg is found in groundwater. The major source of Hg to Wisconsin surface waters is atmospheric deposition from coal fired power plants and from a still operating chlor-alkali plant at Port Edwards. However, this plant is scheduled to be shut down. Nearly 1,200 lakes have fish that exceed the WDNR's standard in 2001 (Wisconsin Academy of Sciences, Arts and Letters, 2003). Elevated Hg levels in groundwater are probably caused by Hg-impaired lakes and connections to groundwater. The high molecular weight of Hg may also be a factor.

In general, TSS and particle-associated substances, e.g., metal concentrations are higher in stormwater than in sanitary sewage. The reason for high sanitary sewage concentrations of these pollutants shown in this study is, as indicated above, the sampling location of sanitary sewage at the influent channel of treatment plants where the

turbulence of inflow prevents particles from settling causing high concentrations of particles and associated pollutants.

7.3.2 CMB Model Pollutant Source Contributions

Statistical results obtained from CMB modeling of CSO pollutant source profiles for two (stormwater and sanitary sewage) and three (stormwater, sanitary sewage, and groundwater) sources are presented in Table 7.2. Relative errors of stormwater, sanitary sewage, and groundwater profiles were assumed to be 0.0616, 0.128, and 0.194, respectively (Table 7.1). As indicated in Christensen et al. (1997), the CMB model fit is considered satisfactory for the $r.e._k \leq 0.50$, fair for $0.50 < r.e._k < 0.70$, and unsatisfactory for $r.e._k \geq 0.70$. The CMB results indicate good agreement between calculated and measured CSO data when modeling two and three sources. The R^2 for two sources (0.779-0.841) is slightly less favorable than that of three sources (0.819-0.853). Note the similarity of α values of sanitary sewage from modeling two and three sources without fecal coliform (0.0377 and 0.0371-0.0374, respectively). Also, the reduction in α for stormwater when modeling three sources is approximately equal to the α value of the third source (0.0853 ± 0.103 or 0.0739 ± 0.112), groundwater. Three sources in CSOs, i.e., stormwater, sanitary sewage, and groundwater, are found to be acceptable based on the CMB model. However, the α values of groundwater have larger uncertainties than their values, indicating that the groundwater source is rather uncertain. Inclusion of *E. coli* and fecal coliform into CMB modeling indicates a slightly less favorable model fit, as reflected by lower values of R^2 , e.g., 0.779 vs 0.841, and higher values of the relative errors for $\chi^2=df$, 0.508 vs 0.438, both for the two-source solution. Similar numbers apply to three-source solution.

The percent relative contributions f (eq 45) of eleven pollutants in CSOs based on two and three sources are shown in Table 7.3. Metals and TSS have much higher percent relative contributions from stormwater than sanitary sewage, even after adding the third source into the model. Furthermore, stormwater contributes higher total phosphorus TP (71 ± 19 % for two and 70 ± 22 % for three sources) and about the same amount of BOD₅ as sanitary sewage and groundwater to CSOs. As one could expect, NH₃ has higher contribution (61 ± 25 % for two and 58 ± 25 % for three sources) from sanitary sewage. Stormwater provides the major source of *E. coli* in the CSOs. Similar contributions between stormwater and sanitary sewage were found for fecal coliform.

Due to the overestimation of the sanitary sewage profile concentrations as discussed earlier, its α value needs to be multiplied by a factor k (eqs 47 and 48) for the estimation of flow contribution. The CSO data with events of low rainfall were used to represent the accurate sanitary sewage profile, and the resulting k value was estimated to be 6.44 ± 1.65 . The flow contribution of sanitary sewage is about 27 %, with at least 65 % stormwater and up to 8.0 % groundwater (Table 7.3).

Table 7.2. Statistical results of the CMB model.

Pollutant	α		$\Sigma \alpha$	$\chi^2 = \text{df}$	R^2	Relative Errors (for $\chi^2 = \text{df}$)
	Sanitary Sewage	Stormwater	Groundwater			
BOD ₅ , TSS, NH ₃ , TP, Cd, Cr, Cu, Pb, Ni, Hg, and Zn	0.0377 ± 0.0243	0.626 ± 0.135		9	0.841	0.438
BOD ₅ , TSS, NH ₃ , TP, Cd, Cr, Cu, Pb, Ni, Hg, Zn, EC, and FC	0.0430 ± 0.0280	0.635 ± 0.155		11	0.779	0.508
BOD ₅ , TSS, NH ₃ , TP, Cd, Cr, Cu, Pb, Ni, Hg, and Zn	0.0374 ± 0.0247	0.559 ± 0.158	0.0853 ± 0.103	8	0.853	0.445
BOD ₅ , TSS, NH ₃ , TP, Cd, Cr, Cu, Pb, Ni, Hg, Zn, and EC	0.0371 ± 0.0271	0.586 ± 0.172	0.0739 ± 0.112	9	0.819	0.488

Note: assuming relative errors of sanitary sewage, stormwater, and groundwater profiles = 0.128, 0.0616, and 0.194, respectively.

Table 7.3. Percent relative contributions of CSO pollutants with uncertainties using CMB model.

Pollutant	Percent relative contribution for 2 sources		Percent relative contribution for 3 sources		
	Sanitary Sewage	Stormwater	Sanitary Sewage	Stormwater	Groundwater
BOD ₅	46 ± 15	54 ± 18	42 ± 15	53 ± 19	5.0 ± 2.0
TSS	9.0 ± 2.1	91 ± 23	8.0 ± 2.2	85 ± 25	7.0 ± 2.0
NH ₃	61 ± 25	39 ± 16	58 ± 25	39 ± 18	3.0 ± 1.3
TP	29 ± 7.6	71 ± 19	28 ± 8.0	70 ± 22	2.0 ± 0.6
Cd	11 ± 2.5	89 ± 22	10 ± 2.6	85 ± 25	5.0 ± 1.4
Cr	19 ± 4.4	81 ± 21	17 ± 4.6	79 ± 23	4.0 ± 1.2
Cu	10 ± 2.3	90 ± 22	9.0 ± 2.4	85 ± 25	6.0 ± 1.6
Pb	2.0 ± 0.6	98 ± 25	2.0 ± 0.6	96 ± 29	2.0 ± 0.7
Ni	9.0 ± 2.0	91 ± 23	7.0 ± 2.2	84 ± 25	9.0 ± 2.5
Hg	19 ± 4.5	81 ± 21	11 ± 6.8	49 ± 31	4.0 ± 2.6
Zn	6.0 ± 1.3	94 ± 24	5.0 ± 1.4	88 ± 26	7.0 ± 1.9
EC	16 ± 3.6	84 ± 21	15 ± 4.1	85 ± 25	
FC	52 ± 19	48 ± 18			
Estimated flow percentage	30	70	27	65	8.0

7.3.3 PMF Model Pollutant Source Profiles

Coefficients of determination (COD), values of the Exner function, and the weighted sum of squared residuals (Q) are shown in Table 7.4. The results indicate an improvement from two to three factors. However, TP, Cd, and Cr have relatively low COD values, even for three factors. The improvement in the Exner function from 0.180 to 0.0747 is substantial. Therefore, based on the diagnostic tools a three-factor solution is significant enough to represent all ten pollutants.

Comparisons of three average matrix loadings (F1, F2, and F3) generated using ten data sets from Monte Carlo simulation and the CSO pollutant source profiles of Table 7.1 are illustrated in Figure 7.1. From the high R^2 value (0.956), loading F1 clearly represents the stormwater profile, and loading F2 is a version of the sanitary sewage profile ($R^2 = 0.932$). This applies to both the two and three-factor solution. The third loading F3 fits the stormwater profile best, but almost equally well the groundwater profile lending support to the suggestion that groundwater is a minor source in CSOs (Table 7.3). However, as noted previously, the associated source contribution factor α (Table 7.2) is rather uncertain, meaning that the groundwater may not be significant source. It should also be noted that the metals content of the third PMF factor (Table 7.5), on an equal flow basis, is much higher than of the corresponding CMB groundwater factor (Table 7.3), but fairly similar to that of stormwater, indicating that the factor is in fact stormwater related. Thus, a different stormwater source, or a stormwater related pollutant source such as erosion of sewer sediment may represent the third loading F3. The flow contribution of sanitary sewage, estimated based on eqs 51 and 52, is about 56

% with at least 26 % stormwater and possibly up to 18 % of another stormwater related source (Table 7.5).

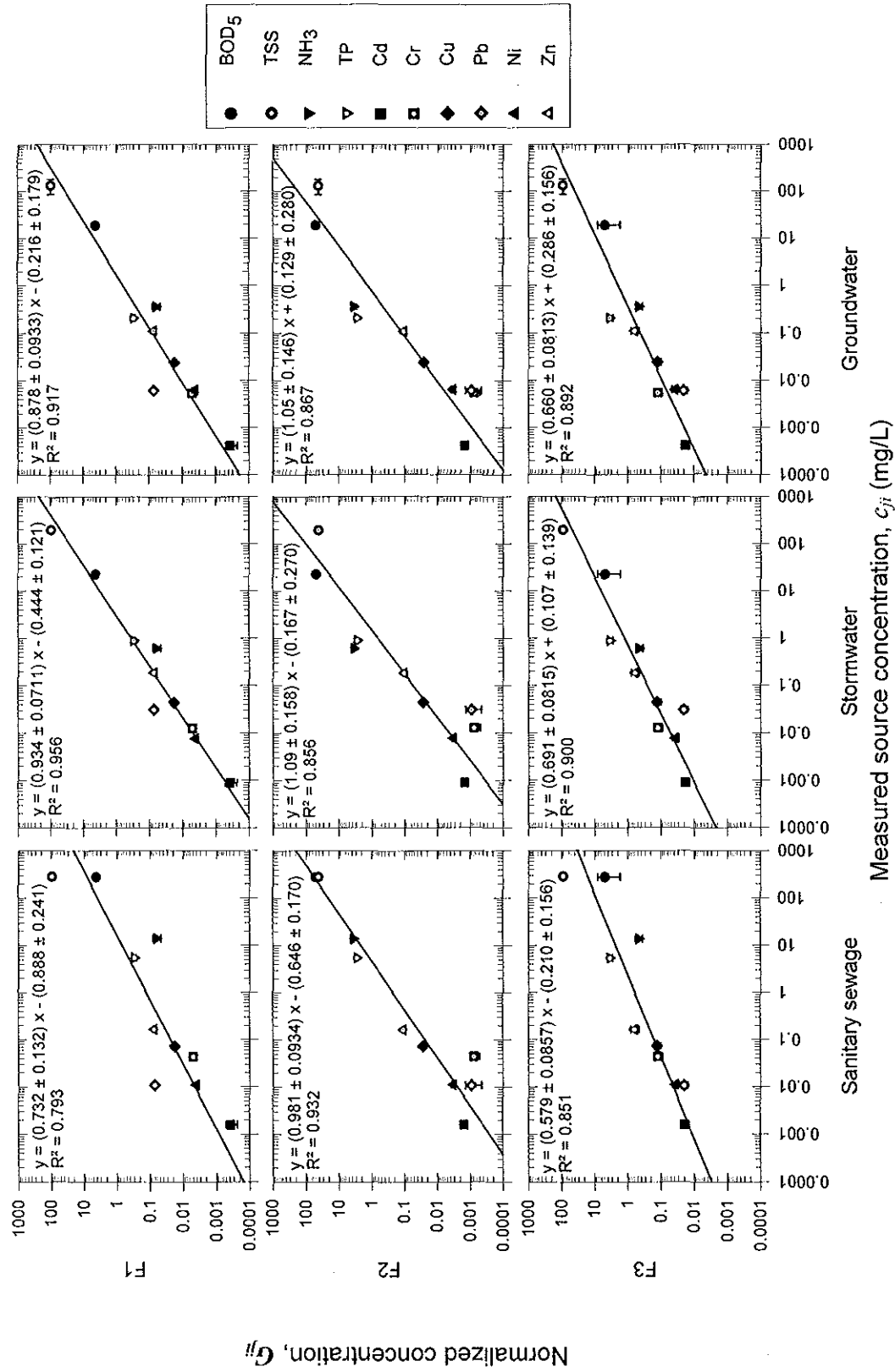


Figure 7.1. Log – linear regressions of PMF estimated normalized source profiles G_{ji} vs. measured source profiles c_{ji} (Table 7.1)

Table 7.4. Results of coefficient of determination (COD) and Exner function for the Milwaukee's combined sewer overflow data set using PMF with NNLS.

Pollutant	Coefficient of determination factors	
	2	3
BOD ₅	0.334	0.428
TSS	0.726	0.909
NH ₃	0.865	0.795
TP	0.316	0.317
Cd	-0.157	0.214
Cr	0.164	0.177
Cu	0.873	0.852
Pb	0.377	0.579
Ni	0.731	0.731
Zn	0.855	0.891
No. of Samples	53	53
Exner	0.180	0.0747
Q ^a	735	515

^a assuming 20 % relative error of the elements of the data matrix;
df = 53(10)-m(53+10), where m = number of factors

Table 7.5. Percent relative contributions of CSO pollutants from Monte Carlo simulation using PMF with NNLS.

Pollutant	Percent relative contribution for 2 factors		Percent relative contribution for 3 factors		
	Factor 1	Factor 2	Factor 1	Factor 2	Factor 3
BOD ₅	18 ± 2.8	82 ± 2.8	18 ± 2.7	78 ± 3.3	4.0 ± 0.7
TSS	75 ± 2.7	25 ± 2.7	60 ± 3.2	25 ± 2.7	15 ± 1.4
NH ₃	7.2 ± 1.7	93 ± 1.7	5.6 ± 1.2	87 ± 2.7	7.6 ± 1.7
TP	30 ± 3.2	70 ± 3.2	13 ± 1.6	59 ± 3.2	28 ± 2.3
Cd	54 ± 3.3	46 ± 3.3	8.2 ± 1.0	22 ± 2.3	70 ± 2.2
Cr	83 ± 2.3	17 ± 2.3	18 ± 1.8	2.5 ± 0.4	79 ± 1.8
Cu	59 ± 3.3	41 ± 3.3	28 ± 2.5	30 ± 2.8	41 ± 2.3
Pb	98 ± 0.7	2.5 ± 0.7	89 ± 1.7	2.0 ± 0.5	9.0 ± 1.4
Ni	69 ± 3.0	31 ± 3.0	29 ± 2.5	19 ± 2.1	52 ± 2.4
Zn	59 ± 3.3	41 ± 3.3	27 ± 2.4	28 ± 2.7	45 ± 2.3
Estimated flow percentage	35 ± 3.3	65 ± 3.3	26 ± 2.7	56 ± 3.4	18 ± 1.6

7.3.4 PMF Model Pollutant Source Contributions

The PMF relative contributions for all ten pollutants based on two and three factors are shown in Table 7.5. The three factor solution corresponds to Figure 7.1. Note that the sanitary sewage loading F2 has similar pollutant contributions for two and three factors, except for Cd and Cr. Loading F1 for two sources is split into F1 and F3 of the three factor solution.

Based on the three-factor solution in Table 7.5, with percent relative contributions of BOD₅ (78 ± 3.3 %), NH₃ (87 ± 2.7 %), and TP (59 ± 3.2 %) of factor 2, sanitary sewage is the dominant source of these pollutants in CSOs. A similar result is obtained for factor 2 of the two-factor solution. Comparing Tables 7.3 and 7.5, both CMB and PMF results show that stormwater, stormwater related sources, and possibly some groundwater, carry more than 50 % of the CSO metals load. Also, both models demonstrate that ≥ 28 % contributions of BOD₅, NH₃, and TP are from sanitary sewage. Especially NH₃ is strongly (≥ 58 %) associated with sanitary sewage. However, most TSS (≥ 75 %) is from stormwater.

While trends are similar for CMB and PMF results, there are some differences, mostly within a factor two. The reasons for this disparity are not clear. As discussed earlier, it is possible that the third source originates inside the combined sewer. Another reason may be that measured data for the CMB model are more extensive (Table 7.1) than for the PMF model. In the latter case we used just the 53 data set listed in Appendix D. However, the PMF results may carry more weight since PMF requires almost no α

priori source information in contrast to CMB modeling where source profiles must be known.

VIII. STORMWATER BEST MANAGEMENT PRACTICES (BMPs)

Many stormwater runoff reduction practices were previously demonstrated and described in MMSD (2007c). The following 10 practices were part of that study:

1. Downspout Disconnection—Disconnection of roof downspouts from sewers and conveyance of roof runoff to pervious land surfaces.



Figure 8.1. Downspout disconnection will keep excess water out of the sewer system.

2. Rain Barrels— Collection of roof runoff in 50-100 gallon barrels, with subsequent release to landscaped areas.
3. Rain Gardens—Small ($\sim 9 \text{ m}^2$) vegetated depressions used to capture runoff and promote infiltration and evapotranspiration.



Figure 8.2. The rain garden at Calumet Auto Parts, Inc., 8501 West Calumet Road in Milwaukee. (MMSD, 2007c).

4. Green Roofs—Soil and vegetation installed on top of a conventional flat or slightly sloped roof. A complete green roof system may include a watertight membrane, protective layer, insulation, irrigation/drainage system, filter layer, soil, and plants.



Figure 8.3. UWM Great Lakes Water Institute green roof. (MMSD, 2007c).

5. Green Parking Lots—Various measures used to reduce the effective impervious area of a parking lot and promote infiltration and/or evapotranspiration.

6. Stormwater Trees—Increasing the coverage of tree canopies to provide stormwater interception and evapotranspiration, along with other ecological benefits.

7. Porous Pavement—The use of porous asphalt or concrete, modular block systems, grass pavers, or gravel pavers to allow stormwater to percolate through the ‘pavement’.



Figure 8.4. Water infiltrates the pervious concrete. (MMSD, 2007c).

8. Inlet Restrictors/Pavement Storage—Flow regulation devices that allow the temporary storage of stormwater on streets and parking lots.



Figure 8.5. Inlet restrictor locations, Prospect Avenue. The dots indicate the location of the inlets. (MMSD, 2007c).

9. Bioretention—Landscaped depressions planted with grass, shrubs, and/or trees. These often utilize a sand/gravel underdrain, mulch, and soil amendments.

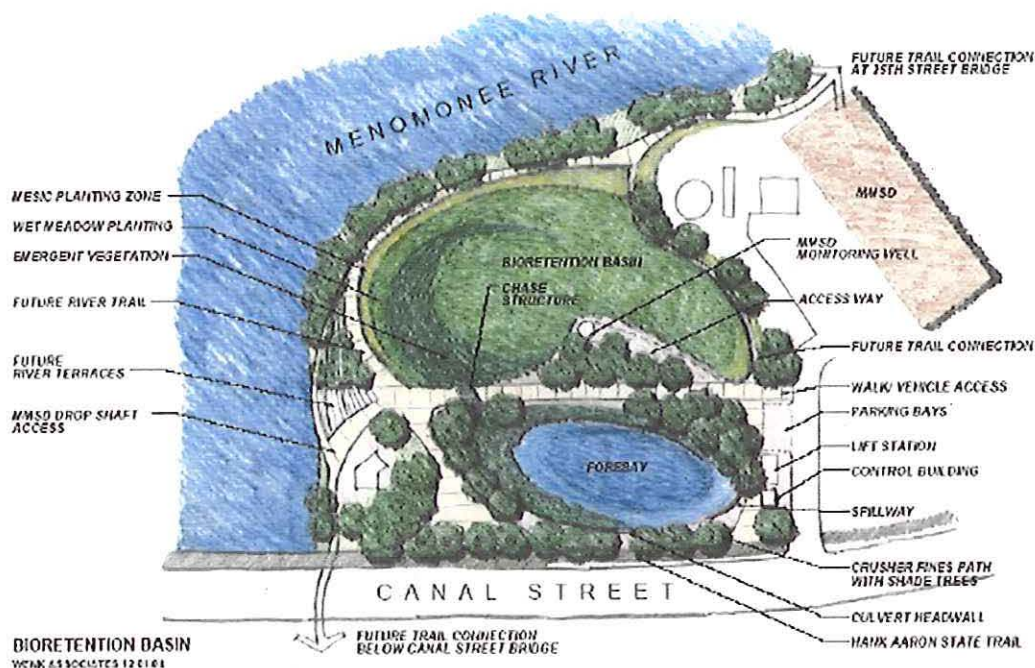


Figure 8.6. Two-acre bioretention system treats stormwater runoff from about 70 acres (28.4 ha) in the Menomonee Valley. (MMSD, 2007c).

10. Onsite Filtering Practices—Practices such as sand filters, bioretention cells, swales, and filter strips that use a filter media (sand, soil, gravel, peat, or compost) to reduce stormwater runoff and capture pollutants.



Figure 8.7. Bioretention swale and rain garden. (MMSD, 2007c).

MMSD (2007c) indicated that in order to reduce stormwater runoff within the separate sewer area, stormwater runoff reduction practices need to be implemented. However, some practices, i.e., downspout disconnection and rain gardens, may contribute more infiltration and inflow (I/I) to sanitary sewers (Shafer, 2006). Other practices, e.g., green roofs and bioretention could be used without increasing the risk of I/I to sanitary sewers. Considering the combined sewer service area, most stormwater runoff reduction practices could significantly reduce combined sewer overflows and the amount of stormwater that would be conveyed to the MMSD's wastewater treatment plants.

This chapter will illustrate how the runoff volume reduction using effective practices can result in a reduction of the runoff pollutant mass based on the load model in Chapters 5 and 6. The average individual storm load may be implied as one component of load allocations (LAs) used to determine the total maximum daily loads (TMDLs) for study pollutants in the area. Design examples of some practices (e.g., detention pond) will be demonstrated based on the overflow velocity.

8.1 Stormwater BMP Removal Efficiencies of An Individual Storm Load.

As discussed in Chapters 5 and 6, the runoff load is

$$M_R = \alpha a \hat{\beta} A t_d (1 - e^{-ckt}) \quad (53)$$

Then,

$$\Delta M_R = ck (\alpha a \hat{\beta} A t_d) e^{-ckt} \Delta t, \quad \Delta t = \text{small time increment} \quad (54)$$

where

$$\Delta V = \hat{\beta} A k \Delta t \quad (55)$$

Equation 54 reduces to

$$\Delta M_R = c(\alpha a t_d) e^{-ckt} \Delta V \quad (56)$$

It can be seen from eq 56 that a reduction of runoff volume will result in a reduction of the runoff pollutant mass.

8.2 Design of Effective Stormwater BMPs.

In Chapter 7, results showed that metals and TSS from stormwater are predominant pollutants in CSOs. One alternative to eliminate CSOs and high discharges of BOD₅, NH₃, and TP is to implement sewer separation in combined sewer areas into sanitary and storm sewers. However, this alternative can be unsuitable unless effective best management practices (BMPs) that target removal of metals, TSS, and bacteria are implemented in the separated storm sewer systems.

Within the separate sewer area in Milwaukee, the polluted stormwater runoff (Soonthornnonda and Christensen, 2007) may cause the local waterways to exceed Wisconsin's State Recreational Water Quality Standards for nutrients and bacteria (U.S. Geological Survey, 2004). Based on MMSD (2007c), it appears that several of the best BMPs (downspout disconnections, rain gardens, porous pavement, bioretention, green parking, and green roofs) can achieve an approximate 30% reduction in peak flows and volumes.

Due to the variety in BMP designs, BMP constructions, and specific site conditions, it is proper to discuss the BMP design using gravity settling and overflow velocity. Minton (2002) stated that flow through swales behave like a sedimentation device for which performance is a function of hydraulic overflow velocity. The fraction

of particles captured in practice follows the classic design of sedimentation facilities on the basis of overflow velocity (Huber et al., 2006):

$$R = 1 - \left(1 + \frac{v_s}{NQ/A} \right)^{-N} \quad (59)$$

where

R = fraction captured

v_s = settling velocity (Stokes' law)

Q = outflow rate

A = basin area

N = number of continuous flow stirred tank reactors in series (CFSTRs)

$q = Q/A$ = overflow rate

The above equation will give the steady state performance of one CFSTR when $N = 1$. In the case of $N \rightarrow \infty$, the equation then becomes

$$R = 1 - e^{-\frac{v_s}{Q/A}} \quad (60)$$

which represents the perfect horizontal plug flow such as a tank or pond (Figure 8.8). The case $N = -1$ corresponds to quiescent settling (e.g., the permanent pool of a wet pond) (Figure 8.9):

$$R = \frac{v_s}{Q/A} = \frac{v_s t_d}{h} \leq 1, \quad v_s \leq \frac{h}{t_d} \quad (61)$$

$$R = 1, \quad v_s \geq \frac{h}{t_d} \quad (62)$$

where

h = basin depth

t_d = detention time

As long as the storm interevent time (antecedent dry time) is higher than the detention time t_d , all particles with settling velocity v_s will be removed.

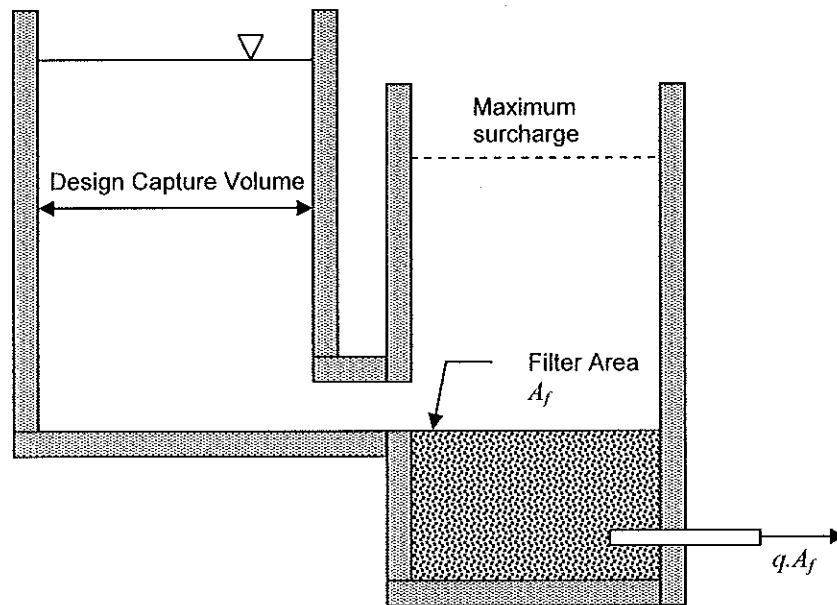


Figure 8.8. Detention basin with controlled release followed by filter media. Source: Wright Water Engineers, Inc. and GeoSyntec Consultants (2007).

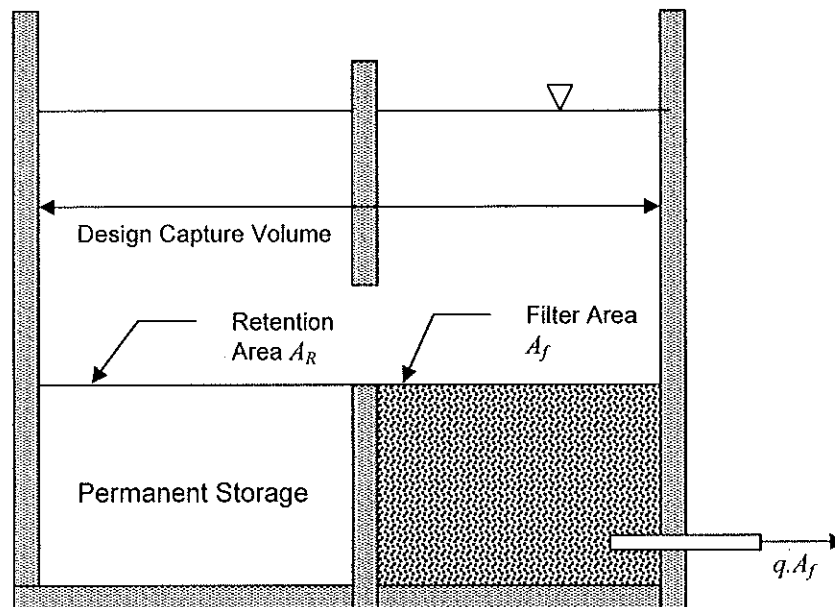


Figure 8.9. Combination of retention pond and media filter. Source: Wright Water Engineers, Inc. and GeoSyntec Consultants (2007).

For the design application of a sedimentation basin, the average runoff volume is assumed to be the capture volume of the basin P_o . The average runoff volume can be computed as

$$V_{runoff} = \hat{\beta} A r \quad (63)$$

where

$\hat{\beta}$ = runoff coefficient

A = drainage area

r = average rainfall depth = 10.2 mm (Chapter 2).

In order to achieve 85% particle removal, the particle size of 2 μm would be obtained using the National Urban Runoff Program (NURP) particle size distribution (U.S. EPA, 1983b). The settling velocity v_s could be estimated based on Stokes' law (25 °C) by assuming particle density of 2650 kg/m^3 . The design overflow rate q would be computed by eqs 60, 61, or 62 depending upon types of BMPs implemented such as a pond or wet pond. The detention time needs to be less than or equal to the interevent time of 2.31 days (Chapter 2). Then, the design of basin depth, $h = \frac{P_o}{A_f} = q t_d$, can be

estimated by using the particle settling velocity v_s , percent solids captured R , and detention time t_d . Tables 8.1 and 8.2 show examples of design calculation sheets for the dry and wet pond regardless of the sediment storage volume, respectively. Figures 8.10 and 8.11 illustrate the design chart of the design capture volume and the filter area for the pond and wet pond.

The following steps are used to design a sedimentation basin as shown in the calculation sheets (Tables 8.1 and 8.2):

- (1) Determine the pollutant fraction captured R using the National Urban Runoff Program (NURP) particle size distribution (U.S. EPA, 1983b). A 2-micron particle size was assumed here, giving $R = 0.85$.

- (2) Calculate the settling velocity for a targeted particle size based on R using

$$\text{Stokes' Equation. } V_s = \frac{\frac{2}{9} \cdot (1 \cdot 10^{-6})^2 \cdot 9.81 \cdot (2650 - 997)}{8.9 \cdot 10^{-4}} = 4.05 \cdot 10^{-6} \text{ m/sec}$$

= 0.35 m/day by assuming particle density of 2650 kg/m³ and temperature of 25 °C.

- (3) Calculate the design overflow rate q using eq 60 (dry pond) and eqs 61

$$\text{and 62 (wet pond). } q = \frac{0.35}{-\ln(1 - 0.85)} = 0.184 \text{ m/day (eq 60) and}$$

$$q = \frac{0.35}{0.85} = 0.411 \text{ m/day (eq 61).}$$

- (4) Select the detention time t_d . The detention time should be less than or equal to the interevent time (2.31 days, see Chapter 2). The detention times of 2.17 (dry pond) and 2.19 (wet pond) were assumed here.

- (5) Determine the design basin depth, $h = 0.184 \cdot 2.17 = 0.40 \text{ m} = 40 \text{ cm}$ for dry pond and $h = 0.411 \cdot 2.19 = 0.90 = 90 \text{ cm}$ for wet pond.

- (6) Check the validity of eq 61: $\frac{0.90}{2.19} = 0.411 \geq 0.350$.

- (7) The runoff volume can be calculated by distributing the 10.2 mm rainfall depth over the drainage area A and the runoff coefficient $\hat{\beta}$ for the given catchment (eq 63). The runoff volume V_{runoff} was assumed to equal the

design capture volume P_o . For example,

$$V_{runoff} = 0.187 \cdot 250 \cdot 10^4 \cdot 10.2 \cdot 10^{-3} = 4,769 \text{ m}^3 \text{ for site SWMI04.}$$

- (8) Plot P_o vs $A_f = \frac{P_o}{h}$, and A_f can be chosen with a given P_o value. For example, filter areas were 12,000 m² for dry pond and 5,300 m² for wet pond. It can be seen that the dry pond may require more spaces than the wet pond when the same design capture volume is applied. In other words, the dry pond may need less design basin depth than the wet pond.

Table 8.1. A design calculation sheet of a dry pond based on the perfect horizontal plug flow and the overflow velocity.

1.	r	0.00000100	m		
	g	9.81	m/sec ²		
	ρ_p	2650	kg/m ³		
	ρ_t	997	kg/m ³		
	η	0.000890	kg-sec/(m-sec ²)		
2.	v_s	0.00000405	m/sec =	0.350	m/day
	R	0.850			
3.	q	0.184	m/d		
	Interevent time	2.31	days		
4.	Select t_d	2.17	days	OK (< Interevent time)	
5.	$h = P_o/A_f$	0.400	m =	40.0	cm

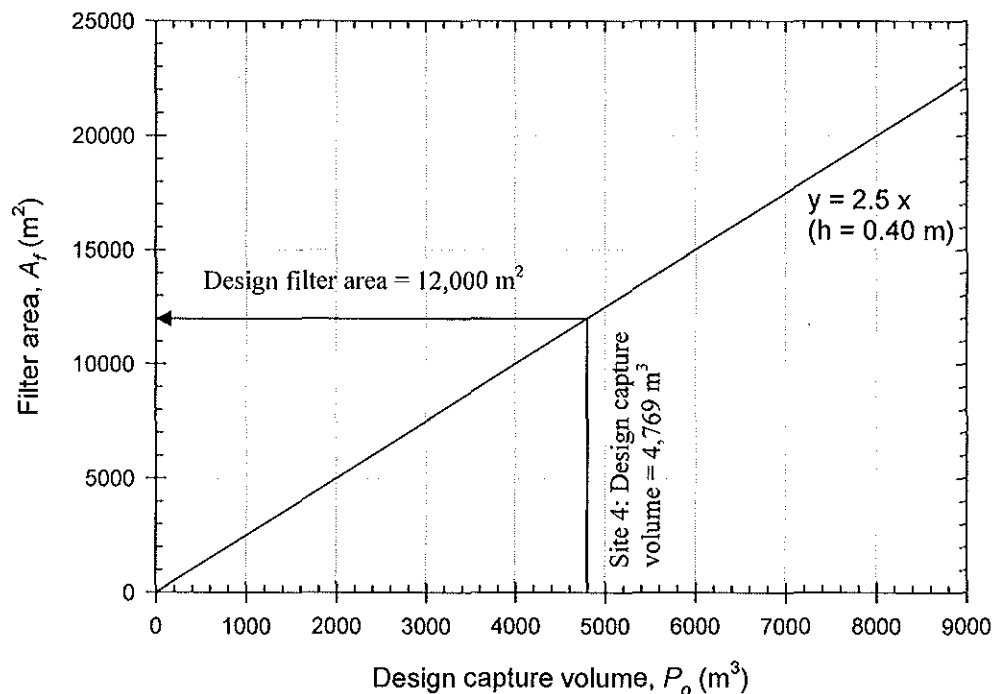
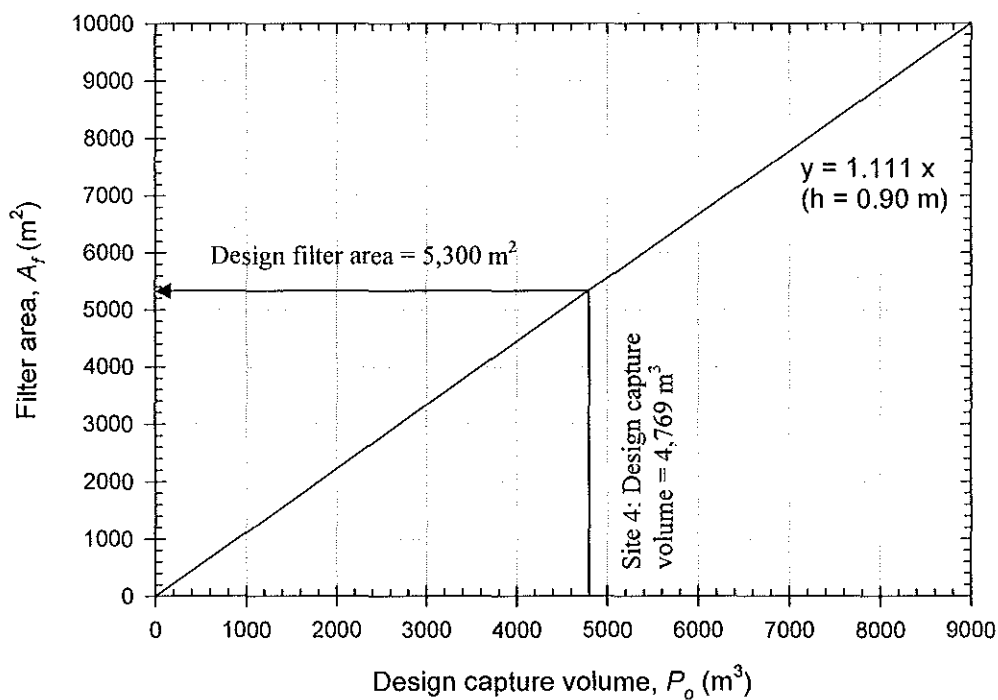


Figure 8.10. A design chart between the design capture volume or runoff volume and the filter area for a pond based on $h = 0.40$ m and $t_d = 2.17$ days.

Table 8.2. A design calculation sheet of a wet pond based on the quiescent settling.

1.	r	0.00000100	m		
	g	9.81	m/sec ²		
	ρ_p	2650	kg/m ³		
	ρ_f	997	kg/m ³		
	η	0.000890	kg-sec/(m-sec ²)		
2.	v_s	0.00000405	m/sec =	0.350	m/day
	R	0.850			
3.	q	0.411	m/d		
	Interevent time	2.31	days		
4.	Select t_d	2.19	days	OK (< Interevent time)	
5.	$h = P_o/A_f$	0.900	m =	90.0	cm
6.	Check h/t_d	0.411	m/day \geq	0.350	m/day

Figure 8.11. A design chart between the design capture volume or runoff volume and the filter area for a wet pond based on $h = 0.90$ m and $t_d = 2.19$ days.

8.3 Examples of Stormwater BMP Technologies Using Settling for Treatment.

8.3.1 Stormceptor®

The Stormceptor® is most commonly used in urban environments where local, regional or national regulations require water quality devices. It can be applied to locations that generate significant amounts of motor vehicle related contaminants and petroleum spills. The system is designed for stormwater quality retrofits for existing developments, industrial and commercial parking lots, automobile service stations, airports and military installations, vehicle loading and unloading areas, new residential developments, re-development in the urban core, manholes and pre-treatment applications.

Under normal (frequent) operating conditions (Figure 8.12), stormwater enters into the upper chamber and is diverted by u-shaped weir, down an orifice of pipe, into the lower chamber. This downward flow is directed through the riser pipe at the circular walls of the upper chamber. Flow horizontally continues to the storm drain outlet. Fine and coarse sediments settle to the floor of the lower chamber, while oil-based contaminants rise and become trapped beneath the fiberglass insert.

For infrequent high flow events (Figure 8.13), peak stormwater flows bypass over the weir and continue through the upper chamber into the storm drain outlet. A portion of incoming sediments continues to be directed by the weir into the lower chamber where they settle. Stormceptor is the only device with an internal by-pass that prevents scouring of trapped pollutants.

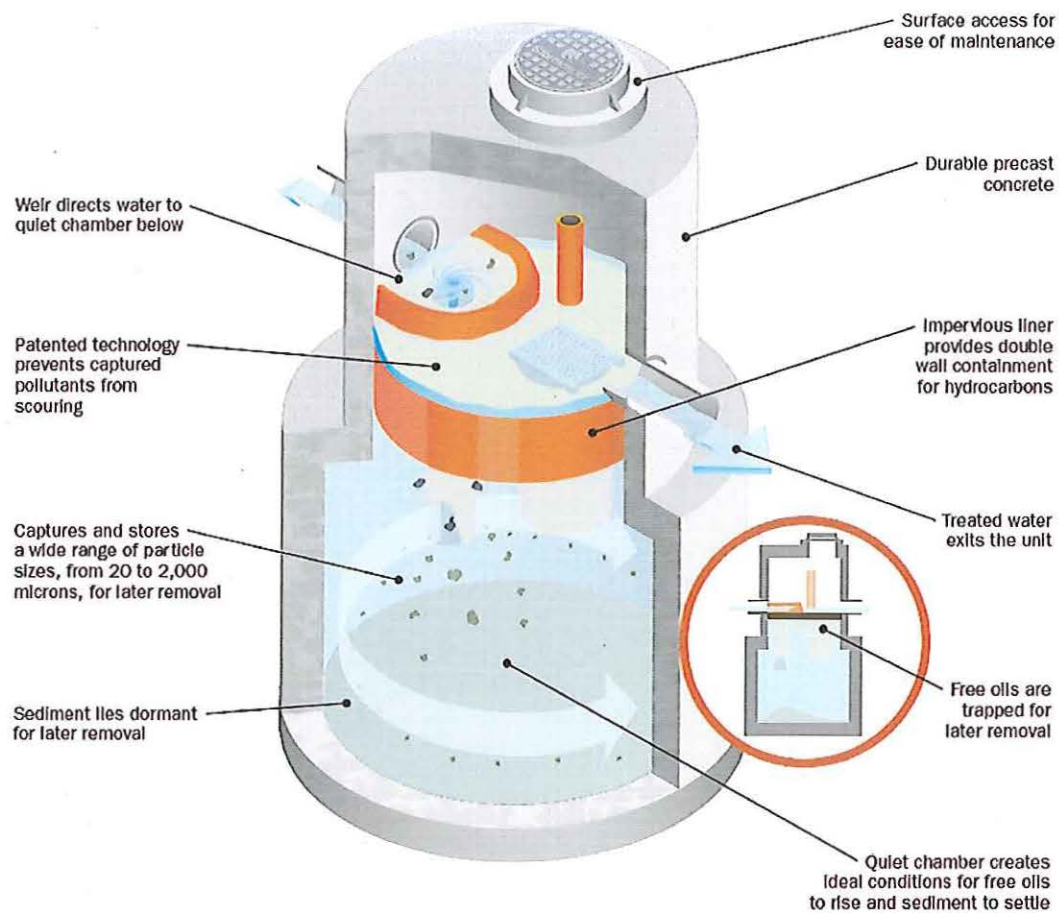


Figure 8.12. The Stormceptor® under normal operating conditions (frequent rainfall).
Source: www.rinkerstormceptor.com.

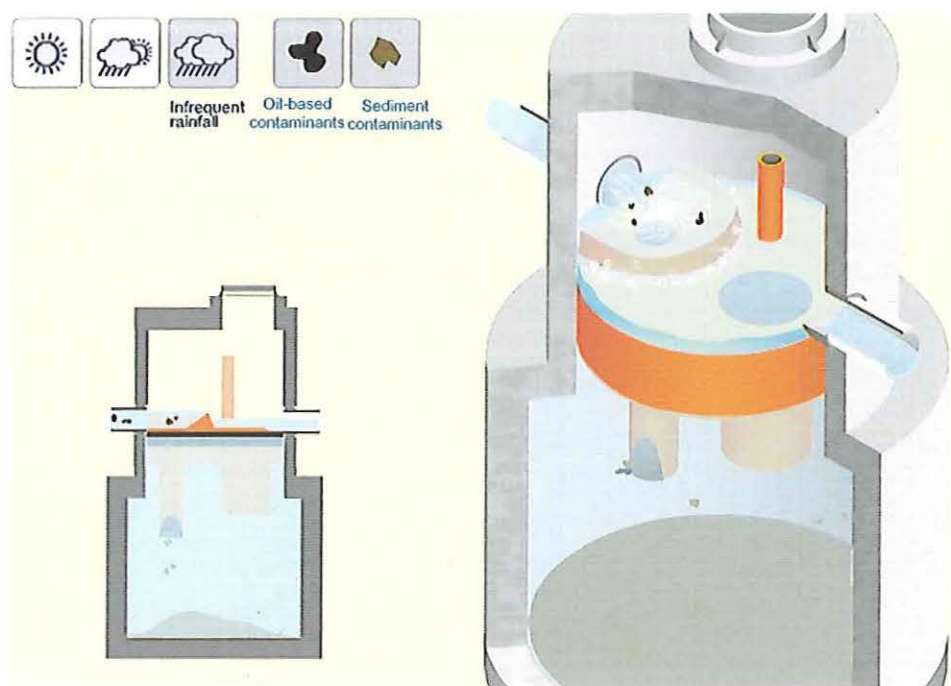


Figure 8.13. The Stormceptor® under by-pass operating conditions (infrequent heavy rainfall). Source: www.rinkerstormceptor.com.

8.3.2 Vortechs®

The Vortechs system is custom-designed by CONTECH Stormwater Solutions engineers. The system is a high-performance hydrodynamic separator that removes hydrocarbon-saturated sediments, sands, silts, oily floatable liquids, heavy metals, and other floatable and settleable debris. Each system is installed below grade which minimizes land consumption. The system's flow controls cause water to decant after a storm event and leave a low water level. These flow controls and large pollutant storage volume result in a low water-to-pollutant ratio, which reduces the cost and frequency of maintenance. The system is designed for residential, industrial, commercial, and municipal applications, parking lots, airport runways, roadways, vehicle maintenance areas, gas stations, and outdoor material storage areas.

Under low flow conditions (green arrow in Figure 8.14), water enters the swirl chamber at a tangent, enhancing gravitational separation. Sinking pollutants stay in the swirl chamber while floating pollutants are stopped at the baffle wall. During larger storms (yellow arrow in Figure 8.14), the water level rises above the low flow control and begins to flow through the high flow control. When the storm drain is flowing at peak capacity, the water surface in the system approaches the top of the high flow control. The system will be sized large enough so that previously captured pollutants are retained in the system even during high intensity storm events. After storm events, treated runoff decants out of the system, and the water level is restored to the invert level of the inlet and outlet pipes.

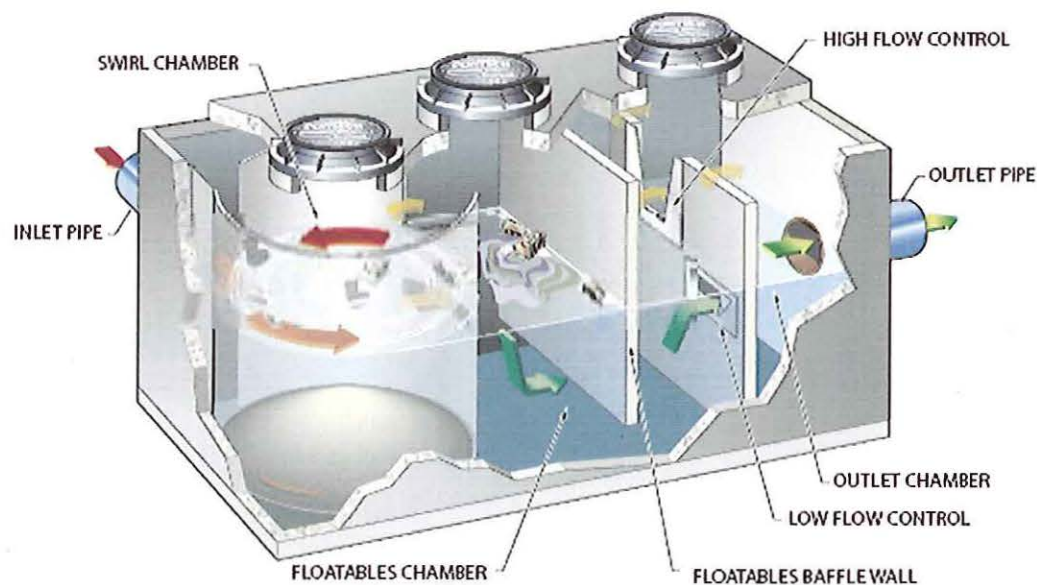


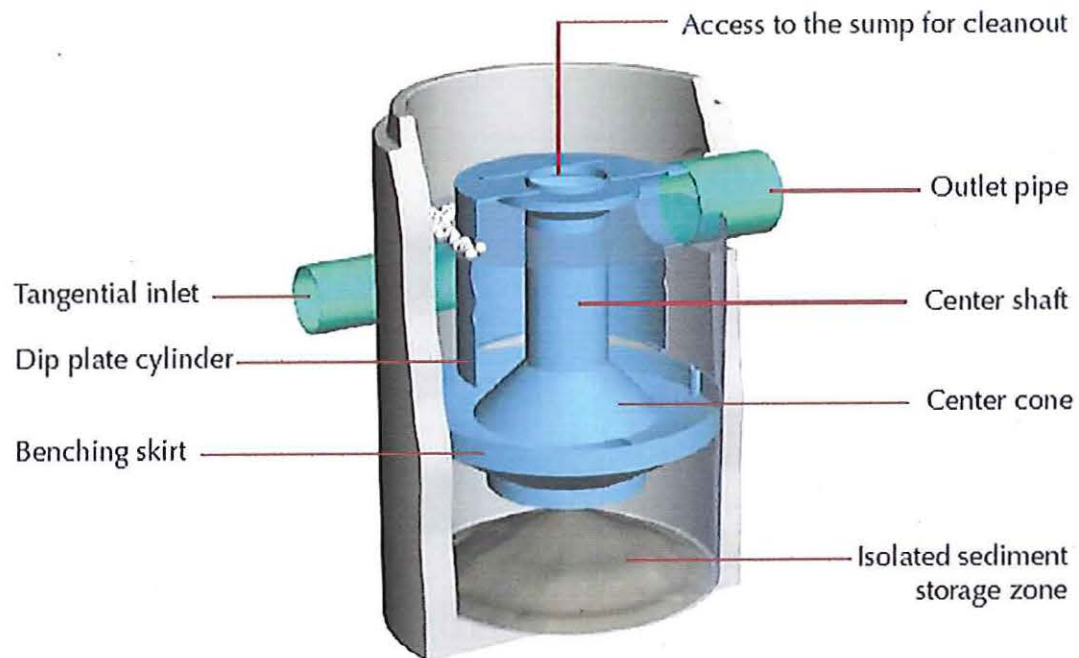
Figure 8.14. The Vortechs system operating under low and high flow conditions. Source: www.contech-cpi.com.

8.3.3 Downstream Defender®

The Downstream Defender® is an advanced vortex separator which is designed to provide high removal efficiencies of settleable solids and their associated pollutants, oil, and floatables over various flow rates. Its flow-modifying internal components designed to advance vortex separation by minimizing turbulence and headloss, enhancing separation, and preventing washout of stored pollutants.

Stormwater enters tangentially into the side of the vessel which generates a rotating flow that spirals around the outside of the dip plate (red arrow in Figure 8.15). Oils, trash and floatable debris rise to the water surface and are trapped in the oil and floatables storage volume (dark red zone in Figure 8.15). While flow continues to spiral down around the dip plate cylinder, low energy vortex motion directs sediment along the benching skirt into the isolated sediment storage zone (bottom zone below the benching skirt). The benching skirt and center cone redirect the rotating flow up and inward between the center shaft and dip plate cylinder away from the stored sediment. The outlet pipe discharges treated effluent from within the dip plate cylinder ensuring the longest possible residence time (blue arrow in Figure 8.15).

(a)



(b)

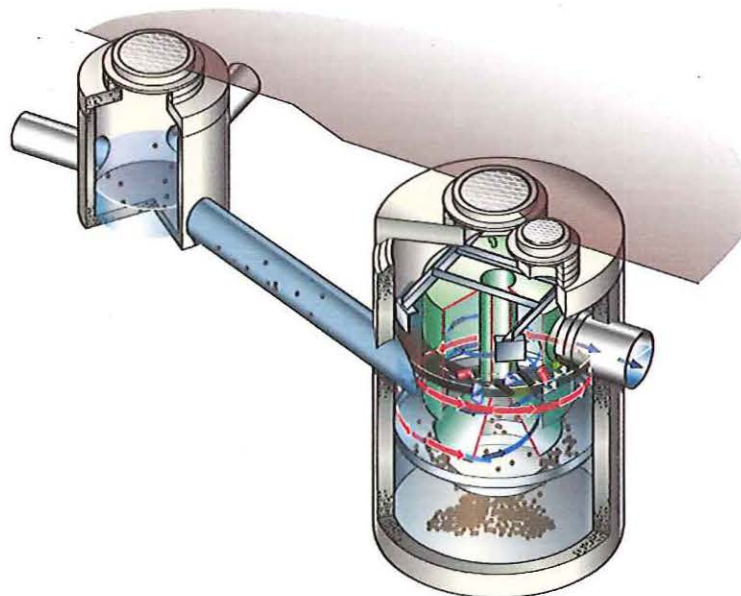


Figure 8.15. Components of the Downstream Defender® (a) and its system while operating (b). Source: www.hydro-international.biz/.

8.3.4 Dry Detention pond

Dry detention ponds (i.e., dry ponds, extended detention basins, detention ponds, and extended detention ponds) are basins whose outlets have been designed to detain stormwater runoff for some minimum time (e.g., 24 hours) to allow particles and associated pollutants to settle. Unlike wet ponds, these facilities do not have a large permanent pool of water (Figure 8.16). They can also be used to provide flood control by including additional flood detention storage.

Dry detention ponds have traditionally been one of the most widely used stormwater best management practices (BMPs). They are typically easier and less expensive to construct as compared to wet detention ponds and more flexible in maintenance and inspection. Hussain et al. (2006) reported that dry detention ponds are an effective option for water quality control such as total suspended solids, volatile suspended solids, particulate phosphorus, and total phosphorus in the stormwater management.

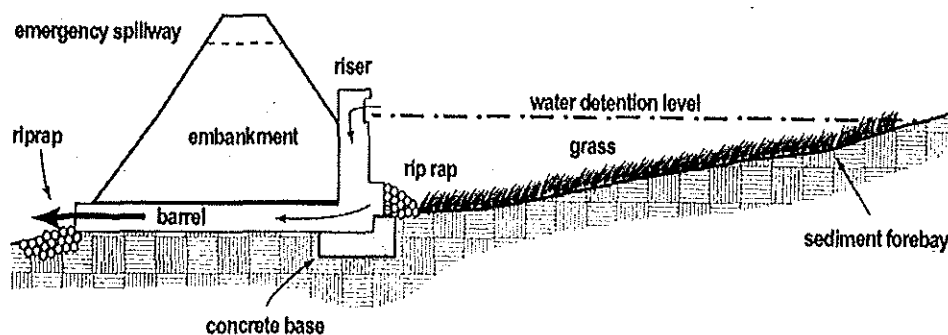


Figure 8.16. Example profiles view of a dry detention pond.

IX. CONCLUSIONS

This dissertation outlines a framework for a comprehensive stormwater quality analysis, with special emphasis on the Greater Milwaukee area. GIS was used to determine drainage area sizes and runoff coefficients of areas for various land uses. The influence of each of several dry periods before a storm event on the calculated load in the stormwater load model for mixed land-use drainage areas was investigated. The CMB and PMF models were applied to apportion pollutant sources of CSOs, and to quantify the fraction of pollutant mass and flow fractions of stormwater and sanitary sewage. The main conclusions of this work are as follows:

1. A topographic map for each storm catchment might not reveal the complete drainage pattern of stormwater runoff. GIS maps including contour data, storm sewer lines, and land use, along with runoff coefficients from original drainage areas are useful to help determine actual drainage area sizes accurately. Runoff coefficients were calculated by an optimization model based on 18 drainage areas and 10 GIS land use subareas. A better understanding of the drainage pattern provides information required to make decisions related to stormwater best management practices (BMPs).
2. Stormwater pollutant loadings were found to be dependent on drainage area, runoff coefficient, land use, antecedent dry period, and duration and intensity of the rainfall. The pollutant load model proposed here can be applied for multiple catchments with various runoff coefficients and types of land use. Land use was modeled by a multiplicative parameter, the land use factor α . The model also

contains an average constituent deposition rate α (kilograms per hectare per day or CFU per hectare per day), such that the deposition rate is $\alpha\alpha$ for each catchment. The lengths of antecedent dry periods were found to be significant parameters determining pollutant concentrations and loadings due to the gradual accumulation of pollutants during several dry periods prior to a storm. An effective accumulation time that considers the residual load from several previous storms was defined. Two previous dry periods in the antecedent dry period function appeared to be sufficient for most pollutants.

3. A washoff model was also developed. The model can be applied to the portion of the hydrograph near the peak, especially when the peak was extended through at least 2 – 3 hours. A good estimate of the transport coefficient for individual pollutants is necessary because the transport coefficient reflects the removal ability of pollutant mass on the surfaces. Typical transport coefficient values found in this study using narrow hydrograph peaks are 4 – 8 times higher than similar values determined previously for single land use areas, or based on the load model for the same drainage areas. Transport coefficients for metals are in decreasing order $\text{Pb} > \text{Ag} > \text{Zn} > \text{Cu} > \text{Ni} > \text{Hg} > \text{Cd}$, reflecting the decreasing degree of particle association. For BOD_5 , suspended solids, bacteria, and phosphorus, the order of transport coefficients are $\text{TSS} > \text{FC} > \text{EC} > \text{BOD}_5 > \text{TP}$, showing the increase in soluble fraction of these pollutants.
4. Both CMB and PMF models are valid for identification of pollutant sources and calculation of pollutant and flow contributions in CSOs. Based on overflow events during 2000 – 2006 for the CMB model and 2004 – 2006 for the PMF

model, three possible sources (stormwater, sanitary sewage, and groundwater) in CSOs were found. Between 27 and 56 % of the flow was from sanitary sewage and at least 26 % from stormwater with up to 18 % from groundwater. Metals and TSS from stormwater were found to be predominant pollutants in CSOs. Sanitary sewage contributed ≥ 28 % of the BOD₅, NH₃, and TP in CSOs. The contribution of sanitary sewage to NH₃ was relative high (≥ 58 %). In order to eliminate CSOs with high amounts of BOD₅, NH₃, and TP from sanitary sewage, sewer separation may be implemented to separate combined sewers into sanitary and storm sewers but this method can be costly and inappropriate unless effective BMPs that target removal of metals, TSS, and bacteria from stormwater are implemented in the separated storm sewer systems. Reduction of CSO pollutants such as Cd, Cr, Cu, Ni, and Zn may be achieved through periodic removal of sewer sediment. In order to effectively reduce other CSO pollutants such as TSS and Pb, it is better to implement BMPs prior to combining stormwater and sanitary sewage, for example, rain gardens, green parking lots, porous pavement, stormceptor®, vortechs®, and downstream defender®.

X. RECOMMENDATIONS

The following practical recommendations can be made to improve water quality on impaired receiving water bodies due to polluted stormwater runoff in the Greater Milwaukee, Wisconsin:

1. The storm sewer lines in GIS shape files for local communities need to be extensively conducted. The GIS maps based on topographical data and storm sewer lines accordance with runoff coefficients can reveal the accurate drainage pattern for each storm catchment.
2. The source apportionment methods outlined here based on CMB and PMF models may be used not only to characterize origin of pollutants and flows in CSOs but also to explore improper connections between sanitary and storm sewers during dry or wet weather flows. The results, which are quantitative, may be used in conjunction with alternative qualitative techniques such as the genetic marker method which can distinguish between fecal bacteria of animal and human origin. For example, genetic marker tests were done by the University of Wisconsin-Milwaukee's Great Lakes Water Institute on samples collected from site SWMI16 (Miller Park east parking lots), and the marker for human fecal bacteria was found. While stormwater is known to contain high levels of bacteria from birds, pets and other animals that are rinsed off parking lots, lawns and streets, it should not contain bacteria from human feces.

3. Future works on source apportionment of dry weather flows and wet at storm sewer outfalls using CMB and PMF models may have to be performed in order to demonstrate the modeling to local municipal engineers.
4. Implementing traditional effective stormwater BMPs such as detention ponds following MMSD stormwater reduction program is key to improve the receiving water quality. However, other technologies that can treat the stormwater such as Stormceter®, Vortechs®, and Downstream defender® may also be applied.

XI. REFERENCES

- Ab Razak, I. A. and Christensen, E. R. (2001). "Water quality before and after deep tunnel operation in Milwaukee, Wisconsin." *Water Res.* 35(11), 2683–2692.
- Adams, B. J. and Papa, F. (2000). *Urban Stormwater Management Planning with Analytical Probabilistic Models*. John Wiley and Sons, New York, NY.
- Akan, A. O. (1988). "Derived frequency-distribution for storm runoff pollutant." *J. Environ. Eng.* 114, 1344–1351.
- Alley, W. M. (1981). "Estimation of impervious-area washoff parameters." *Water Resour. Res.* 17(4), 1161–1166.
- Alley, W. M. and Smith, P. E. (1981) "Estimation of accumulation parameters for urban runoff quality modeling." *Water Resour. Res.* 17 (6), 1657–1664.
- Alley, W. M. and Veenhuis, J. E. (1983). "Effective impervious area in urban runoff modeling." *J. Hydraul. Eng.*, 109, 313–319.
- American Public Health Association (APHA), American Water Works Association (AWWA) and Water Environment Federation (WEF) (1998). *Standard Methods for the Examination of Water and Wastewater*. 20th ed., APHA, Washington, D.C.
- Bannerman, R. T., Owens, D. W., Dodds, R. B. and Hornewer, N. J. (1993). "Sources of pollutants in Wisconsin stormwater." *Water Sci. Technol.* 28, 241–259.
- Barrett, M. E., Irish Jr., L. B., Malina Jr., J. F. and Charbeneau, R. J. (1998). "Characterization of highway runoff in Austin, Texas, Area." *J. Environ. Eng.* 124(2), 131–137.
- Berbee, R., Rijs, G., Brouwer, R. and Velzen, L. (1999). "Characterization and treatment of runoff from highways in the Netherlands paved with impervious and pervious Asphalt," *Water Environ. Res.* 71(2), 83–190.
- Brewer, P. (1997). "Vehicles as a Source of Heavy Metal Contamination in the Environment. M.Sc. Thesis, University of Reading, Berkshire, United Kingdom.
- Brezonik, P. L. and Stadelmann, T. H. (2002). "Analysis and predictive models of stormwater runoff volumes, loads, and pollutant concentrations from watersheds in the Twin Cities Metropolitan area, Minnesota, USA." *Water Res.* 36, 1743–1757.

- Brown and Caldwell (2004). Analysis of Pollutant Loading Changes Resulting From Sewer Separation Within MMSD System. Memorandum to Members of the Mayor's Audit Committee. Milwaukee Metropolitan Sewerage District (MMSD), Wisconsin.
- Butcher, J. B. (2003). "Buildup, washoff, and event mean concentrations." *J. Am. Water Resour. Assoc.* 39,1521-1528.
- Bzdusek, P. A., Christensen, E. R., Lee, C. M., Pakdeesusuk, U. and Freedman, D. L. (2006a). "PCB congeners and dechlorination in sediments of Lake Hartwell, South Carolina, determined from cores collected in 1987 and 1998." *Environ. Sci. Technol.* 40, 109-119.
- Bzdusek, P. A., Lu, J. and Christensen, E. R. (2006b). "PCB congeners and dechlorination in sediments of Sheboygan River, Wisconsin, determined by Matrix Factorization." *Environ. Sci. Technol.* 40, 120-129.
- Cameron, R. and Green, D. M. (2005). Salt Spring Island electoral area stormwater quality. Annual Report. Capital regional district scientific programs, Environmental services department, Victoria, BC.
- Charbeneau, R. J. and Barrett, M. E. (1998). "Evaluation of Methods for Estimating Stormwater Pollutant Loads." *Water Environ. Res.* 70(7), 1295-1302.
- Chen, J. and Adams, B. J. (2006). Analytical urban storm water quality models based on pollutant buildup and washoff processes." *J. Environ. Eng.* 132,1314-1330.
- Christensen, E. R. and Guinn, V. P. (1979). "Zinc from Automobile Tires in Urban Runoff." *ASCE J. Environ. Eng.* 105(1), 165-168.
- Christensen, E. R., Li, A., Ab Razak, I. A., Rachdawong, P. and Karls, J. F. (1997). "Sources of Polycyclic Aromatic Hydrocarbons in sediments of the Kinnickinnic River, Wisconsin." *J. Great Lakes Res.* 23(1), 61-73.
- Colman, J. A.; Rice, K. C. and Willoughby, T. C. (2001). Methodology and Significance of Studies of Atmospheric Deposition in Highway Runoff. U.S. Geological Survey Open-File Report 01-259. U.S. Geological Survey, Northborough, Massachusetts.
- Cooper, J. A. and J. G., Watson, Jr. (1980). "Receptor oriented methods of air particulate source apportionment." *J. Air Pollut. Control Assoc.* 30(10), 1116-1125.
- Elliott, A. H. and Trowsdale, S. A. (2007). "A Review of Models for Low Impact Urban Stormwater Drainage." *Environ. Modell. Softw.* 22(3), 394-405.

- Ellis, J. B., Revitt, D. M., Harrop, D. O. and Beckwith, P. R. (1987). The contribution of highway surfaces to urban stormwater sediments and metal loadings." *Sci. Total Environ.* 59, 339-349.
- Field, R., Pitt, R., Lalor, M., Brown, M., Vilkelis, W. and Phackston, E. (1994). "Investigation of dry-weather pollutant entries into storm-drainage systems." *ASCE J. Environ. Eng.* 120(5), 1044-1066.
- Fries, J. S., Characklis, G. W. and Noble, R. T. (2006) "Attachment of fecal indicator bacteria to particles in the Neuse river estuary, N.C." *J. Environ. Eng.* 132, 1338-45.
- Gilbert, R. O. (1987). *Statistical Methods for Environmental Pollution Monitoring*, John Wiley & Sons, Inc.
- Gromaire, M. C., Garnaud, S., Saad, M. and Chebbo, G. (2001). "Contribution of different sources to the pollution of wet weather flows in combined sewers." *Water Res.* 35(2), 521-533.
- Grottke, M. (1987). "Runoff Quality from a Street with Medium Traffic Loading." *Sci. Total Environ.* 59, 457-466.
- Harrison, R. M. and Johnston, W. R. (1985). "Deposition Fluxes of Lead, Cadmium, Copper and Polynuclear Aromatic Hydrocarbons (PAH) on the Verges of a Major Highway." *Sci. Total Environ.* 46, 121-135.
- Henry, R. C., Lewis, C. W., Hopke, P. K. and Williamson, H. J. (1984). "Review of receptor model fundamentals." *Atmos. Environ.* 18 (8), 1507-1515.
- Hicks, B. B. (1997). "Atmospheric Deposition and Its Effects on Water Quality," in *workshop on research Needs for Coastal Pollution in Urban Areas*, E. R. Christensen and C. R. O'Melia (Eds.), Milwaukee, WI.
- Hilborn, J. and Sill, M. (1990). Canadian Perspectives on Air Pollution. SOE Report 90-1. Environment Canada, Ottawa, Ontario.
- Hopke, P. K. (1985). *Receptor Modeling in Environmental Chemistry*. Wiley-Interscience, New York.
- Huber, W. C. (1986). "Deterministic Modeling of Urban Runoff Quality," in *Proceedings, Urban Runoff Pollution*. H. C. Torno et al. (Eds.), Springer-Verlag, Berlin, 167-242.
- Huber, W. C., Lai, F., Clannon, L. and Stouder, M. (2006). "Modeling concepts for BMP/LID Simulation." *BMP Technology in Urban Watersheds: Current and*

Future Conditions. Edited by Field, E., Struck, S. D., Tafuri, A. N., Ports, M. A., Clar, M., Clark, S., and Rushton, B., ASCE, Virginia, 221-231.

- Hussain, C. F., Brand, J., Gulliver, J. S. and Weiss, P. T. (2006). Water Quality Performance of Dry Detention Ponds with Under-Drains. Final Report to Minnesota Department of Transportation, Research Services Section, St. Paul, Minnesota.
- James, W. and Boregowda, S. (1986). "Continuous Mass-Balance of Pollutant Build-up Processes," in *Proceedings, Urban Runoff Pollution*. H. C. Torno et al. (Eds.), Springer-Verlag, Berlin, 243-272.
- Kim, L. H., Kayhanian, M., Lau, S. L. and Stenstrom, M. K. (2005). "A new model approach—First flush metal mass loading." *Water Sci. Technol.* 51(3-4), 159–167.
- Kim, L. H., Zoh, K. D., Jeong, S. M., Kayhanian, M. and Stenstrom, M. K. (2006). "Estimating pollutant mass accumulation on highways during dry periods." *ASCE J. Environ. Eng.* 132(9), 985–993.
- Klemm, R. F. and Grey, J. M. L. (1982). A Study of the Chemical Composition of Particulate Matter and Aerosols over Edmonton. Report RMD 82/9. Prepared for the Research Management Division by the Alberta Research Council.
- Lalor, M. (1994). An assessment of non-stormwater discharges to storm drainage systems in residential and commercial land use areas. Ph.D. dissertation, Department of Civil and Environmental Engineering, Vanderbilt University, Nashville, Tennessee.
- Larsen, R. K. and Baker, J. E. (2003) "Source apportionment of polycyclic aromatic hydrocarbons in the urban atmosphere: a comparison of three methods." *Environ. Sci. Technol.* 37, 1873–1881.
- Lawson, C. L. and Hanson, R. J. (1974). *Solving Least Squares Problems*. Prentice-Hall, New Jersey.
- Lee, H. S., R. A. Wadden and P.A. Scheff. (1993). "Measurement and evaluation of acid air pollutants in Chicago using an annular denuder system." *Atmos. Environ. Part A Gen. Top.* 27A (4), 543–553.
- Lee, H., Lau S-L., Kayhanian, M. and Stenstrom, M. K. (2004). "Seasonal first flush phenomenon of urban stormwater discharge," *Water Res.* 38, 4153-4163.
- Legret, M. and Pagotto, C. (1999). "Evaluation of pollutant loadings in the runoff waters from a major rural highway." *Sci. Total Environ.* 235, 143–150.

- McCuen, R.H. (2004). *Hydrologic analysis and design*. 3rd ed., Pearson Prentice Hall, New Jersey.
- Milwaukee Metropolitan Sewerage District (MMSD) (2007a). MMSD Laboratory QA/QC Program. MMSD, Milwaukee, Wisconsin.
- Milwaukee Metropolitan Sewerage District (MMSD) (2007b). Screening Alternatives. MMSD 2020 Facilities Plan. MMSD, Milwaukee, Wisconsin.
- Milwaukee Metropolitan Sewerage District (MMSD) (2007c). The application of stormwater runoff reduction best management practices in metropolitan Milwaukee. Stormwater runoff reduction program final report. MMSD, Milwaukee, Wisconsin.
- Milwaukee Metropolitan Sewerage District (MMSD) (2003). Stormwater Monitoring Program. MMSD, Milwaukee, Wisconsin.
- Minton G. R. (2002). Stormwater Treatment; Biological, Chemical and Engineering Principles. Resource Planning Associates, Seattle, Washington.
- Muirhead, R. W., Collins, R. P. and Bremer, P. J. (2006). "Interaction of *Escherichia coli* and soil particles in runoff." *Appl. Environ. Microbiol.* 72, 3406-11.
- New South Wales Environment Protection Authority (NSW EPA) (2005). What is urban stormwater?. NSW EPA, Department of Environment and Climate Change, New South Wales, Australia. <http://www.epa.nsw.gov.au/stormwater/whatis/index.htm>
- Niehus, C. A. (1997). Characterization of Stormwater Runoff in Sioux Falls, South Dakota, 1995–96. U.S. Geological Survey of Water Resources Investigation Report 97-4070. U.S. Geological Survey, Rapid City, South Dakota.
- Novotny, V., Sung, H. M., Bannerman, R. and Baum, K. (1985). "Estimating Non-point Pollution from Small Urban Watersheds," *Journal of the Water Pollution Control Federation* 57(4), 339-348.
- Osuch-Pajdzinska, E. and Zawilski, M. (1998). "Model of storm sewer discharge: I Description." *J. Environ. Eng.* 124, 593-9.
- Paatero, P. (1997). "Least squares formulation for robust nonnegative factor analysis." *Chemom. Intell. Lab. Syst.* 37, 23-35.
- Petersen, T. M., Rifai, H. S., Suarez, M. P. and Stein, A. R. (2005). "Bacteria loads from point and nonpoint sources in an urban watershed." *J. Environ. Eng.* 131, 1414-25.

- Pitt, R., Chaturvedula, S., Karri, V. and Nara, Y. (2004). "Source verification of inappropriate discharges to storm drainage systems." Proceeding of 77th Annual Water Environment Federation Technical Exhibition and Conference. Water Environment Federation, October 2-6, New Orleans, Louisiana.
- Pitt, R., Field, R., Lalor, M., Adrian, D. D. and Barbe, D. (1993). Investigation of Inappropriate Pollutant Entries into Storm Drainage Systems: A User Guide. Rep. No. EPA/600/SR-92/238. Storm and Combined Sewer Pollution Control Program (Edison, N.J.). US Environmental Protection Agency (EPA), Ohio.
- Pitt, R., Williamson, D., Voorhees, J. and Clark, S. (2004). "Review of historical street dust and dirt accumulation and washoff data." *In Effective Modeling of Urban Water Systems, Monograph 1*. Computational Hydraulics International, Guelph, Ontario, Canada.
- Randall, C. W., Grizzard, T. J., Helsel, D. R. and Griffin, D. M. (1982). "Comparison of Pollutant Mass Loads in Precipitation and Runoff in Urban Areas," *in Proceedings, Urban Stormwater Quality, Management and Planning*. B. C. Yen (Ed.), Water Resources Publications Highlands Ranch, CO, 29-38.
- Revitt, D. M., Hamilton, R. S. and Warren, R. S. (1990). "The transport of heavy metals within a small urban catchment." *Sci. Total Environ.* 93, 359-73.
- Sabin, L. D., Lim, J. H., Stolzenbach, K. D. and Schiff, K. C. (2005). "Contribution of trace metals from atmospheric deposition to stormwater runoff in a small impervious urban catchment." *Water Res.* 39, 3929-3937.
- Sansalone, J. J., Hird, J. P., Cartledge, F. K. and Tittlebaum, M. E. (2005). "Event-based stormwater quality and quantity loadings from elevated urban infrastructure affected by transportation." *Water Environ. Res.* 77, 348-365.
- Sartor, J. D., Boyd, G. B. and Agardy, F. J. (1974). "Water Pollution Aspects of Street Surface Contaminants." *J. Water Pollut. Control Fed.* 46(3), 458-467.
- Sawyer, C. N., McCarty, P. L. and Parkin, G. F. (2003). *Chemistry for environmental engineering and science*. McGraw-Hill, New York.
- Segarra-Garcia, R. and Loganathan, G. V. (1994). "A stochastic pollutant load model for the design of stormwater detention facilities." *Water Sci. Technol.* 29, 327-35.
- Shafer, K. (2006). "Milwaukee's Integrated Approach, A Watershed Moment." *BMP Technology in Urban Watersheds: Current and Future Conditions*. Edited by Field, E., Struck, S. D., Tafuri, A. N., Ports, M. A., Clar, M., Clark, S., and Rushton, B., ASCE, Virginia, 18-23.

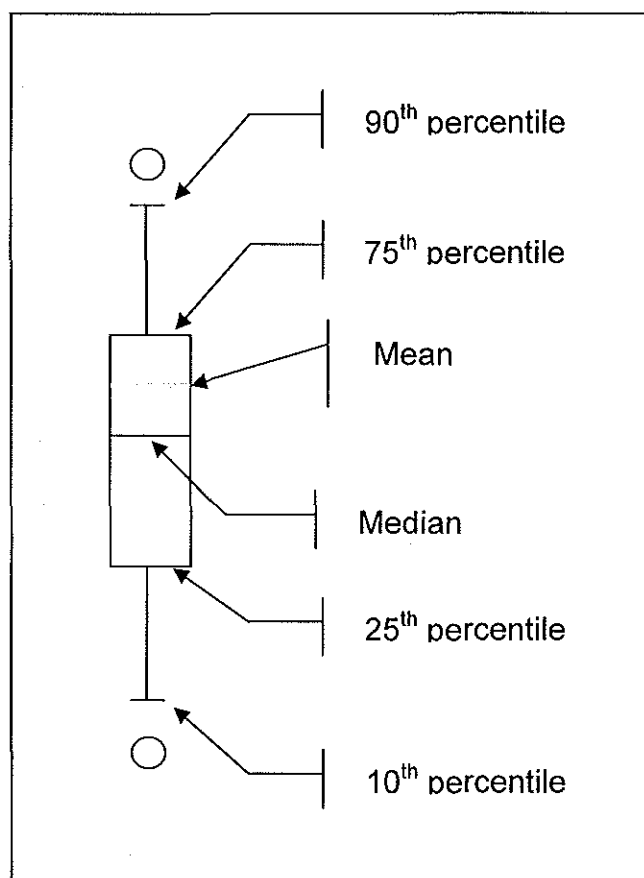
- Soonthornnonda, P. and Christensen, E. R. (2005) MMSD Stormwater Monitoring Program Data Analysis 2004–2005. Final Report. University of Wisconsin-Milwaukee: Milwaukee, Wisconsin.
- Soonthornnonda, P. and Christensen, E. R. (2007a). “A load model based on antecedent dry periods for pollutants in stormwater.” *Water Environ. Res.* In press.
- Soonthornnonda, P. and Christensen, E. R. (2007b). “Source apportionment of pollutants and flows of combined sewer wastewater.” *Water Res.* In revision.
- Soonthornnonda, P., Christensen, E. R., Boudjou, U., Singer, M., Bate, T., Magruder, C. and Waldmer, E. (2007a). “An evaluation of separating combined sewers and its effect on water quality in the Greater Milwaukee, Wisconsin area.” Proceeding of 80th Annual Water Environment Federation Technical Exhibition and Conference. Water Environment Federation, October 13–17, San Diego, California.
- Soonthornnonda, P., Christensen, E. R., Liu, Y. and Li, J. (2007b). “A washoff model for stormwater pollutants.” *Sci. Total Environ.* Submitted.
- Soonthornnonda, P., Seth, I., Liu, Y., Li, J. and Christensen, E. R. (2006). MMSD expanded stormwater monitoring program, data analysis, 2000–2006. 1st Interim Report. University of Wisconsin-Milwaukee, WI.
- Su, M. C. and Christensen, E. R. (1997). “Apportionment of sources of polychlorinated dibenzo-p-dioxins and dibenzofurans by a chemical mass balance model.” *Water Res.* 31 (12), 2935–2948.
- Texas Transportation Institute (2005). Urban Mobility Study for Milwaukee. Texas A&M University: College Station, Texas.
http://mobility.tamu.edu/ums/congestion_data/tables/milwaukee.pdf.
- Thomson, N. R., McBean, E. A., Snodgrass, W. and Mostrenko, I. (1997). “Sample Size Needs for Characterizing Pollutant Concentration in Highway Runoff.” *J. Environ. Eng.* 123(10), 1061–1065.
- U.S. Environmental Protection Agency (U.S. EPA) (1983a). Methods for chemical analysis of water and wastes. EPA-600/ 4-79-020. U.S. EPA, Cincinnati, Ohio.
- U.S. Environmental Protection Agency (U.S. EPA) (1983b). Final report of the nationwide urban runoff program. Water planning division, U.S. EPA, Washington, D.C.
- U.S. Environmental Protection Agency (U.S. EPA) (1986). Quality Criteria for Water, Gold Book, EPA-440/5-86-001. U.S. EPA, Washington, D.C.

- U.S. Environmental Protection Agency (U.S. EPA) (1994). Determination of Mercury in Water by Cold Vapor Atomic Absorption Spectrometry. U.S. EPA, Cincinnati, Ohio.
- U.S. Environmental Protection Agency (U.S. EPA) (1996). Test Methods for Evaluating Solid Waste, Physical/Chemical Methods (SW-846). U.S. EPA, Washington, D.C.
- U.S. Environmental Protection Agency (U.S. EPA) (1999). NPDES Multi-Sector Storm Water General Permit Monitoring Guidance. Office of Water, NPDES Program Branch, U.S. EPA, Washington, D.C.
- U.S. Environmental Protection Agency (U.S. EPA) (2000). Final Reissuance of National Pollutant Discharge Elimination System (NPDES) Storm Water Multi-Sector General Permit for Industrial Activities, EPA-65/FR-64745. U.S. EPA: Washington, D.C.
- U.S. Environmental Protection Agency (U.S. EPA) (2004). National Recommended Water Quality Criteria. Office of Water, Office of Science and Technology, U.S. EPA, 4304T, Washington, D.C.
- U.S. Geological Survey (USGS) (2004). Water-Resources-Related Information for the Milwaukee Metropolitan Sewerage District Planning Area, Wisconsin, 1970-2002. Water-Resources Investigation Report 03-4240. USGS, Reston, Virginia.
- Wade, T. J., Pai, N., Eisenberg, J. N. S. and Colford, J. M. (2003). "Do US Environmental Protection Agency water quality guidelines for recreational waters prevent gastrointestinal illness? A systematic review and meta-analysis." *Environ. Health Perspect.* 111, 1102-1109.
- Waller, D., and Hart, W. C. (1986). "Solids, Nutrients and Chlorides in Urban Runoff," *Proceedings of Urban Runoff Pollution*, H. C. Torno et al. (Eds.), Springer-Verlag, Berlin, 59-85.
- Warner, L. R., Sokhi, R. S., Luhana, L., Boulter, P. G. and McCrae, I. (2002). "Non-Exhaust Particle Emissions from Road Transport." *Proceedings of 11th International Conference, Transport and Air Pollution*, Graz, Austria, June 19-21, Institute for Internal Combustion Engines and Thermodynamics, Graz University of Technology, 265-272.
- Waschbusch, R. J., Selbig, W. R. and Bannerman, R. T. (1999). Sources of phosphorus in stormwater and street dirt from two urban residential basins in Madison, Wisconsin, 1994-95. Water-Resources Investigations: Report 99-4021. U.S. Geological Survey, USA.
- Water, Soil and Hydro-Environmental Decision Support System (WATERSHEDSS) (2003). A Decision Support System for Nonpoint Source Pollution Control. North Carolina State University, Raleigh, NC. <http://www.water.ncsu.edu/watershedss/>

- Watson, J. G., Cooper, J. A. and Huntzicker, J. J. (1984). "The effective variance weighting for least squares calculations applied to the mass balance receptor model." *Atmos. Environ.* 18(7), 1347–1355.
- Westerlund, C., Viklander, M. and Backstrom, M. (2003). "Seasonal variations in road runoff quality in Lulea, Sweden." *Water Sci. Technol.* 48(9), 93-101.
- Wisconsin Academy of Sciences, Arts and Letters (WASAL) (2003). Waters of Wisconsin: The Future of Our Aquatic Ecosystems and Resources. A report of WASAL. WASAL, Madison, Wisconsin.
- Wisconsin Department of Natural Resources (WDNR) (2002). Stormwater discharge permits, NR 216. WDNR, Madison, Wisconsin.
- Wisconsin Department of Natural Resources (WDNR) (2003). WPDES Permit No. WI-0036820-02-0. WDNR, Madison, Wisconsin.
- Wisconsin Department of Natural Resources (WDNR) (2007). Groundwater Retrieval Network (GRN). WDNR, Madison, Wisconsin.
[http://prodoasext.dnr.wi.gov/inter1/grn\\$.startup](http://prodoasext.dnr.wi.gov/inter1/grn$.startup)
- Wisconsin state climatology office (2005). Long-term variability in seasonal snowfall at Milwaukee. Atmospheric and Oceanic Sciences Department, University of Wisconsin, Wisconsin.
<http://www.aos.wisc.edu/~sco/stations/mke/milwaukee.html>.
- Wright Water Engineers, Inc. and GeoSyntec Consultants (2007). International Stormwater Best Management Practices Database Data Entry Spreadsheets. Interim User's Guide. Interim Release, Version 1.0. Urban Water Resources Research Council (UWRRC), U.S. EPA Office of Water, Washington, D.C.

XII. APPENDICES

Appendix A First Flush and Later-Time Concentrations



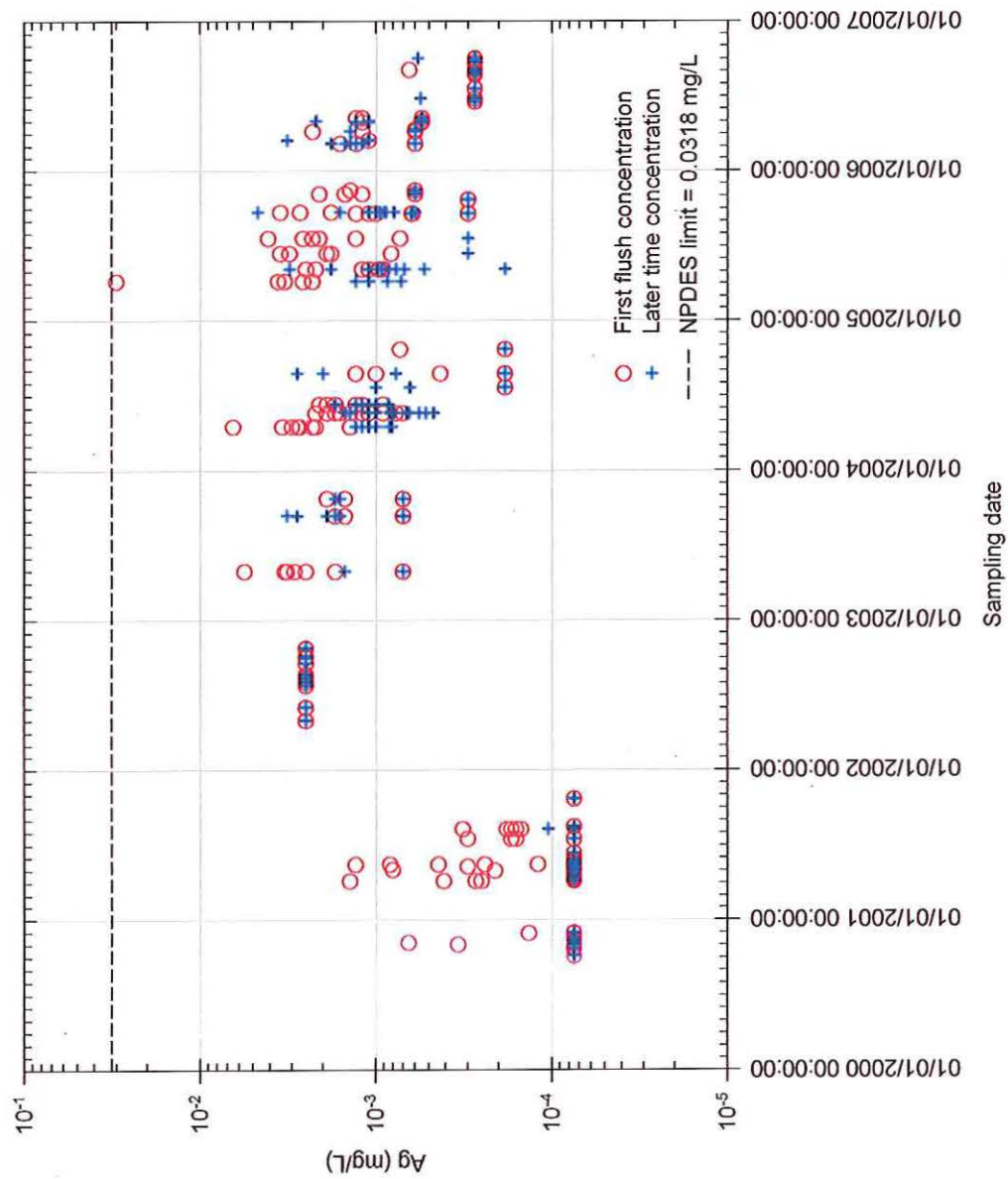


Figure A - 1. First flush and later-time concentrations of Ag in stormwater.

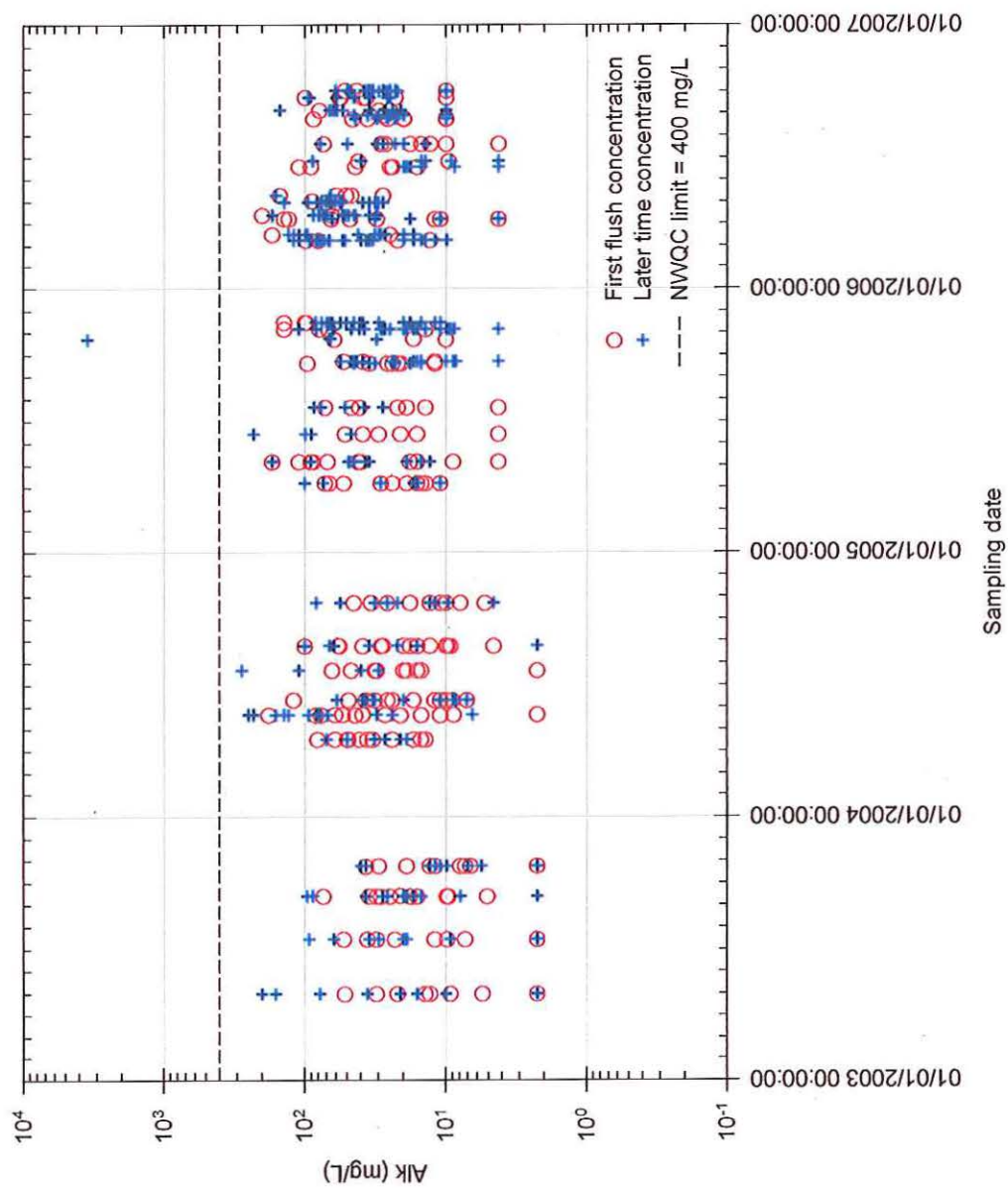


Figure A - 2. First flush and later-time concentrations of Alk in stormwater.

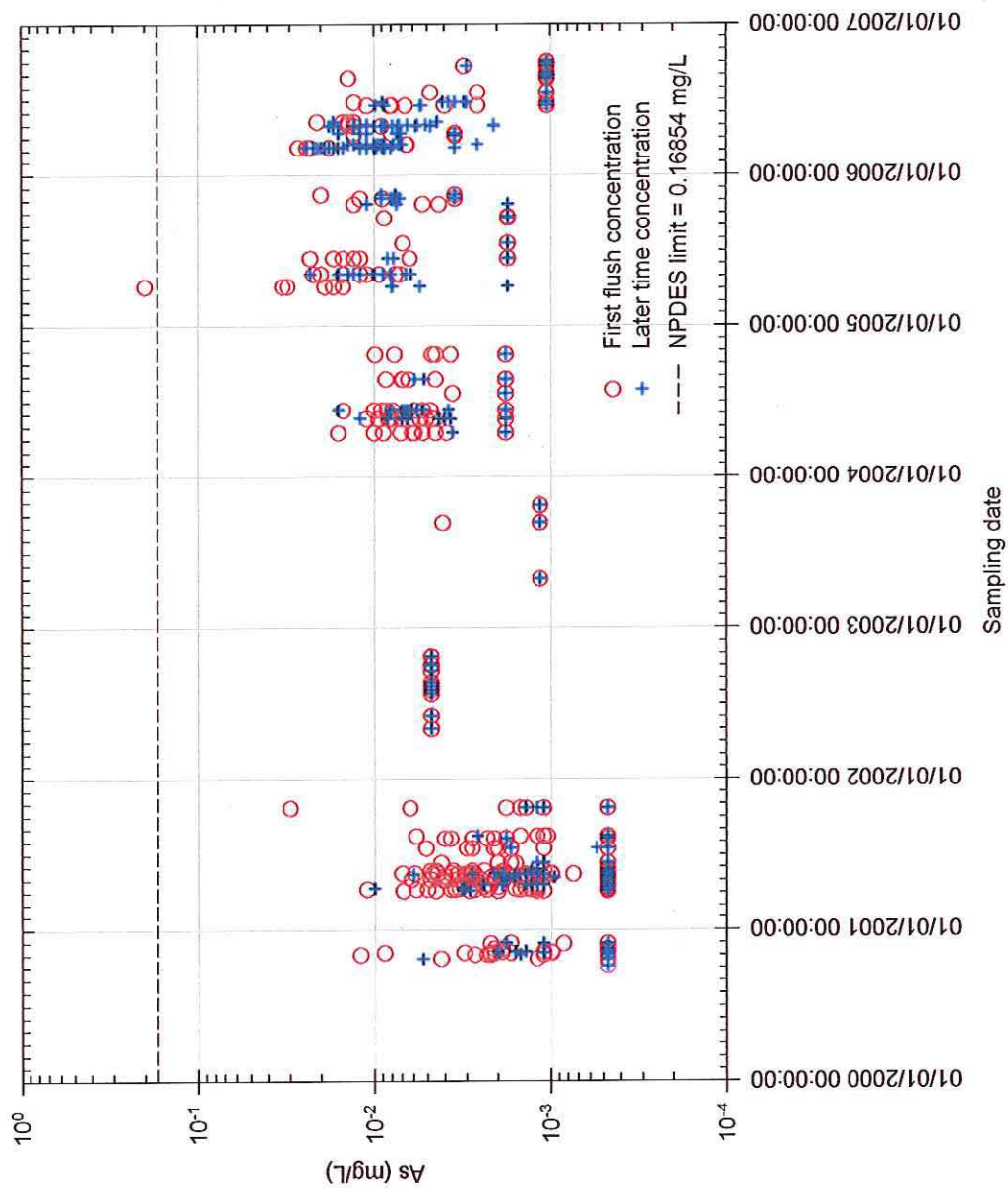


Figure A - 3. First flush and later-time concentrations of As in stormwater.

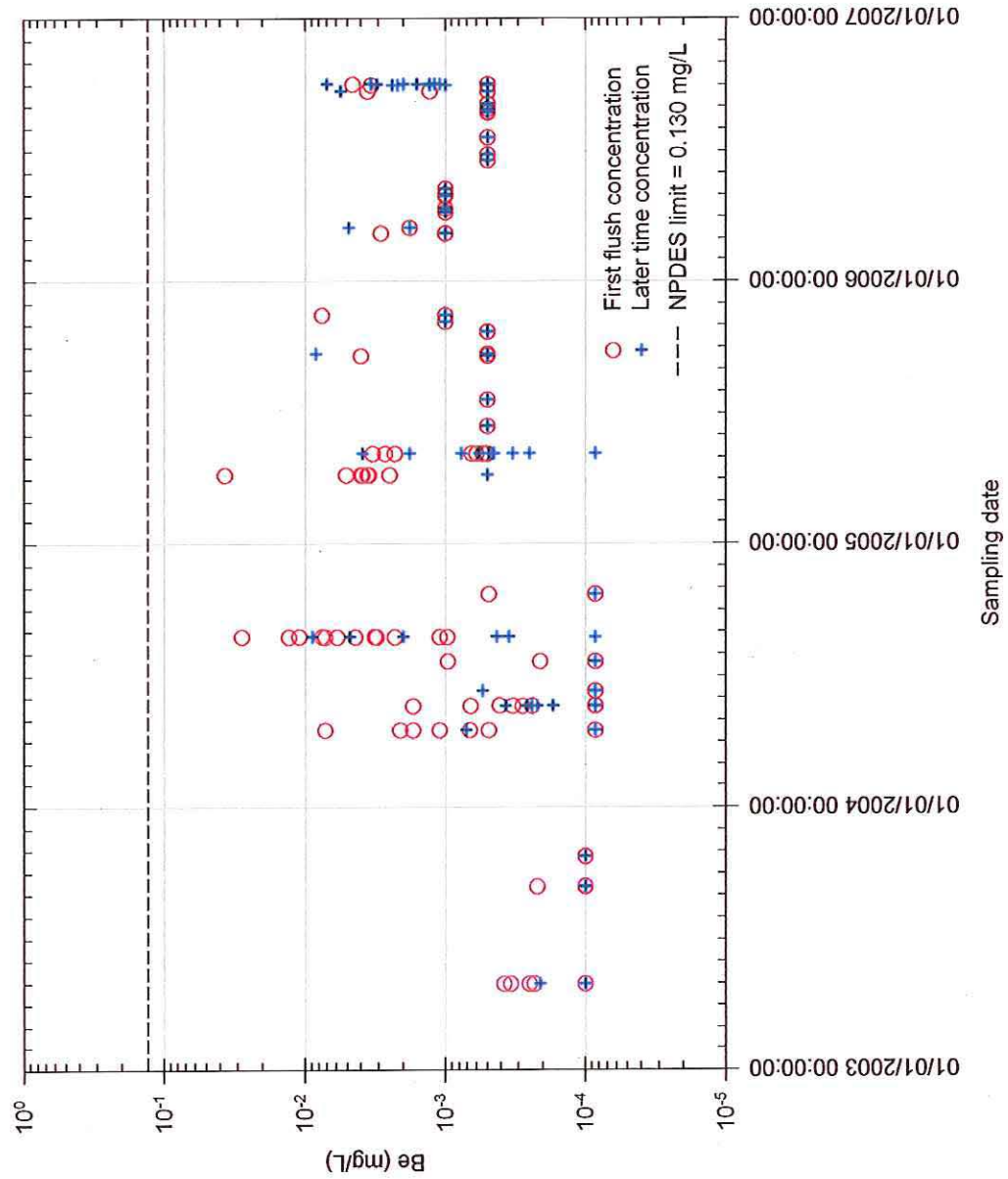


Figure A - 4. First flush and later-time concentrations of Be in stormwater.

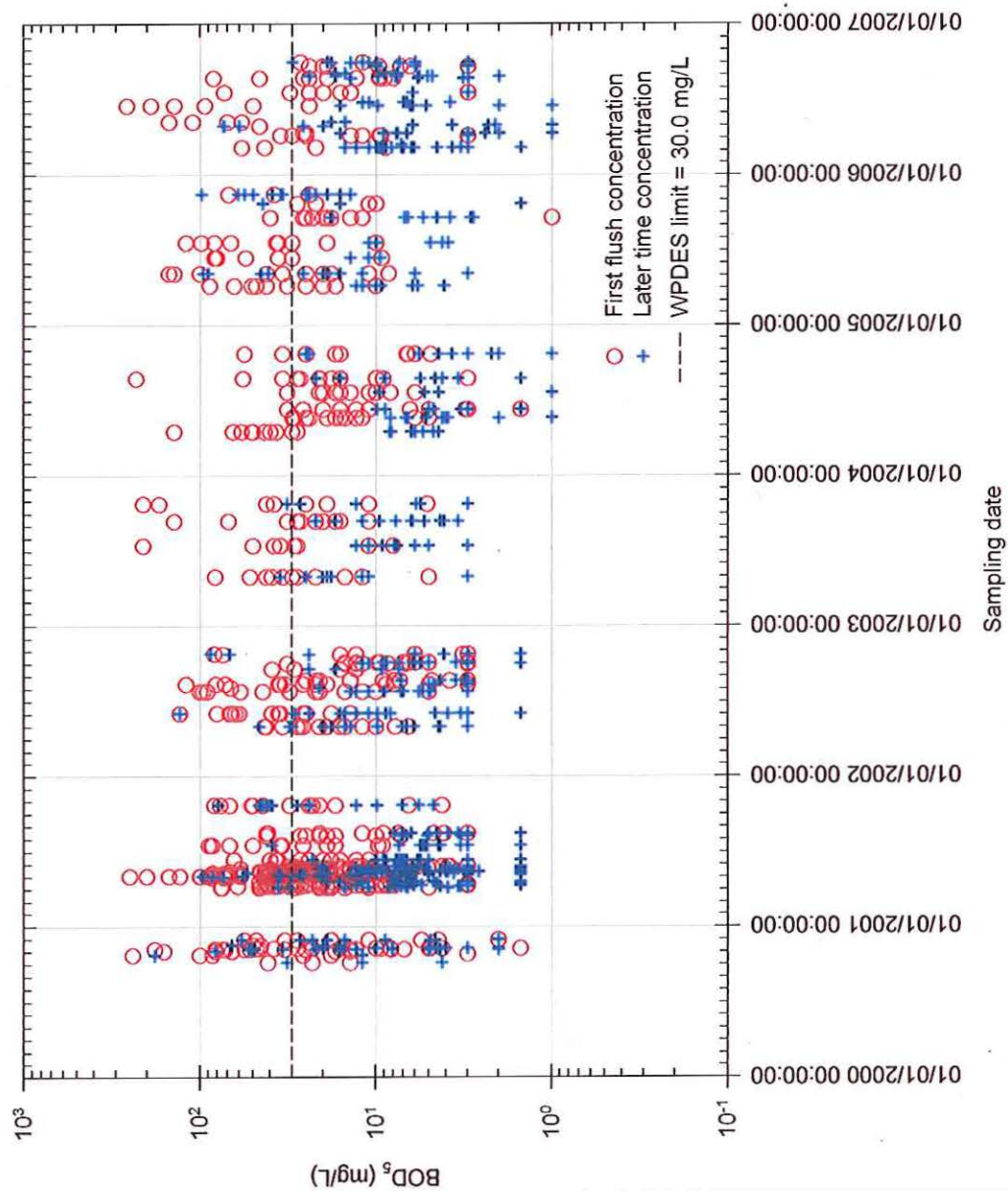


Figure A - 5. First flush and later-time concentrations of BOD₅ in stormwater.

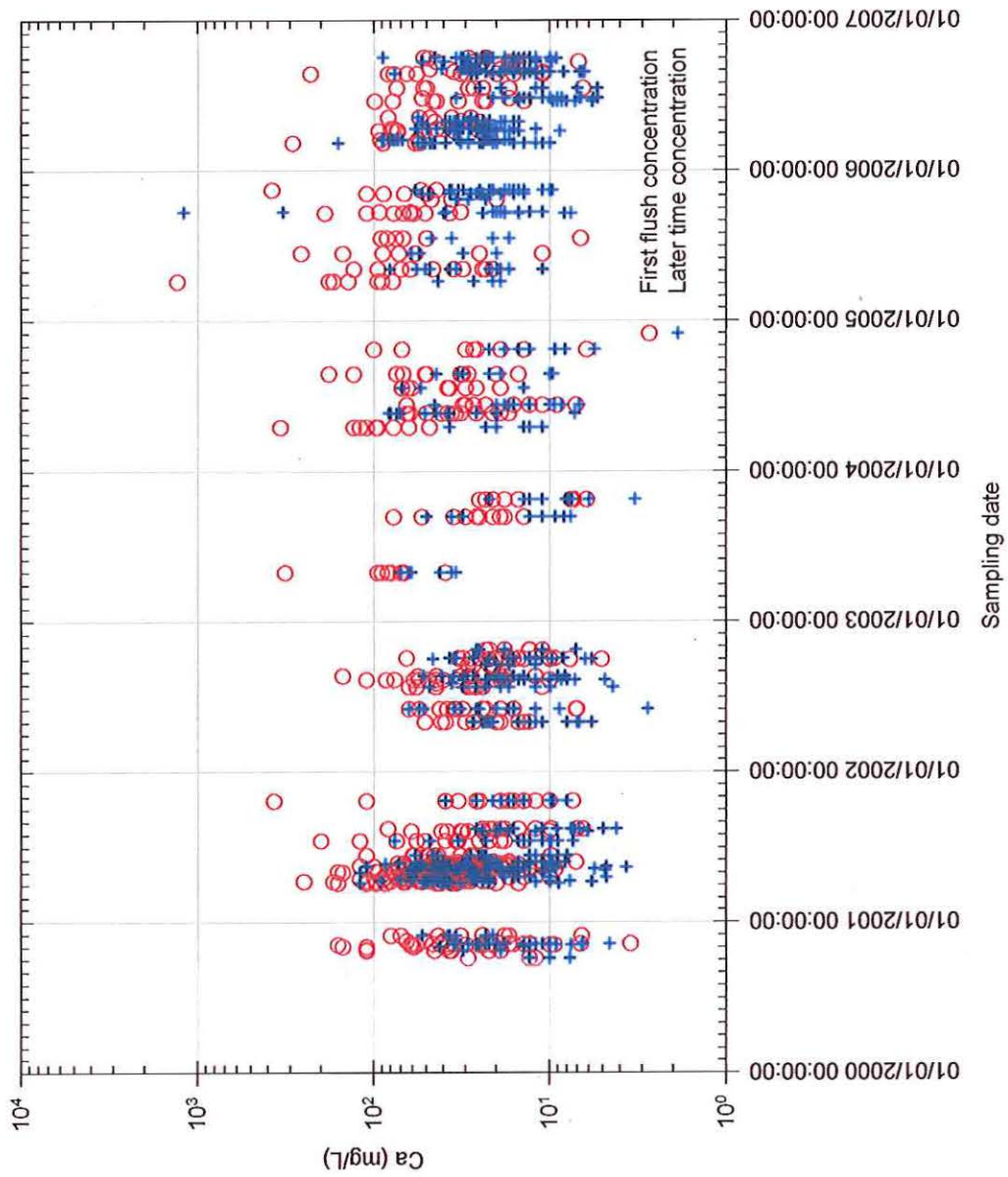


Figure A - 6. First flush and later-time concentrations of Ca in stormwater.

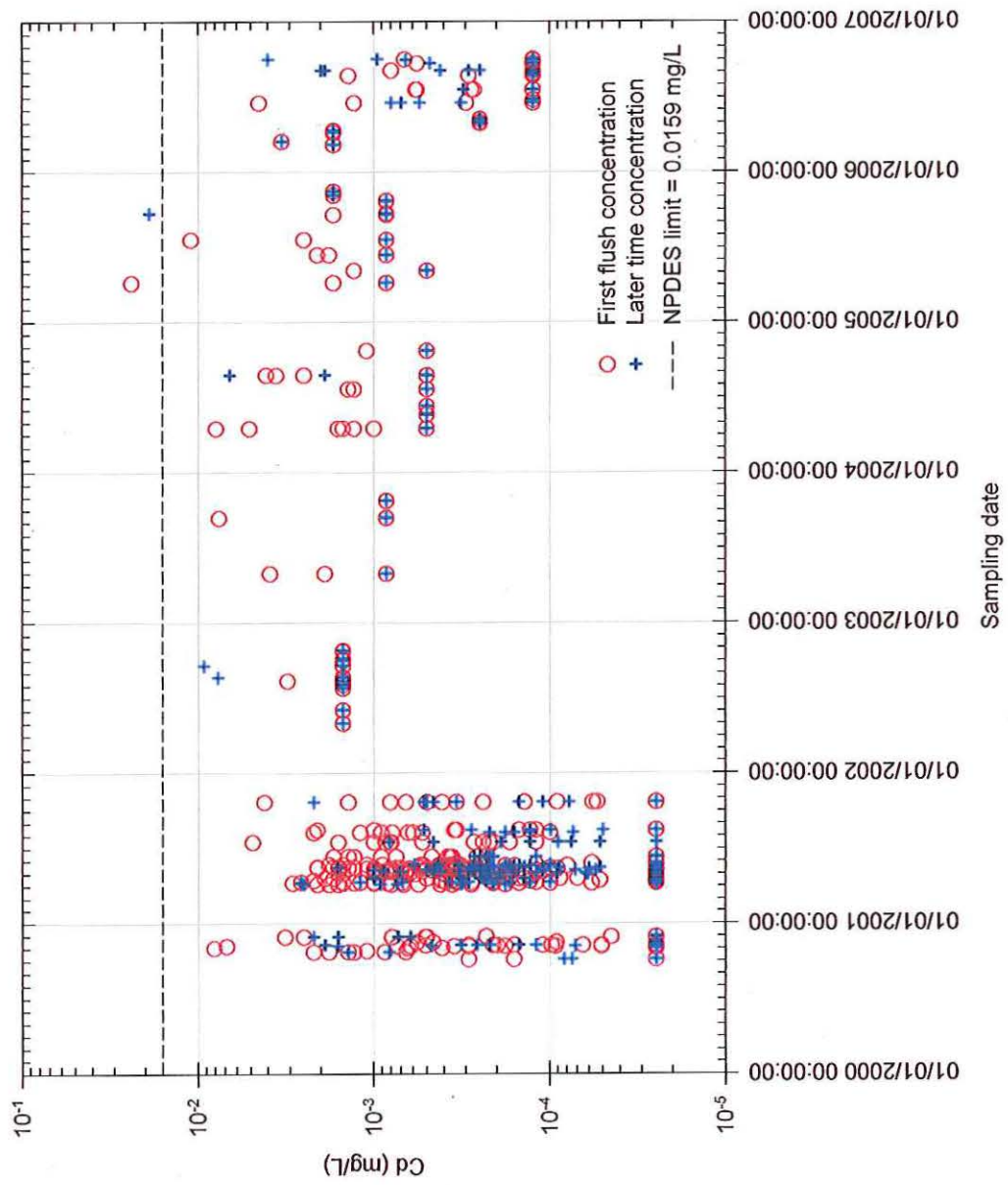


Figure A - 7. First flush and later-time concentrations of Cd in stormwater.

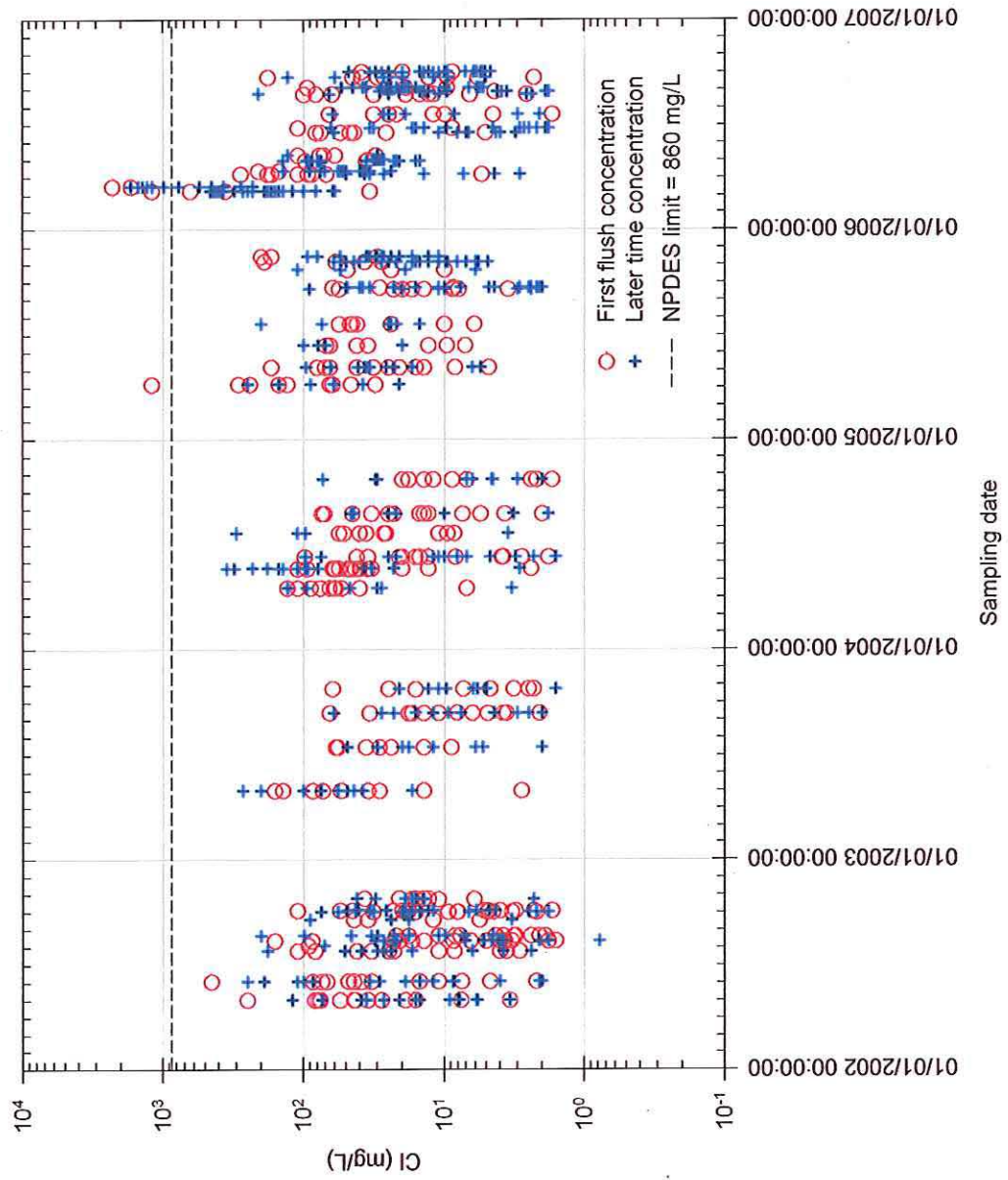


Figure A - 8. First flush and later-time concentrations of Cl⁻ in stormwater.

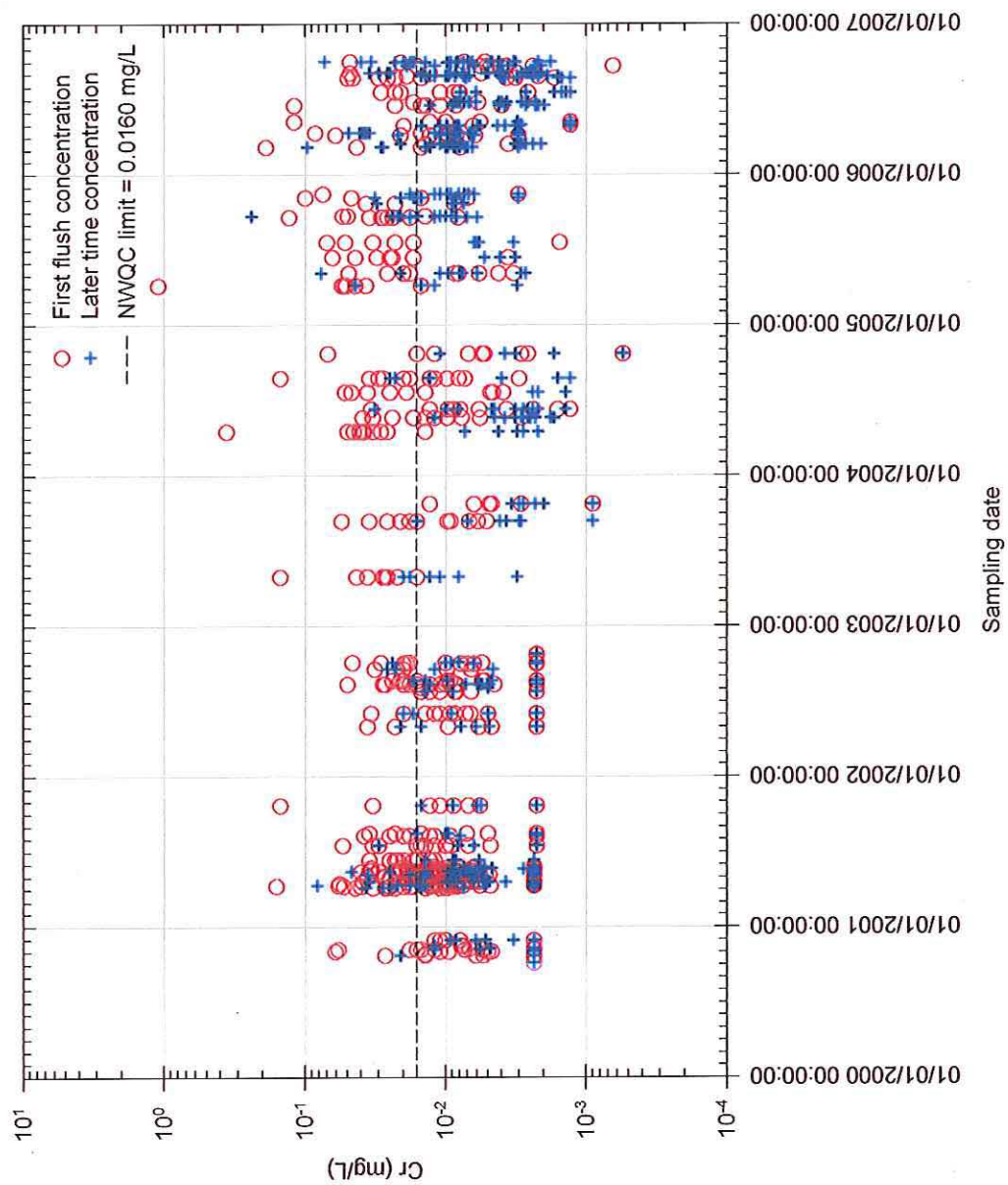


Figure A - 9. First flush and later-time concentrations of Cr in stormwater.

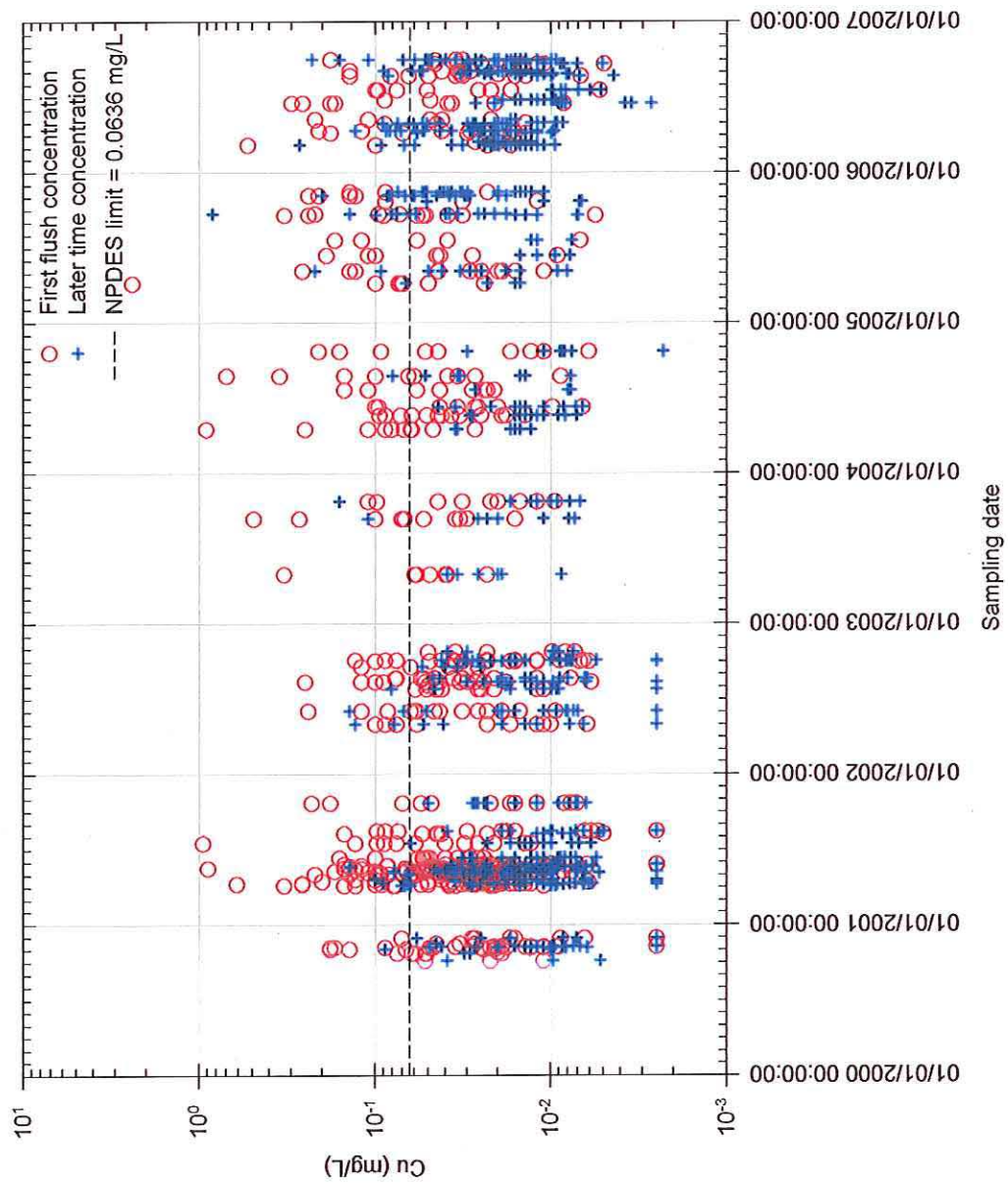


Figure A - 10. First flush and later-time concentrations of Cu in stormwater.

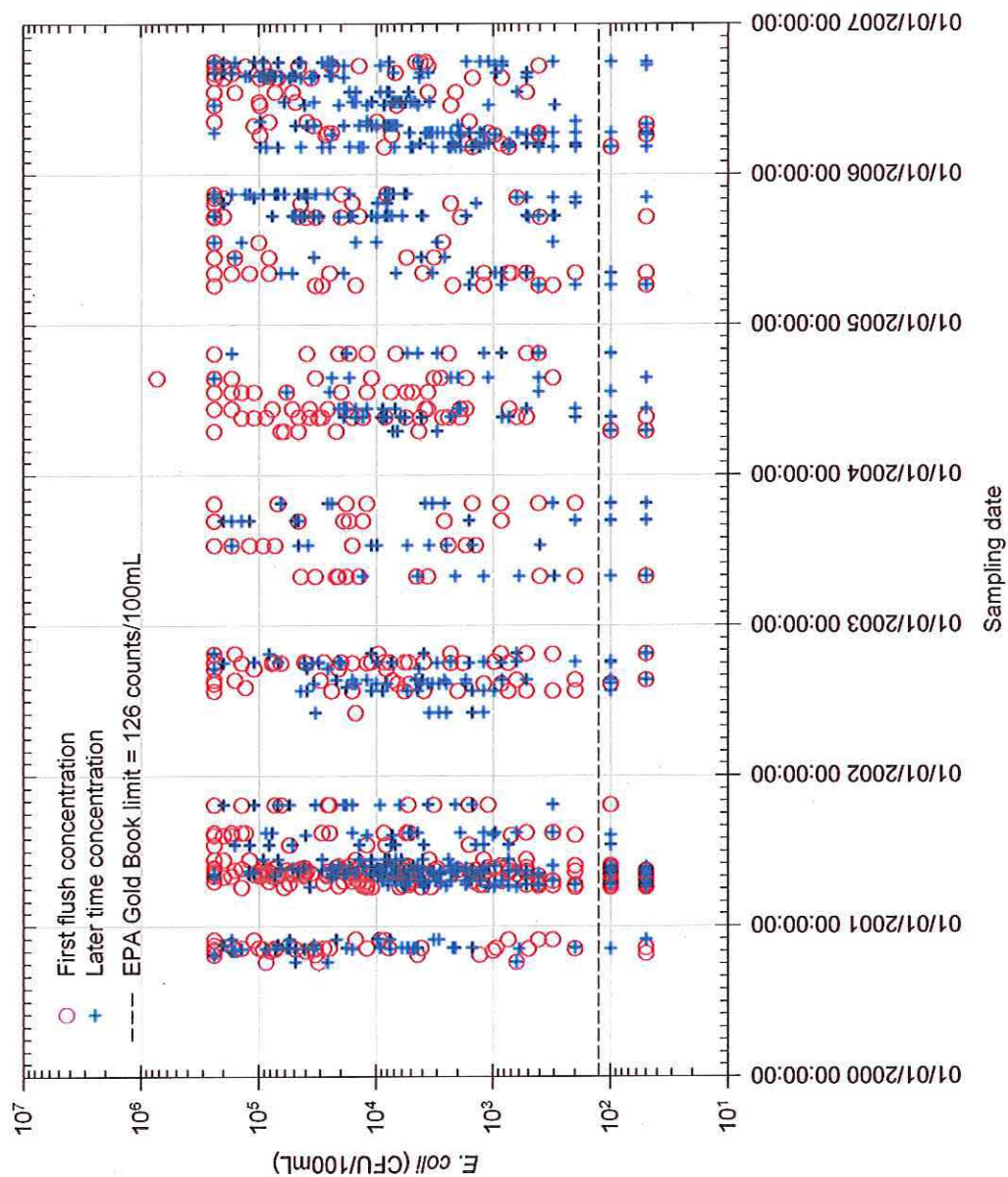


Figure A - 11. First flush and later-time concentrations of EC in stormwater.

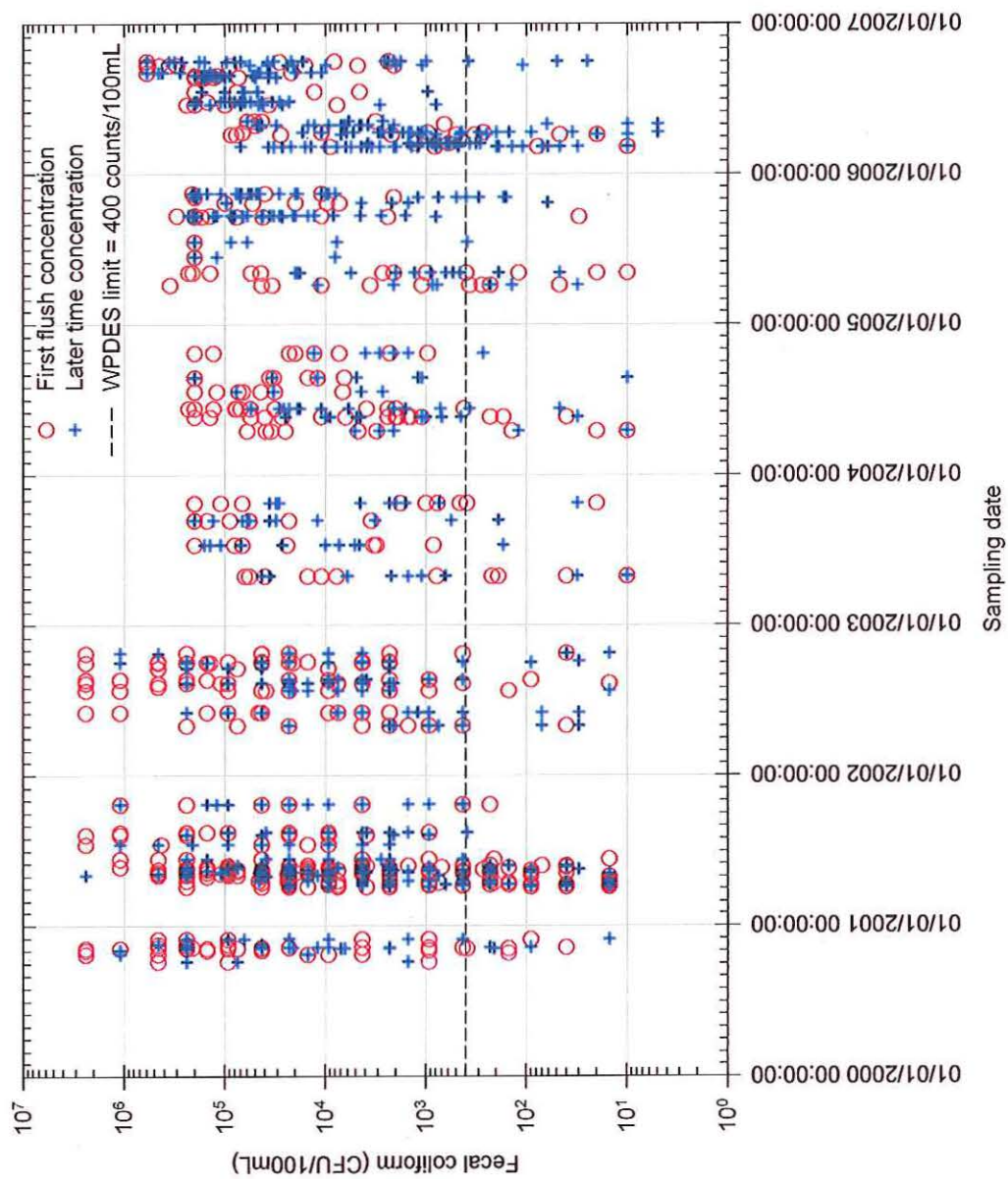


Figure A - 12. First flush and later-time concentrations of FC in stormwater.

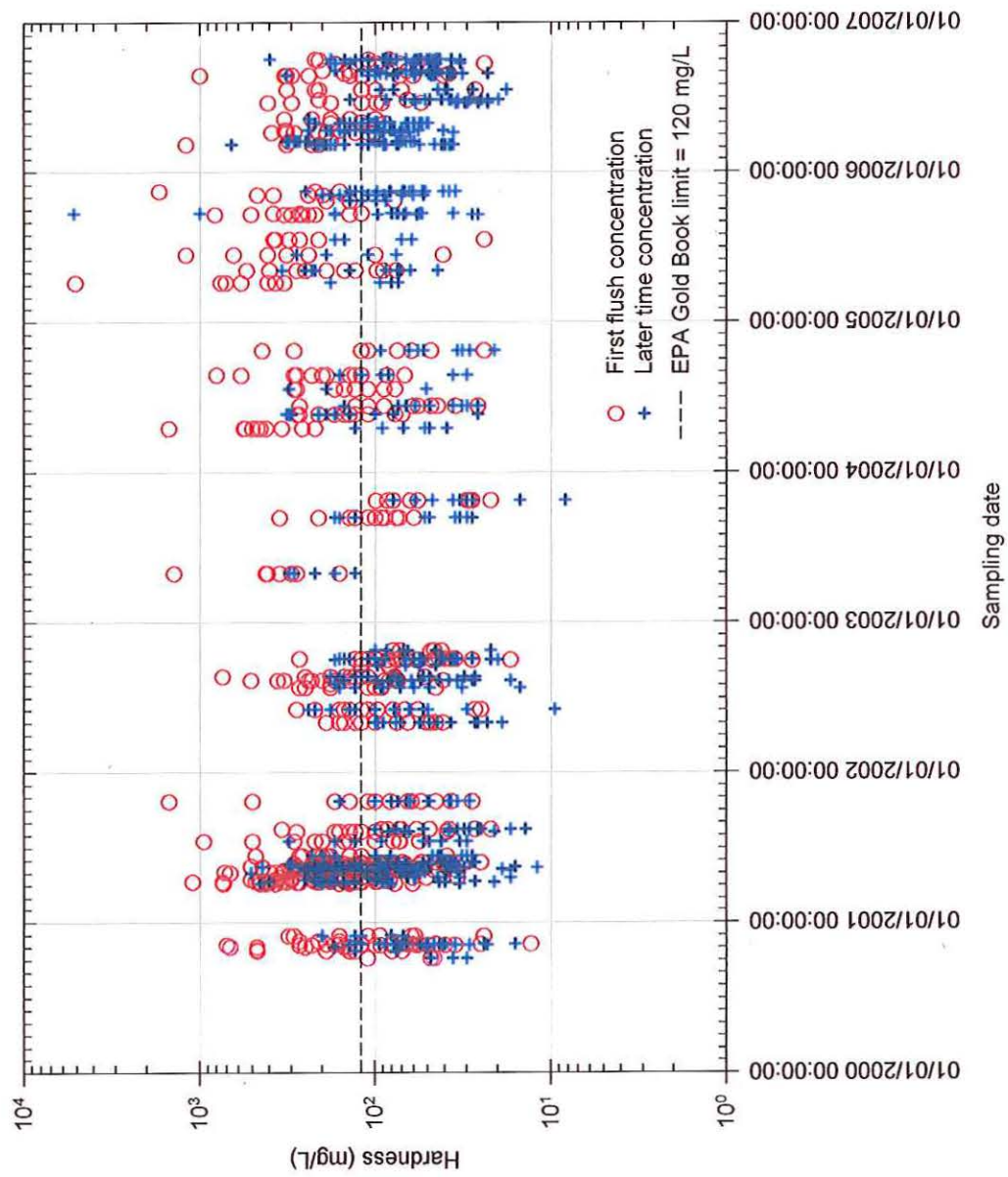


Figure A - 13. First flush and later-time concentrations of Hard in stormwater.

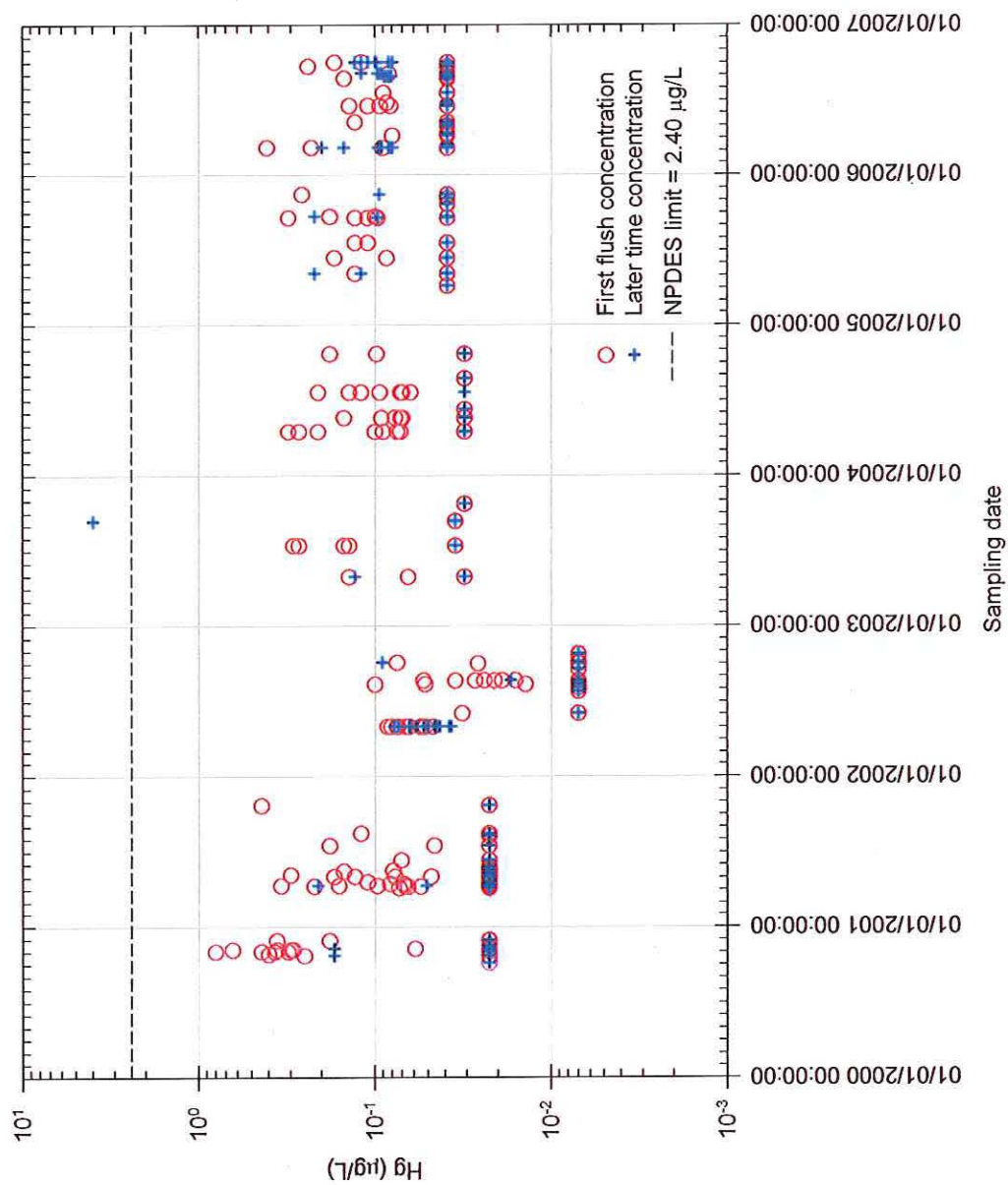


Figure A - 14. First flush and later-time concentrations of Hg in stormwater.

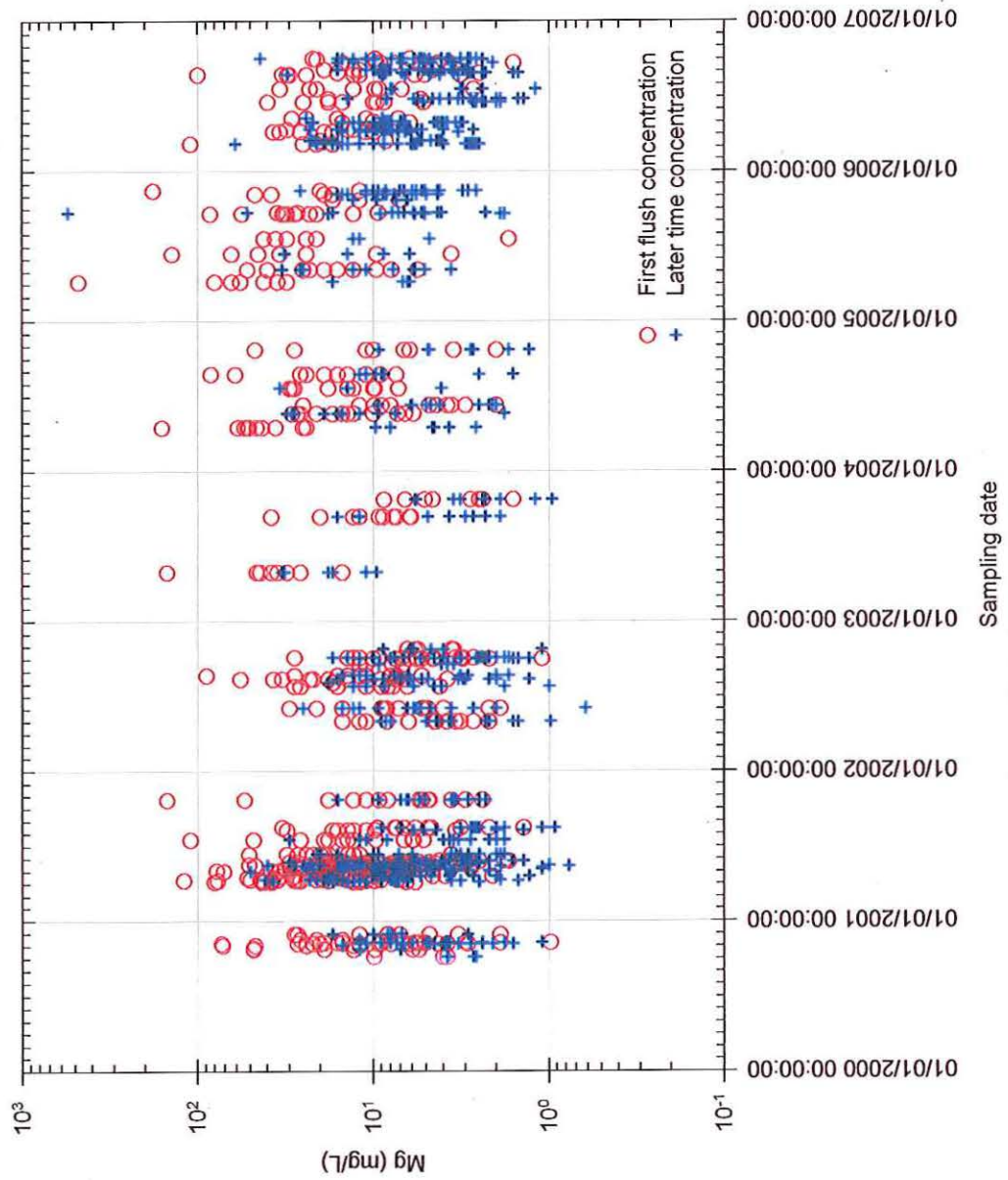


Figure A - 15. First flush and later-time concentrations of Mg in stormwater.

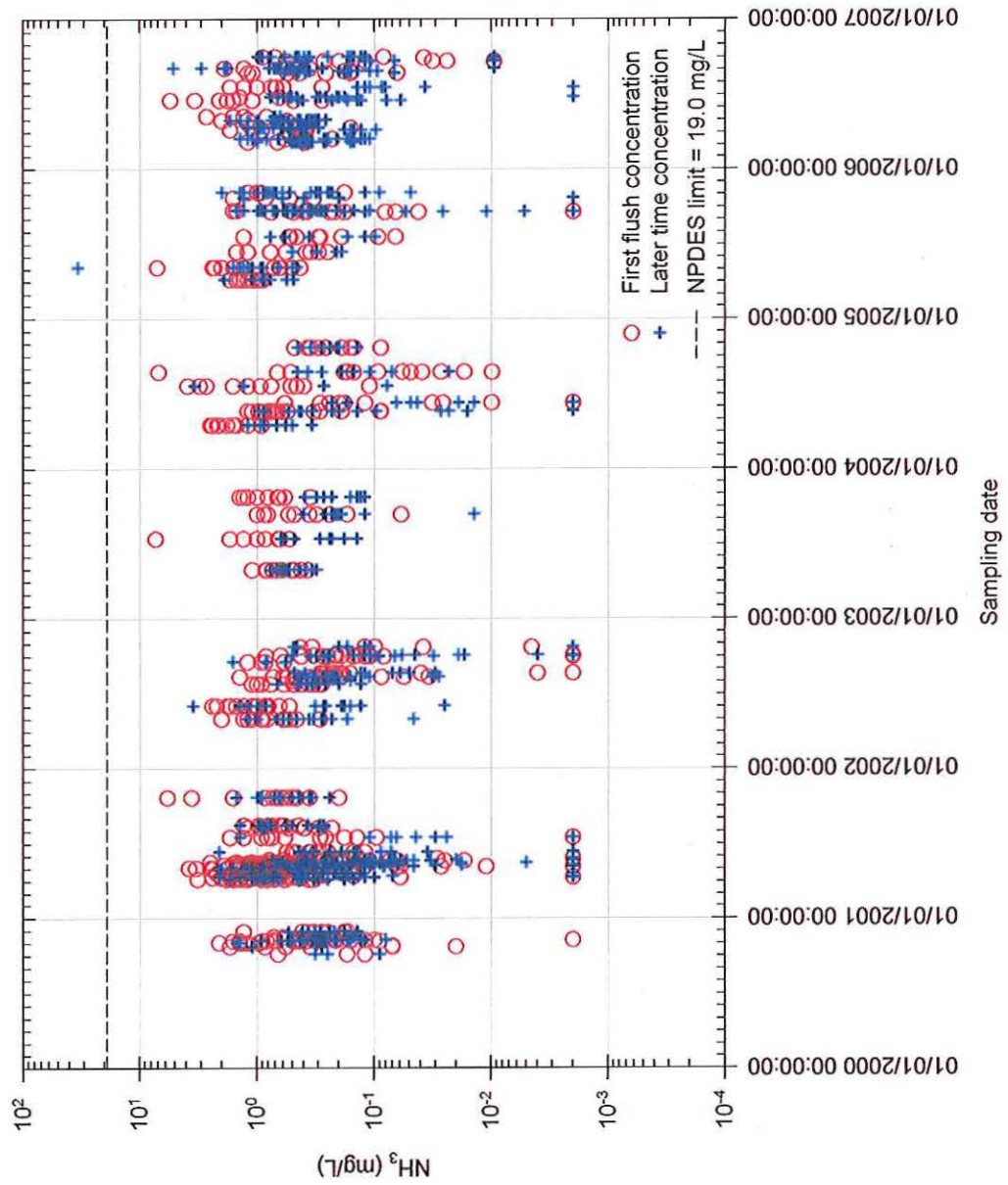


Figure A - 16. First flush and later-time concentrations of NH_3 in stormwater.

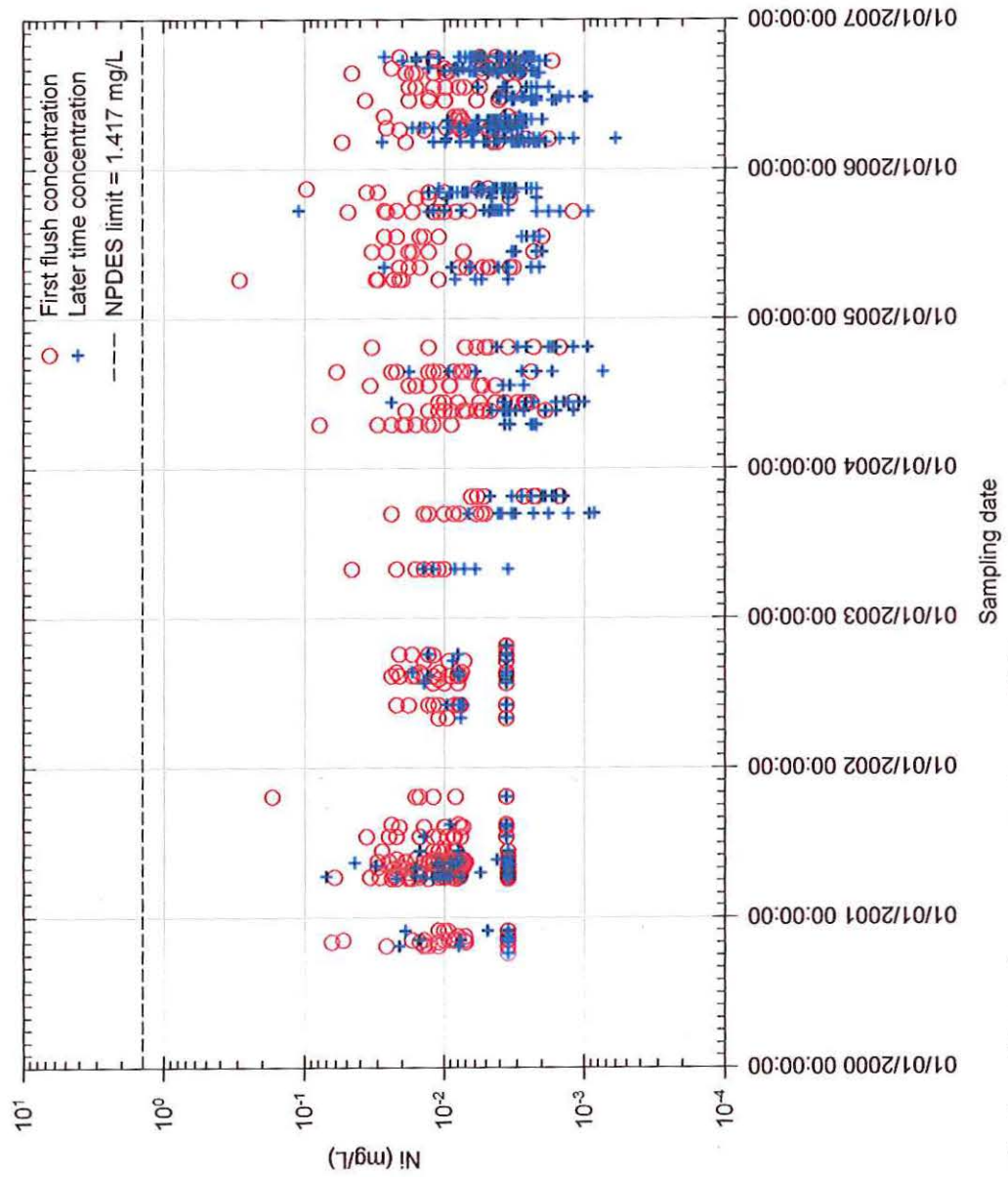


Figure A - 17. First flush and later-time concentrations of Ni in stormwater.

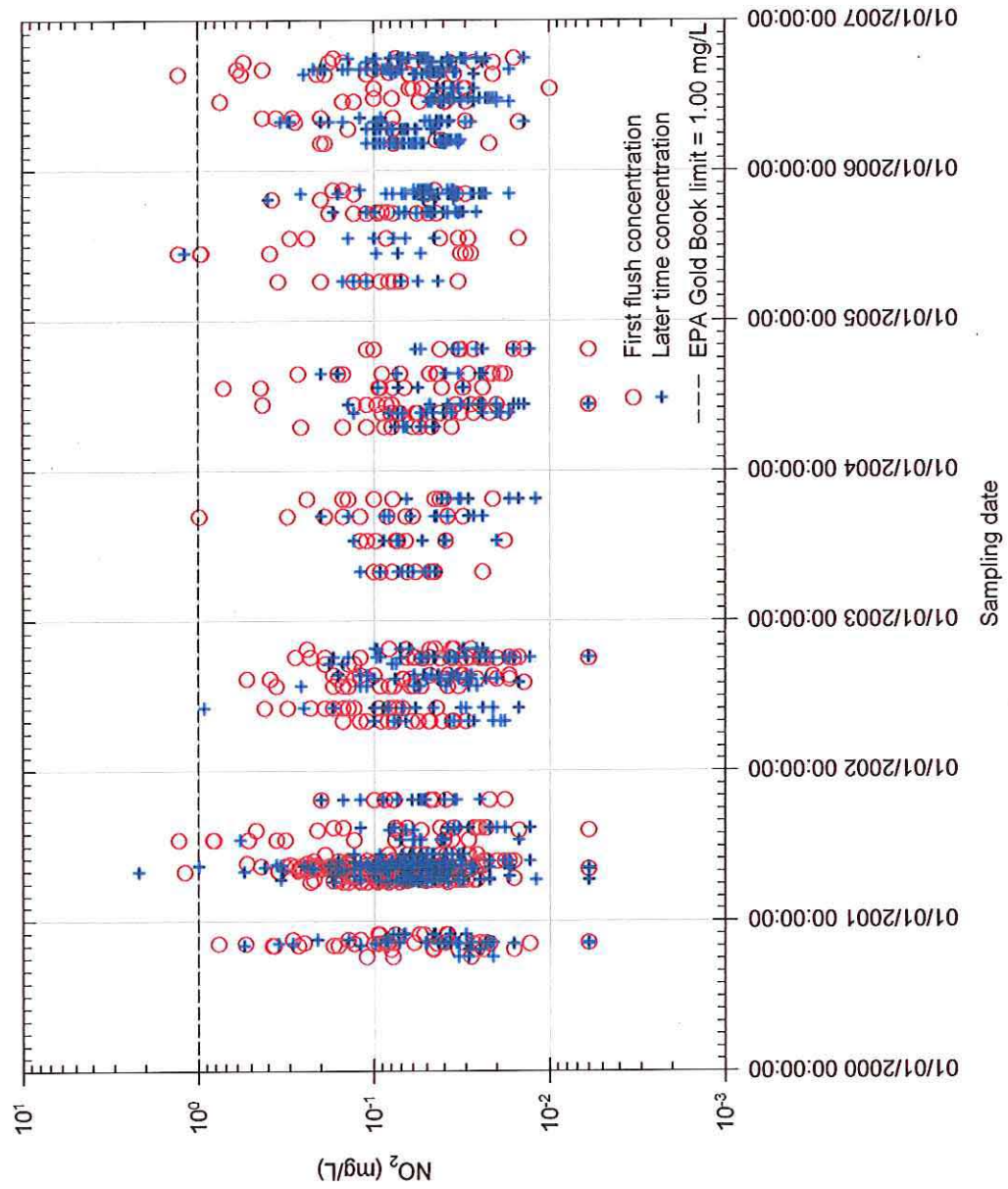


Figure A - 18. First flush and later-time concentrations of NO_2 in stormwater.

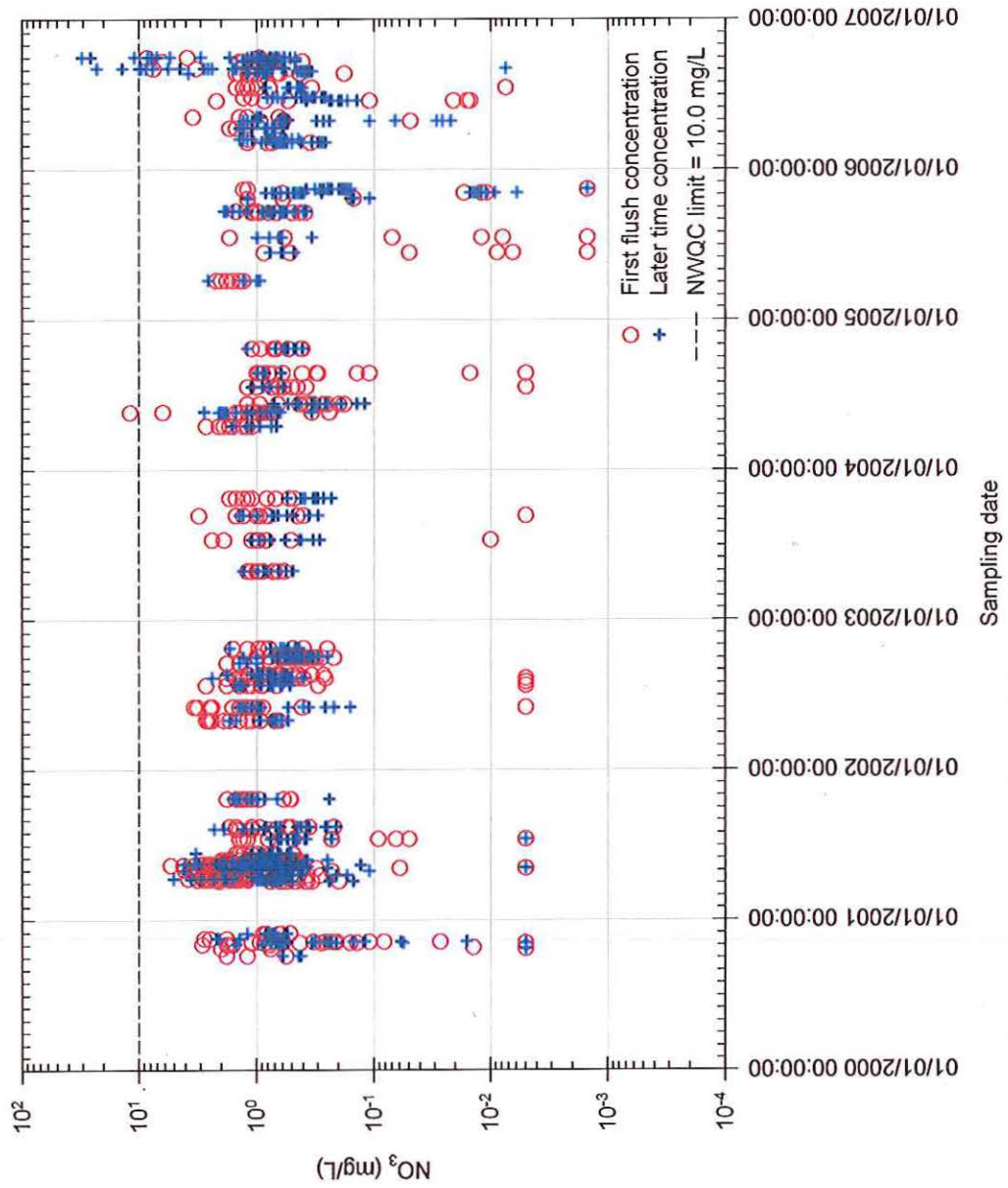


Figure A - 19. First flush and later-time concentrations of NO_3 in stormwater.

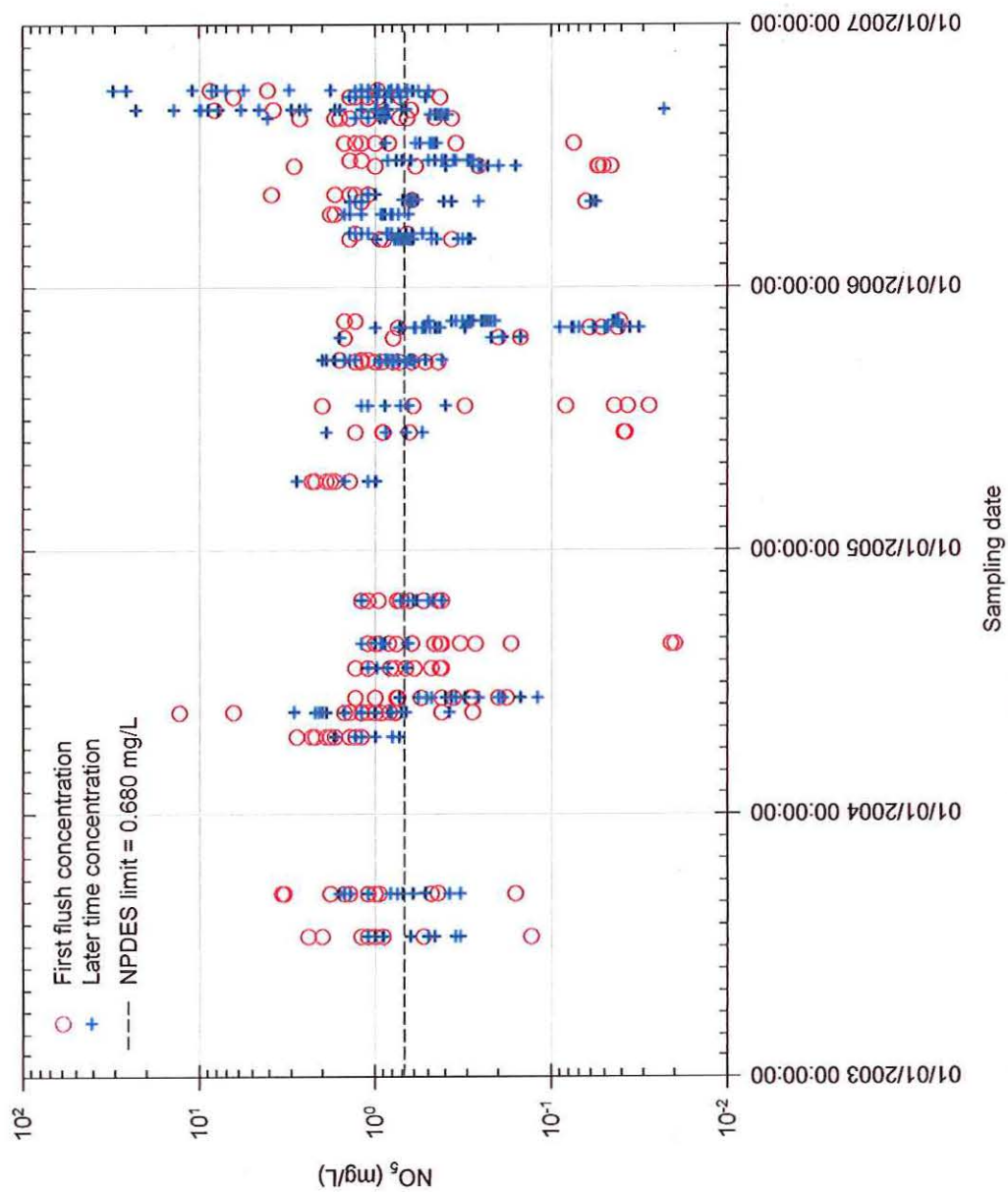


Figure A - 20. First flush and later-time concentrations of NO_3^- in stormwater.

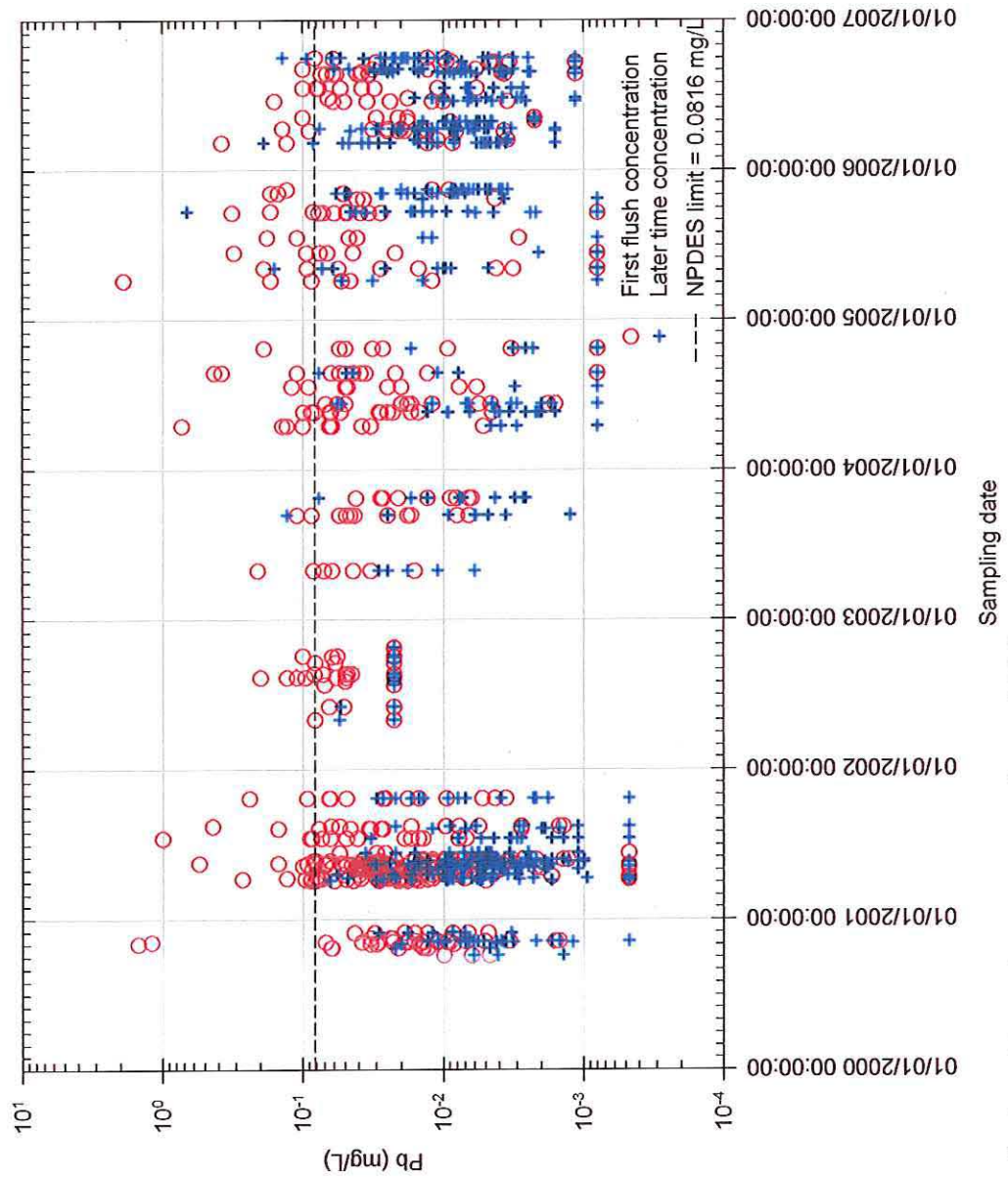


Figure A - 21. First flush and later-time concentrations of Pb in stormwater.

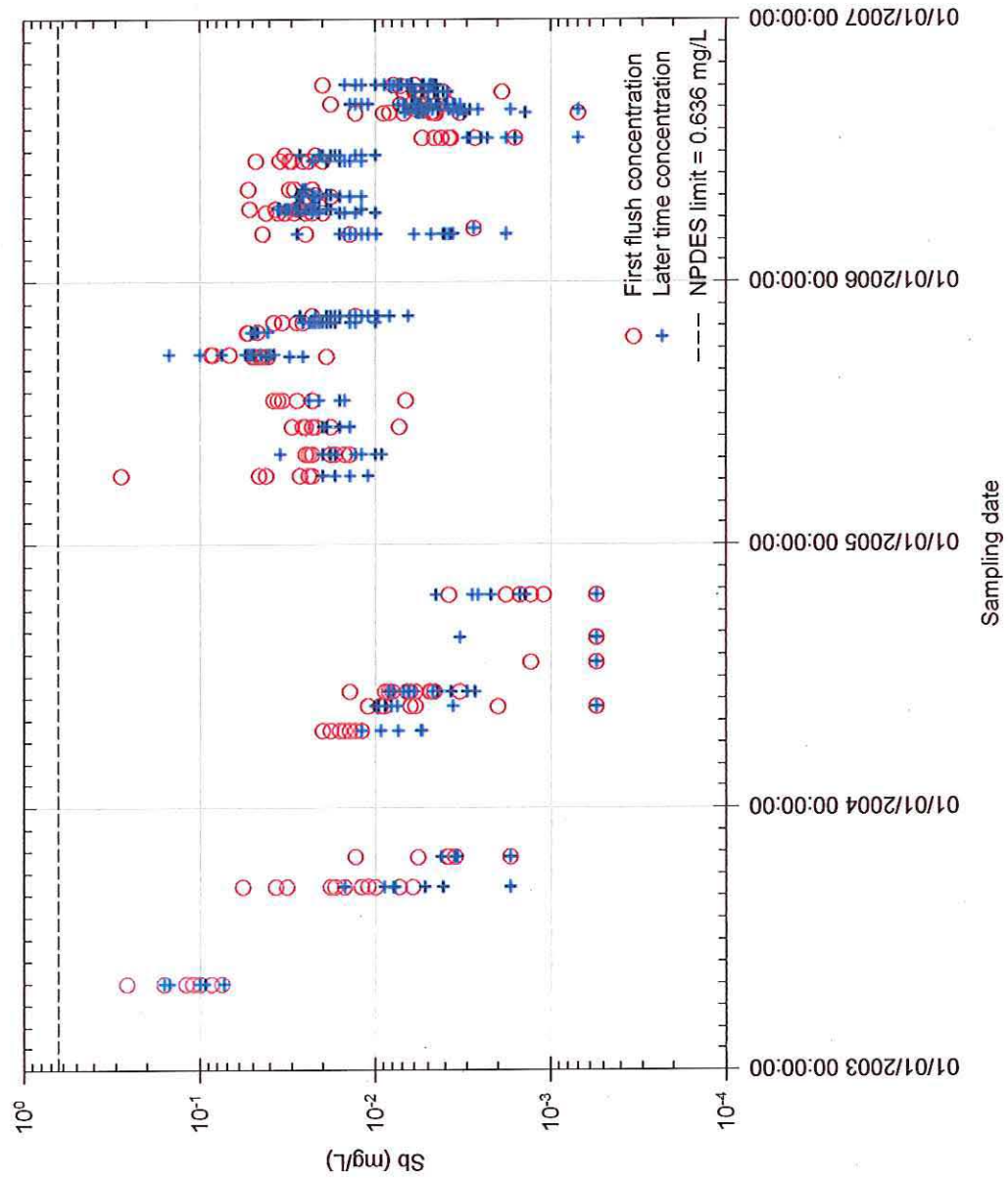


Figure A - 22. First flush and later-time concentrations of Sb in stormwater.

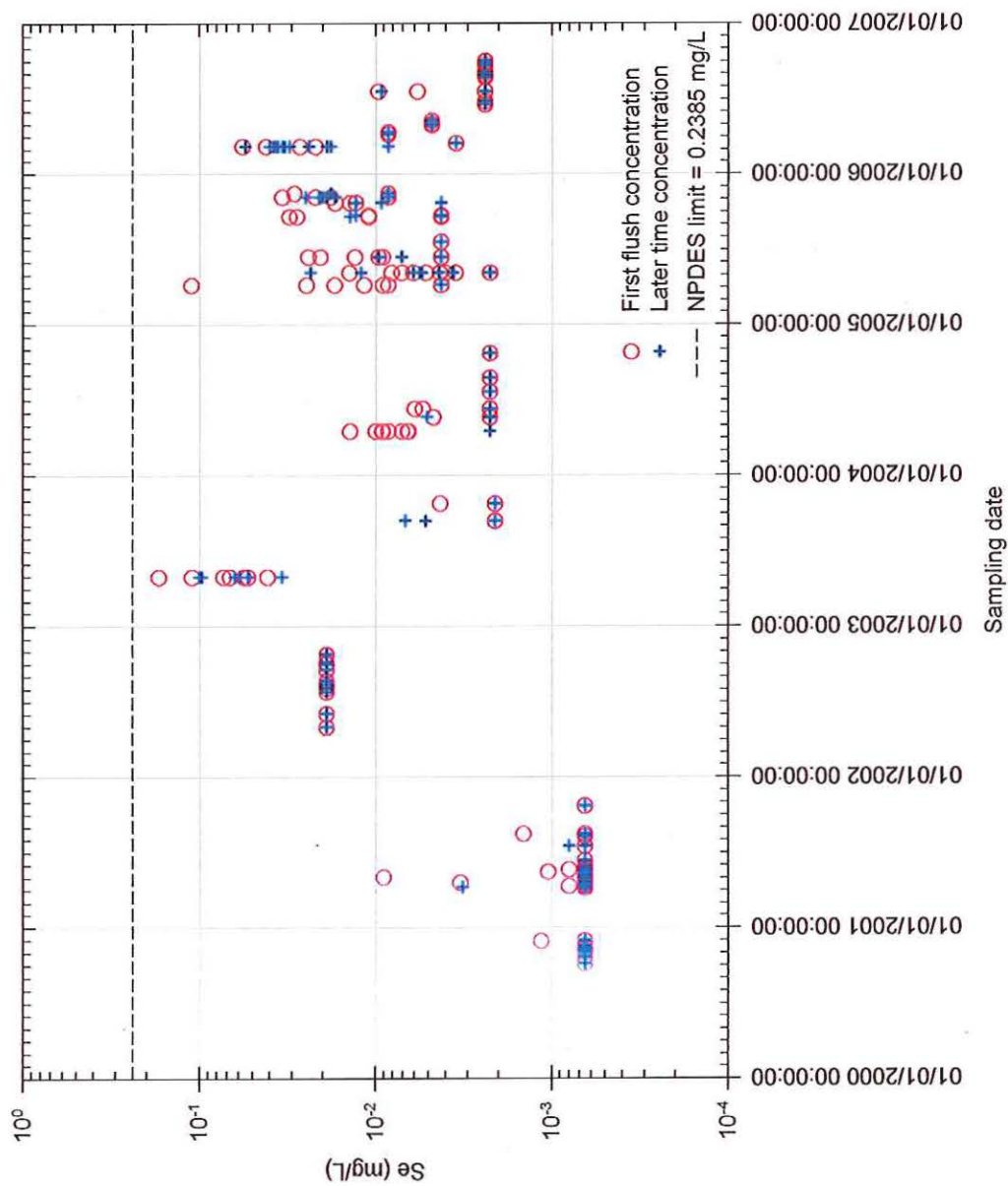


Figure A - 23. First flush and later-time concentrations of Se in stormwater.

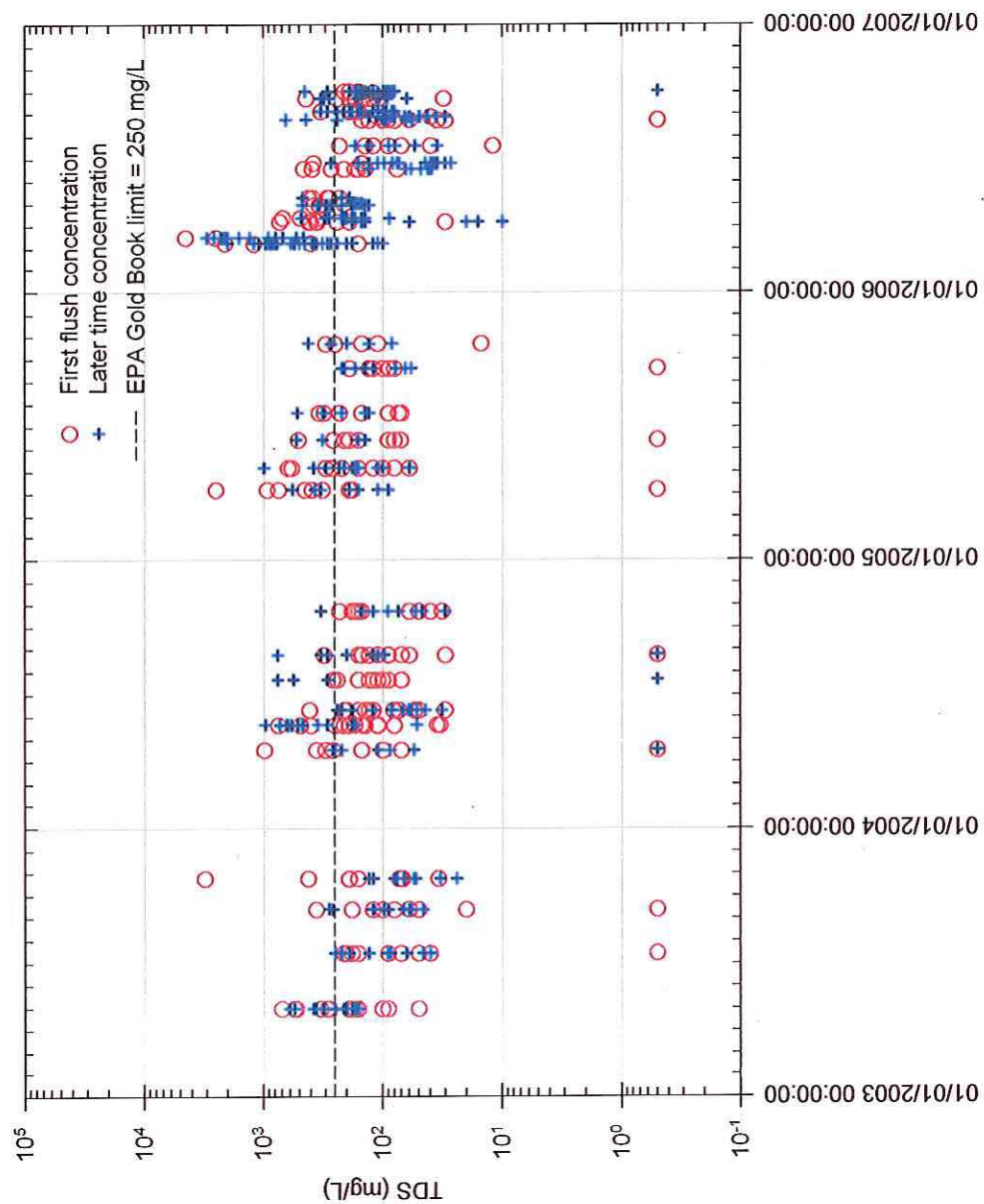


Figure A - 24. First flush and later-time concentrations of TDS in stormwater.

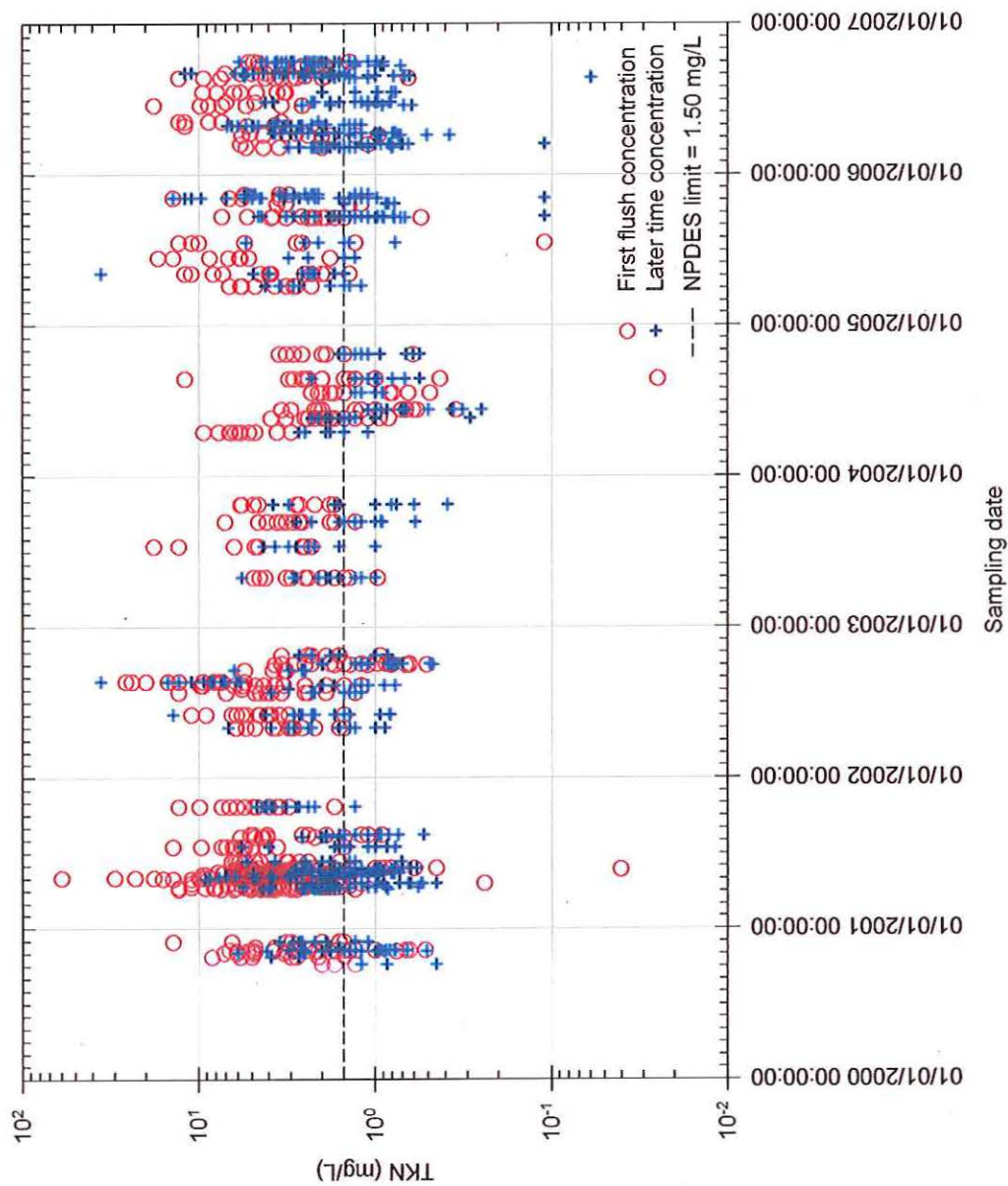


Figure A - 25. First flush and later-time concentrations of TKN in stormwater.

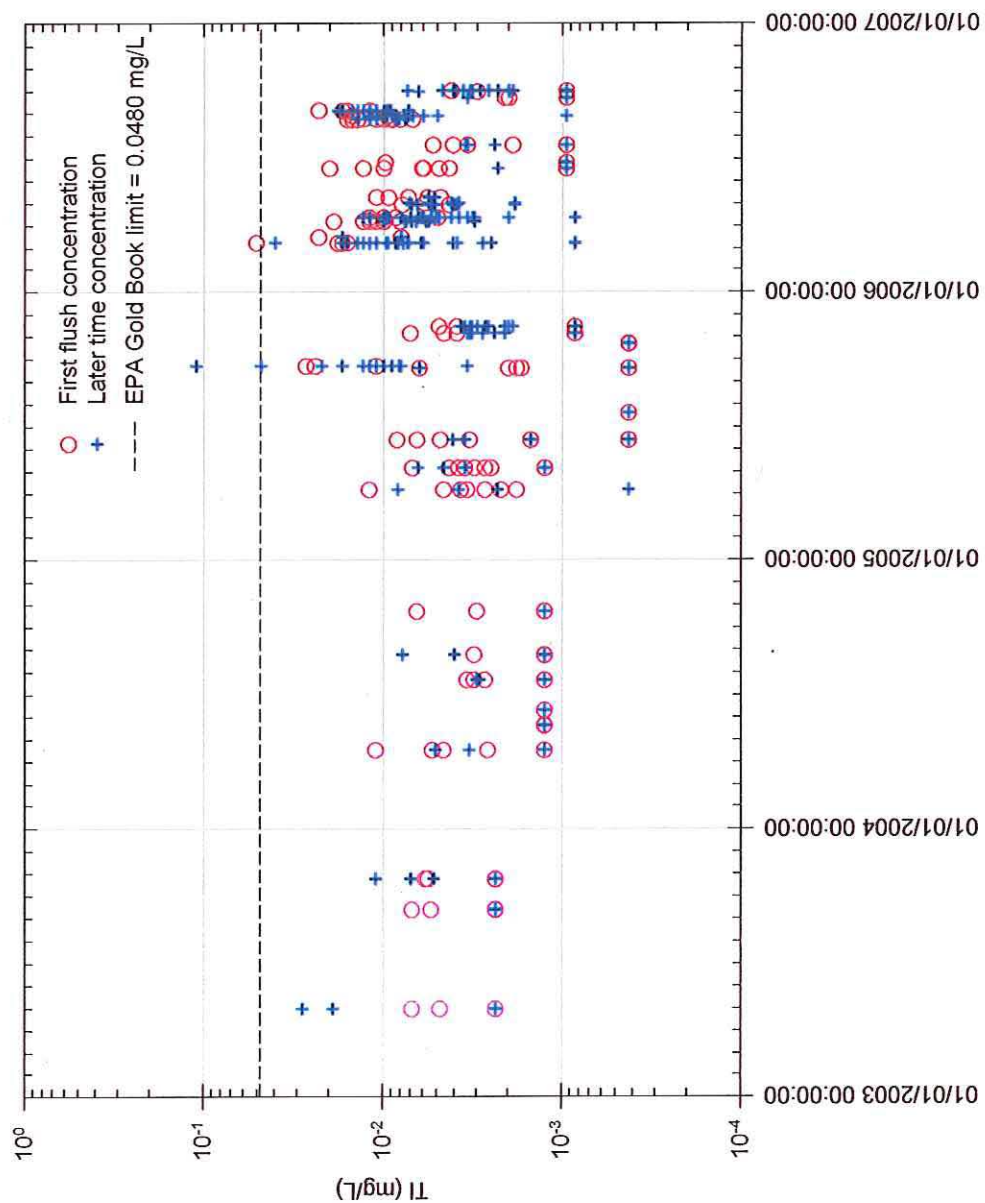


Figure A - 26. First flush and later-time concentrations of Tl in stormwater.

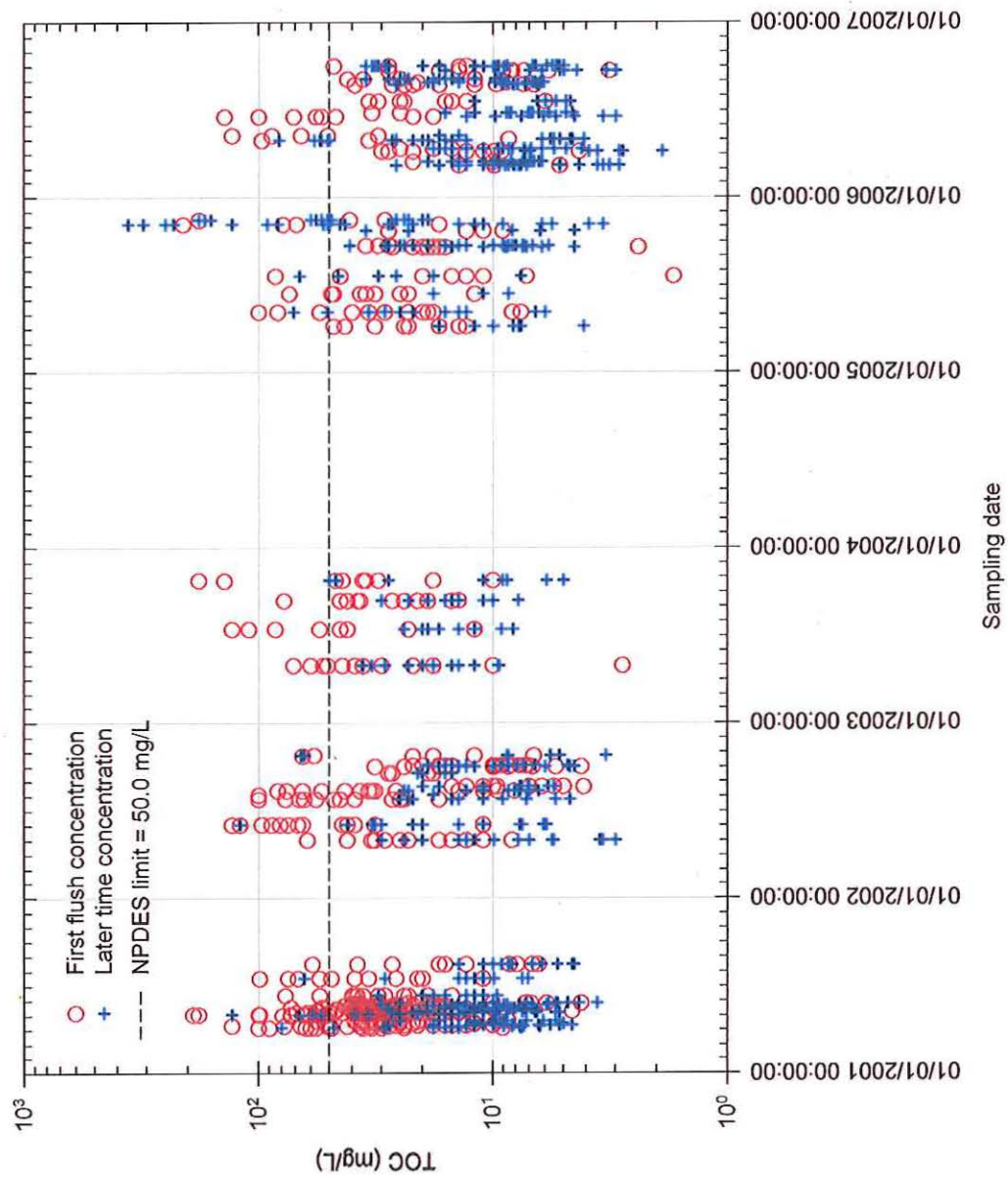


Figure A - 27. First flush and later-time concentrations of TOC in stormwater.

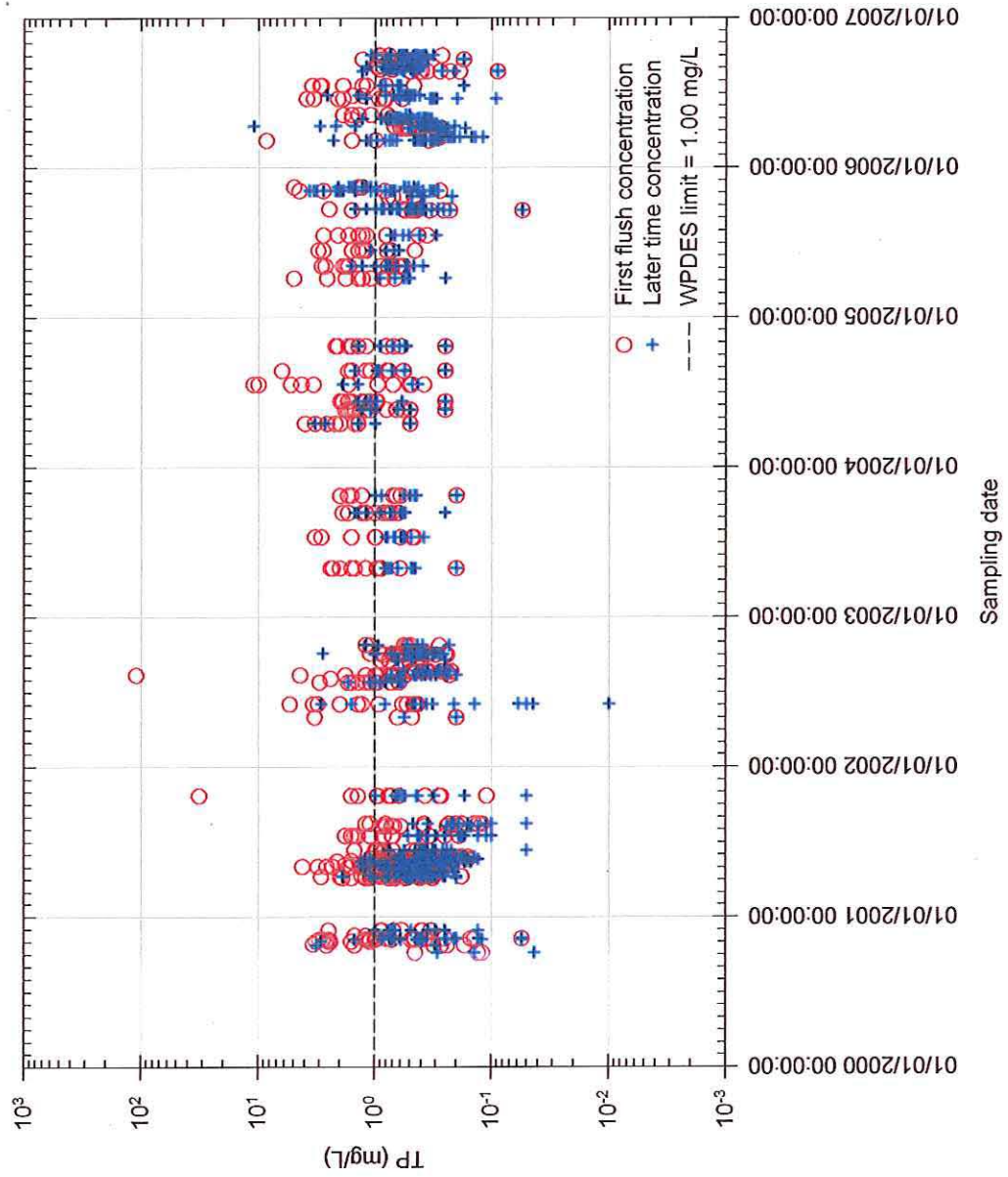


Figure A - 28. First flush and later-time concentrations of TP in stormwater.

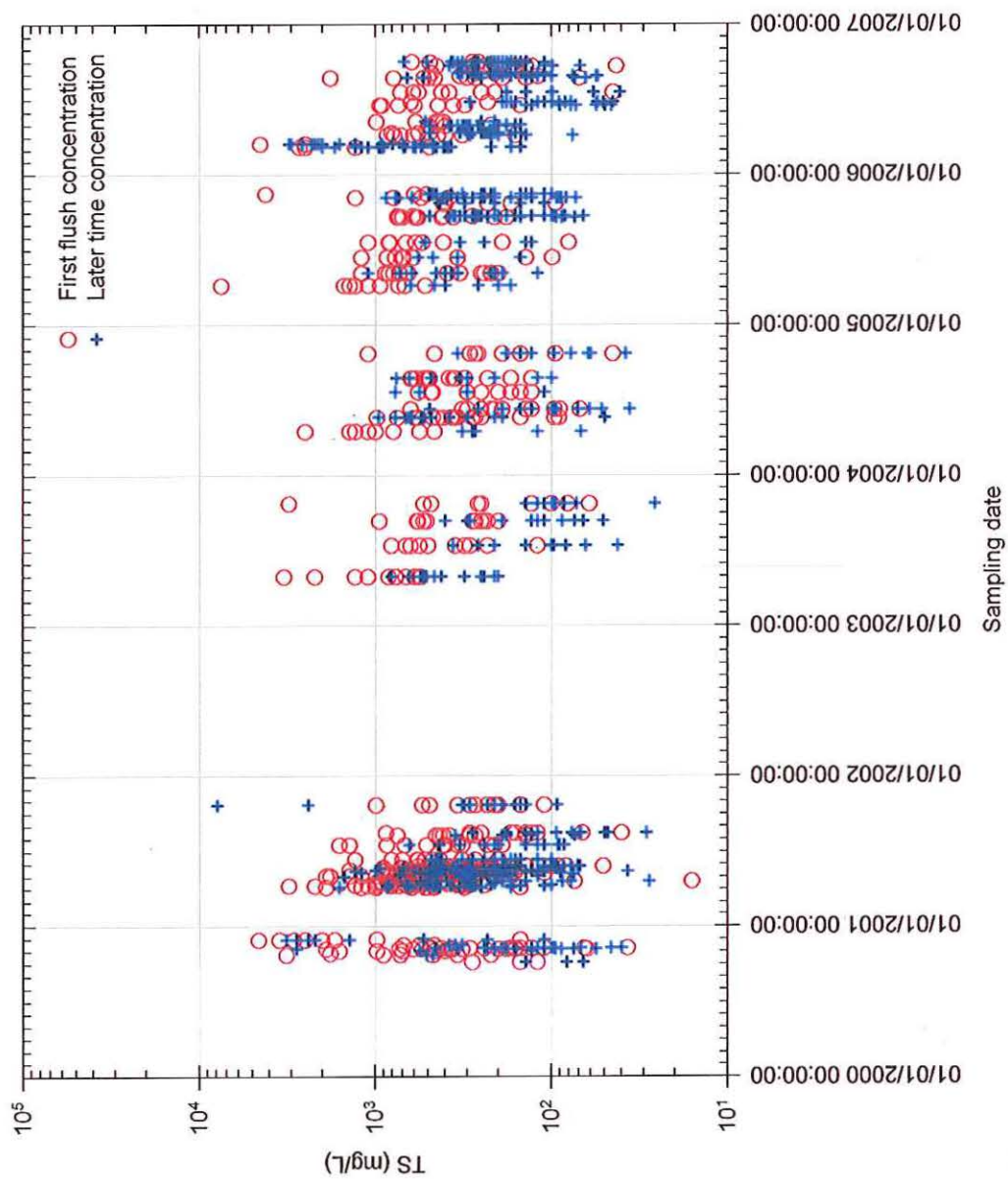


Figure A - 29. First flush and later-time concentrations of TS in stormwater.

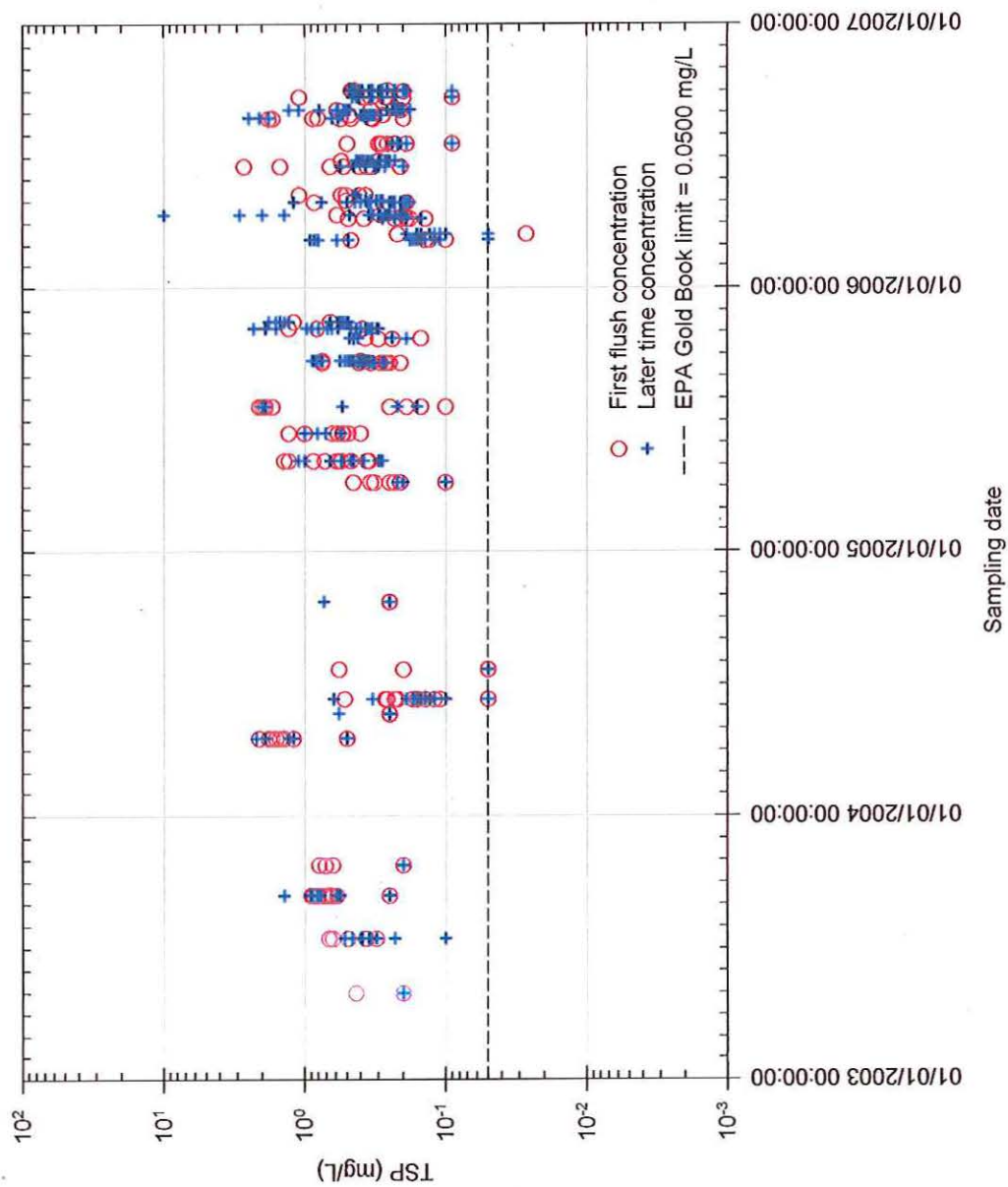


Figure A - 30. First flush and later-time concentrations of TSP in stormwater.

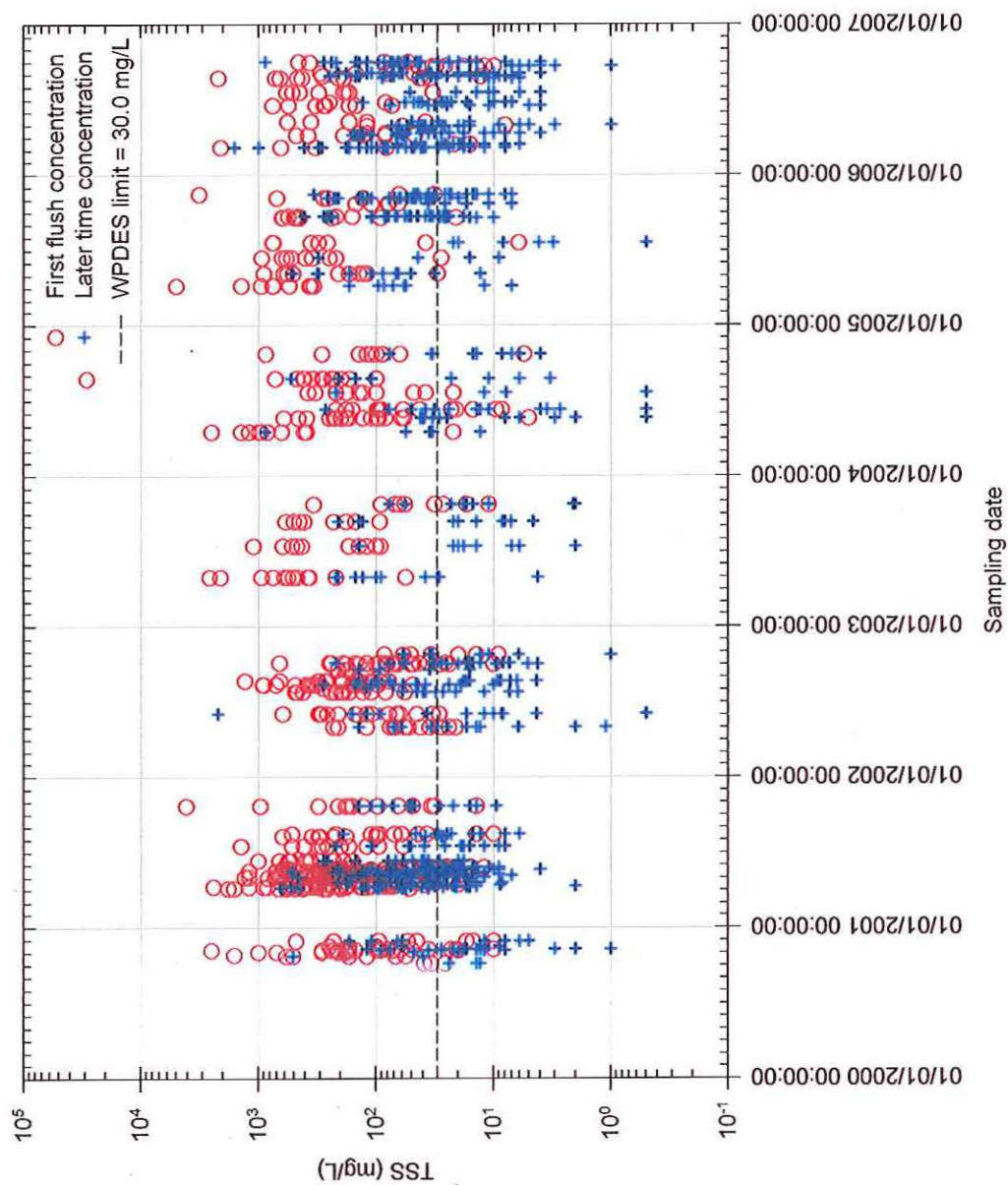


Figure A - 31. First flush and later-time concentrations of TSS in stormwater.

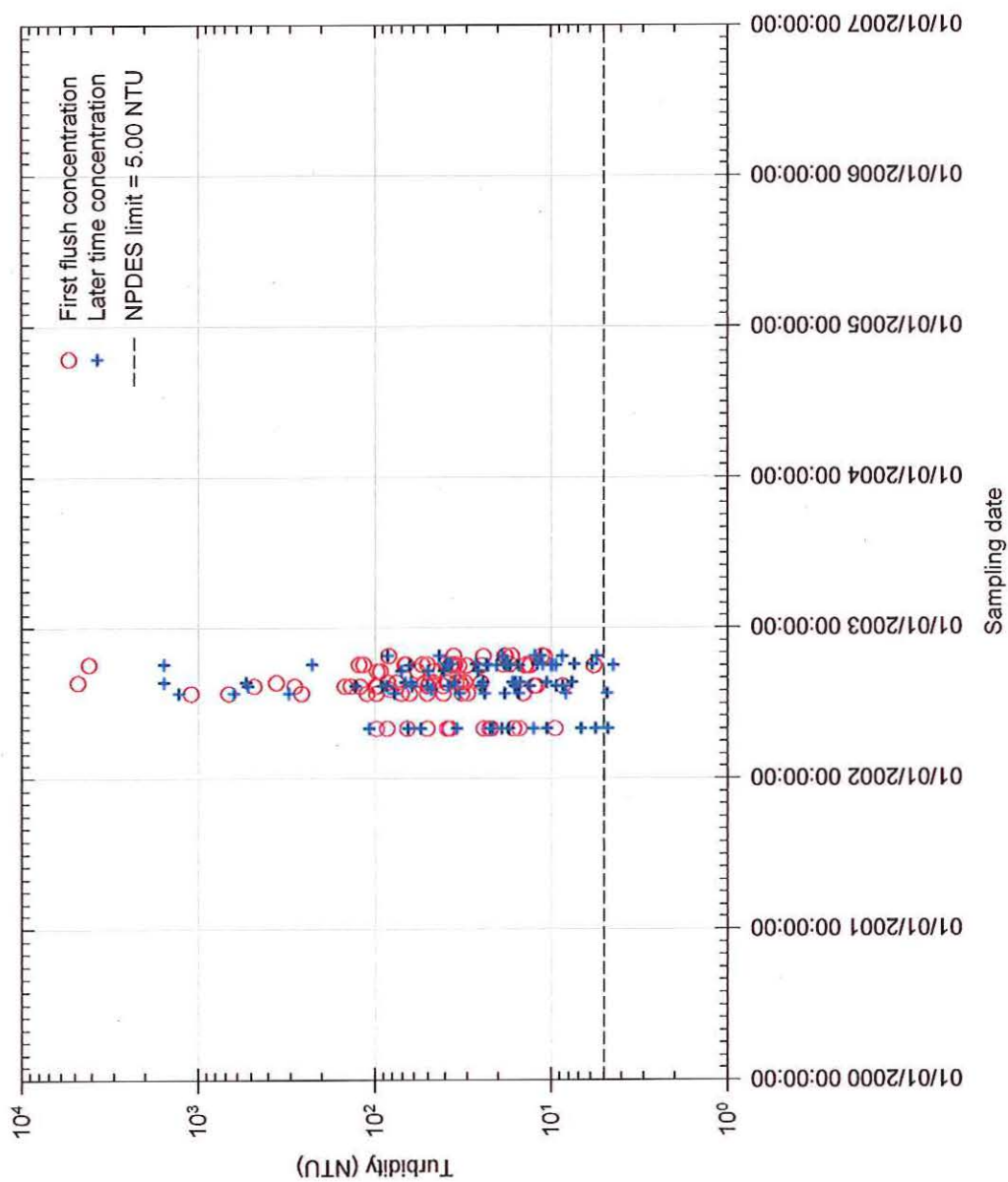


Figure A - 32. First flush and later-time concentrations of turbidity in stormwater.

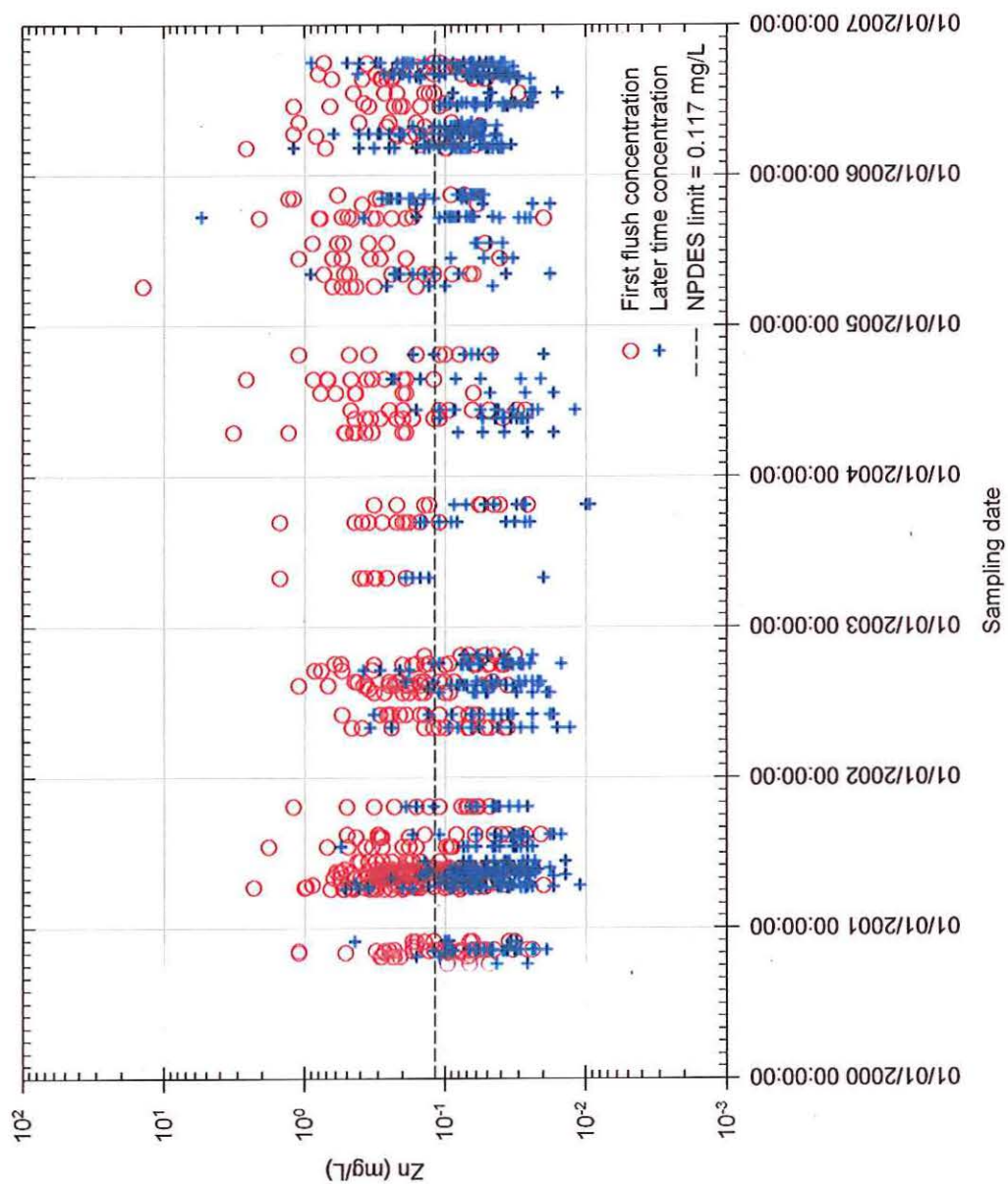


Figure A - 33. First flush and later-time concentrations of Zn in stormwater.

Appendix B Pollutant Concentrations in Stormwater per Site

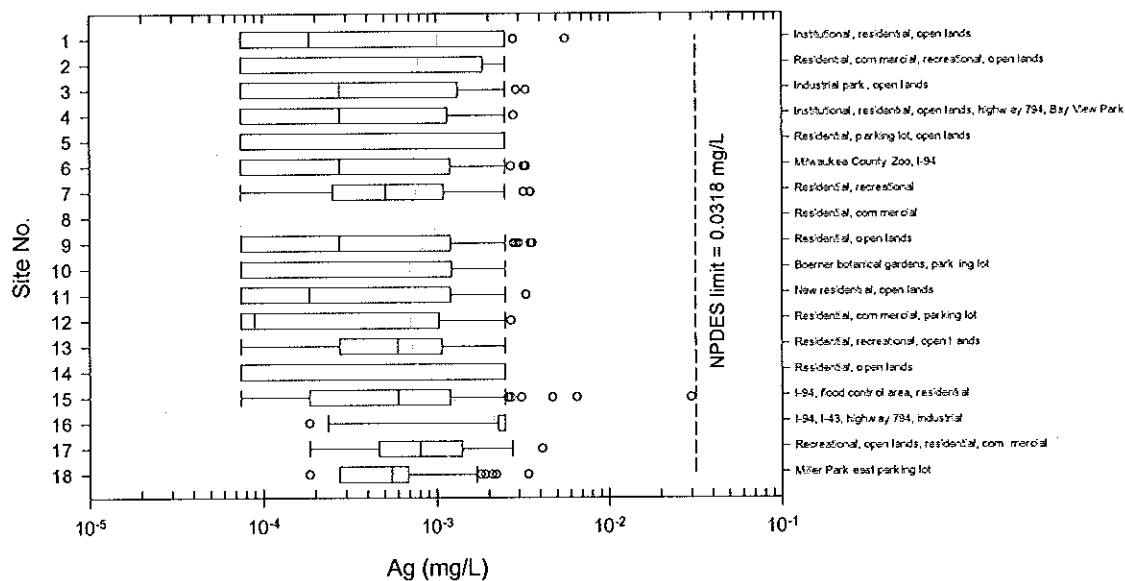


Figure B - 1. Box plots of Ag in stormwater per site.

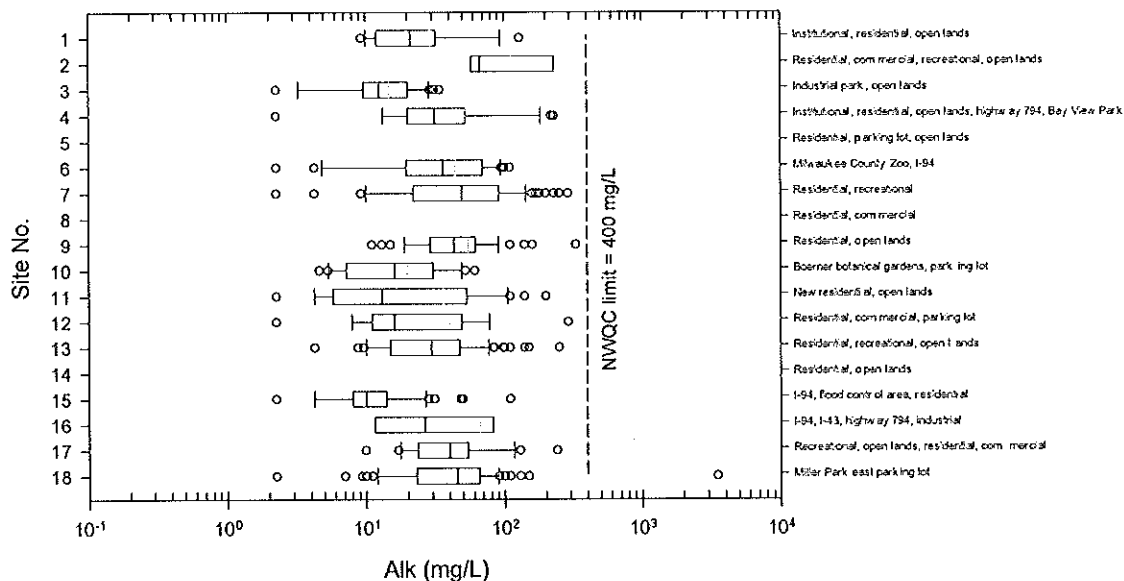


Figure B - 2. Box plots of Alk in stormwater per site.

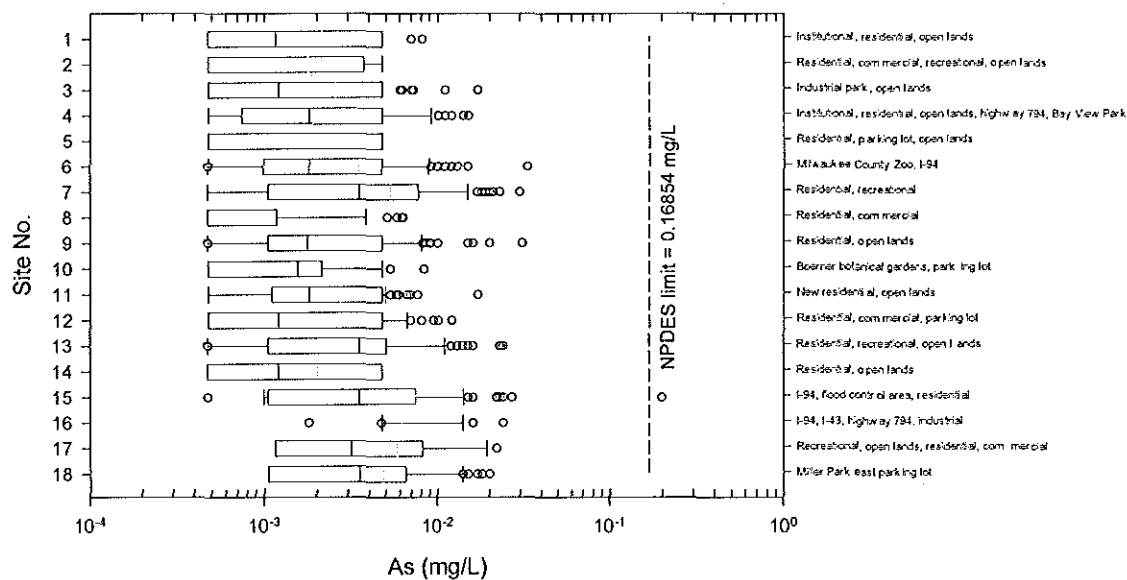


Figure B - 3. Box plots of As in stormwater per site.

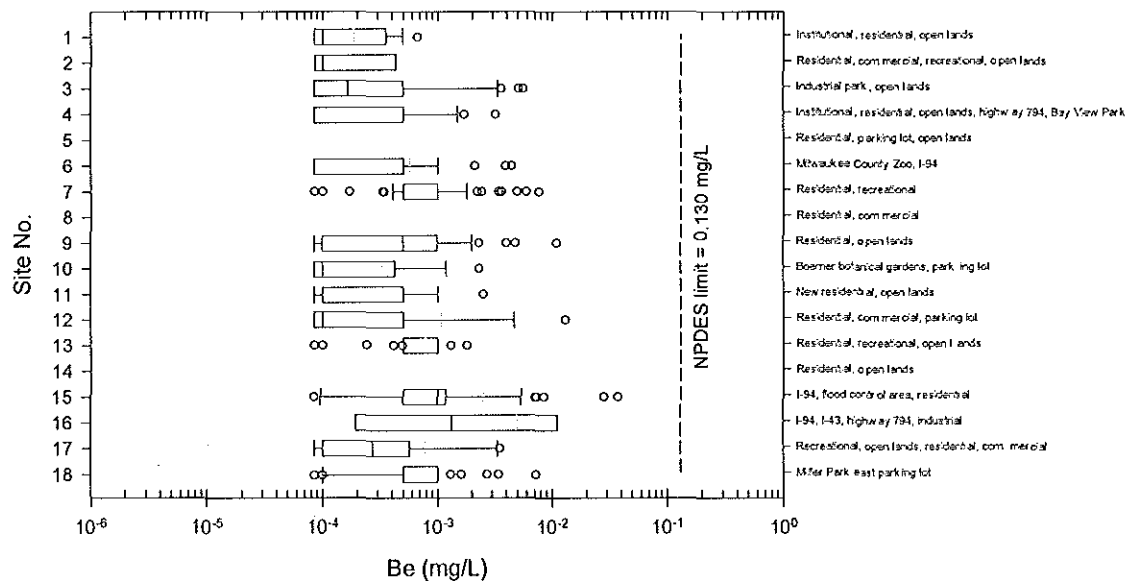


Figure B - 4. Box plots of Be in stormwater per site.

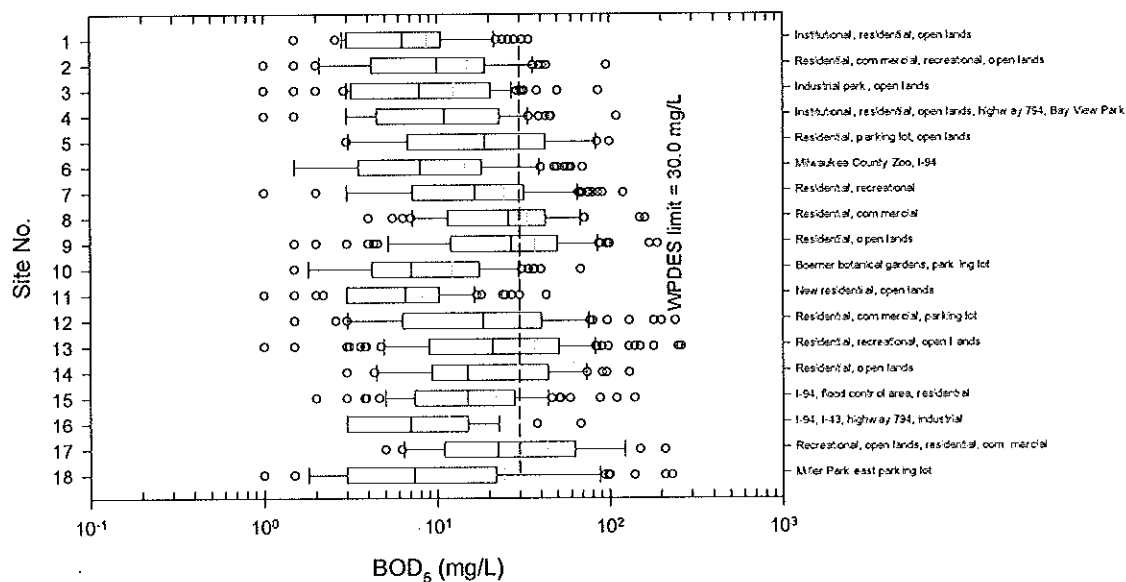


Figure B - 5. Box plots of BOD_5 in stormwater per site.

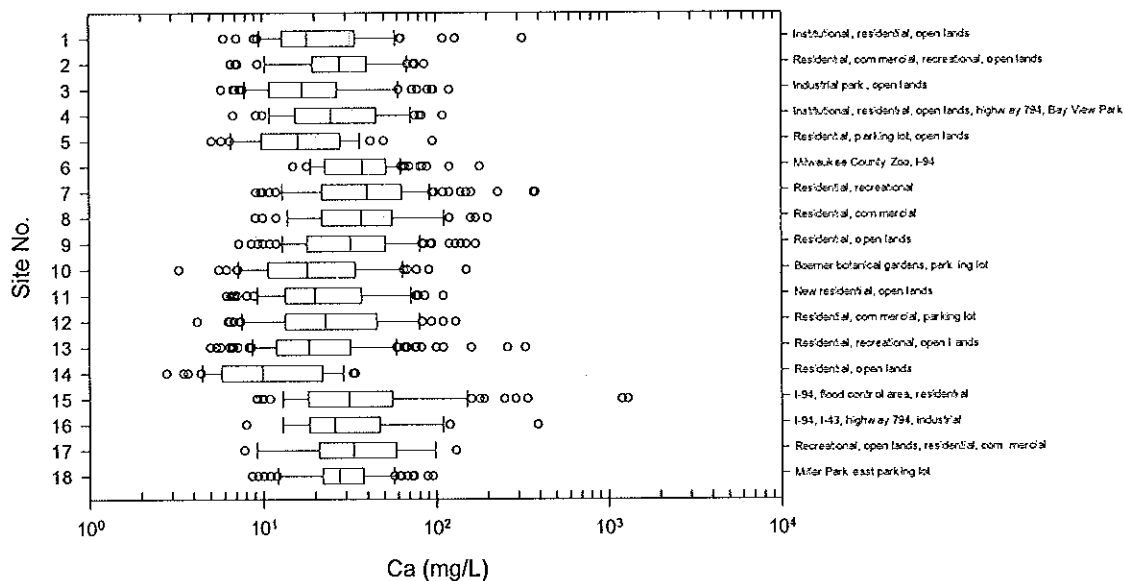


Figure B - 6. Box plots of Ca in stormwater per site.

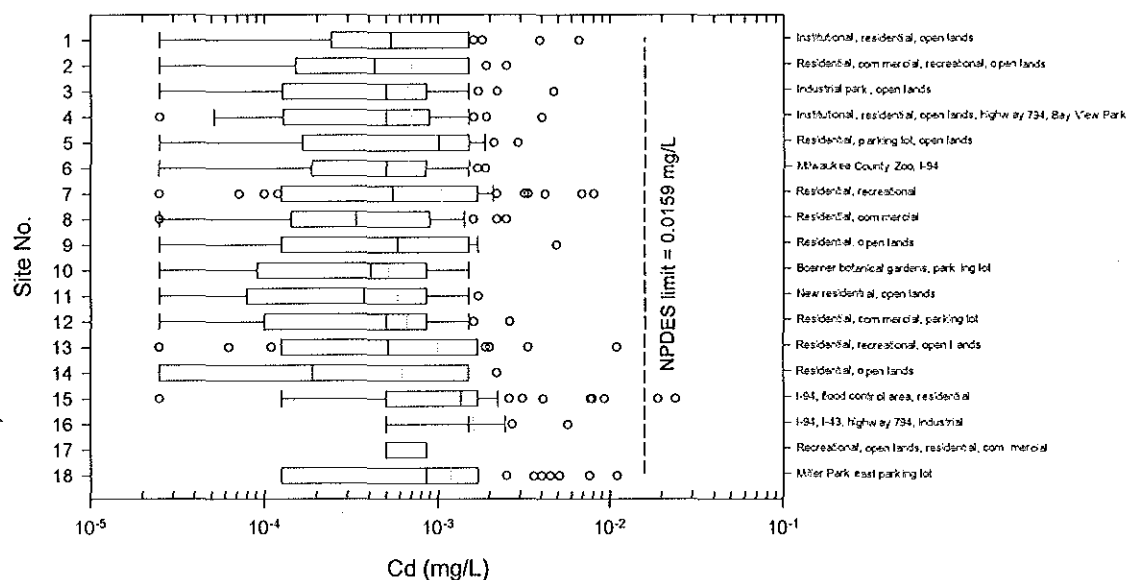


Figure B - 7. Box plots of Cd in stormwater per site.

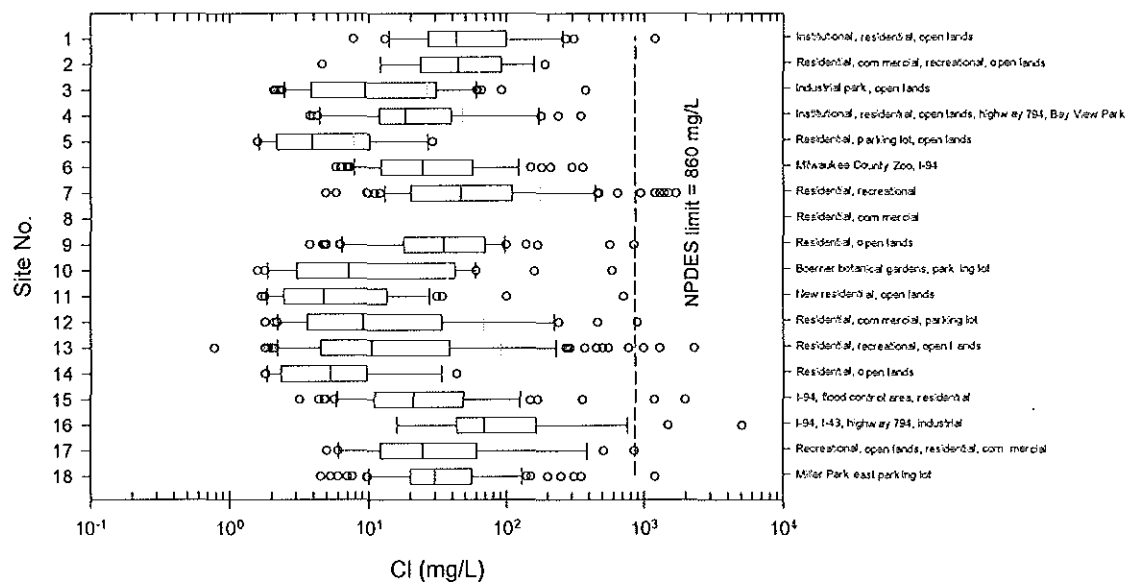


Figure B - 8. Box plots of Cl in stormwater per site.

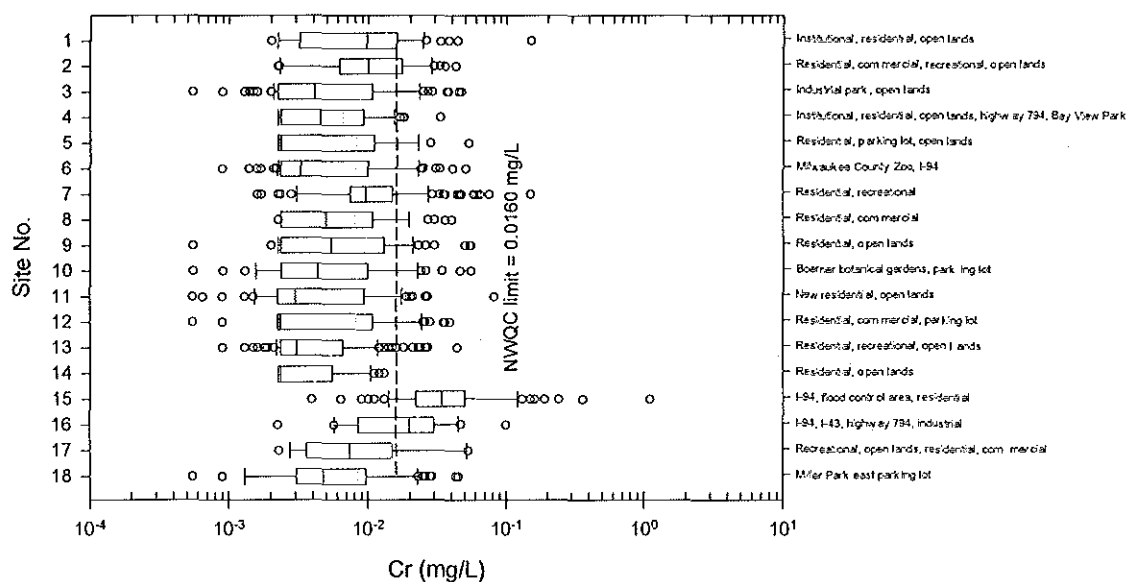


Figure B - 9. Box plots of Cr in stormwater per site.

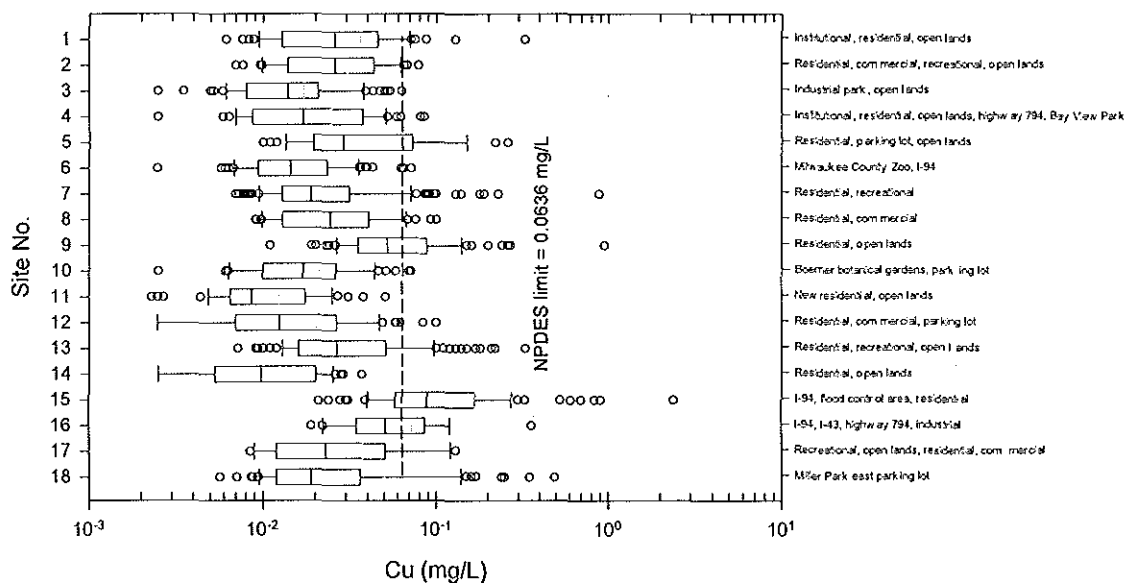


Figure B - 10. Box plots of Cu in stormwater per site.

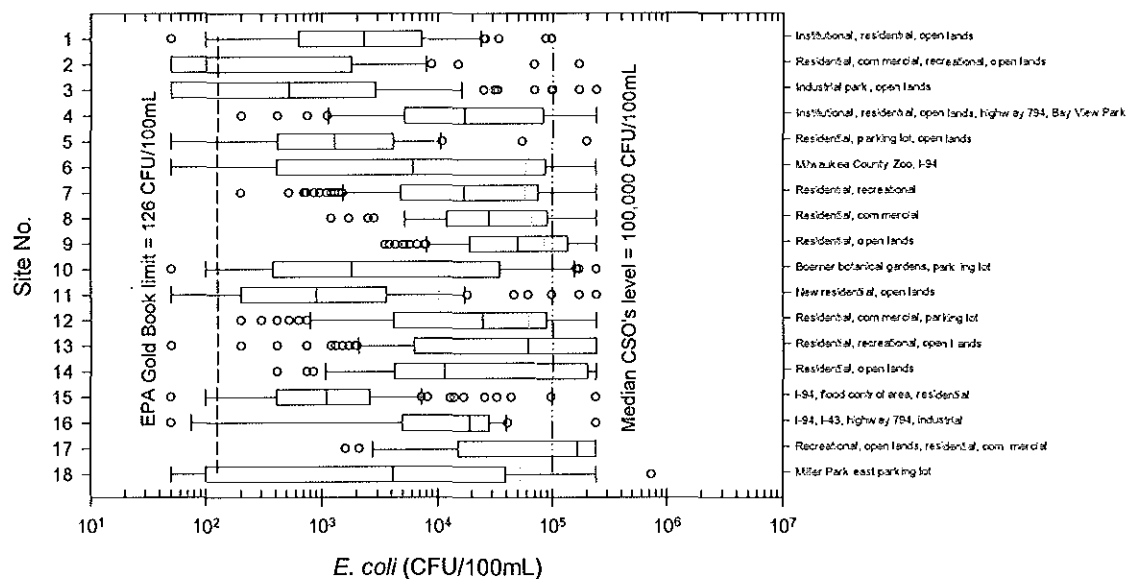


Figure B - 11. Box plots of EC in stormwater per site.

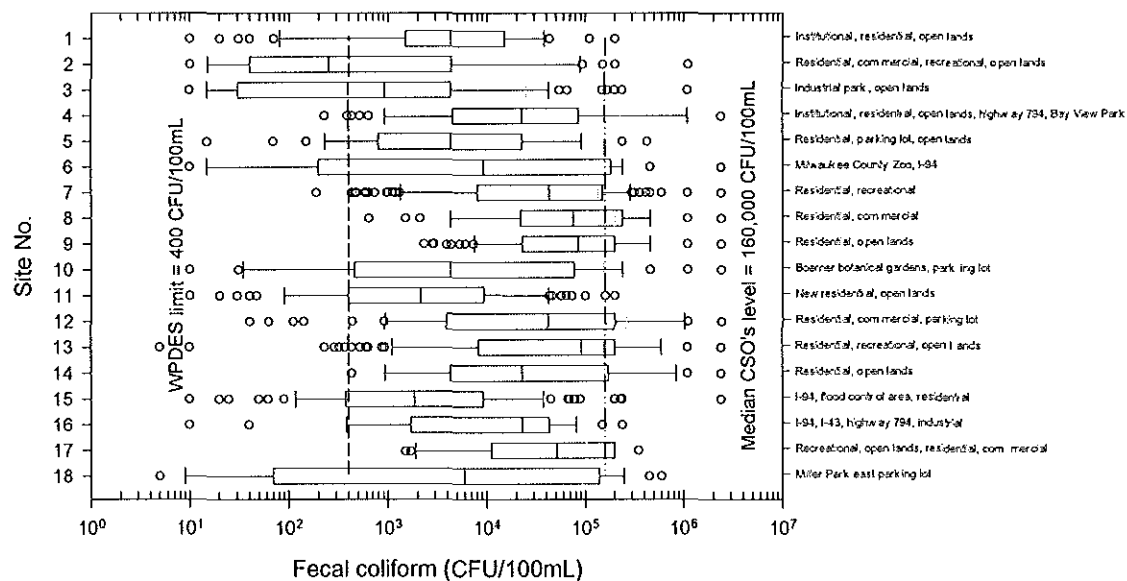


Figure B - 12. Box plots of FC in stormwater per site.

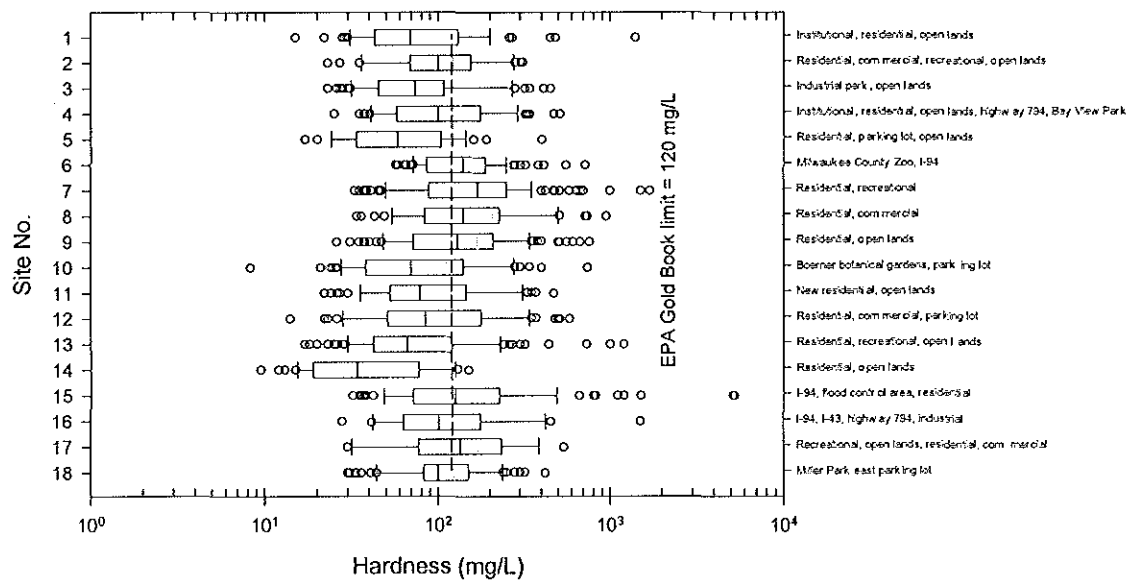


Figure B - 13. Box plots of Hard in stormwater per site.

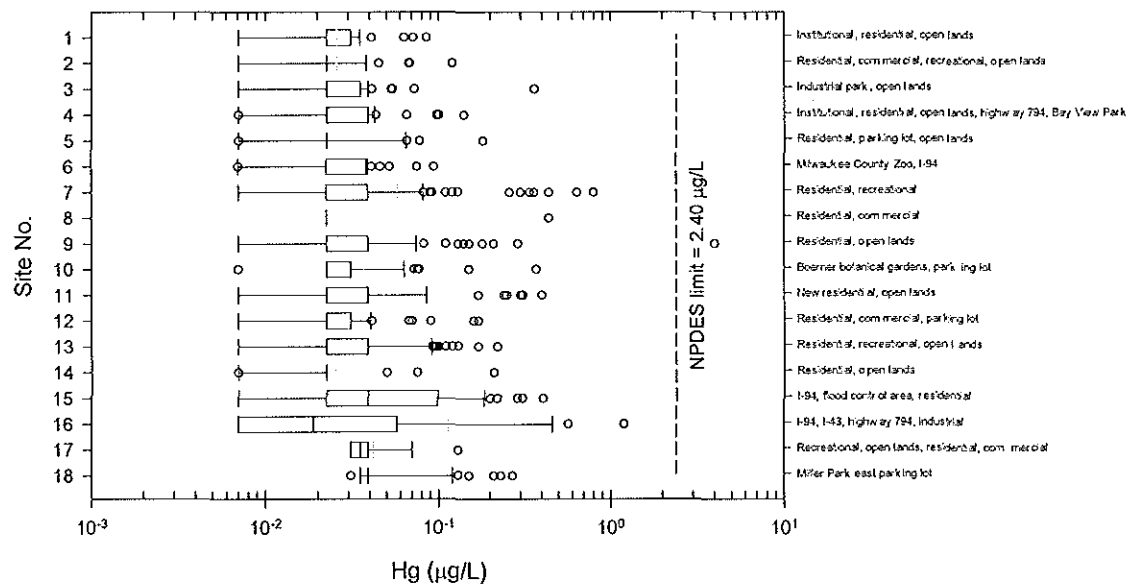


Figure B - 14. Box plots of Hg in stormwater per site.

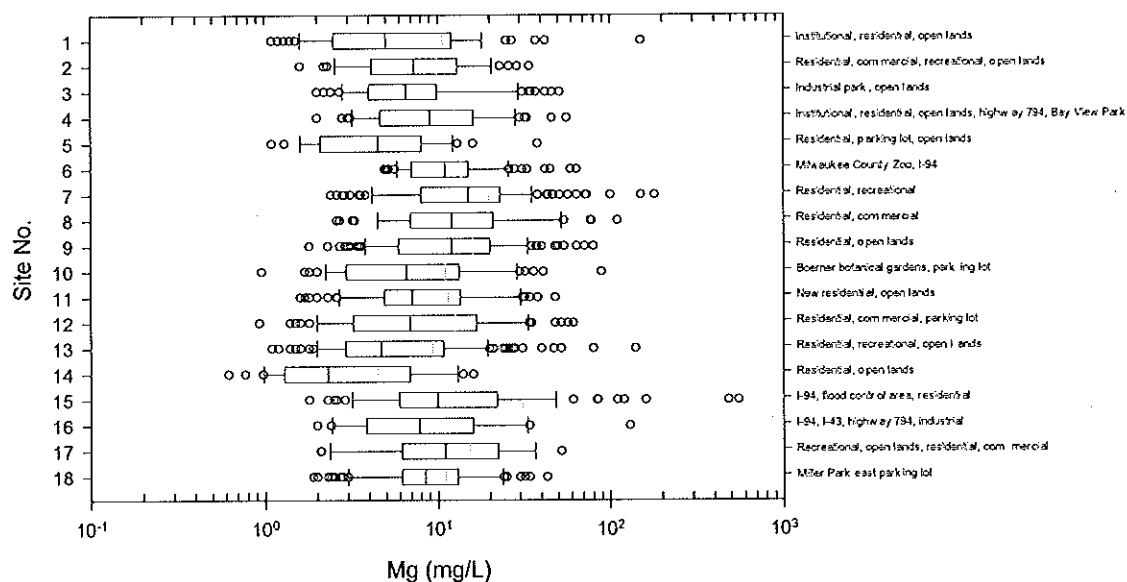
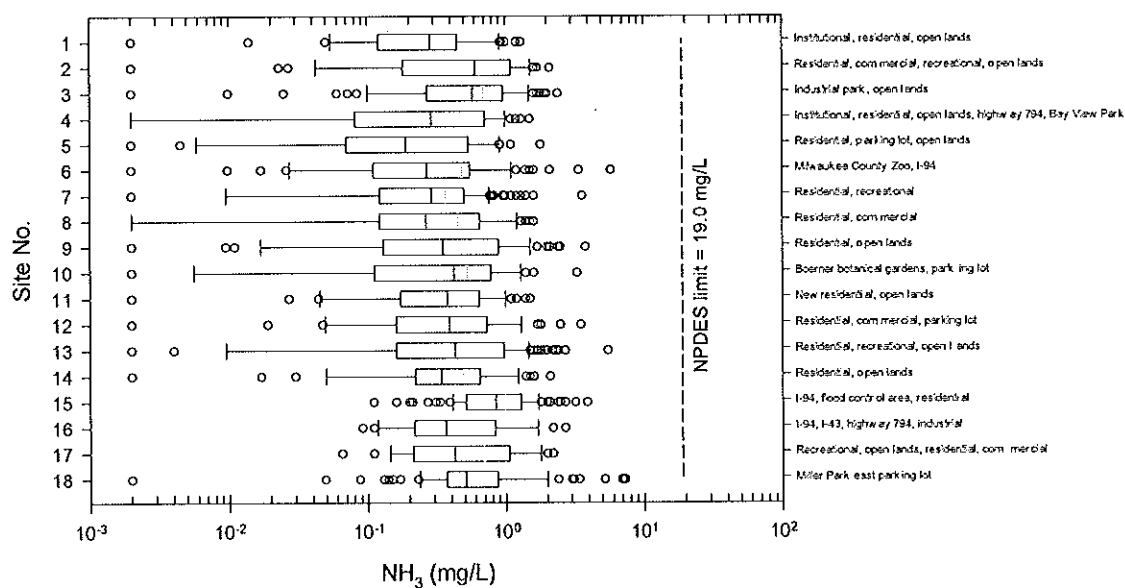


Figure B - 15. Box plots of Mg in stormwater per site.

Figure B - 16. Box plots of NH₃ in stormwater per site.

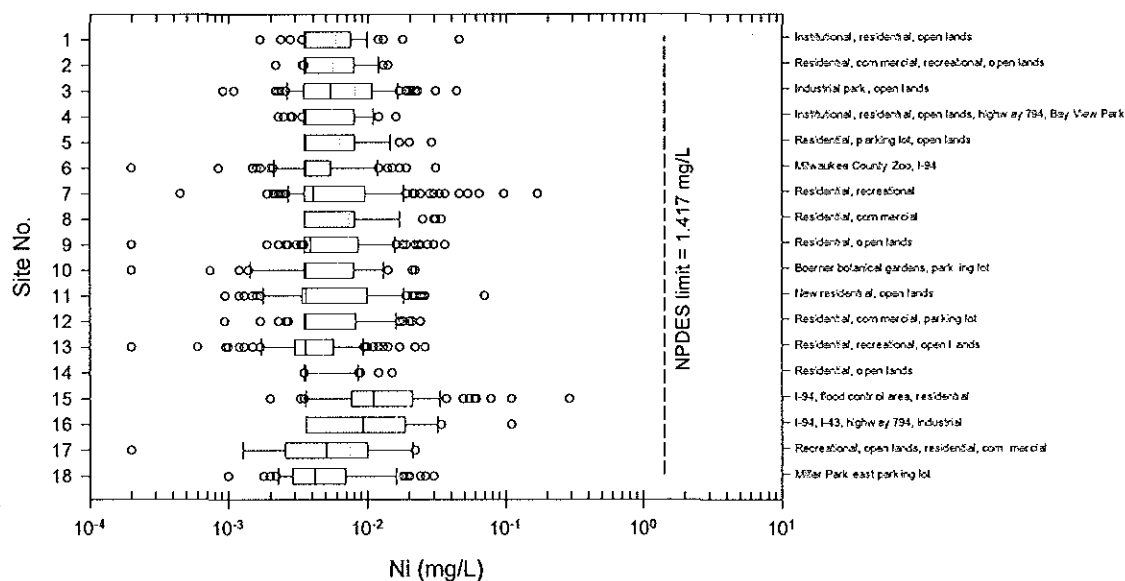


Figure B - 17. Box plots of Ni in stormwater per site.

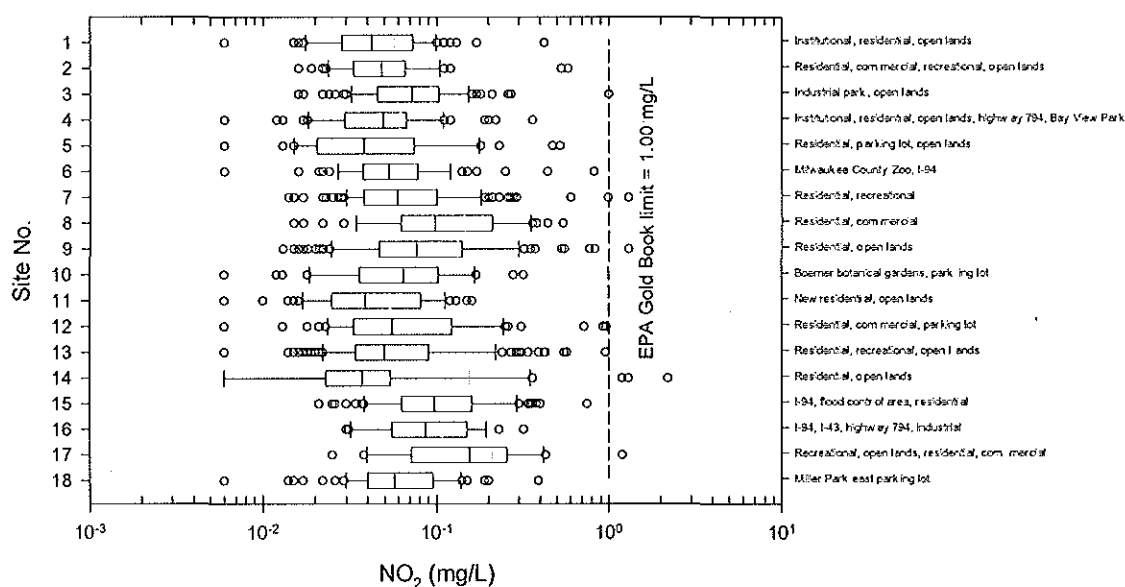


Figure B - 18. Box plots of NO_2 in stormwater per site.

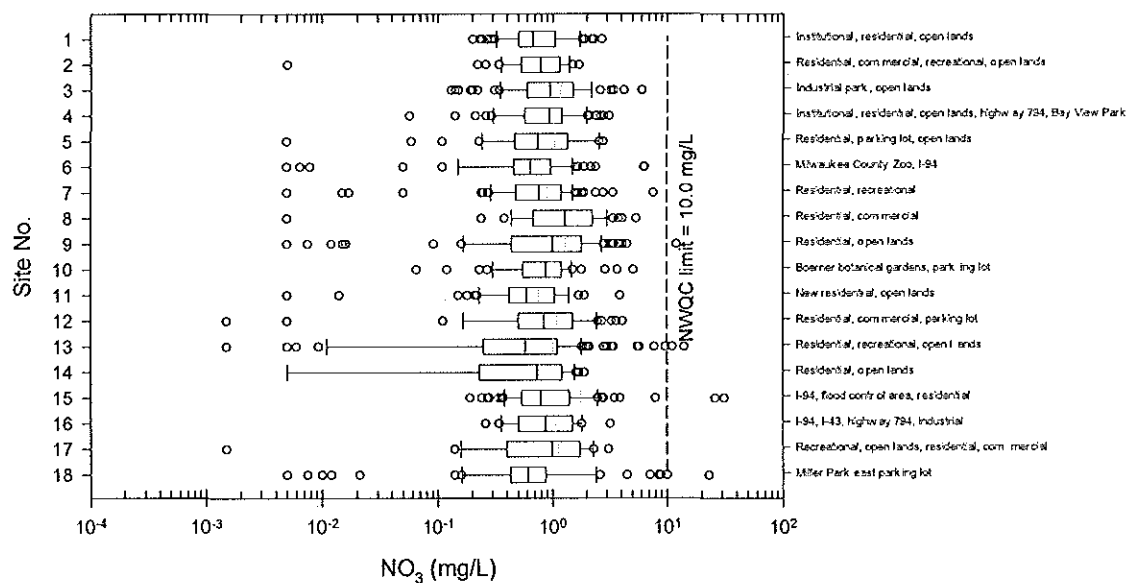


Figure B - 19. Box plots of NO_3 in stormwater per site.

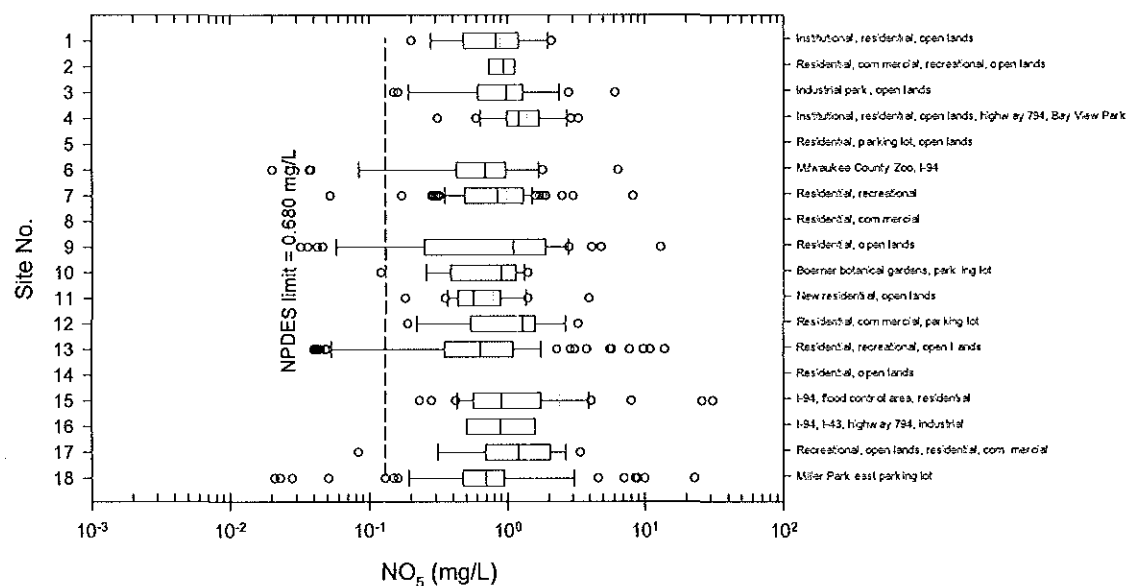


Figure B - 20. Box plots of NO_5 in stormwater per site.

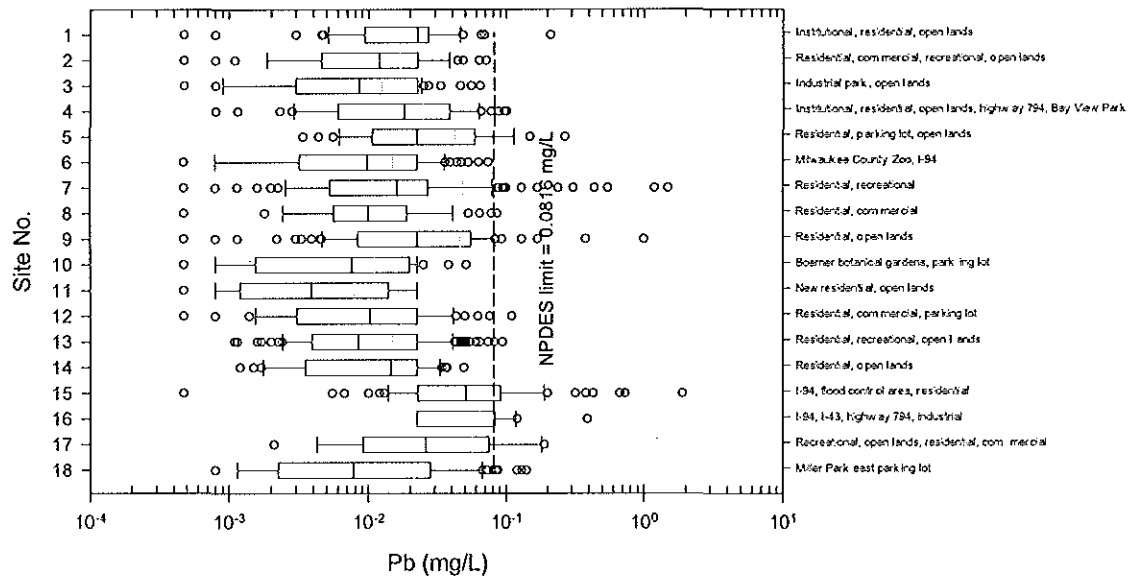


Figure B - 21. Box plots of Pb in stormwater per site.

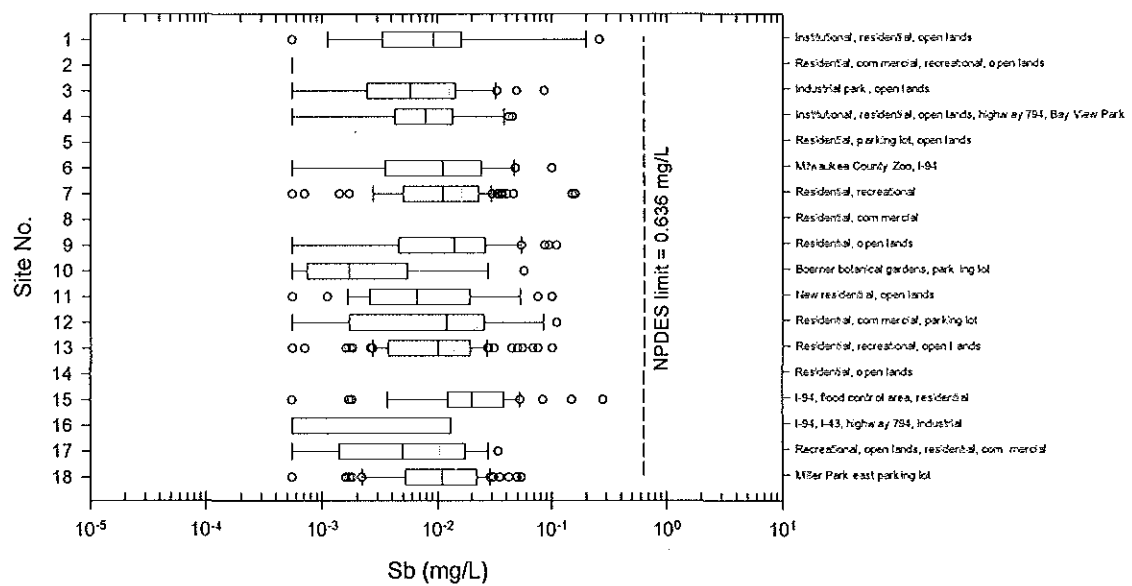


Figure B - 22. Box plots of Sb in stormwater per site.

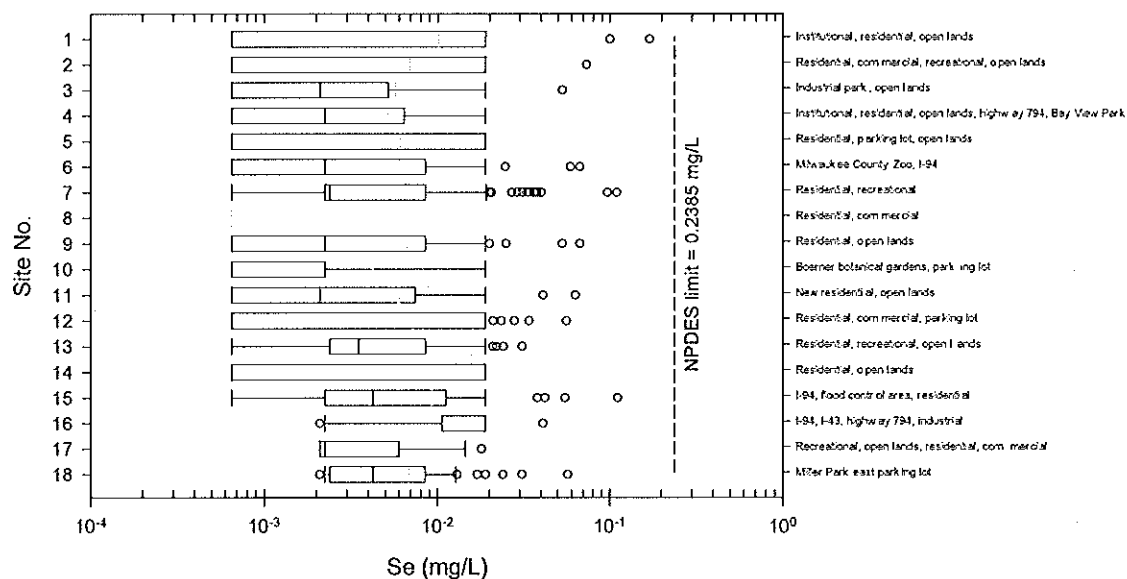


Figure B - 23. Box plots of Se in stormwater per site.

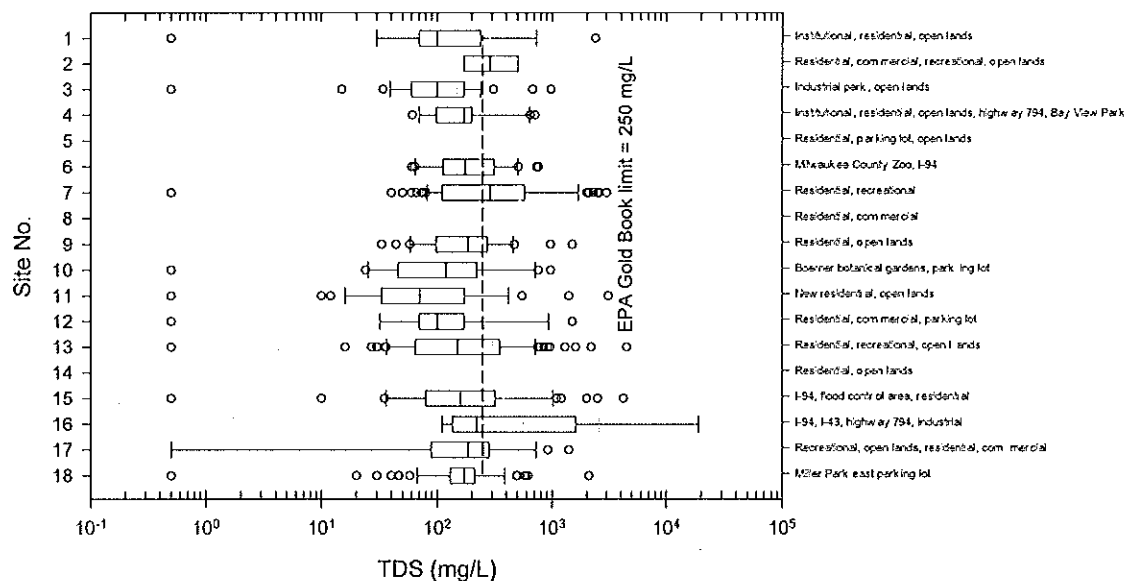


Figure B - 24. Box plots of TDS in stormwater per site.

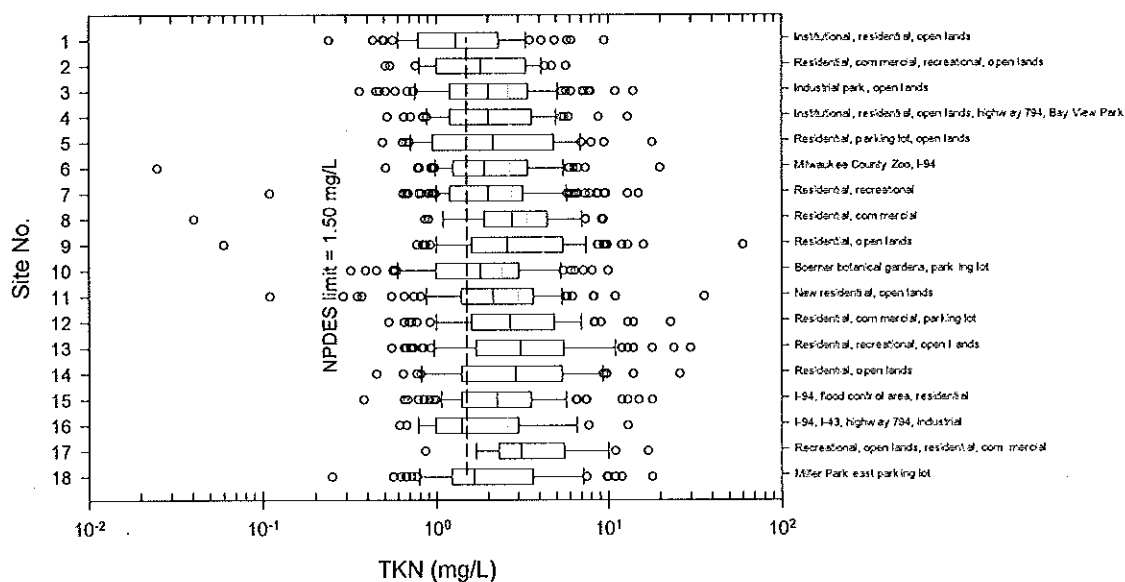


Figure B - 25. Box plots of TKN in stormwater per site.

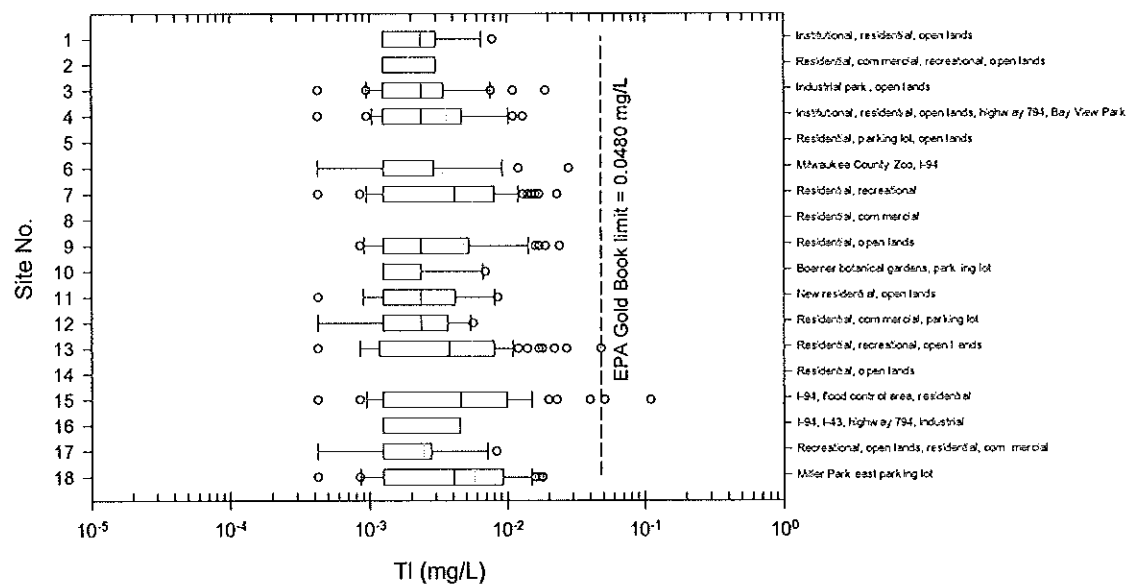


Figure B - 26. Box plots of TI in stormwater per site.

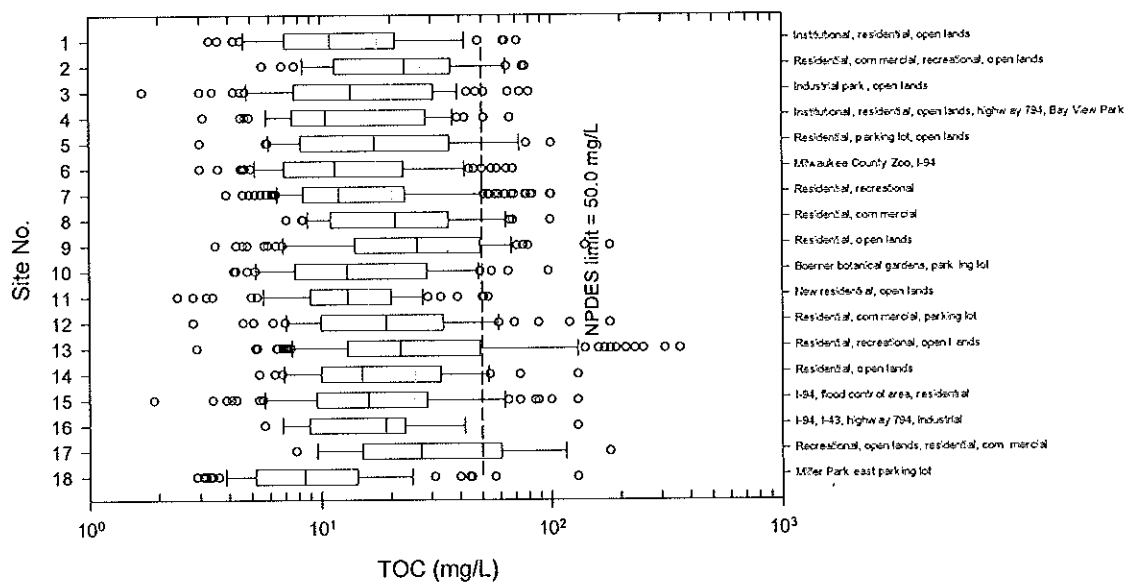


Figure B - 27. Box plots of TOC in stormwater per site.

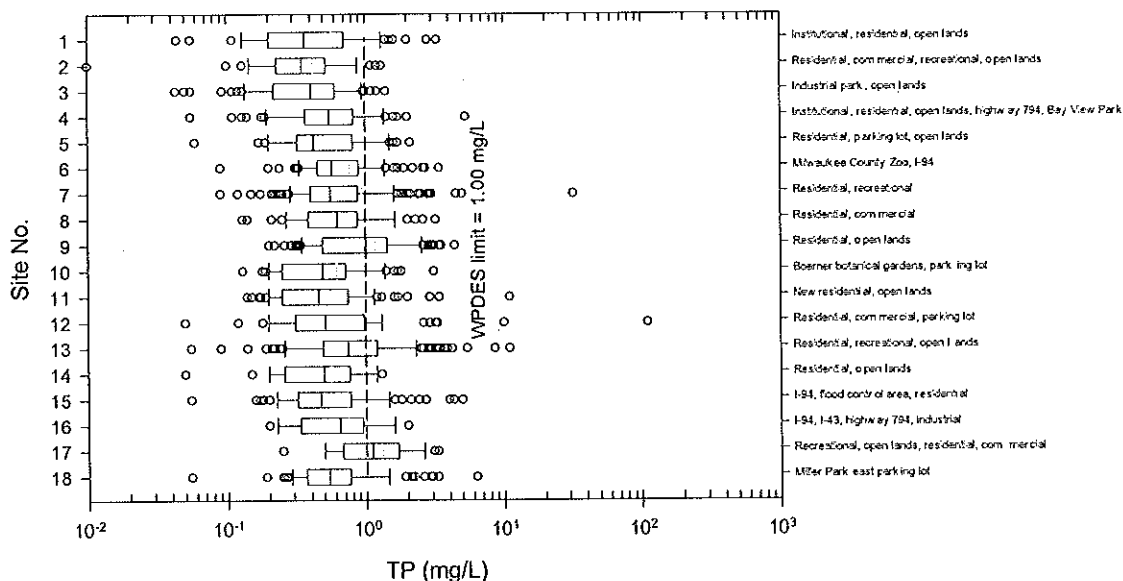


Figure B - 28. Box plots of TP in stormwater per site.

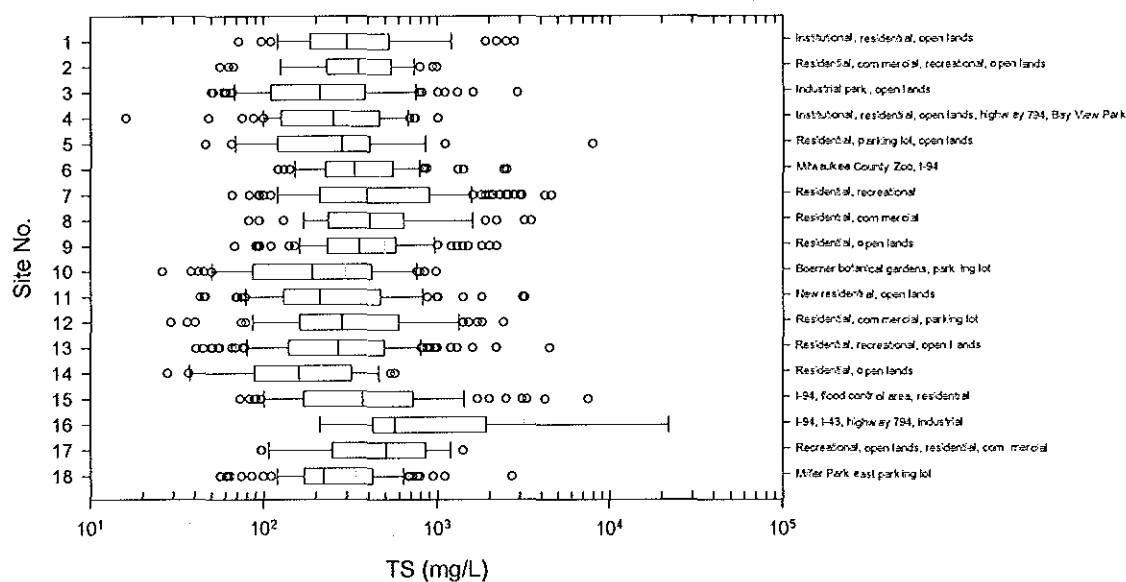


Figure B - 29. Box plots of TS in stormwater per site.

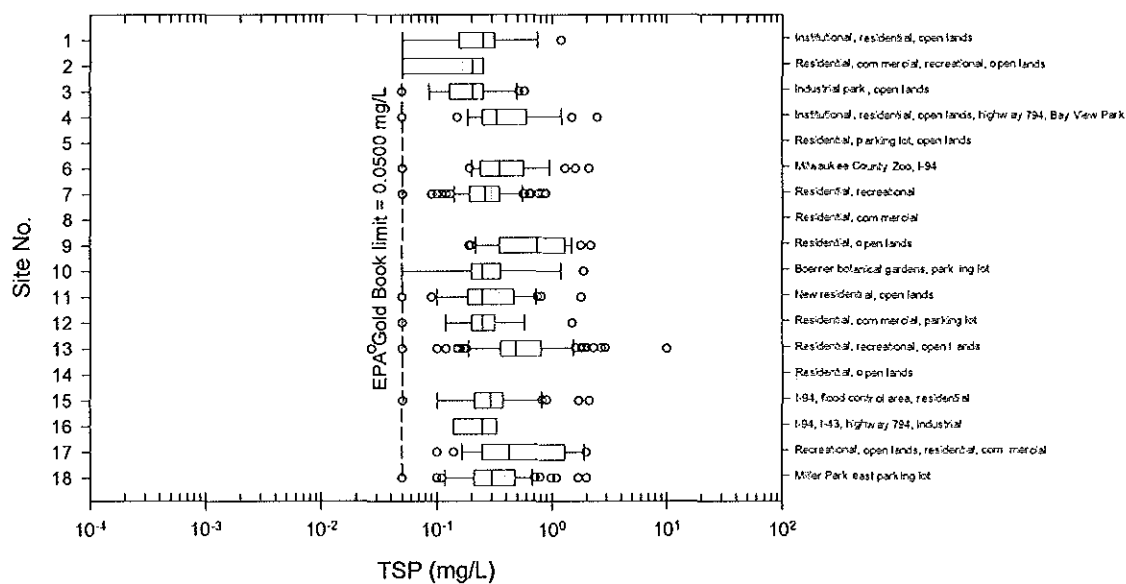


Figure B - 30. Box plots of TSP in stormwater per site.

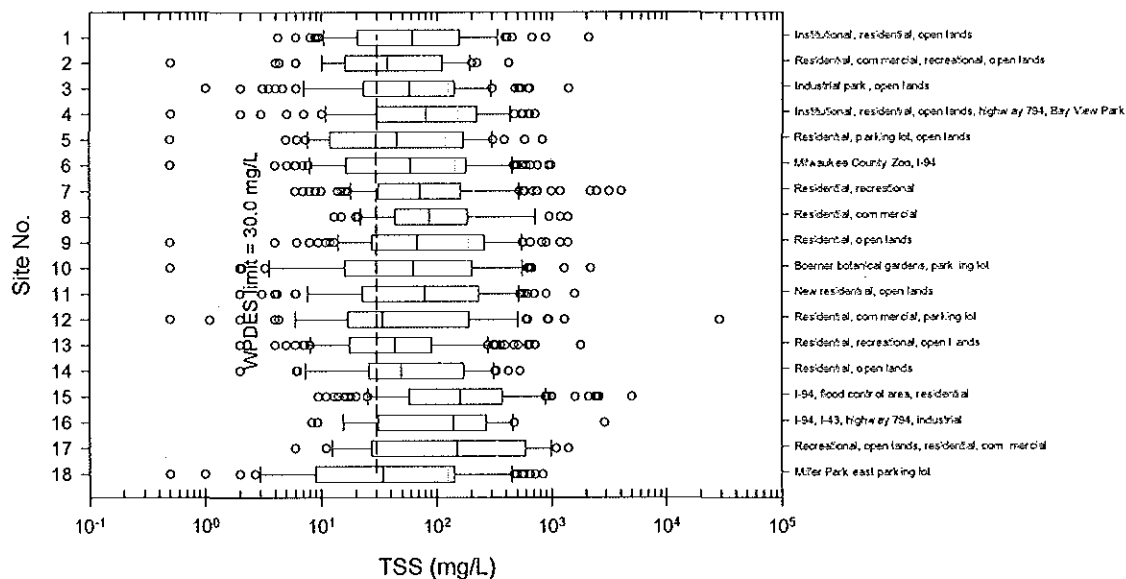


Figure B - 31. Box plots of TSS in stormwater per site.

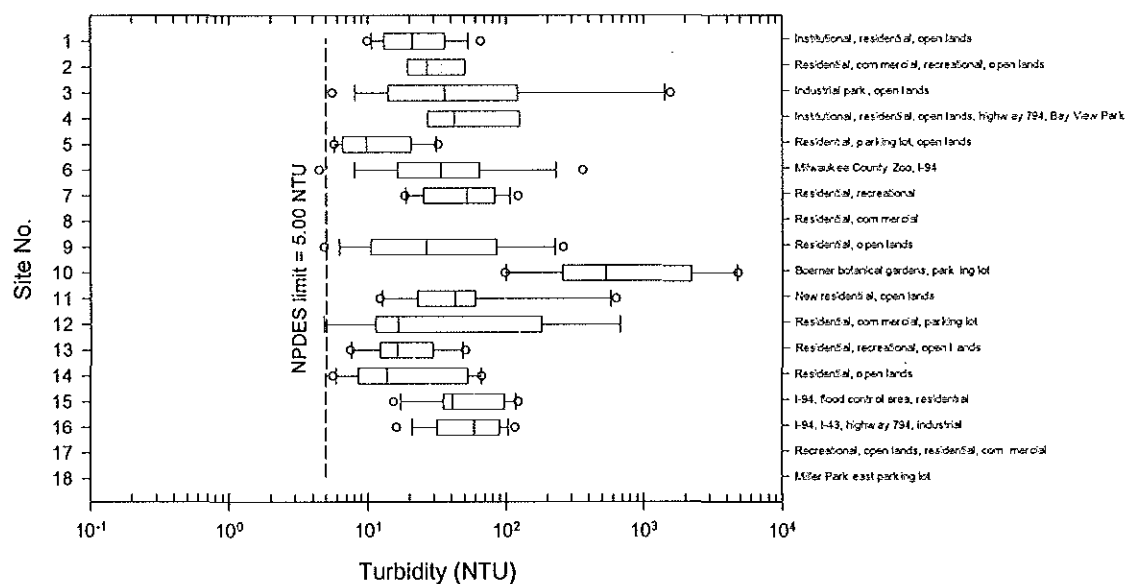


Figure B - 32. Box plots of turbidity in stormwater per site.

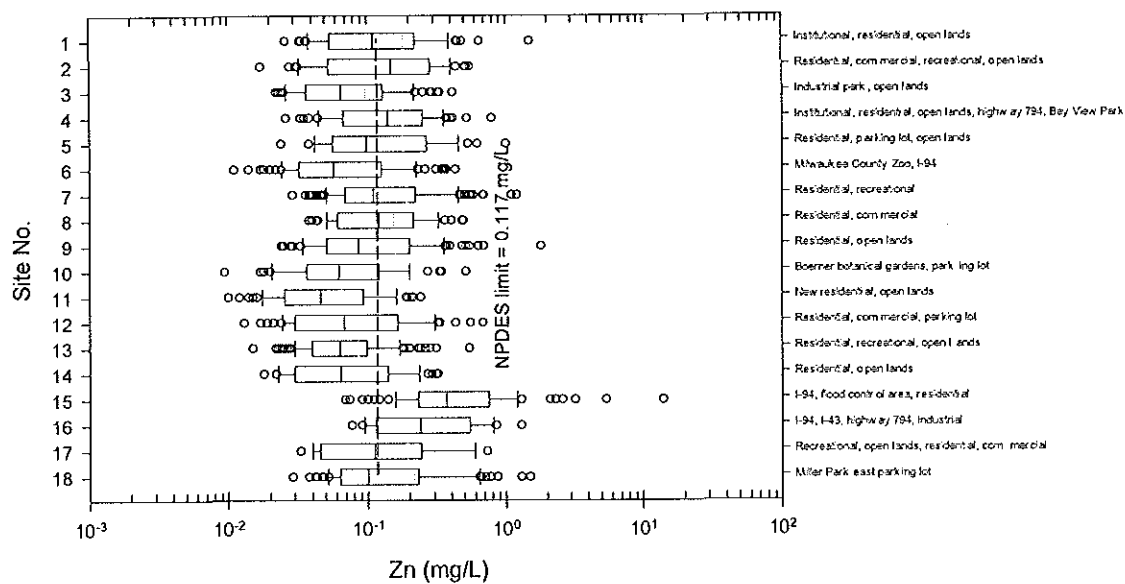


Figure B - 33. Box plots of Zn in stormwater per site.

Appendix C Pollutant Concentrations in Stormwater per Season

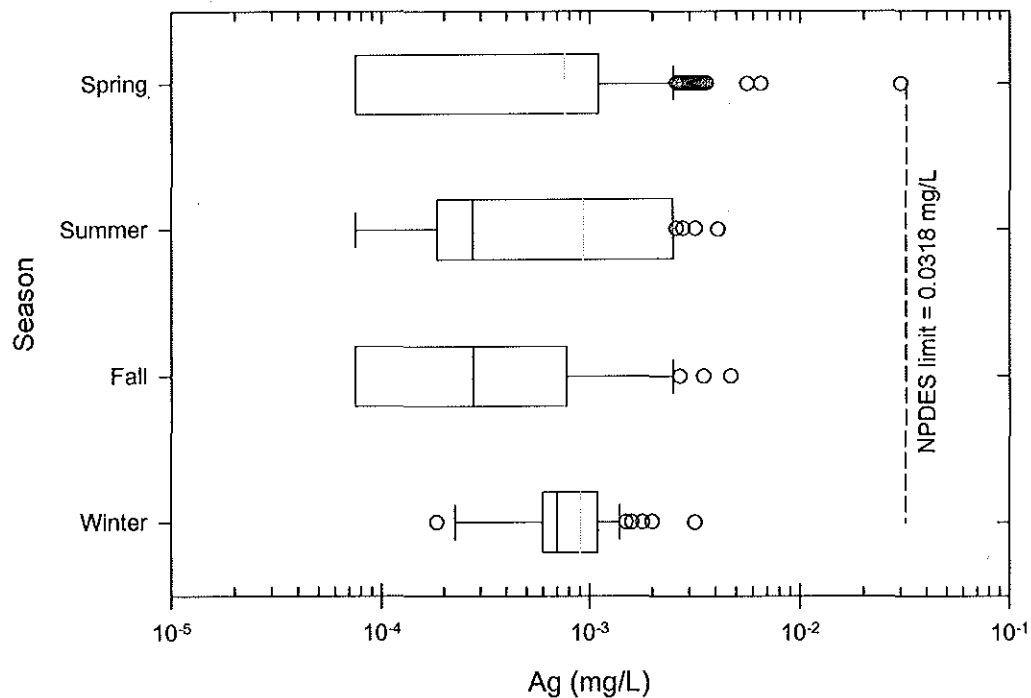


Figure C - 1. Box plots of Ag in stormwater per season.

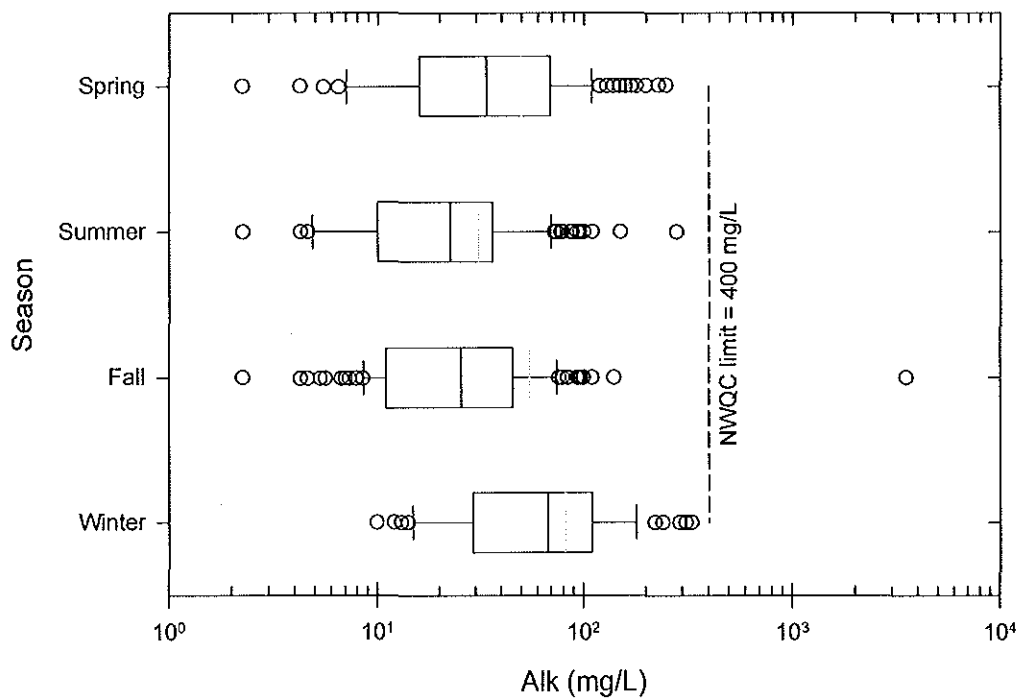


Figure C - 2. Box plots of Alk in stormwater per season.

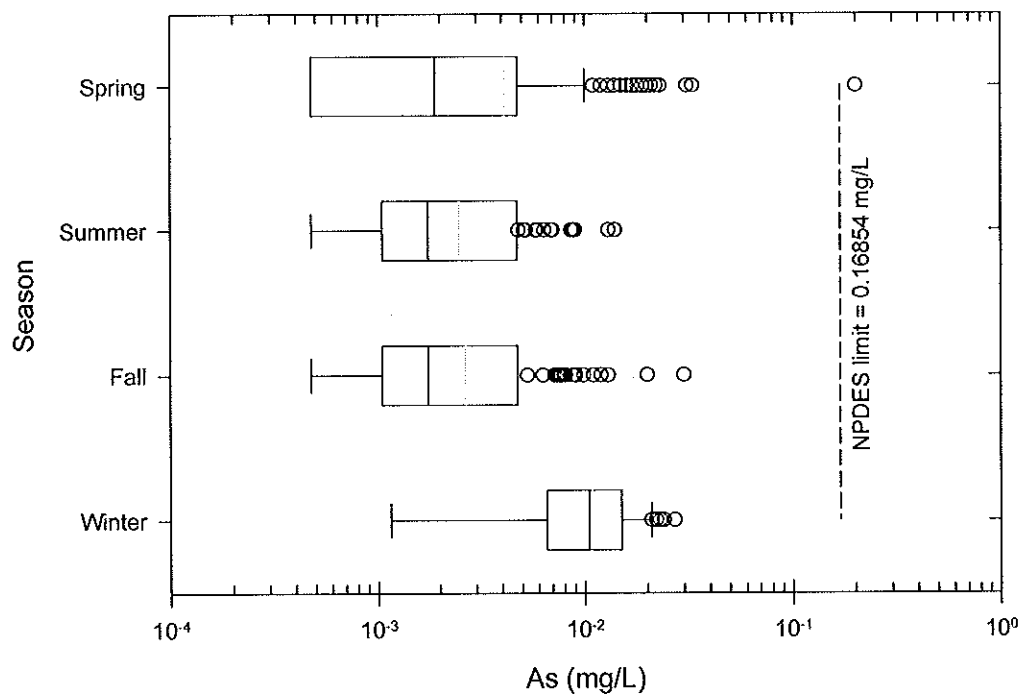


Figure C - 3. Box plots of As in stormwater per season.

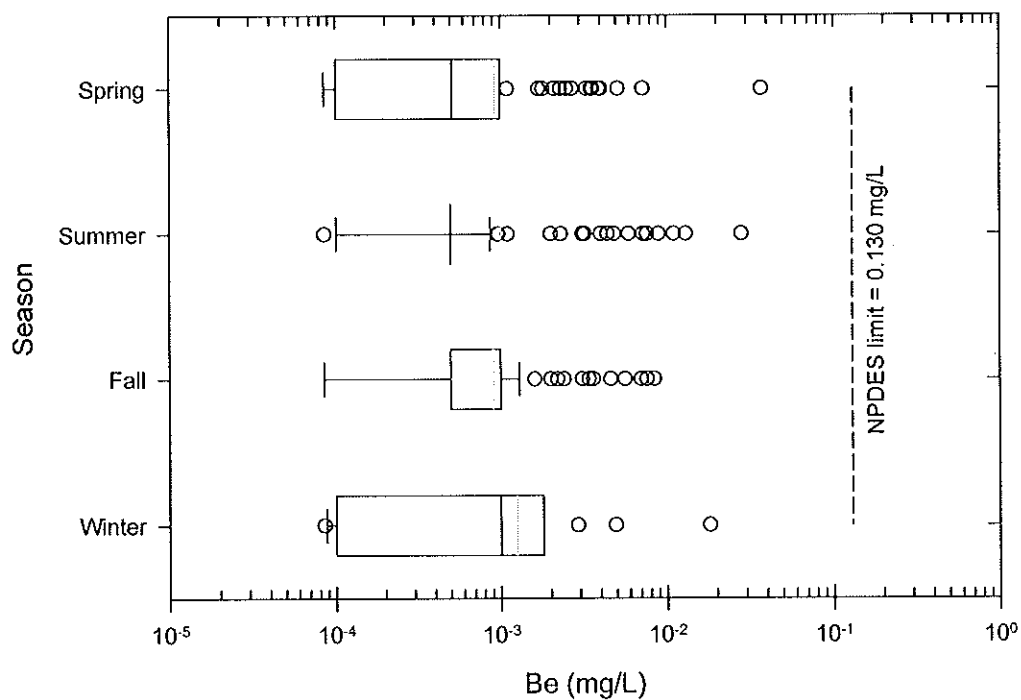


Figure C - 4. Box plots of Be in stormwater per season.

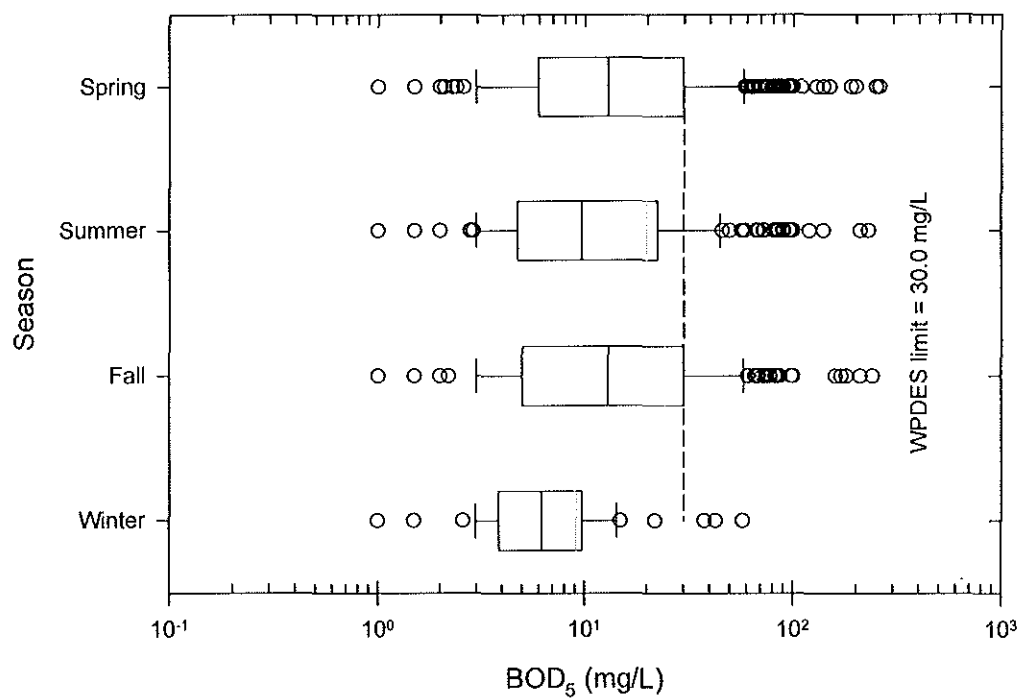


Figure C - 5. Box plots of BOD₅ in stormwater per season.

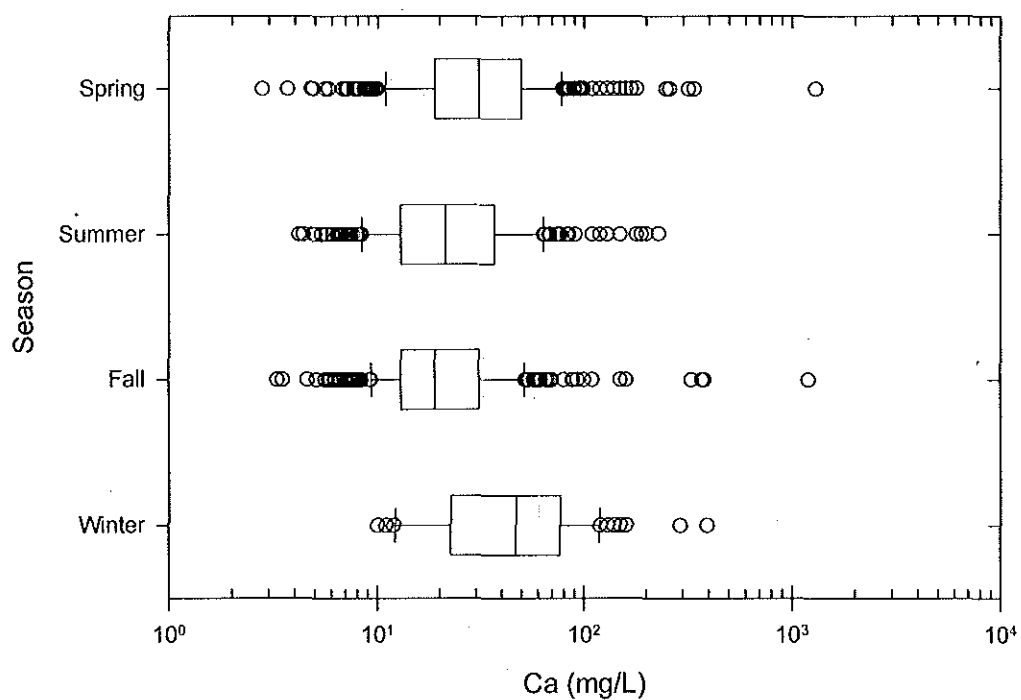


Figure C - 6. Box plots of Ca in stormwater per season.

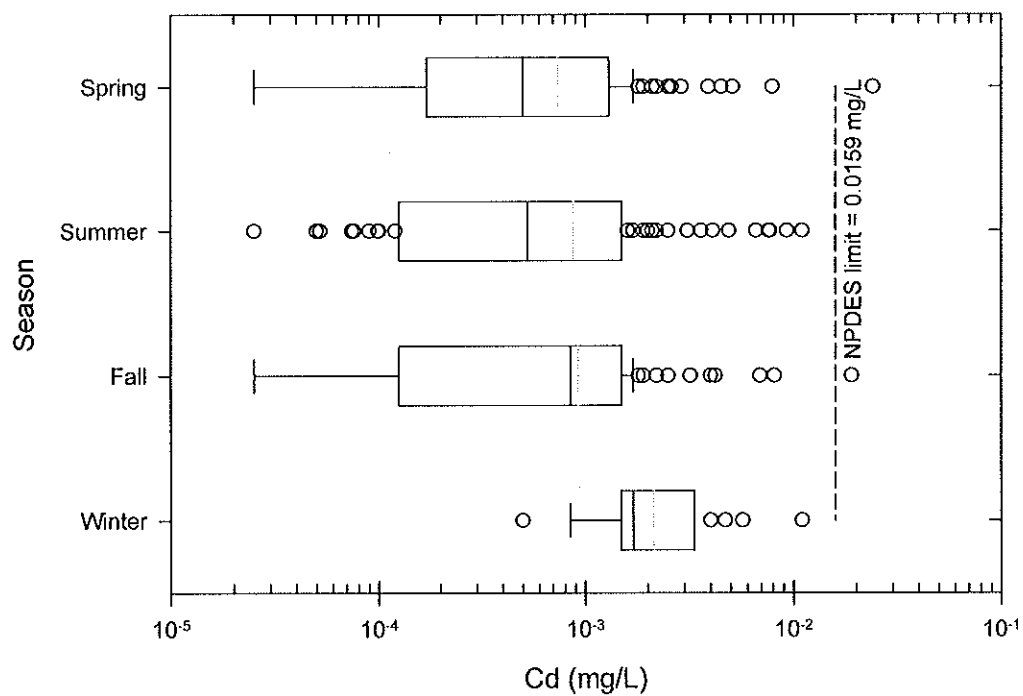


Figure C - 7. Box plots of Cd in stormwater per season.

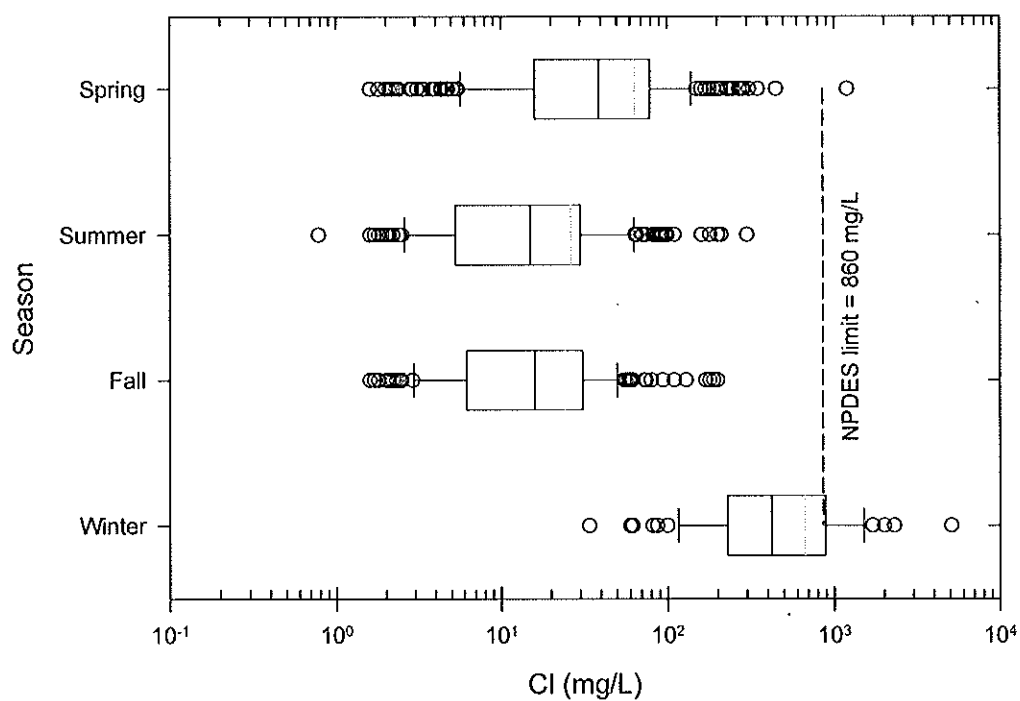


Figure C - 8. Box plots of Cl in stormwater per season.

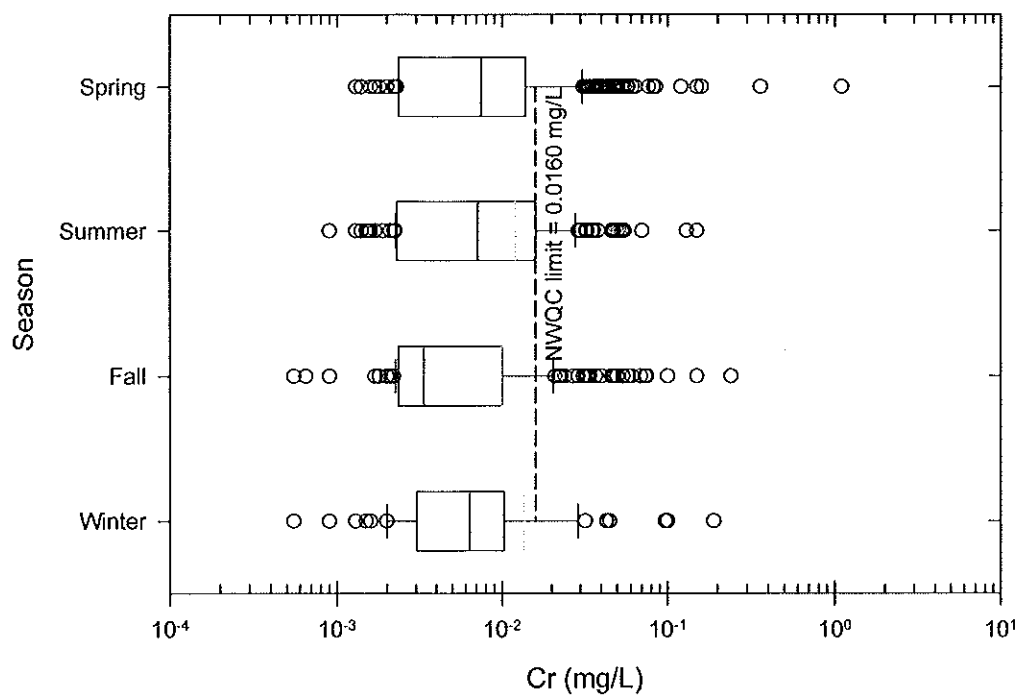


Figure C - 9. Box plots of Cr in stormwater per season.

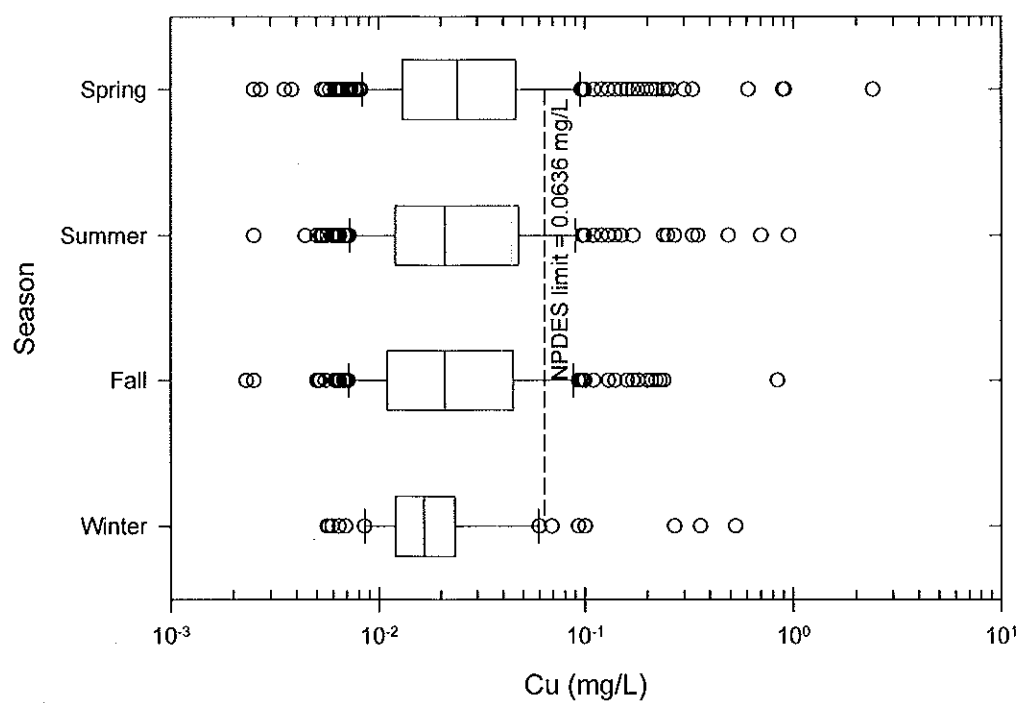


Figure C - 10. Box plots of Cu in stormwater per season.

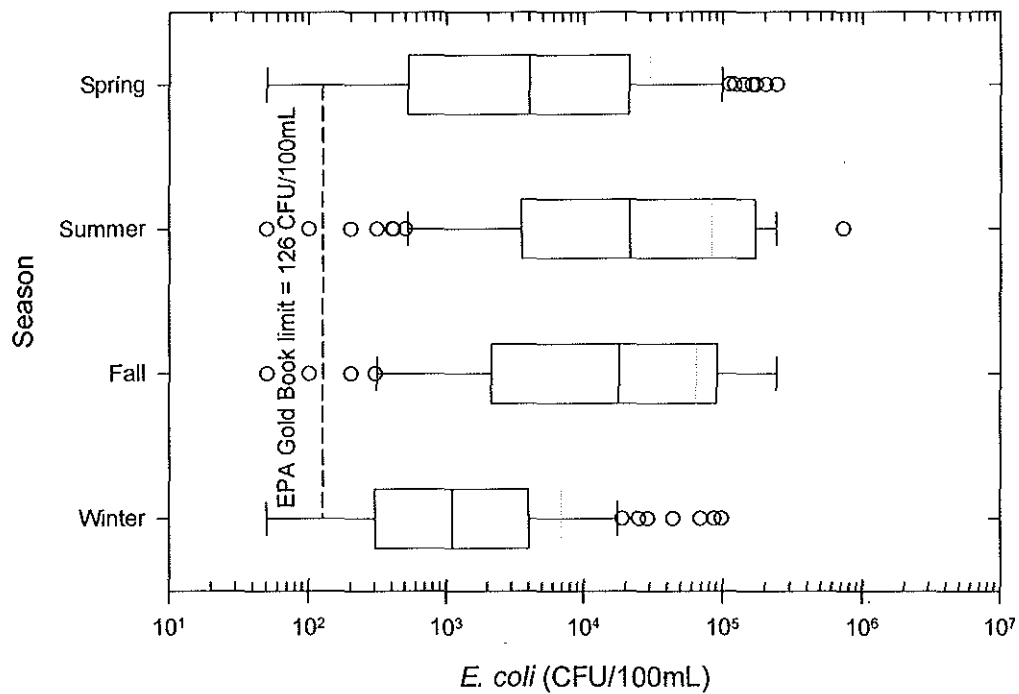


Figure C - 11. Box plots of EC in stormwater per season.

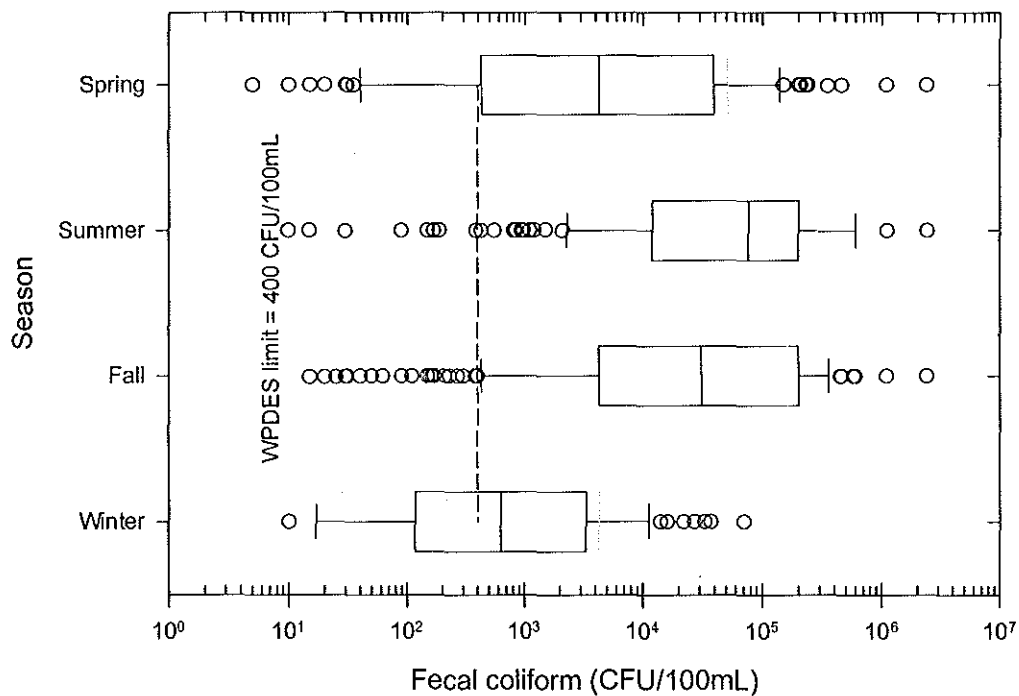


Figure C - 12. Box plots of FC in stormwater per season.

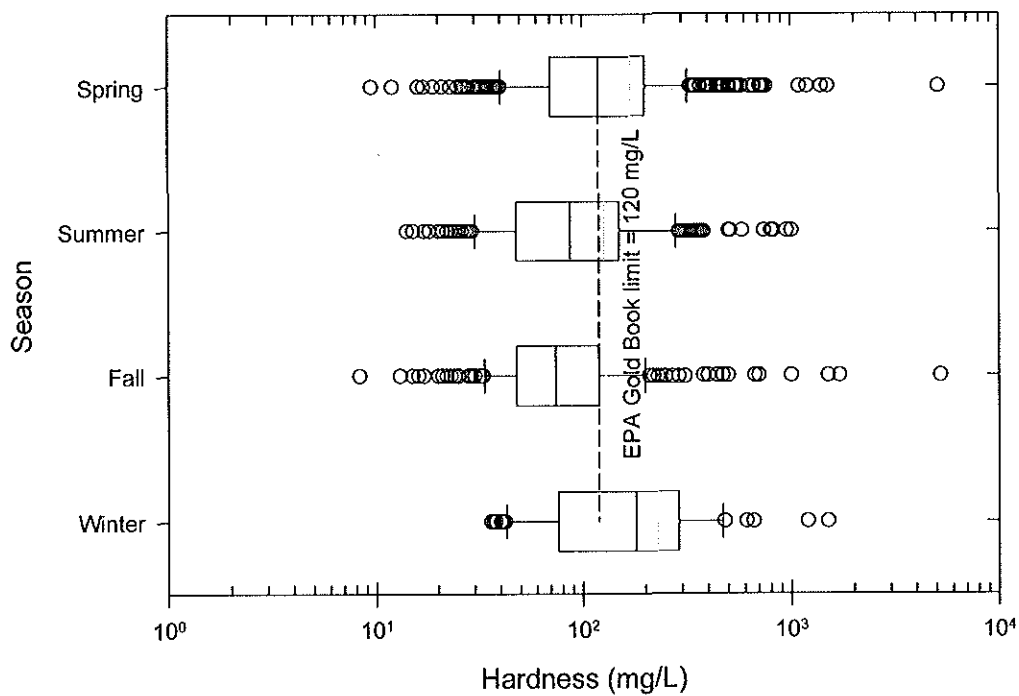


Figure C - 13. Box plots of Hard in stormwater per season.

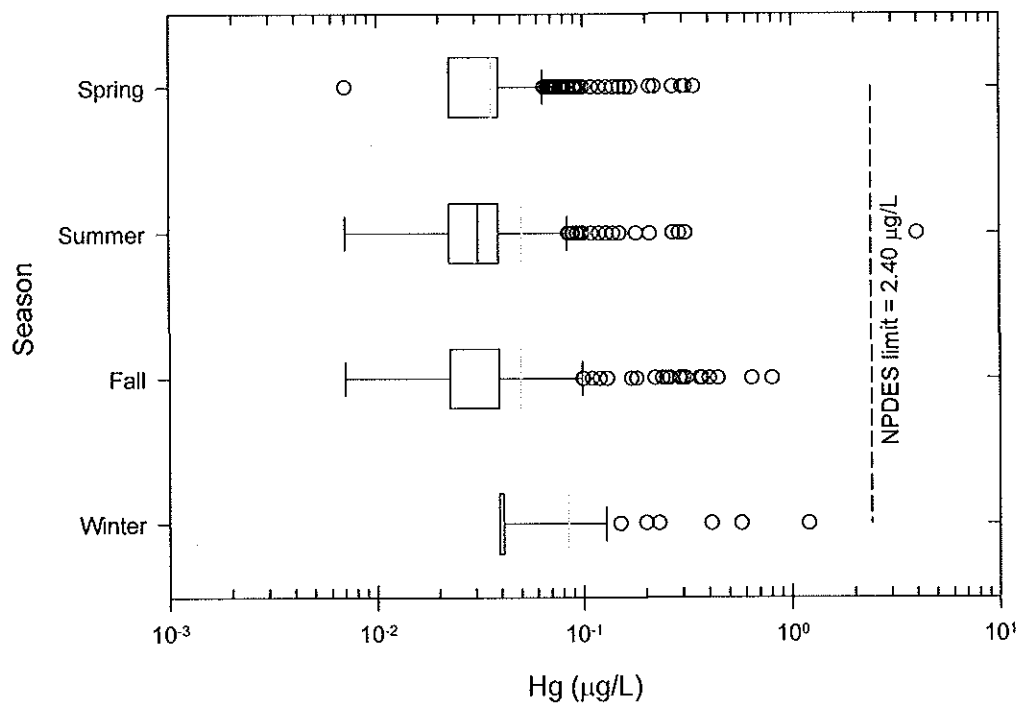


Figure C - 14. Box plots of Hg in stormwater per season.

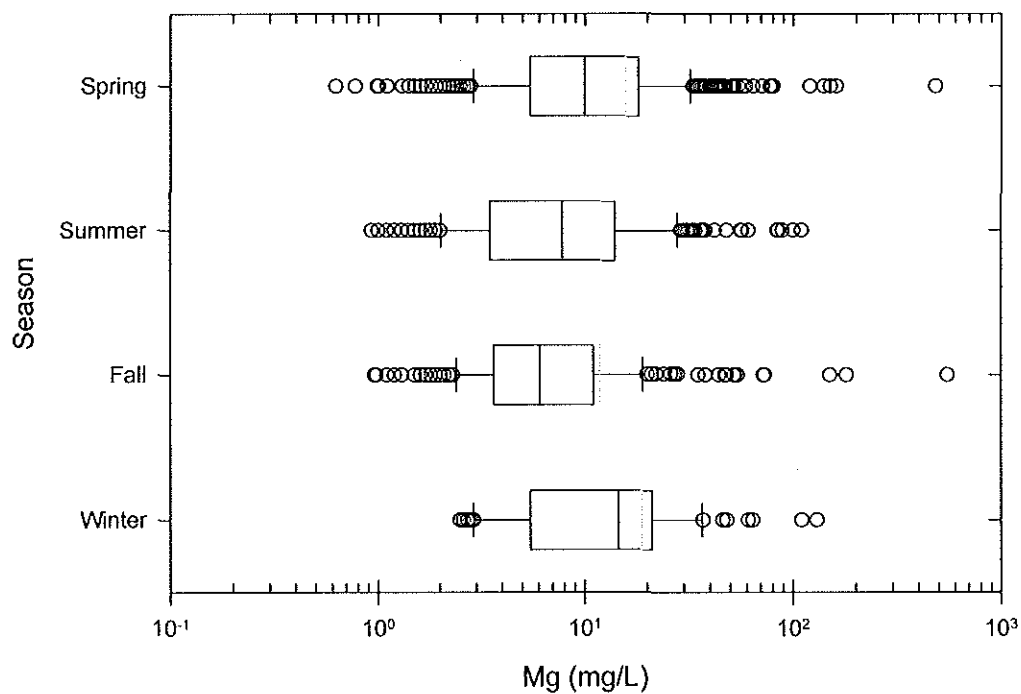


Figure C - 15. Box plots of Mg in stormwater per season.

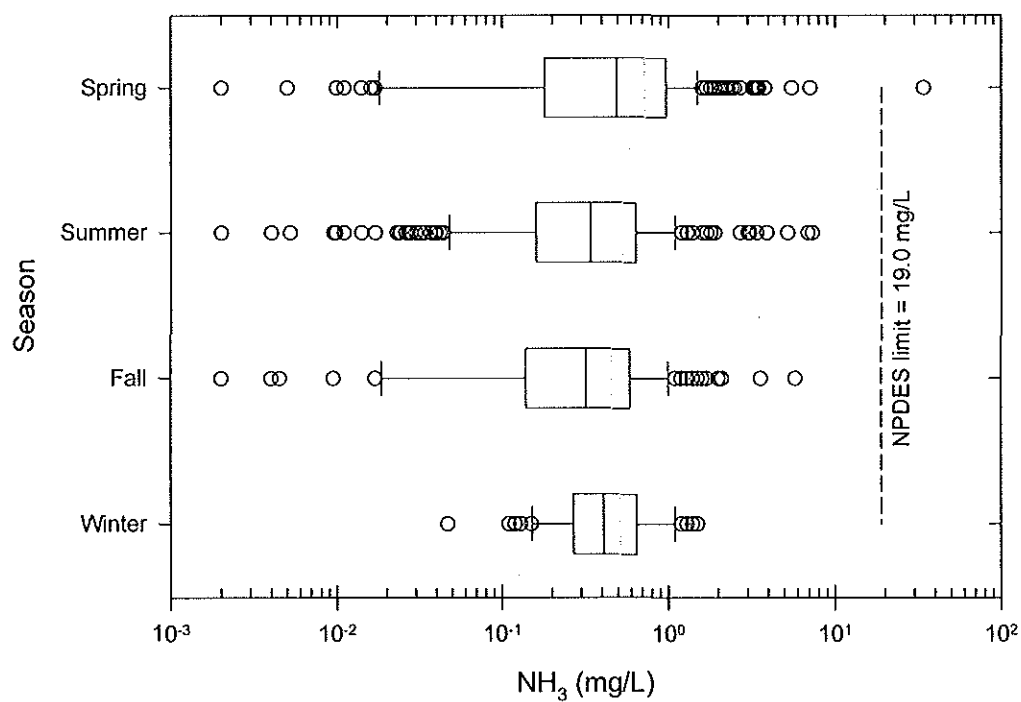


Figure C - 16. Box plots of NH_3 in stormwater per season.

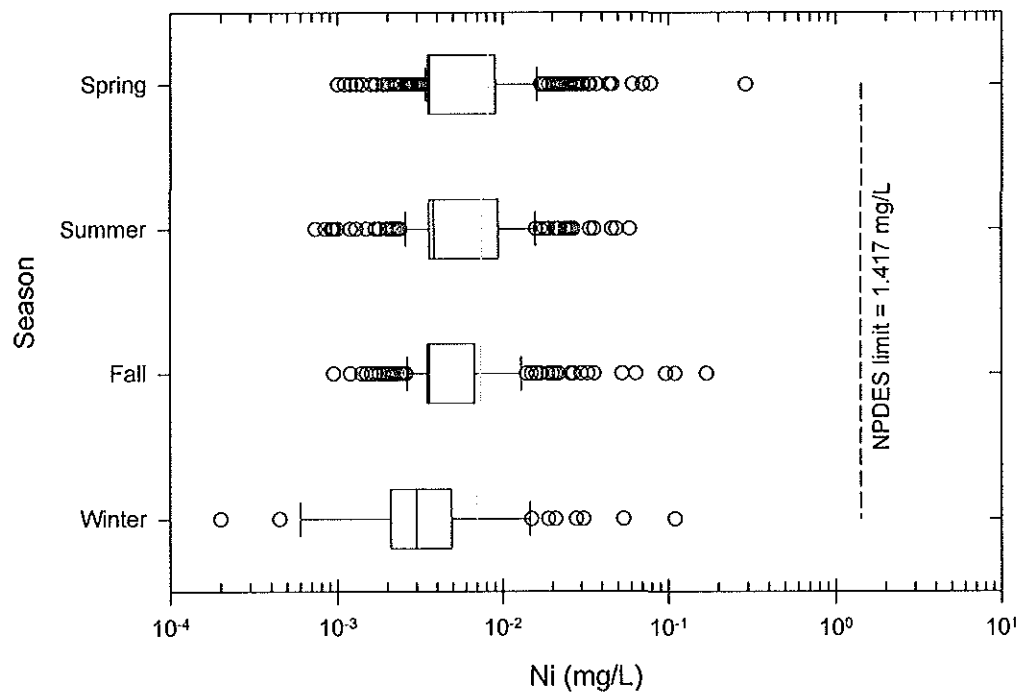


Figure C - 17. Box plots of Ni in stormwater per season.

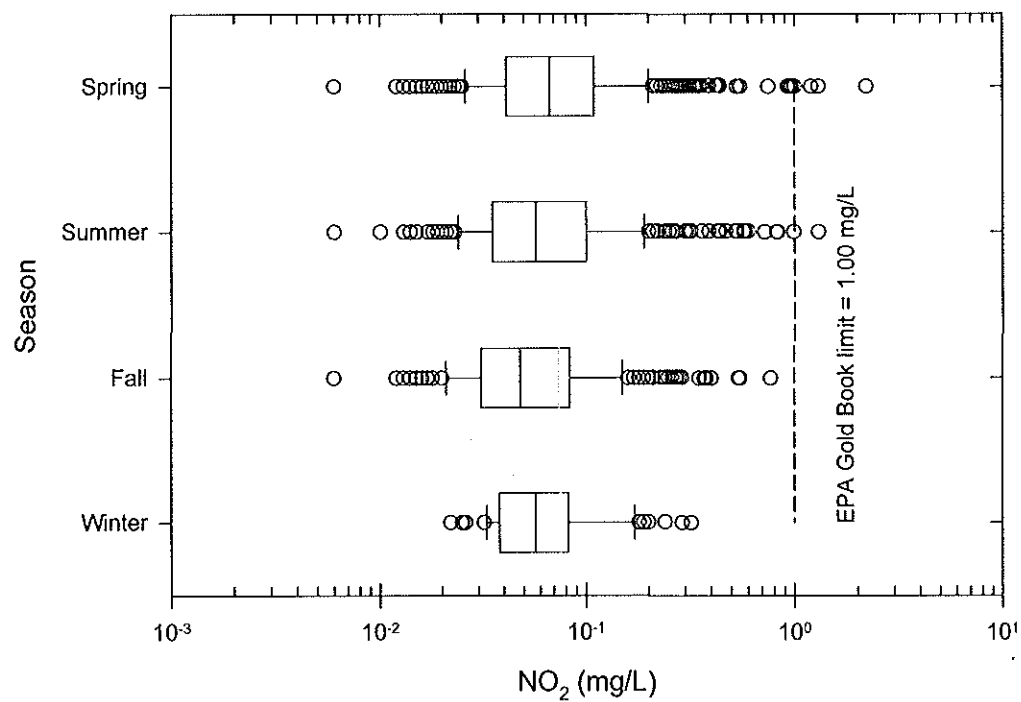


Figure C - 18. Box plots of NO_2 in stormwater per season.

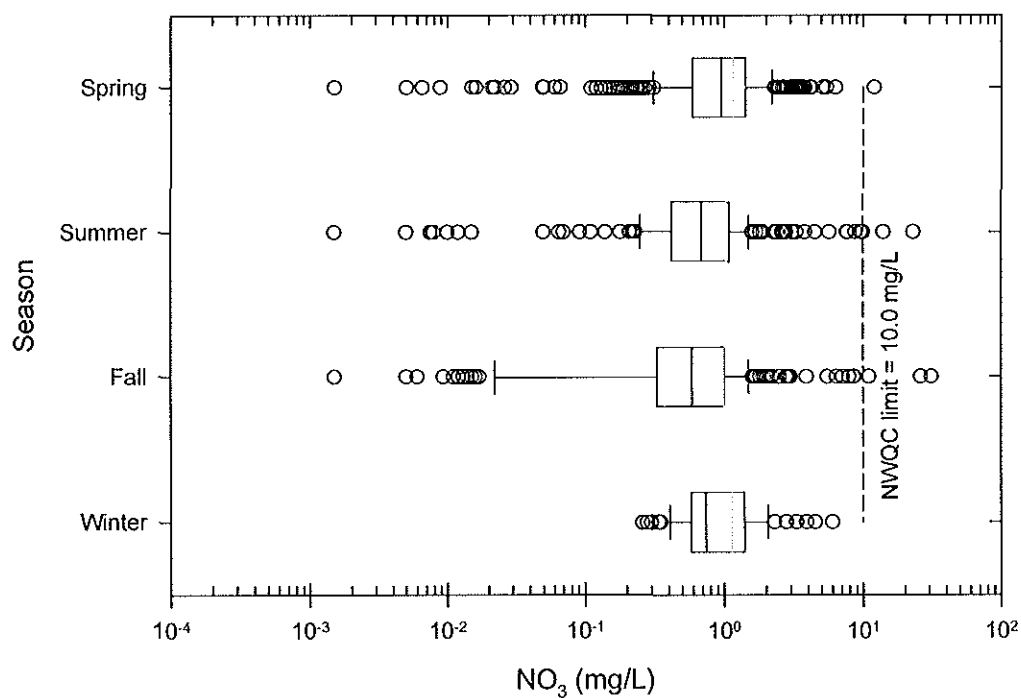


Figure C - 19. Box plots of NO_3 in stormwater per season.

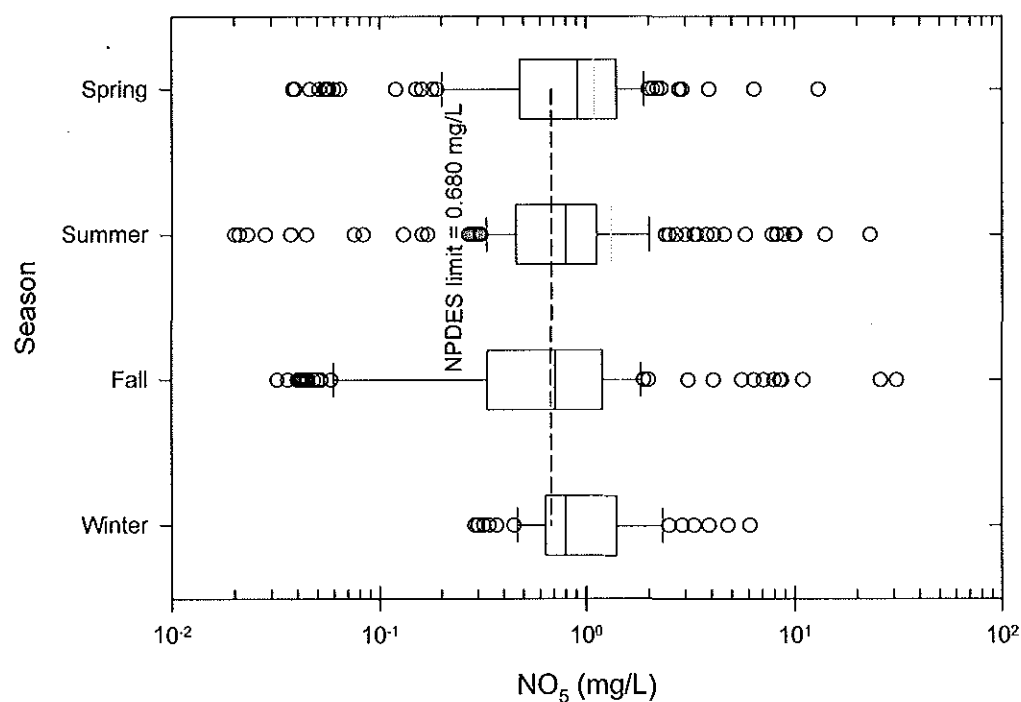


Figure C - 20. Box plots of NO_5 in stormwater per season.

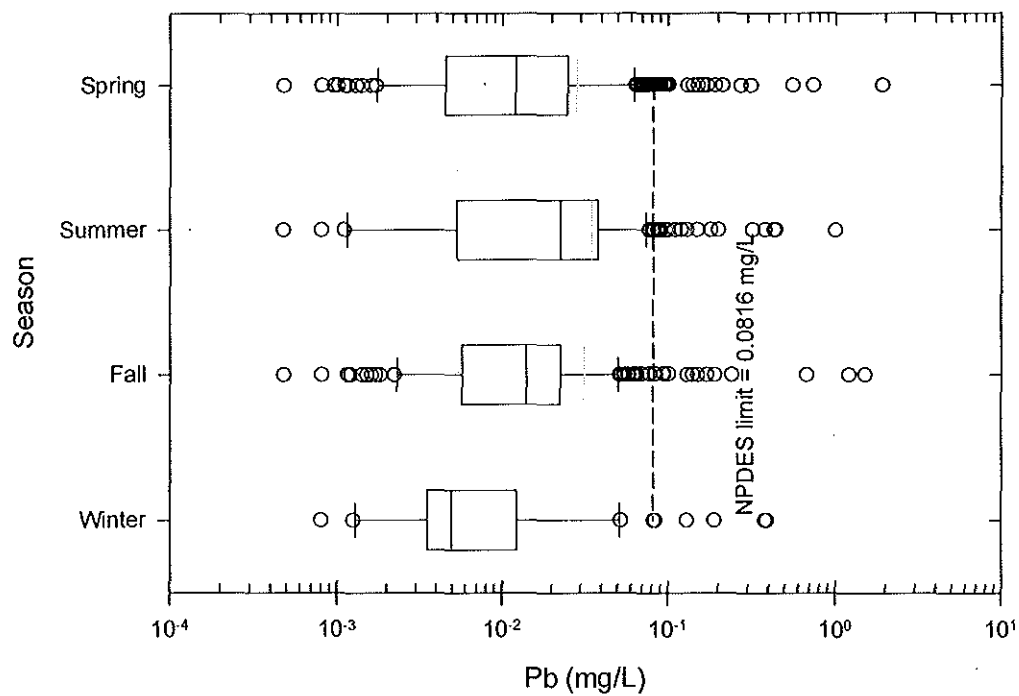


Figure C - 21. Box plots of Pb in stormwater per season.

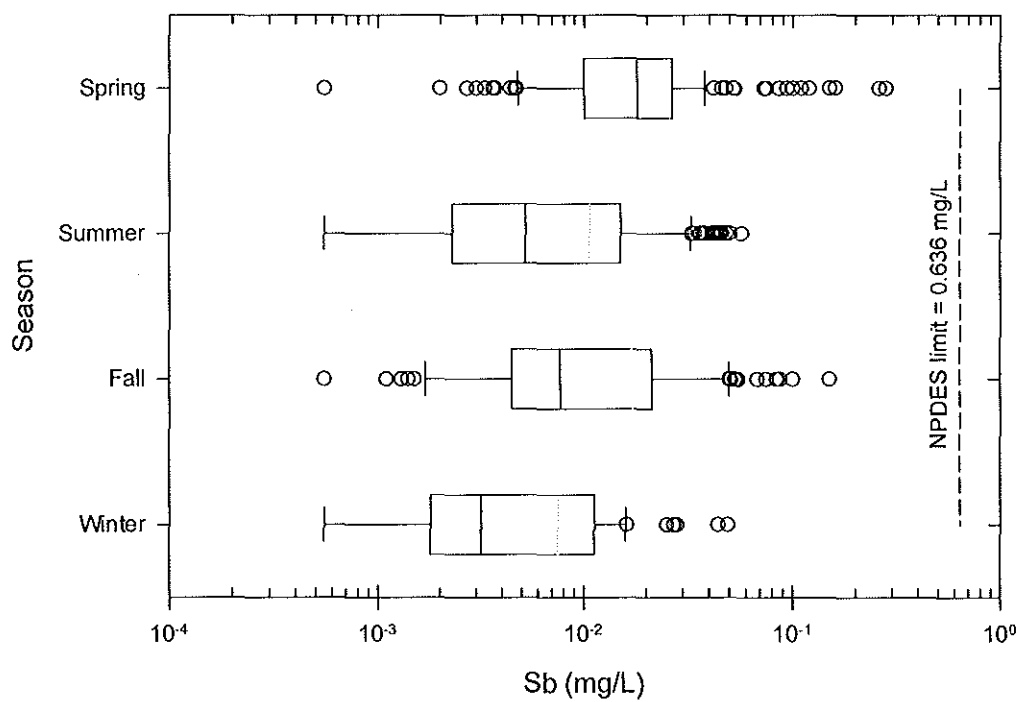


Figure C - 22. Box plots of Sb in stormwater per season.

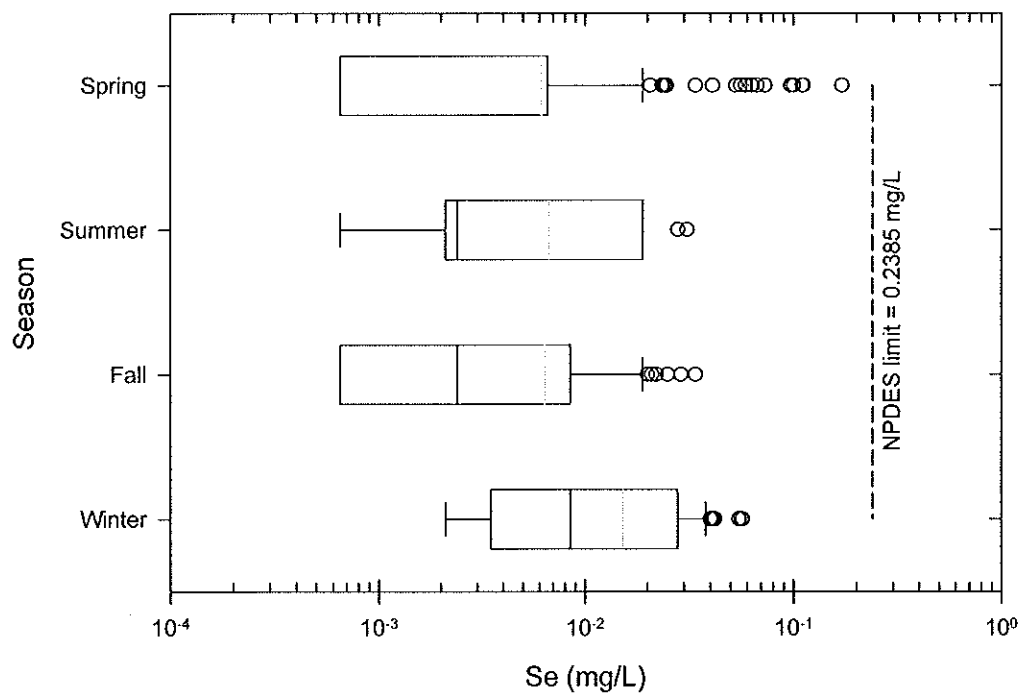


Figure C - 23. Box plots of Se in stormwater per season.

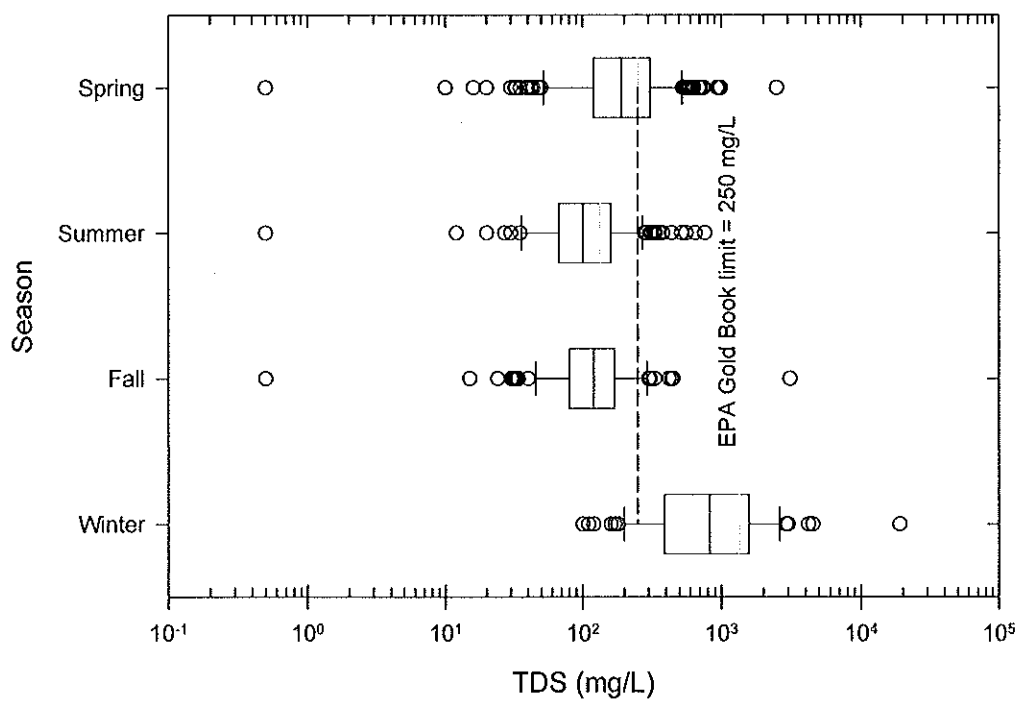


Figure C - 24. Box plots of TDS in stormwater per season.

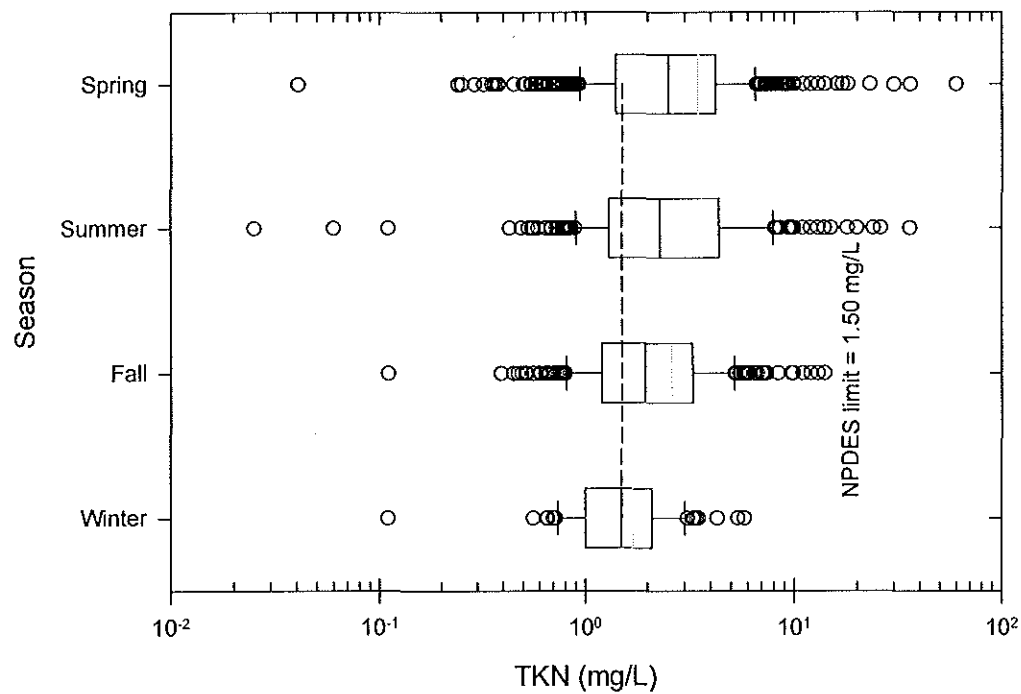


Figure C - 25. Box plots of TKN in stormwater per season.

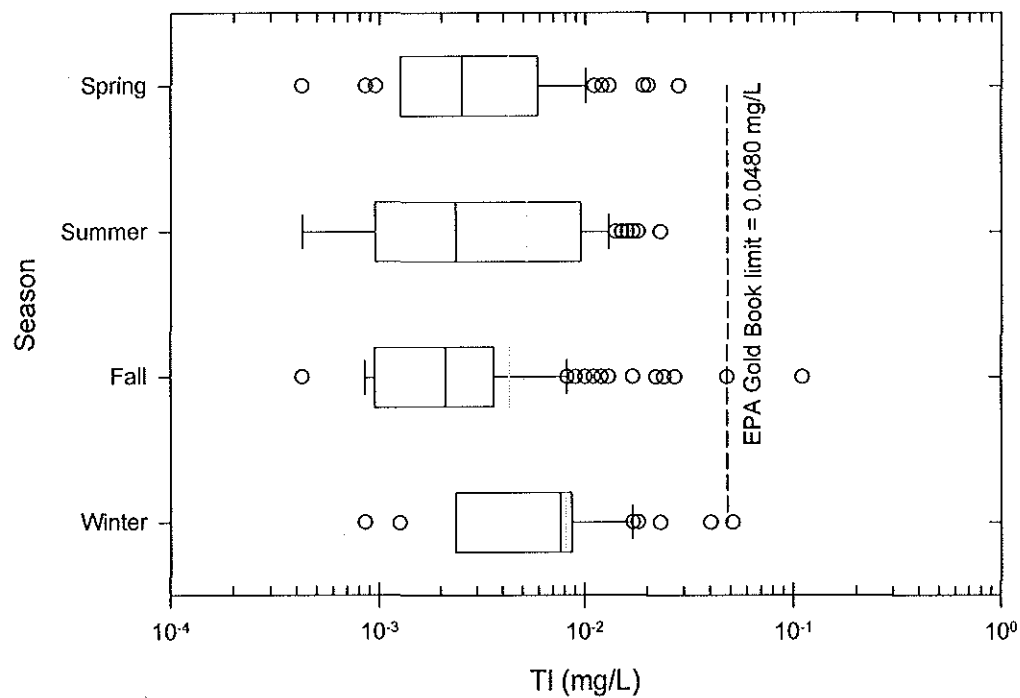


Figure C - 26. Box plots of TI in stormwater per season.

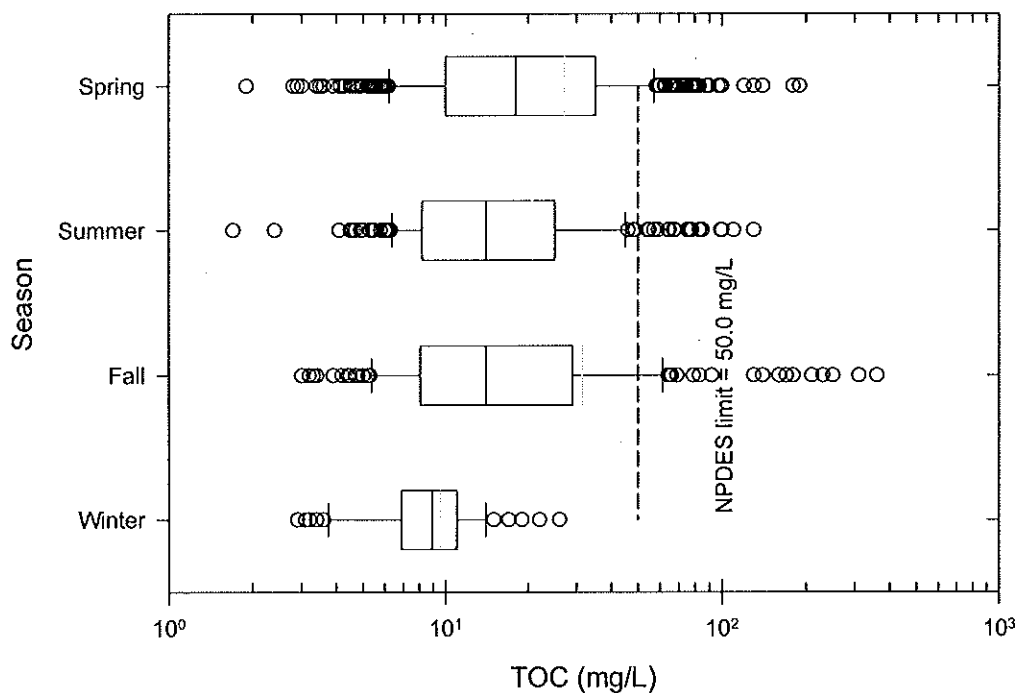


Figure C - 27. Box plots of TOC in stormwater per season.

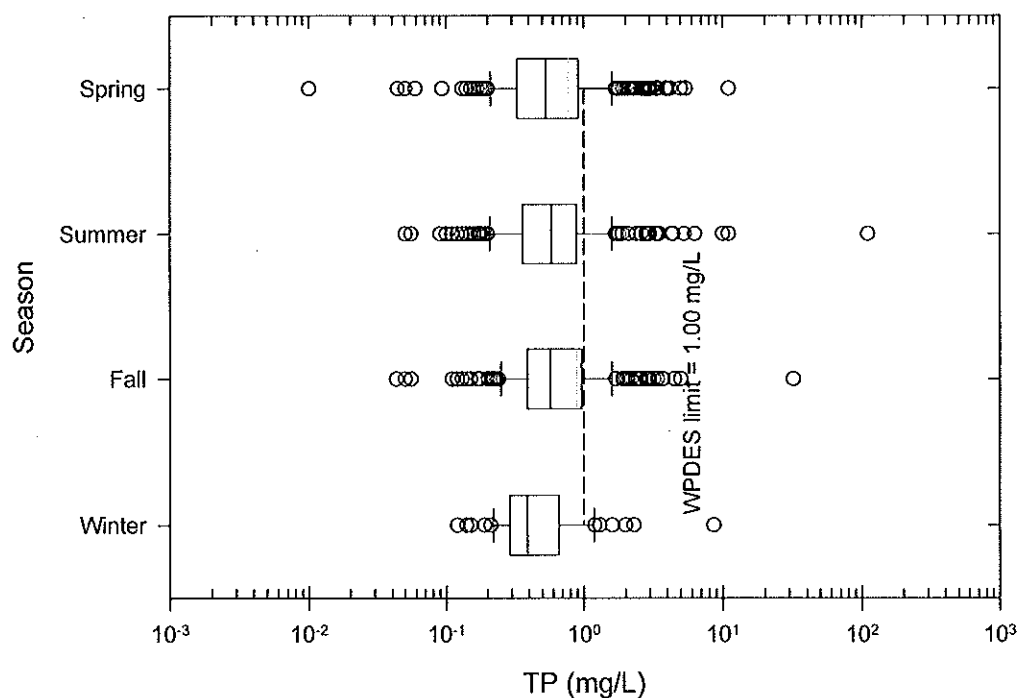


Figure C - 28. Box plots of TP in stormwater per season.

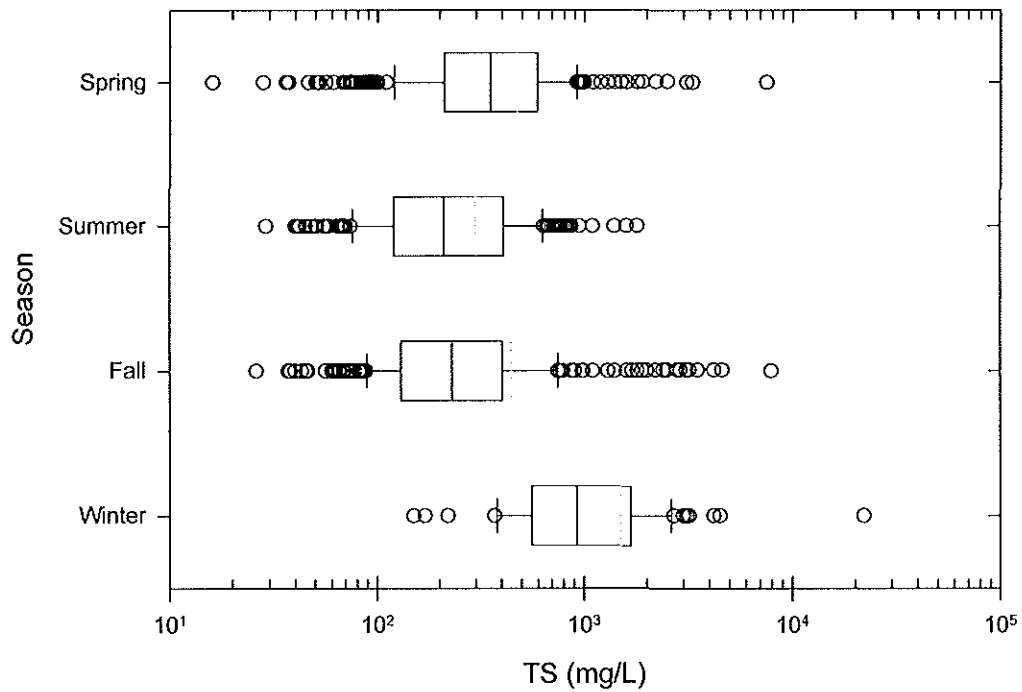


Figure C - 29. Box plots of TS in stormwater per season.

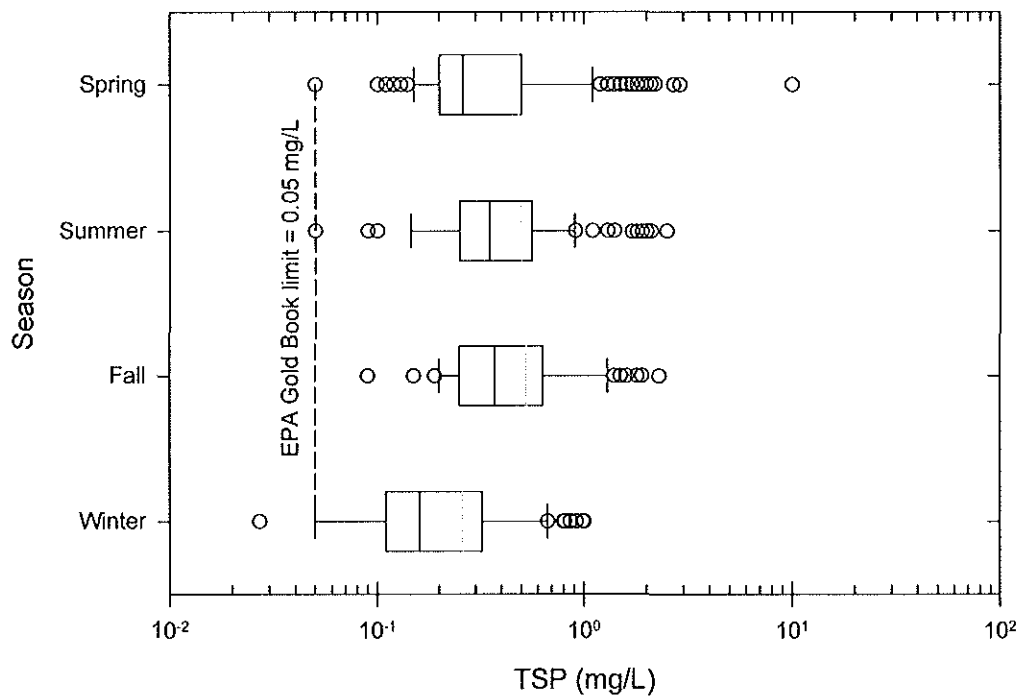


Figure C - 30. Box plots of TSP in stormwater per season.

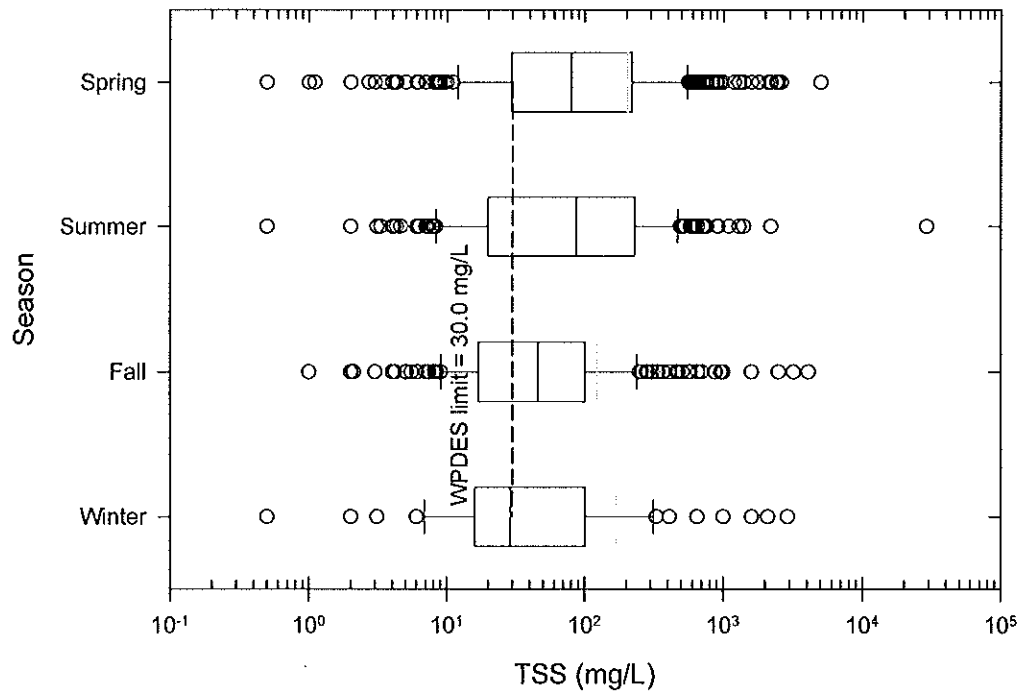


Figure C - 31. Box plots of TSS in stormwater per season.

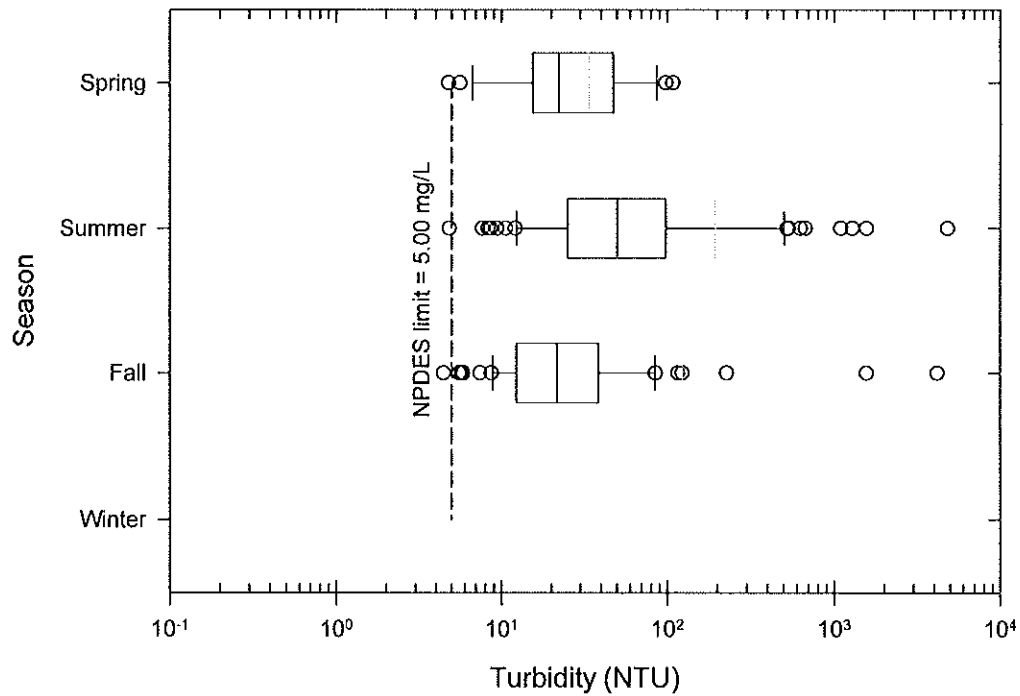


Figure C - 32. Box plots of turbidity in stormwater per season.

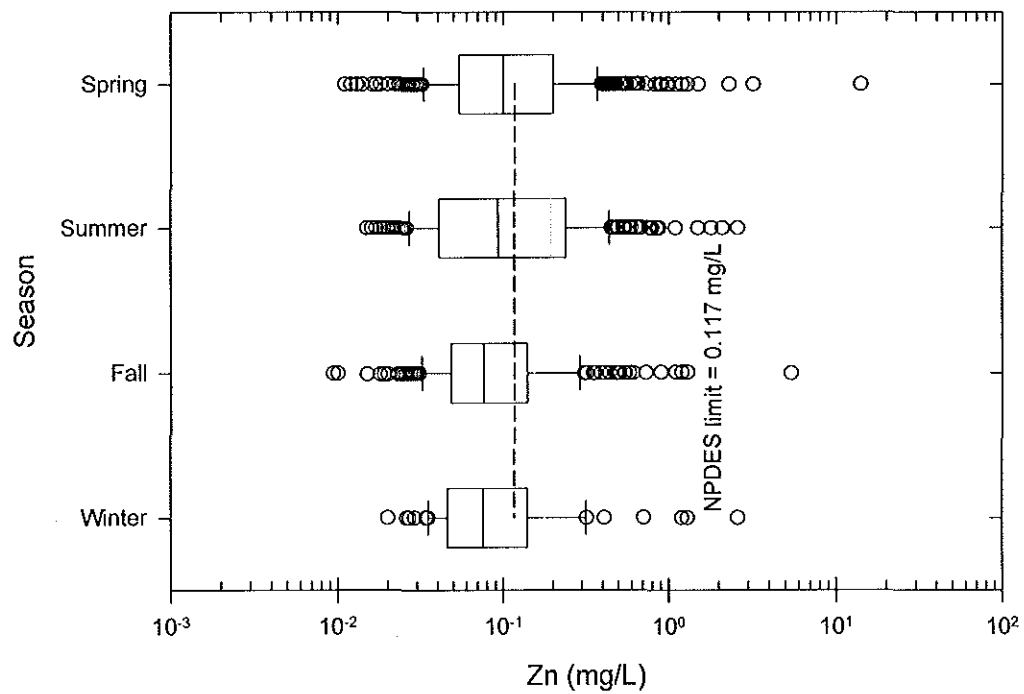


Figure C - 33. Box plots of Zn in stormwater per season.

Appendix D Combined sewer overflow data (mg/L) in the Milwaukee's Combined Sewer Service Area

Table D - 1. Data matrix for PMF modeling.

Site	Date	Pollutant									
		BOD ₅	TSS	NH ₃	TP	Cd	Cr	Cu	Pb	Ni	Zn
IssCT02	5/22/2004	36	27	1.3	0.99	0.00085	0.0009	0.0099	0.00125	0.0019	0.049
IssCT07	5/14/2004	25	66	0.92	1	0.0017	0.017	0.039	0.053	0.0057	0.13
IssCT07	5/22/2004	53	43	1.1	0.94	0.00085	0.067	0.017	0.016	0.0034	0.064
IssCT08	5/14/2004	15	97	0.73	1.2	0.0017	0.025	0.025	0.065	0.0074	0.12
IssCT08	5/22/2004	9.2	63	0.57	0.69	0.00085	0.0046	0.015	0.013	0.0023	0.057
IssCT34	5/13/2004	15	340	1	1.2	0.0017	0.018	0.049	0.16	0.012	0.22
IssCT34	5/20/2004	18	46	0.78	0.75	0.0017	0.0036	0.018	0.019	0.0028	0.082
IssCT56	5/13/2004	88	220	1.5	1.3	0.0022	0.016	0.043	0.14	0.012	0.25
IssCT56	5/22/2004	77	73	1.6	2.4	0.00085	0.0039	0.03	0.017	0.0035	0.082
IssCT56	9/25/2005	3	37	0.095	0.46	0.0034	0.016	0.026	0.029	0.0087	0.11
IssCT56	3/13/2006	80	53	0.72	0.84	0.00085	0.008	0.015	0.016	0.0044	0.093
IssKK01	5/14/2004	15	60	1.3	1.1	0.0017	0.025	0.024	0.036	0.015	0.1
IssKK01	5/22/2004	14	36	1.5	0.98	0.00085	0.0035	0.011	0.017	0.0024	0.056
IssKK01	9/25/2005	3	77	0.095	0.61	0.0017	0.013	0.017	0.06	0.0045	0.095
IssKK02	5/14/2004	15	28	1.4	1.4	0.0017	0.006	0.02	0.015	0.0021	0.06
IssKK02	5/22/2004	4	31	0.73	0.67	0.00085	0.0023	0.0095	0.0062	0.0019	0.056
IssKK02	3/13/2006	2	11	0.4	0.41	0.00085	0.0048	0.007	0.0008	0.0015	0.041
IssKK03	5/13/2004	15	170	1.2	1.5	0.0017	0.013	0.045	0.16	0.0079	0.19
IssKK03	5/22/2004	14	26	0.95	0.74	0.00085	0.0028	0.015	0.02	0.0018	0.057
IssKK03	9/25/2005	14	63	0.52	0.58	0.0017	0.013	0.017	0.032	0.0046	0.08
IssKK04	5/14/2004	63	35	2.1	2.9	0.0017	0.0038	0.025	0.0066	0.0034	0.071
IssKK04	5/22/2004	12	18	0.74	0.71	0.00085	0.0009	0.016	0.0095	0.0021	0.051
IssLMN	5/13/2004	17	73	1	1.4	0.0017	0.0065	0.027	0.057	0.0053	0.11
IssLMN	5/22/2004	3	6.7	0.28	0.54	0.00085	0.0019	0.0081	0.0042	0.0018	0.023
IssLMN	9/26/2005	6.7	28	0.52	0.51	0.0017	0.0083	0.017	0.01	0.0095	0.079
IssLMN	3/13/2006	4.6	17	0.64	0.47	0.00085	0.0052	0.0078	0.0044	0.0023	0.048
IssLMS	5/14/2004	15	67	0.59	5.1	0.0017	0.0059	0.015	0.022	0.0063	0.063
IssLMS	5/22/2004	13	11	1.1	0.8	0.00085	0.0018	0.009	0.0074	0.0016	0.04
IssNS04	5/13/2004	15	150	1.1	1	0.0017	0.015	0.047	0.045	0.011	0.12
IssNS04	5/21/2004	10	28	0.43	0.5	0.0017	0.0027	0.017	0.0055	0.0034	0.038
IssNS04	3/13/2006	13	21	0.9	0.87	0.00085	0.0047	0.012	0.0029	0.0023	0.057
IssNS05	5/14/2004	15	43	1	1.6	0.0017	0.0071	0.019	0.045	0.0044	0.11
IssNS05	5/22/2004	4	51	0.59	0.57	0.00085	0.0037	0.014	0.029	0.0029	0.075
IssNS06	5/14/2004	15	16	1.2	1.7	0.0017	0.0049	0.014	0.019	0.0026	0.048
IssNS06	5/22/2004	3	18	0.43	0.54	0.00085	0.0043	0.011	0.009	0.0027	0.096
IssNS06	9/25/2005	3	49	0.095	0.48	0.0017	0.01	0.02	0.027	0.0061	0.07
IssNS06	3/13/2006	2	13	0.39	0.42	0.00085	0.0046	0.01	0.0061	0.0014	0.045
IssNS07	5/13/2004	15	140	0.81	1.1	0.0017	0.019	0.041	0.094	0.0063	0.14
IssNS07	5/21/2004	20	33	0.98	0.87	0.0017	0.0028	0.016	0.02	0.0028	0.058
IssNS07	3/13/2006	30	30	1.6	1	0.00085	0.0047	0.0086	0.0074	0.003	0.052

Appendix D

Table D – 1 (*continued*)

Site	Date	Pollutant									
		BOD ₅	TSS	NH ₃	TP	Cd	Cr	Cu	Pb	Ni	Zn
IssNS08	5/14/2004	27	170	0.81	2.1	0.0017	0.014	0.053	0.069	0.016	0.15
IssNS08	5/21/2004	24	73	1	0.88	0.0017	0.0072	0.029	0.024	0.0053	0.081
IssNS08	3/13/2006	11	32	0.85	0.73	0.0075	0.0071	0.0099	0.0085	0.0033	0.083
IssNS09	5/14/2004	15	170	0.45	1.9	0.0022	0.016	0.038	0.2	0.013	0.19
IssNS09	5/21/2004	6	110	0.32	0.66	0.0017	0.011	0.02	0.045	0.0053	0.084
IssNS10	5/14/2004	15	31	0.59	1	0.0017	0.0079	0.017	0.016	0.003	0.064
IssNS10	5/22/2004	8.6	41	1.1	0.68	0.00085	0.0069	0.016	0.011	0.0033	0.069
IssNS10	9/26/2005	3	37	0.095	0.42	0.0017	0.015	0.022	0.089	0.0036	0.083
IssNS11	5/13/2004	15	180	0.81	1	0.0017	0.013	0.04	0.06	0.011	0.14
IssNS11	5/21/2004	6.4	35	0.43	0.56	0.0017	0.004	0.013	0.014	0.0025	0.063
IssNS11	3/13/2006	16	21	1.2	0.75	0.00085	0.01	0.013	0.0046	0.0021	0.1
IssNS12	5/13/2004	15	110	1	1	0.0017	0.0094	0.026	0.35	0.0065	0.15
IssNS12	5/21/2004	6.4	23	0.39	0.59	0.0017	0.0022	0.0093	0.01	0.0021	0.051

XIII. CURRICULUM VITAE

Puripus Soonthornnonda

PLACE OF BIRTH

Yala, Thailand

EDUCATION

1992 – 1996 B.S. Major: Civil Engineering,

Sirindhorn International Institute of Technology, Thammasat University, Thailand

1998 – 2001 M.S. Major: Civil Engineering,

Bradley University, Peoria, Illinois

MEMBERSHIPS

IAGLR	International Association for Great Lakes Research
WEF	Water Environment Federation

DISSERTATION TITLE

Stormwater Quality Characterization, Modeling, and Management for the Greater Milwaukee Area, Wisconsin.

REFEREED JOURNAL PUBLICATIONS

1. Liu, Y., **Soonthornnonda, P.**, Li, J. and Christensen, E. R. (2007). "GIS in urban stormwater modeling: Determination of drainage areas and runoff coefficients." *Environ. Sci. Technol.* In preparation.
2. **Soonthornnonda, P.**, Christensen, E. R., Liu, Y. and Li, J. (2007). "A washoff model for stormwater pollutants." *Sci. Total Environ.* Submitted.

3. **Soonthornnonda, P.** and Christensen, E. R. (2007). "Source apportionment of pollutants and flows of combined sewer wastewater." *Water Res.* Accepted.
4. **Soonthornnonda, P.** and Christensen, E. R. (2007). "A load model based on antecedent dry periods for pollutants in stormwater." *Water Environ. Res.* In press.
5. Dilmaghani, S., Henry, I. C., **Soonthornnonda, P.**, Christensen, E. R. and Henry, R. C. (2007). "Harmonic analysis of environmental time series with missing data or irregular sample spacing." *Environ. Sci. Technol.* 41(20), 7030–7038.
6. Seth, I., **Soonthornnonda, P.** and Christensen, E. R. (2006). "Use of GIS in urban storm-water modeling." *J. Environ. Eng.* 132(12), 1550–1552 (Editorial).

CONFERENCE PRESENTATIONS

1. **Soonthornnonda, P.**, Christensen, E. R., Boudjou, U., Singer, M., Bate, T., Magruder, C. and Waldmer, E. (2007). "An evaluation of separating combined sewers and its effect on water quality in the Greater Milwaukee, Wisconsin area." 80th Annual Water Environment Federation Technical Exhibition and Conference. Water Environment Federation, October 13–17, San Diego, California, USA.
2. Magruder, C., Waldmer, E., Singer, M., Boudjou, U., Christensen, E. R. and **Soonthornnonda, P.** (2007). "Urban runoff as a public health concern in the Greater Milwaukee area." World Environmental & Water Resources Congress. Environment & Water Resources Institute, American Society of Civil Engineers, May 14–19, Tampa, Florida, USA.
3. **Soonthornnonda, P.**, Seth, I., Liu, Y., Shedivy, P., Christensen, E. R. and Li, J. (2006). "A study of runoff coefficients related to characteristics of monitored catchments in Milwaukee area, USA." 49th Annual Conference on Great Lakes Research. International Association for Great Lakes Research, May 22–26, University of Windsor, Ontario, Canada.

TECHNICAL REPORTS

1. **Soonthornnonda, P.**, Liu, Y., Li, J. and Christensen, E. R. (2007). Milwaukee Metropolitan Sewerage District (MMSD) expanded stormwater monitoring program, data analysis, 2000–2006, contract: M03023E01. Final report. MMSD. In preparation.
2. **Soonthornnonda, P.**, Liu, Y., Li, J. and Christensen, E. R. (2007). Milwaukee Metropolitan Sewerage District (MMSD) expanded stormwater monitoring program, data analysis, 2000–2006, contract: M03023E01. Interim report II. MMSD.

3. **Soonthornnonda, P.**, Seth, I., Liu, Y., Li, J. and Christensen, E. R. (2006). Milwaukee Metropolitan Sewerage District (MMSD) expanded stormwater monitoring program, data analysis, 2000–2006, contract: M03023E01. Interim report I. MMSD.
4. **Soonthornnonda, P.** and Christensen, E. R. (2005). Milwaukee Metropolitan Sewerage District (MMSD) stormwater monitoring program, data analysis, 2000–2004, contract: M03023P01. Final report. MMSD.



12/10/07

Major Professor

Date